Gas–Liquid Mixing in Turbulent Systems

JOHN C. MIDDLETON

BHR Group Ltd.

JOHN M. SMITH

University of Surrey

11-1 INTRODUCTION

There are many processes in which gas–liquid contacting is important. Gas must be *effectively* and *efficiently* contacted with liquid to provide mass transfer (absorption or desorption; absorption of gas into liquid to produce a chemical reaction is often a particularly critical duty). Sometimes the gas merely provides energy (via buoyancy, level rise, bubble wakes, bubble coalescence, or gas expansion) for mixing the liquid.

Different contexts bring different challenges. Fermentations and effluent treatment can be at very large scale but the product value and workup tend to be comparatively low, so mixer capital and energy are important, whereas mass transfer requirements can be modest (fortunate if the microorganisms are shear sensitive). Gas–liquid reactions in low viscosity liquids

- Are often also at large scale
- Have reaction selectivity issues involving the dissolved gas concentration
- Have rapid reactions with large exotherms
- Involve subsequent processing producing comparatively valuable products

So for these, scale-up, liquid mixedness, and mass and heat transfer are important but impeller capital and energy cost are not. Chlorinations and sulfonations

tend to be fast reactions with soluble gases, so high mass transfer intensity with short contact time is efficient. With oxidations the gas is less soluble, but selectivity is often critical. Hydrogenations involve longer contact times, often with gas recycling (compression safety issues!) and solid particles to be kept in suspension.

11-1.1   New Approaches and New Developments

How is this chapter different from previous texts on gas–liquid mixing? First, it takes the viewpoint of a practitioner with the task of designing or scaling-up a process vessel, so the spectrum of information, conflicts, and priorities is always in view. There is mention of the more academic side when it helps to provide understanding and therefore confidence in the design methods. Second, there are reviews of some newer features, such as:

- The behavior of high-vapor-pressure systems, which may be either boiling or hot sparged
- The behavior at "high" (>0.08 m/s) superficial gas velocity (often found in industry, yet very little researched and very different from the usual regime reported in the literature)
- The extended range of impellers, including concave blade designs and up-pumping wide-blade hydrofoils
- The correlation of gas recirculation ratio and its value in calculating mass transfer driving force correctly

11-1.2   Scope of the Chapter

Table 11-1 lists many of the process considerations that will influence the selection of equipment for gas–liquid contacting operations. The equipment possibilities are

Table 11-1   Process Factors Controlling the Selection of Gas–Liquid Contacting Equipment

Required residence time for either phase
Allowable pressure drop
Relative flow rates of gas and liquid
Need for countercurrent contact
Local mass transfer performance (dispersion size and turbulent mass transfer)
Need to supply or remove heat
Corrosion considerations
Presence of solid particles
Foaming behavior and phase separation
Relative importance of micromixing
Flow pattern requirements of reaction scheme
Interaction of reaction with mass transfer
Rheological behavior in laminar and transitional flow regimes

Table 11-2 General Classification of Gas–Liquid Reactors

Contactors in which the liquid flows as a thin film
Packed columns
Trickle bed reactors
Thin-film reactors
Rotating disk reactors
Contactors in which gas is dispersed into the liquid phase
Plate columns (including control cycle reactors)
Mechanically agitated reactors (principally stirred tanks)
Bubble columns
Packed bubble columns
Sectionalized bubble columns
Two-phase horizontal contactors
Co-current pipeline reactors
Coiled reactors
Plunging jet reactors, ejectors
Vortex reactors
Contactors in which liquid is dispersed in the gas phase
Spray columns
Venturi scrubbers

outlined in Table 11-2, with their main operational characteristics (at least when arising in air–water systems) presented in Table 11-3.

The emphasis is on providing practical advice, underpinned as much as possible by analysis of the basic mechanisms involved. We consider turbulent systems, concentrating on stirred vessels with "high-speed" agitators (i.e., not anchors or helical ribbons) and certain static mixers. Stirred vessels are very commonly used for gas–liquid reactions on account of their flexibility and good performance for mass and heat transfer, so much of this chapter is concerned with them.

Static mixers operating in turbulent flow can be useful where plug flow and/or higher intensity of mass transfer are required and their short contact time is acceptable. For some cases, other equipment is more suitable (see Figure 11-3); for example:

- Bubble columns (cheaper than stirred vessels; if modest mass transfer performance is acceptable) (Deckwer, 1992) and gas-lift recirculating columns
- Ejectors (Nagel et al., 1973; Zlokarnik, 1979) and plunging jets (van de Sande and Smith, 1973, 1974; Bin and Smith, 1982)
- Sprays (low liquid hold-up)
- Packed towers and plate columns (countercurrent flow)
- In-line rotor–stator mixers (for high viscosity liquids)

The topics covered in this chapter include mass transfer, liquid mixedness, liquid and gas flow patterns and residence time distribution, gas fraction ("gas hold-up"), and impeller power demand. Bubble size is important in all these

Table 11-3 Characteristics of Gas–Liquid Contacting Equipment[a]

Type of Absorber	Typical Gas Velocity × 10² (m/s)	Residence Time Distribution		Residence Time of Liquid	Fractional Liquid Holdup	$k_L \times 10^4$ (m/s)	a (m²/m³)	$k_L a \times 10^2$ (s⁻¹)
		Gas	Liquid					
Film type: packed column and trickle bed reactors	10–100	Plug	Plug	Very low	0.05–0.1	0.3–2	2–35	0.06–7
With gas dispersed as bubbles in liquids								
Bubble columns	1–30	Plug	Mixed	Unlimited	0.6–0.8	1–4	2.5–100	0.25–40
Packed bubble columns	1–20	Plug	Mixed	Unlimited	0.5–0.7	1–4	10–30	1–12
Bubble cap plate columns	50–200	Plug	Mixed	Unlimited	0.7–0/7	1–4	10–40	1–16
Plate columns without downcomers	50–300	Plug	Mixed	Limited variation	0.5–0.5	1–4	10–20	1–8
Mechanically agitated contactors	0.1–2	Mixed	Mixed	Unlimited	0.5–0.8	1–5	20–100	2–50
Horizontal pipeline contactors	5–300	Plug	Plug	Low	0.1–0.8	2–6	10–40	2–24
Static mixers	0.05–20	Plug	Plug	Low	0.01–0.99	1–20	10–100	10–200
With liquid dispersed in gas								
Spray columns	5–300	Mixed	Plug	Very low	—	0.5–1.5	2–15	0.1–2.25
Sieve plate in spray regime	100–300	Plug	Mixed	Unlimited	—	1–3	5–20	0.5–6

[a]These are comparative values only, based on air and water. See also Table 13-9.

aspects of gas–liquid mixing, so some remarks on breakup and coalescence are also included, partly to illustrate the difficulty of providing accurate design correlations. Heat transfer is often important, and although in many cases the agitation required for gas dispersion is more than adequate to satisfy the demands of heat transfer, there is insufficient information on the effects of gassing to include a worthwhile discussion in this chapter.

This chapter covers only processes with low viscosity liquids: those in which turbulent or near-turbulent flow is achievable in practice. For stirred vessels this implies an impeller Reynolds number $ND^2\rho/\mu > {\sim}10^4$, or for static mixers and the like, a Reynolds number $UD\rho/\mu > {\sim}3000$. The dispersion of gases into viscous liquids is a different problem and largely outside the scope of this chapter. In such fluids the dispersion action is best achieved by elongating and folding the gas into the liquid, a principle that is exploited in a variety of beaters and rollers exemplified by those empirically developed for the food-processing industry over the last 2000 years. Rotor stator devices can also be used as a means of bringing these high viscosity fluids into turbulent motion, but the high viscosities and small clearances involved make this difficult to achieve. Various static mixers can be reasonably successful in achieving dispersion, notably the various Sulzer or Koch SMX designs.

It is worth mentioning that in many processes the avoidance of air entrainment and/or the removal of bubbles from viscous liquid is a greater problem. Lowering the pressure to increase bubble volume and reducing the liquid viscosity by heating and/or spreading the liquid into thin films are probably the most generally used techniques to de-gas viscous fluids.

Computational fluid dynamics (CFD) is now quite well established as a tool for modeling mixing processes with single-phase systems, but its success in predicting multiphase coalescing or dispersing flows has hitherto been limited. A brief overview in the context of the modeling of gas–liquid systems has been included in Section 11-3.1.

11-1.3   Gas–Liquid Mixing Process Objectives and Mechanisms

11-1.3.1   Turbulent Mechanisms. The processes of liquid mixing, generation of interface area, and gas–liquid mass transfer in turbulent systems are controlled primarily by the *power* dissipated in the fluids and the *gas volume fraction* ϕ. The power (together with the fluid properties) influences the *bubble size*. The gas is broken up into a dispersion of bubbles in a high-shear zone such as at the discharge from the sparger holes in a bubble column, the impeller tips in an agitated vessel, or the gas inlet and wall-shear zones in a static mixer. It is the power dissipated in that zone which controls the bubble breakup process. However, with agitated vessels the design correlations are commonly based on the average energy dissipation per unit mass in the vessel, $P/\rho V$. The power in this expression is the sum of the shaft power and the (principally potential) energy introduced as a result of injecting the gas at depth (Middleton et al., 1994). It may be noted that the ratio of local to average energy dissipation rates can be large and will differ between impeller types.

The bubbles may or may not subsequently recoalesce to some extent, depending on the local fluid dynamics and the interfacial behavior. The unpredictability of this rules out a priori prediction of bubble size and interface area in general, so design via scale-up from experiments is preferred. The *gas fraction* in an agitated vessel is determined by the bubble size and the degree of bubble recirculation [itself a function of agitation, bubble size, and scale (Middleton, 1997)]. For a static mixer, ϕ is largely set by the ratio of the average gas flow to liquid flow, but with corrections for bubble "slip," which depend on flow orientation and the bubble size.

11-1.3.2 *Factors Influencing the Power*.
In a given baffled agitated vessel, with given fluid properties, the independent variables controlling P and ϕ are the impeller type, impeller diameter, impeller speed, and gas rate. However, the gas rate for a process is usually set by the process flow sheet, that is, by the stoichiometry and the required inlet and outlet gas compositions (or absorption efficiency), so the contribution of gas buoyancy to the total energy dissipation rate is fixed. Calculation of the other (usually main) contribution, being the impeller power input per unit mass, $P/\rho V$, is well established for single-phase systems. For some (unfortunately, still common) impeller types such as the Rushton disk turbine and the downflow pitched blade turbine, the impeller power draw is greatly reduced when gas is introduced. The power draw is affected by the degree of gas recirculation and to some extent by the detailed geometry of the equipment. Modern gas–liquid impellers, such as the concave-blade disk turbines (Scaba SRGT, Chemineer BT6 and CD6 impellers, and the Lightnin R130; sample shown in Figure 11-5) and the up-pumping wide-blade hydrofoils (Lightnin A345, Prochem Maxflow, APV B6; sample shown in Figure 11-5), maintain more than 70% of their ungassed power draw on gassing.

For an inline mixer, a value for the specific power $(P/\rho V)$ can easily be estimated from the manufacturer's (or measured) friction factor, adjusted for the gas–liquid ratio using the correction of Lockhart and Martinelli (1944). Although this may not be rigorously applicable, some success has been achieved by applying the approach to static mixers using the laminar gas–turbulent liquid regime factors.

11-1.3.3 *Liquid Mixing*.
The bulk circulation is the rate-determining step for *liquid mixing* (*blending)* in stirred vessels. The turbulence ensures that mixing on smaller scales (mesomixing and micromixing) is comparatively fast. (Note, however, that extremely fast reactions can be even faster than the micromixing.) Again, the gas affects this. At modest gas rates, the gas affects the intensity of liquid mixing because of its effect on the impeller power, and its location because of changes to the flow field. At high gas fractions, presumably, the gas buoyancy must contribute.

11-1.3.4 *Gas–Liquid Mass Transfer*.
Good *mass transfer* performance requires large interface area between gas and liquid (resulting directly from small bubble size and high gas fraction, given the fixed gas rate) and a high

mass transfer coefficient (associated with local levels of turbulence). A high gas fraction is not always desirable since the profitability of a reactor is largely controlled by the quantity of liquid it contains. Excessive gas retention may also lead to overreaction. It is only necessary to allow enough time for the required mass transfer.

11-1.3.5   Heat Transfer. *Heat transfer* in the turbulent regime is essentially a macromixing process. Heat transfer coefficients are controlled by the turbulence levels (hence boundary layer thickness) near the heat transfer surfaces. In many cases the process demands of suspension or dispersion and mass transfer are more than sufficient to ensure adequate heat transfer.

11-1.3.6   Solid Particles. *Particle suspension* from the base and *drawdown* from the surface are often required in gas–liquid agitated vessels and are influenced in a complex manner by gassing. There are no well-established correlations for the influence of gas. Particle suspension is probably controlled by the energy and frequency of turbulent bursts, and drawdown by details of local flow patterns and vorticity at the surface, both of which could be expected to be affected by the presence of gas bubbles.

11-1.3.7   Flow Patterns. Flow patterns can be important. A "slow" reaction scheme (occurring in the bulk liquid) with competing steps may exhibit selectivity dependent on the local concentration of a liquid or dissolved gas reactant. In this case the liquid flow pattern (i.e., whether the liquid undergoes backmixing or plug flow or, as is almost always the case, somewhere in between) is important. A "fast" reaction scheme (occurring mainly near the gas–liquid interface) with dependence of selectivity on local dissolved gas concentration, will be sensitive to the history of gas concentration in the bubbles as they travel through the reactor. In other words, the selectivity will be sensitive to the degree of backmixing of the gas phase, and therefore to the bubble flow pattern. Even for simple gas–liquid mass transfer, the gas flow pattern is critical unless a very small proportion of the dissolvable gas is absorbed per pass. For example, if 95% of the inlet dissolvable gas is absorbed, its mean concentration in the gas phase (and hence its mean transfer rate to the liquid), if in plug flow, is 5.17 times that for an perfectly backmixed gas phase.

Here a conflict can arise in an agitated vessel. High power input per unit mass is required to enhance mass transfer area and heat transfer coefficient, but this will result in a high degree of gas recirculation, reducing the mean gas phase concentration "driving force" for mass transfer. Local shear rates will also increase with power input. The balance will vary with scale.

11-2   SELECTION AND CONFIGURATION OF GAS–LIQUID EQUIPMENT

Tables 11-1, 11-2, and 11-3 give an indication of the aspects to be considered in this section which gives a procedure for defining the components of gas–liquid

mixing equipment. The procedure applies only to low viscosity liquids in which turbulent flow can be achieved. If it is not clear whether it is practical to achieve turbulent flow, an outline design will be useful. For example, if an agitated vessel is to be used (see below), take a typical power number (e.g., 0.8 if a Lightnin A345 upflow hydrofoil is to be used, or 5.0 for a six-blade Rushton turbine) and an impeller diameter of 0.4T (or 0.33T), where T is the intended vessel diameter, and calculate the speed N required to provide a specific power input of, say, 2 kW m^{-3} (see Section 11-1.4.2). The Reynolds number can then be calculated and compared with that required to give turbulent mixing. If the fluid is non-Newtonian, an appropriate viscosity will be that at a shear rate of about 10 times N, the agitator speed (Metzner and Otto, 1957; see Section 9-3). Skelland (1967) gives a table of the constant for a number of impeller types.

First the *gas entry method* can be decided. With a vessel, the gas is preferably *sparged* in through a dip pipe discharging (preferably via a sparge
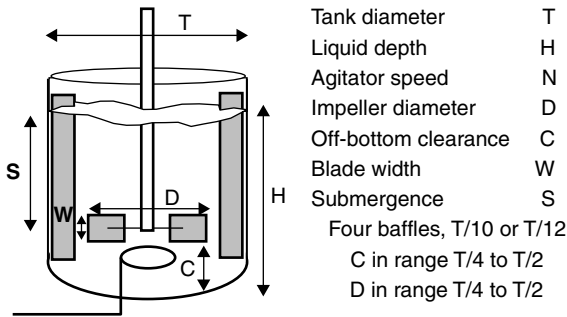

Tank diameter	T
Liquid depth	H
Agitator speed	N
Impeller diameter	D
Off-bottom clearance	C
Blade width	W
Submergence	S

Four baffles, T/10 or T/12
C in range T/4 to T/2
D in range T/4 to T/2

Figure 11-1   Standard vessel geometry (single impeller, H ~ T).
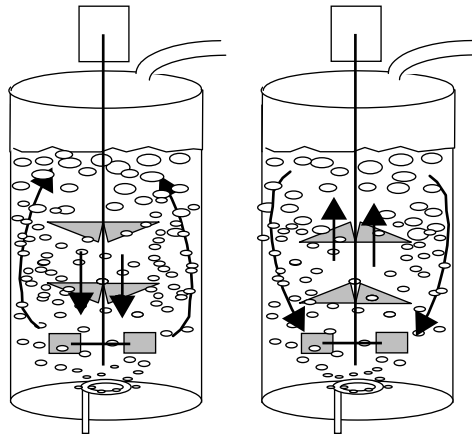

Figure 11-2   Multiple-impeller agitators, down- and up-pumping hydrofoils above a radial dispersing impeller.

ring of diameter less than the impeller diameter) underneath the impeller (see Figures 11-1 and 11-2). This ensures that the gas has a good chance of being dispersed into fine bubbles by the impeller, providing a high gas–liquid contact area. For in-line mixing, gas will generally be fed to the inlet of a static mixer (see Figure 11-3), preferably via an axially positioned feed pipe or, with larger mixer diameters, via a multipoint distributor.
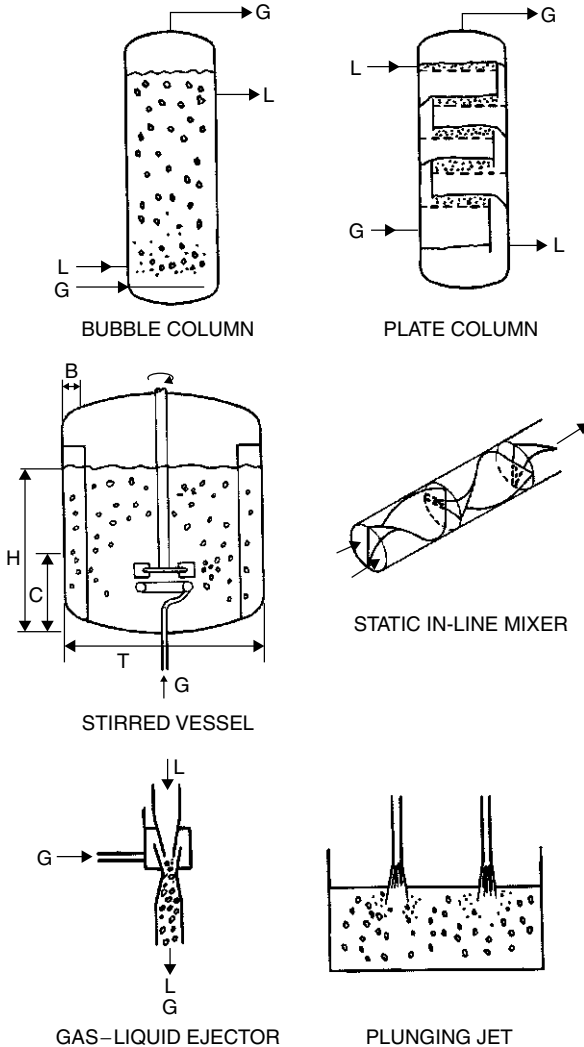

Figure 11-3 Gas–liquid contacting equipment for low viscosity liquids. (From Middleton, 1997; reproduced by permission of Butterworth–Heinemann.) An illustration of gas–liquid contacting is included on the Visual Mixing CD affixed to the back cover of the book.

In some cases, sufficient gas pressure may not be available (e.g., if avoiding the dangers of compressing hydrogen) and the gas can be drawn in by means of the energy in the liquid flow. In a vessel, gas is drawn down from the headspace using, preferably, a proprietary *self-inducing agitator*, which draws gas down a hollow shaft to the impeller (see Figure 11-4). An impeller near the surface is sometimes used to draw in gas, although this arrangement can be unstable and very sensitive to small changes of level. For in-line mixing, an *ejector*, in which gas is sucked in and dispersed by entrainment into a liquid jet, may well be chosen (see Figure 11-3).
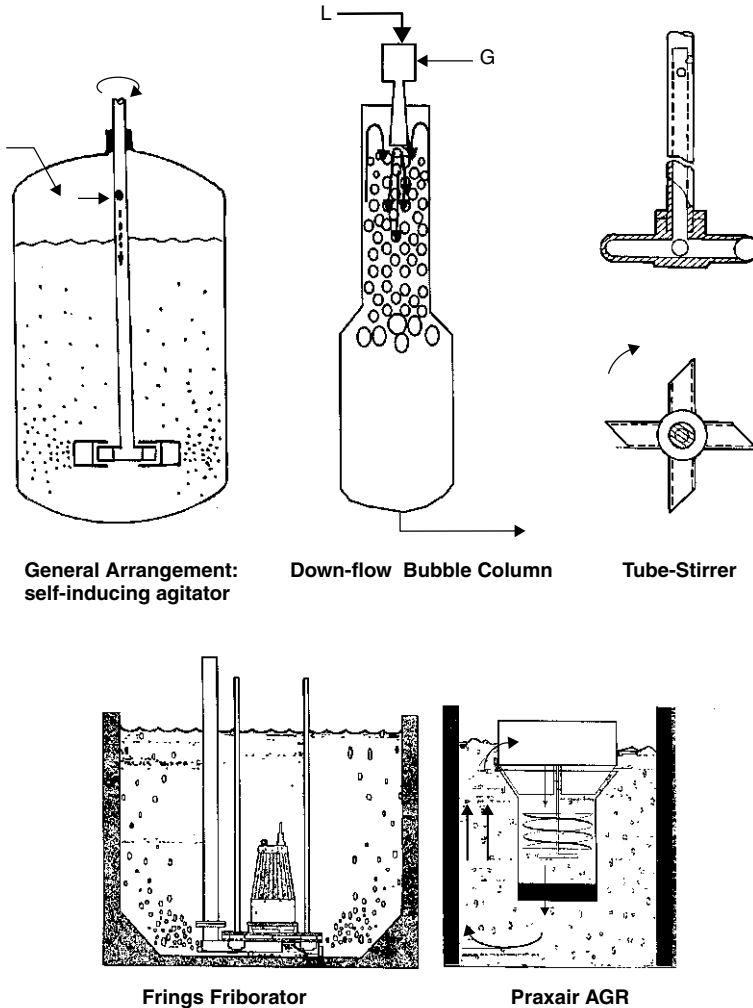

General Arrangement: **Down-flow Bubble Column**   **Tube-Stirrer**
self-inducing agitator

Frings Friborator   **Praxair AGR**

Figure 11-4   Self-inducing gas–liquid equipment. (Part from Middleton, 1997; reproduced by permission of Butterworth–Heinemann.)

11-2.1 Sparged Systems

The next choice concerns the intensity of mass transfer and turbulence required. For a first selection, three levels can be defined [see Middleton (1997, Sec. 15.1) for more detail, and also Section 11-6.3 for reacting systems]:

1. *Low intensity:* $k_L a$ values (air–water equivalent) of order 0.005 s^{-1}; for slow reactions, without a severe particle suspension or heat transfer duty. Large liquid volume is required since the reaction occurs throughout the liquid phase. Here a *bubble column* should be considered: possibly with packing to enhance the plug flow characteristics of the gas. Where it is appropriate to enhance the driving force for mass transfer by using countercurrent flow, or if the liquid needs to be nearer plug flow, a *plate column* may be selected. To meet low cost and intensity requirements when liquid flow pattern is not an issue, *plunging jets* could be considered. See Figure 11-3 and Table 11-3.
2. *Moderate intensity:* $k_L a$ of order 0.05 s^{-1}; for fast reactions with other slower steps; where particle suspension and/or heat transfer require enhancement. *Agitated vessels* are useful here, and indeed are often selected where the intensity needs are uncertain, or may vary widely (as in general-purpose reactors). The larger top surface area per unit volume than can be achieved with bubble columns allows higher exit gas flow rates without liquid entrainment and carryover.
3. *High intensity:* $k_L a$ of order 0.5 s^{-1}; for very fast reactions and short residence times: *Static mixers in turbulent flow* offer plug flow in both phases. *Thin-film contactors* such as wiped-film columns or spinning disks offer large surface per unit volume, giving very rapid mass transfer and evaporative flux.

11-2.2 Self-Inducers

A variety of *surface aerators* are available that entrain gas into a liquid surface, but these are generally applicable only in the wastewater treatment area. The simplest self-inducer for an *agitated vessel* is an impeller located near the surface, sometimes with the upper part of the baffles removed so as to encourage the formation of a surface vortex. This is, however, a sensitive and unstable arrangement. It is better, although probably more expensive, to use a self-inducing impeller system in which gas is drawn down a hollow shaft to the low-pressure region behind the blades of a suitable, often shrouded impeller (see Figure 11-4). Various proprietary designs are available, such as the Ekato gasjet Praxair AGR and the Frings Friborator (see Figure 11-4).

Self-inducing impellers are not generally successful for drawing gas down to depths greater than about 2.5 m. Success of scale-up while changing to an undersparged system will be uncertain. With limited pressure differences across the orifices there is a potential danger of plugging when operating in systems liable to cause reactor fouling.

In either case the achievable gas flow rates and gas penetration depths are limited, so large scale units may not be very successful. Scale-up will normally be on the basis of maintaining a given impeller Froude number, and as the equipment becomes larger, this will inevitably result in operation at very high specific power input levels. Performance can be sufficient for some fermentations and hydrogenations but is generally insufficient to satisfy the demands of higher intensity reactions.

Higher intensity self-induction can be achieved by an *ejector* (or *eductor*), in which a liquid stream (either the feed stream or the circulating stream of a loop reactor) is used to draw in gas and disperse it with high $k_L a$. The loop also usually contains a pump, heat exchanger, and a gas disengagement space. In the special case of total absorption, where there is no exit gas, a *downflow bubble column* may be suitable (Figure 11-4): Gas and liquid flow in at the top and the gas is dispersed, perhaps using an ejector. The bubbles are held in the downflow liquid stream until they disappear.

11-2.3 Recommendations for Agitated Vessels

Since agitated vessels are so common, it is worth noting some points arising from recent work that lead to recommended designs for turbulent systems. Most of this work has been with sparged systems, but the remarks on impeller blade shapes may also apply to self-inducers.

11-2.3.1 Sparged Stirred Vessel Geometry. As mentioned above, the gas should be fed beneath the impeller such that the impeller will "capture" the rising gas plume. With radial or upward flow impellers it is sufficient to use a sparger that has a smaller diameter than the impeller itself (a ring sparger of diameter about 0.75D is recommended). To provide the maximum gas contact time, the impeller should be near the base of the vessel but not so near as to inhibit its liquid pumping action: a clearance of T/4 is recommended. The bubble breakup mechanism relies on a high relative velocity between the blades and the liquid, so wall baffles are necessary to restrict the circumferential motion of the liquid. They also enhance the vertical motion of the liquid and hence the mixing of the liquid bulk and the recirculation of liquid and gas back to the impeller, increasing the gas hold-up. For any single impeller this recirculation is favored by an aspect ratio liquid height/vessel diameter $\equiv$ H/T of about 1. All of these factors lead to a recommended geometry, which is illustrated in Figure 11-1.

A vessel of larger aspect ratio may be required, for example, to:

- Obtain more wall surface for heat transfer
- Provide a longer contact time for the gas
- Give a staged countercurrent system
- Circumvent a mechanical limitation on available vessel diameter

In this case, more than one impeller will be required (see Section 11-2.3.3).

11-2.3.2 *Impeller Type*. An impeller that approximately maintains the ungassed power level when gas is introduced will give more stable operation and minimal scale-up difficulties. Recommended types (Figure 11-5) include, for radial flow, hollow-blade designs such as the Scaba SRGT, Chemineer CD6 or BT6, Lightnin R130, or for axial flow, an upward-pumping wide-blade hydrofoil such as the Lightnin A345 or A340 or the Prochem-Chemineer MaxfloW. Downflow hydrofoils or pitched blade turbines may be unstable during gas–liquid operation (Chapman et al., 1983; Nienow et al., 1986; Hari-Prajitno et al., 1998). The liquid flow induced by a downpumping impeller is opposed to the natural tendency of buoyant gas to rise. With a single impeller this is evidenced in the transition between indirect and direct loading that occurs as the gas flow is increased (Warmoeskerken et al., 1984). At certain impeller speeds there may be an accumulation of gas below the impeller plane which can become hydrodynamically unstable. These physical phenomena, which are independent of scale, have been found, within the authors' experience, to lead to an unpredictable loading of the impeller and a source of mechanical problems (see Section 11-4.2).

A single upflow hydrofoil may not be optimum in a vessel with H = T, if the D/T ratio is larger than say 0.5 (which may occur if high $P/\rho V$ is required), since recirculation will be localized and zones of high local gas fraction will be formed.[1]

11-2.3.3 *Multiple Impellers*. In vessels taller than H/T = 1.2, or when Reynolds numbers are below about 5000, additional impellers may be required. These would improve the liquid mixing, but also, especially in the heterogeneous
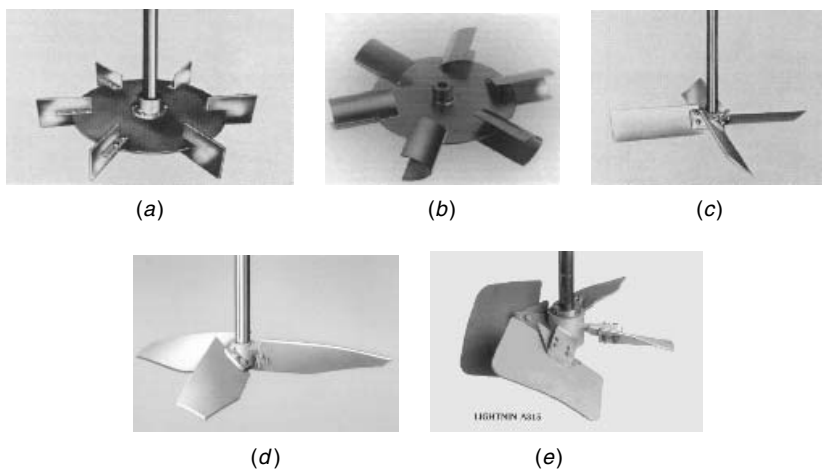
(a)   (b)   (c)

(d)   (e)

Figure 11-5 Various impellers: (*a*) Rushton disk turbine; (*b*) hollow-blade turbine; (*c*) pitched blade turbine; (*d*) narrow-blade hydrofoil; (*e*) wide-blade hydrofoil.

---

[1] *Editors' note:* The question of up-pumping versus down-pumping axial impellers for gas–liquid operation is still under active investigation.

regime or at high gas velocities, will help to redisperse and redistribute gas from the large bubbles which otherwise tend to bypass the impellers. Generally, spacing between impellers should be larger than their diameter D; otherwise, the flow patterns will interact and the power dissipated by the combined impellers will be less than the sum of the individuals. Multiple radial impellers tend to generate zoned or compartmentalized flow fields, in contrast with the better top-to-bottom circulation generated by multiple axial flow configurations. A combination of a radial flow impeller to produce dispersion together with one or more axial flow impellers is often recommended. Many operators use upward-pumping wide-blade hydrofoils (D/T approximately 0.6) even though there is a tendency for these to develop regions of very high gas fraction in the upper part of the vessel (Smith et al., 2001b).

11-2.3.4   *High Gas Velocities*. In high gas velocity systems (superficial gas velocity >0.02 to 0.03 m/s, the lower value referring to lower N), gas fraction and mass transfer do not increase with impeller power as might be expected, and much of the gas flows through as large bubbles (Gezork et al., 2000). This is the heterogeneous regime (see Section 11-3.1).

11-2.3.5   *Boiling (Nonsparged) Systems*. Although purely boiling systems are not very common, they do arise in certain polymerizations (e.g., propylene), liquid-phase exothermic reactions, and evaporative crystallization (e.g., sugar, salt). To avoid cavitation and maintain known impeller performance, impellers such as the axial flow A315u or the radial flow BT6 should be selected. These are suitable for single impeller installations as well as for the uppermost impeller of multiple impeller agitators (see Section 11-4.3).

11-2.3.6   *Near-Boiling Gas Sparged Systems*. Gas sparged or gas evolving hot systems pose different problems. Ventilated cavities (see Section 11-3.1) will almost inevitably develop, so impellers should be selected from those which maintain the power input level on gassing. Again, deep hollow-blade radial flow impellers or upward-pumping wide-blade hydrofoils are suitable. If a multiple-impeller agitator is preferred, consideration should be given to using impellers of differing diameters in order to limit the development of zones of very high void fraction, which might lead to overreaction, near the level of the uppermost impeller (see Section 11-4.4).

11-2.3.7   *Other Points*. In a three-phase reactor it is necessary to ensure that the requirements of solid suspension and gas dispersion are separately satisfied. Liquid macromixing may be as much a limitation as gas–liquid mass transfer, especially in larger gas–liquid reactors. A model comparing the kinetics of the uptake of the dissolved gas by the reaction with the supply rate via the liquid from a bubble will be useful.

11-3   FLOW PATTERNS AND OPERATING REGIMES

Characterization of the flow pattern of either phase is often limited to the ideals of perfect plug flow or fully backmixed flow (see Chapter 1). In practice, it is necessary to consider degrees in between: many in-line mixers such as ejectors and static mixers in turbulent flow achieve a close approximation to plug flow for both phases, but in industrial agitated vessels a close approach to complete backmixing is rare for either phase. If gas–liquid mass transfer is the process rate-controlling step, the flow pattern of the gas is important: Typically, it has a very great effect on the rate of mass transfer, as illustrated in Section 11-3.1. If the limiting step is reaction in the bulk liquid phase, the liquid-phase flow pattern (residence time distribution if continuous flow) may be important (see Section 11-1.3.7).

For batch systems a stirred vessel or loop reactor with an in-line mixer is used. Where plug flow is required, for long residence times a cascade of stirred vessels or loop reactors is commonly used, and for short residence times the choice will often be a static mixer or ejectors. For continuous flow systems requiring an approach to backmixed flow, stirred vessels or loop reactors are indicated.

11-3.1   Stirred Vessels: Gas Flow Patterns

In the *homogeneous regime* in an agitated vessel, the superficial gas velocity, $v_S < 0.02$ to 0.03 m/s (lower value for lower N), and the bubbles have a monomodal size distribution with a small mean size, generally between 0.5 and 4 mm. Here, the impeller controls the flow pattern and bubble size. At higher gas superficial velocities, the *heterogeneous regime* occurs (Gezork et al., 2000), in which the bubble size distribution is bimodal, with some large bubbles (say 10 mm or greater), and is controlled more by the gas velocity (possibly void fraction) than by the agitator. In this regime the influences of impeller speed and gas rate are different from those in the homogeneous regime, as will be seen in Sections 11-4 and 11-5.

Gas flow pattern is important. It controls the degree of recirculation and backmixing of the gas phase, which in turn determines the mean concentration driving force for mass transfer. It can also profoundly affect the liquid-phase macrocirculation and homogenization. One way to quantify the gas backmixing is to use the *recirculation ratio*, α (van't Riet, 1976), defined as the ratio of the gas flow recirculated to the impeller to that sparged. Since in the homogeneous regime gas is mixed with other gas only at the impeller, α represents the degree of backmixing of the gas. This implies that there is little coalescence in the bulk of the two-phase mixture in the reactor. In large scale equipment (larger than about 1 m³) liquid velocities are usually less than in small scale vessels, so even when the gas distribution is described as homogeneous (e.g., monomodal in size distribution), it is unusual for much gas to be recirculated below the level of the (bottom) impeller.

For a standard baffled agitated vessel with H = T and a single *six-flat-blade disk turbine* of D/T = 0.3 to 0.5 operating within the range PT/V = 500 to

5000 Wm^{-2} and $v_S = 0.005$ to 0.04 ms^{-1} (i.e., in the homogeneous regime), a correlation for the degree of gas recirculation, α, in terms of power per unit volume is proposed (Middleton, 1997):

$$\alpha = c \left(\frac{PT}{V} \right)^{1.42} \tag{11-1}$$

where c is a constant equal to 18×10^{-6} for water (a *coalescing* system) or 21×10^{-6} for ionic solutions (*noncoalescing*), with P in watts, T in meters, and V in cubic meters.

[Note that this is empirical and is not dimensionally consistent, but it will give a guide for other systems, using the water value for liquids without surface active solutes. It covers the useful regimes above the loading point (see below).] No correlations are available for other impeller types and vessel configurations, but CFD may be used to calculate gas recirculation, using a suitable estimate or measured value for the mean bubble size.

α is used in mass transfer calculations to estimate the overall mean concentration driving force, as follows: If ΔC is the mean mass transfer driving force $(C^* - C_L)$, where C^* is the equilibrium dissolved gas concentration at the gas–liquid interface and C_L is the bulk dissolved gas concentration, the mean driving force for the vessel is given approximately by

$$\Delta C = \frac{\Delta C_{IN} - \Delta C_{OUT}}{(\alpha + 1) \ln[(\Delta C_{IN} + \alpha \Delta C_{OUT})/(\alpha + 1)\Delta C_{OUT}]} \tag{11-2}$$

(For α in the range 0.1 to 10, this gives values about 10 to 20% low.)

The flow pattern of the gas depends on the regime of gas–impeller interaction. For six-blade disk-turbine impellers, three regimes of flow in the vessel can be defined, as shown in Figure 11-6:
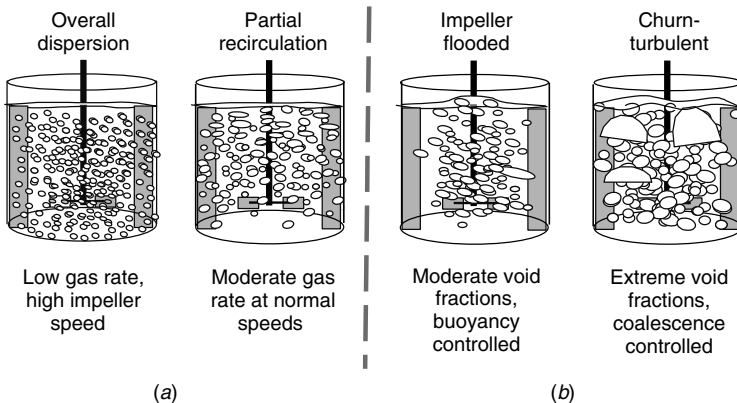

Figure 11-6 Typical void fraction distributions in vessels with a single impeller: (*a*) impeller-controlled regimes; (*b*) void fraction-controlled regime.

1. *Flooding* in which the impeller is overwhelmed by gas and gas–liquid contact; mixing, and so on, are very poor

2. *Loading* in which the impeller disperses the gas through the upper part of the vessel

3. *Complete dispersion* in which gas bubbles are distributed throughout the vessel and significant gas is recirculated back to the impeller

These are closely related to the regimes of gas–impeller interaction: As more gas is fed to the impeller (or speed diminishes), there is more tendency for gas to be accumulated in the low-pressure regions behind the blades, forming ventilated "cavities." When these are large they can cause a profound reduction in the power number of the impeller (related to their obstruction of the liquid discharge from the impeller) (see Figure 11-7 and Section 11-4.2) and hence in its performance for mixing, mass, and heat transfer. This is particularly important for flat-blade turbines with four, six, or eight blades. For six-blade disk turbines the cavity regime is best obtained from the flow regime maps of Warmoeskerken and Smith (1986) (Figure 11-8) [also summarized in Middleton (1997)] since they are dimensionless and tested for several scales.

However, it should be noted that the published maps for disk turbines refer only to impellers with $D = 0.4T$; for other ratios the regime boundaries should be adjusted using the appropriate correlations given below. The transitions between the various regimes generated by a gassed Rushton turbine can be characterized with the main dimensionless numbers, the gas flow number ($Fl_G = Q_G/ND^3$), the impeller Froude number ($Fr = N^2D/g$), and the geometry (D/T) (Smith et al., 1987):

1. Below a certain minimum speed, the impeller has no discernible action. This is approximately when
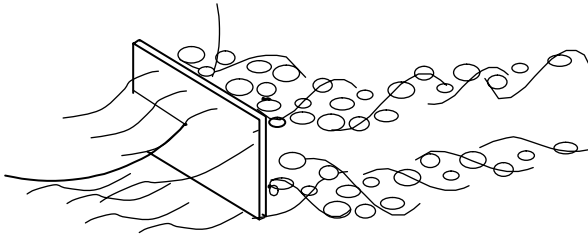
$$Fr < 0.04 \qquad (11\text{-}3)$$

2. The gas flow will swamp the impeller (flooding) if

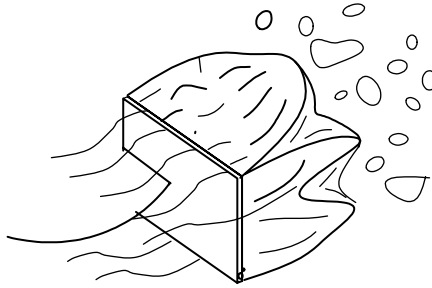$$Fl_G > 30Fr \left(\frac{D}{T}\right)^{3.5} \qquad (11\text{-}4)$$

3. Large cavities are developed by a Rushton turbine when

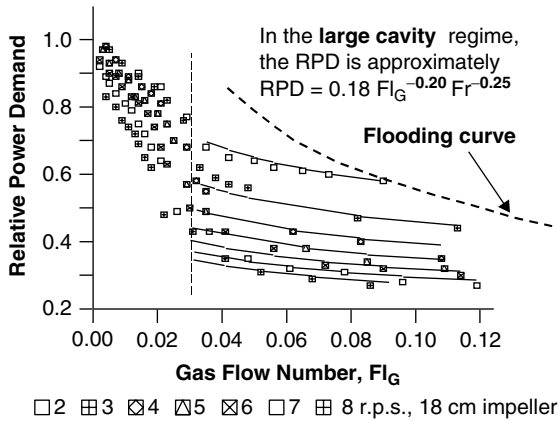$$Fl_G > {\sim}0.025 \left(\frac{D}{T}\right)^{-0.5} \qquad (11\text{-}5)$$

The constant in this expression has a weak dependence (to the power of about 0.2) on the scale of the equipment.

Figure 11-7 (*a*) and (*b*) ventilated gas cavity forms [(*a*) vortex cavities; (*b*) large cavity] on turbine blades and (*c*) relative power demand for a gassed Rushton turbine (D/T = 0.4). (Data from Warmoeskerken et al., 1982.)

4. Nienow et al. (1977) developed a relationship for the speed of a Rushton turbine that would recirculate a given gas rate which can be reformulated and expressed as

$$Fl_G < 13 Fr^2 \left(\frac{D}{T}\right)^{5.0} \tag{11-6}$$

Regimes: (1) below minimum dispersion speed (2) vortex cavities, no recirculation (3) vortex cavities with recirculation, (4) flooded, (5) loaded with large cavities (6) large cavities with recirculation.
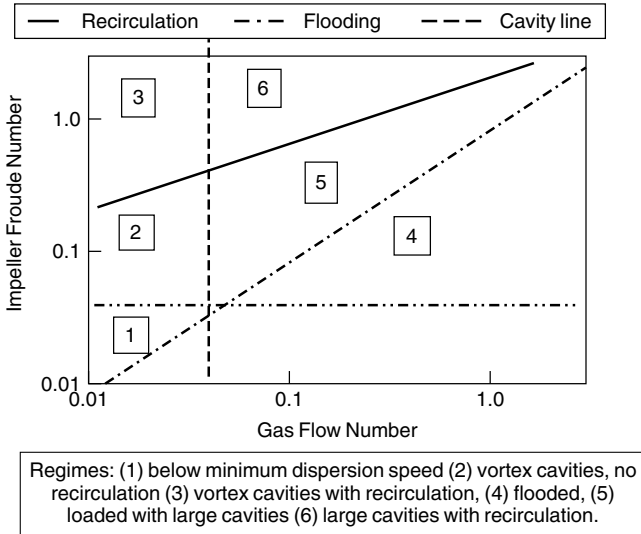
Figure 11-8   Flow map for single Rushton turbine (T/D = 2.5).

These equations allow us to predict the operating conditions in any equipment. In the large-cavity regime of gassed aqueous systems, a good approximation for the gassed power of a single Rushton turbine (D/T = 0.4) is given by

$$\text{RPD} = \frac{P_G}{P_U} = 0.18 Fl_G^{-0.20} Fr^{-0.25} \tag{11-7}$$

and lines corresponding to this equation can easily be added to the flow map. A similar map has been produced for a concave-blade impeller similar to the CD6 (Warmoeskerken, and Smith, 1989). It should be pointed out that non-Newtonian systems behave differently at transitional Reynolds numbers [see Middleton (1997) for a brief summary].

With axial flow impellers in down-pumping mode, two important regimes are identified: direct and indirect loading (Warmoeskerken et al., 1984) (Figure 11-9). At lower gas rates and higher impeller speeds, the downflow from the impeller dominates and gas enters the impeller from above; this is known as *indirect loading*. If the gas buoyancy dominates, the gas loads the impeller directly, and the impeller now pumps radially with much diminished power number (see Figure 11-10 and Section 11-4.2). Operation near the transition is to be avoided since the regime can flip unstably, giving rise to serious mechanical and operational problems. It is preferable to avoid this possibility altogether by operating in upward-pumping mode. Here the gas and liquid flows are not in conflict, and the power curve with gassing is stable and much flatter (Figure 11-11).
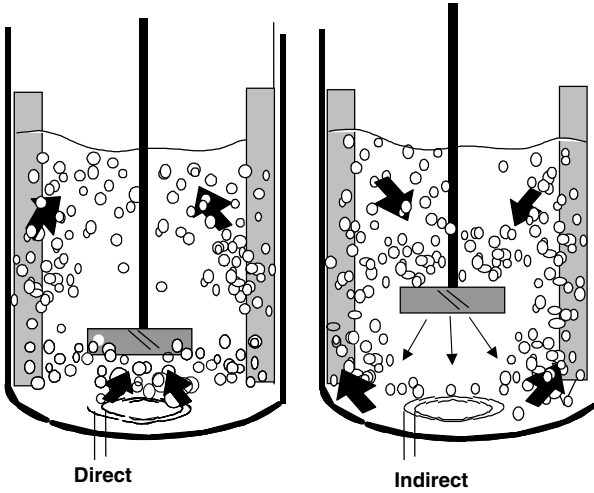
Figure 11-9   Direct and indirect loading of a downward-pumping axial flow impeller.
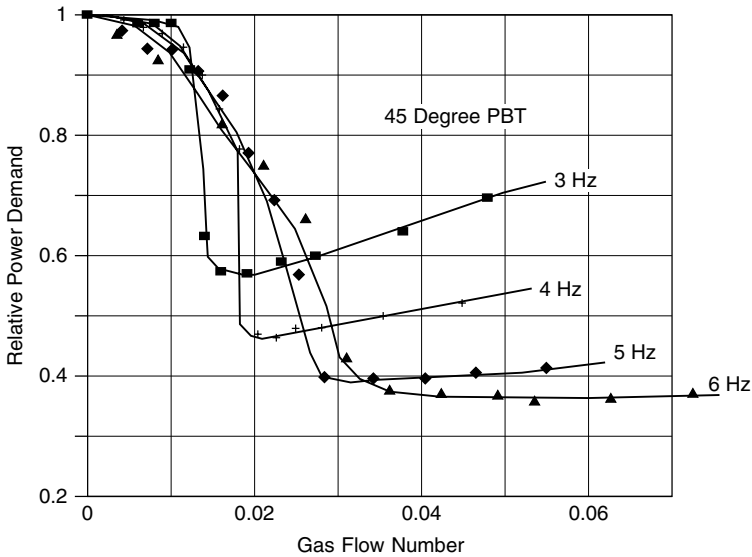

Figure 11-10   RPD For a down-pumping 45° pitched blade turbine. (From Warmoesker-ken et al., 1984.)

11-3.1.1   Flow Computation.   As was remarked in Section 11-1.2, CFD is now quite well established as a tool for modeling mixing processes in single-phase systems, although the currently popular Reynolds-averaging models using the k–ε turbulence model are not appropriate for the local turbulence conditions
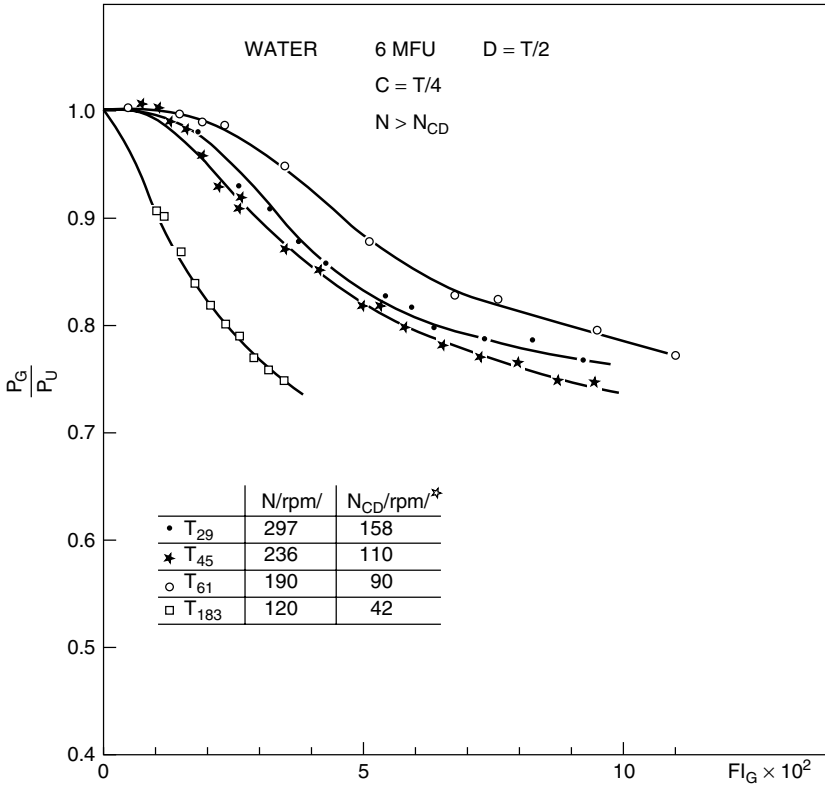
Figure 11-11 Power curves for typical upflow pitched blade turbines. T_{29} data in a 29 cm diameter vessel, etc. (From Nienow et al., 1987.)

around the impeller. Most CFD packages now offer a version of two-phase treatment, generally either particle tracking or a full Eulerian solution for each phase. In the former a selection of bubbles can be tracked as "particles," but a bubble size has to be assumed, and it is also assumed that the liquid flow patterns are unchanged by the gas, so that this is appropriate only for low gas fractions of small bubbles. In due course it is to be expected that a full two-phase treatment will account for interactions between the phases, bubble breakup, and coalescence, but development of these is in the early stages. Computational meshes can now be generated that are sufficiently fine to model the vortices behind the blades, but the remarks above concerning poor prediction of local turbulence still apply, and the gas cavities, if present, have still to be adequately modeled.

11-3.2 Stirred Vessels: Liquid Mixing Time

There is some conflict in the literature as to the effect of gassing on liquid mixing time in the homogeneous regime. However, the effects can all be related to the

reduction in power number caused by gassing, as described above. Cooke et al. (1988) found some success by substituting $(P/V)^{1/3}$ for N in the usual expression for turbulent mixing (Nt_M = constant): This correlated single phase and gassed cases (for subsurface addition) when the total of the gassed impeller shaft power together with the gas buoyancy power was used.

Recent work (Gao et al., 2000; Zhao et al., 2001) has compared liquid mixing times in ungassed, cold, and hot sparged and boiling conditions. It was shown that in an aerated "standard" tank, the mixing time correlates with the specific power input ($W \, kg^{-1}$) and superficial gas velocity ($m \, s^{-1}$), provided that both the possible changes in the relative power demand of the impeller and the potential energy added by the sparged gas (the saturated volume in hot operation) are taken into consideration. The surprising result was that mixing in a truly boiling system is significantly faster than would be expected on this basis, although, of course, with most of the gas being released near the liquid surface in a truly boiling liquid, the potential energy term is difficult to evaluate. Addition at the boiling liquid surface gave more rapid overall liquid blending than addition near the impeller—this is the only situation in which this has been found to be the case. It should be noted that recent (to date unpublished) work implies that this result does not necessarily apply when a combination of a radial flow impellers surmounted by strongly pumping axial flow impellers is used, although there are still advantages from surface addition in a compartmentalized reactor mixed with a multiple-impeller agitator.

As stated above, at high superficial gas velocities, in the heterogeneous regime, large bubbles are formed which rise faster than the liquid and take some liquid with them within their wakes. Since only a few of these will be recirculated, there is a net upflow of liquid produced by the large bubbles. Presumably this will enhance liquid mixing and reduce the mixing time, but this awaits quantification and correlations (Gezork et al., 2000, 2001).

When multiple impellers are used, care must be taken in their selection for gas–liquid systems. For example, a vessel of H = 3T with three radial flow Rushton turbines gives rise to "compartmentalization" of the flow with poor overall top-to-bottom mixing: mixing times can be very much longer than with similar specific power input in a tank with H = T mixed by a single impeller (Cooke et al., 1988). Mixing times for a combination of one to three radial flow impellers for Re > 4400 were well correlated by

$$t_{M90\%}[Po(RPD)]^{0.33}N \left(\frac{D}{T}\right)^{2.4} \left(\frac{T}{H}\right)^{2.4} = 3.3 \qquad (11\text{-}8)$$

The same vessel with a Rushton turbine at the bottom surmounted by two down-flow axial impellers gave less compartmentalization and a mixing time of seven times the H = T single-Rushton value. The best option in this case is probably three upflow hydrofoils (such as the Lightnin A345). Even these give some localized circulation loops, and these dominate at transitional Reynolds numbers. Overall mixing time is not always the full story. There are generally some comparatively dead zones (e.g., in the bottom corners or near the surface) in an

agitated vessel, and these may be a problem with some processes, with solids deposition or fouling, for example.

CFD (as described above) has been used to predict mixing times in liquid-phase systems. In the authors' experience, once the tracer input condition has been carefully modeled to match an experiment, reasonable agreement with experimental values has been obtained for axial flow impellers. For radial flow impellers, the predicted mixing times were longer than the measured values: this appears to be caused by inadequate description of the vertical transfer between the blade vortices in the impeller discharge stream. The effects of gassing have, however, not been explored.

11-4 POWER

This section deals only with turbulent flow conditions. In this regime power dissipation is the controlling factor for mixing and phase dispersion. For in-line mixers the power is derived from the flow energy of the fluid, and for stirred vessels it is obtained from the impeller and, where density differences occur, from buoyancy forces.

11-4.1 Static Mixers

Noting that power = volumetric flow rate × pressure drop, the overall power per unit mass of liquid is straightforward to calculate for single-phase systems given the friction factors and voidage fraction in the mixer as supplied by mixer manufacturers or measured in the laboratory. For gas–liquid systems the volume of fluid in the mixer must be multiplied by $(1 - \phi)$ to obtain the liquid volume, so the gas fraction ϕ must be known (see Section 11-5). It has been found that the Lockhart–Martinelli (1944) correction for the effect of the gas phase on pressure drop in pipe flow can be applied to static mixers with reasonable accuracy ($\pm 20\%$).

11-4.2 Gassed Agitated Vessels, Nonboiling

11-4.2.1 Single Impellers. The well-known equation for impeller power is often modified for gas–liquid systems to give

$$P = Po(RPD)\rho N^3 D^5 \tag{11-9}$$

where RPD is the relative power demand or gassing (or K) factor (P_G/P_U), which depends on the blade shape, Q_G, N, and D. It generally decreases with increased dimensionless gas rate [or gas flow number ($Fl_G = Q_G/ND^3$)]. The value of RPD is particularly important for six-blade disk turbines and for downflow pitched blade turbines and hydrofoils, since it can easily fall as low as 0.4, as shown in Figure 11-7. For the recommended impellers with parabolic concave blades, such

as the Scaba SRGT or Chemineer BT6, it falls to only about 0.9 (and only then at high flow numbers); with the semicircular blades of the Chemineer CD6, it falls to about 0.7. Where higher power numbers are required, flat-blade turbines with more than six blades (preferably 12 or 16) have been used, for which RPD eventually drops to about 0.4 but not until much higher flow numbers than for six flat blades (Figure 11-7). The RPD of up-pumping wide-blade hydrofoils remains close to 1.0, as shown in Figure 11-11.

This behavior has been shown (Bruijn et al., 1974; Warmoeskerken and Smith, 1982) to be related to the buildup of cavities of gas behind the blades, as described in Section 11-3.1. The flatter the blade, the larger the cavities that can form. These act as though they obstruct the passage of liquid through the impeller, and it is this that most directly reduces the effective power number [a summary of cavity formation and its effect on power can be found in Middleton (1997)]. The best way to predict the gassing effect (RPD) is first to predict the cavity regime, then obtain the value of RPD for that regime. The results in Bruijn et al. (1974) may be interpreted to relate RPD to the cavity regime to within engineering tolerance:

$$\text{vortex} - \text{clinging cavities:} \quad \text{RPD} \sim 0.9$$

three clinging + three large cavities:

$$\text{RPD} \approx 0.18 \text{Fl}_G^{-0.20} \text{Fr}^{-0.25} \tag{11-10}$$

$$\text{six large cavities:} \quad \text{RPD} \sim 0.5 \rightarrow 0.4$$

Intermediate conditions are less distinct.

Where axial flow impellers are preferred, they should be operated in the upflow direction, when they are stable and suffer only modest power drop on gassing (e.g., RPD for an upflow pitched blade turbine or a Lightnin A345 falls only to about 0.75, even at high gas rates). Downflow axial flow impellers, especially pitched blade turbines and narrow-blade hydrofoils, have a seriously unstable operating regime in gassed systems and suffer a drastically sharp fall in RPD under particular conditions (the direct–indirect loading transition) with dire consequences, such as fluctuating process performance, rapid seal and bearing wear, and high risk of shaft failure. However, wide-blade hydrofoils can be quite effective, especially as the upper impellers in multiple-impeller agitators.

With pitched blade impellers, cavities form in an analogous way to their development behind Rushton turbine blades. It is a convenient approximation to assume that indirect loading produces vortex cavities and direct-loading large cavities, although in reality the transition may occur at slightly different loadings. The RPD curves for downward-pumping pitched blade turbines are more complex than those for radial flow impellers since the liquid discharge is acting against the gas rising from the sparger. As was the case with radial flow impellers, the gassed RPD of a pitched blade impeller depends on both the gas flow number and the Froude number. The curves shown in Figure 11-10 are for a down-pumping 0.18 m (∼7 in.) diameter impeller with four 45° blades in a 0.44 m (18 in.) tank. The 45° impeller in down-pumping mode is fairly unstable, especially at low

speeds. Even at the highest speed used (6 s^{-1}), the rate of power drop is much steeper than that found with a Rushton turbine (Figure 11-7).

For all down-pumping PBT impellers, the RPD lines cross over and do not follow the orderly progression found with radial flow turbines. General sensitivity to the geometry of down-pumping two-phase hydrodynamics, particularly with respect to the transition between direct and indirect loading, has discouraged the construction of flow maps for these turbines.

Design for mass transfer entails producing a given impeller power, so it is the product of power number Po and the gassing factor (RPD) that is of importance. A summary of typical values for popular impellers at high gas flow number (say, 0.1) may be useful for guidance (Table 11-4). An example of the calculation of power for an agitated reactor is given in Example 11-1.

A very popular basis for predicting gassed power is the equation proposed by Michel and Miller (1962), which arrives at a value of the gassed power in terms of the product of the square of the ungassed power draw, the impeller pumping, ND^3, and the gas rate raised to the arbitrary power of 0.56: $[P_U^2 ND^3/Q_G^{0.56}]^{0.45}$. Unfortunately, as Nienow et al. pointed out in 1977, this equation is specious, effectively depending on a plot of $N^3 D^5$ against $N^7 D^{13}$. To emphasize this point, Figure 11-12 shows the all-too-plausible correlation of gassed power (P_G) against $P_U^2 ND^3/Q_G^{0.56}$ based on allocating random numbers to N and D in the ranges 2 to 9 and 0.2 to 1.5, respectively, and random numbers for the parameters that really matter, RPD (in the range 0.35 to 1.0) and Q_G (10 to 1000 L per minute). A plot of the values of RPD versus Q_G actually used to generate these "data" is shown in Figure 11-13.

Table 11-4 Comparative Gassed Power for Various Impellers

Impeller Type	Po	$(RPD)_{Fl=0.1}$
Radial flow		
6 blade disk turbine[a] D = T/3	5	0.4
12 blade disk turbine, D = T/3	10	0.6
18 blade disk turbine, D = T/3	12	0.7
Chemineer CD6	2.3	0.8
Chemineer BT6	2.0	0.9
Scaba 6SRGT	1.5	0.9
Axial upflow		
4 pitched blade turbine, D = T/3, C = T/3	1.3	0.75
6 pitched blade turbine, D = T/3, C = T/3	1.7	0.75
Lightnin A345, D = 0.4T	0.8	0.75
Axial downflow		
4 pitched blade turbine, D = T/3, C = T/3	1.3	0.3
6 pitched blade turbine, D = T/3, C = T/3	1.7	0.4
Prochem MaxfloW 5, D = 0.45T	1.3	0.7
Lightnin A315, D = 0.4T	0.8	0.7

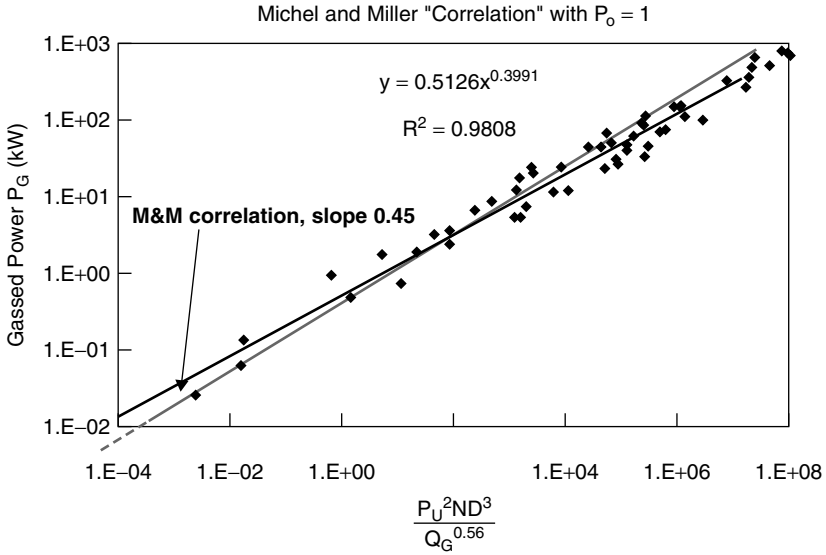[a] This is actually a function of scale (see Bujalski et al., 1987).
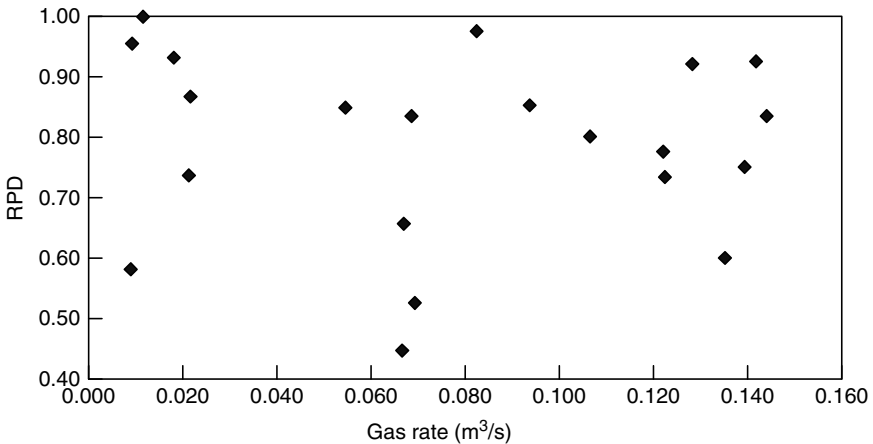
Figure 11-12   Michel–Miller relationship.

Figure 11-13   Random numbers used in generating Figure 11-12.

Example 11-1: Power Draw of an Agitated Reactor. A 5 m^3 vessel (177 ft^3 or 1320 gal) has an impeller 0.52 m (1.7 ft) in diameter and an ungassed power number of 5.0 driven at 42 rpm in water (density 62.4 lb/ft^3 and viscosity 1 cP). What is the ungassed power draw of this impeller? (*Ans.* 65.2 W.) If the gas flow number is 0.04, what is the gassed power demand? (*Ans.* 55.7 W.)

Table 11-5

Name	SI Value	SI Unit	U.S. Engg. Value	U.S. Engg. Unit
N	0.7	s^{-1}	42	rpm
D	0.52	m	1.71	ft
T	1.3	m	4.27	ft
H	3.77	m	12.4	ft
V	5	m^3	1320	gal
Po	5		5	
Fl_G	0.04		0.04	
Q_G	0.00394	m^3/s	0.14	ft^3/sec
Fr	0.026		0.026	
RPD	0.854		0.854	
Re	189 000		189 000	
P_U	65.2	W	0.0874	hp
P_G	55.7	W	0.0746	hp
g	9.81	m/s^2	32.2	ft/sec^2
ρ_L	1000	kg/m^3	62.4	lb/ft^3
μ_L	0.001	Pa · s	0.00067	lb_m/ft-sec

See Table 11-5 for the calculations. The relevant equations, which are solved using TK Solver or a similar program, are

$$Fl_G = \frac{Q_G}{ND^3} \qquad Fr = \frac{N^2D}{g} \qquad P_U = Po \cdot N^3 D^5 \rho_L$$

$$RPD = 0.18 Fr^{-0.25} Fl_G^{-0.20} \qquad P_G = RPD \cdot P_U$$

11-4.2.2 *Multiple Impellers*. Assuming that the lowest impeller is used for the primary gas dispersion, the upper impellers are not loaded by all the gas entering through the sparger (Smith et al., 1987). It can be assumed for the purpose of power demand estimation that upper impellers experience about half the total gas rate. This can be illustrated on a flow regime map (Figure 11-14).

Example 11-2: Power Demand of a Large Fermenter. The agitator in a 20 m^3 fermenter agitator is to have a lower dispersing impeller ($Po_2 = 5.0$) surmounted by a wide-blade hydrofoil, ($Po_1 = 1.0$). The fermenter height is twice the tank diameter and the hydrofoil impeller is to be 40% of the tank diameter. When aerated, the lower impeller is expected to have an RPD of 0.7 and the upper impeller an RPD of 0.9. It is desired that the same energy should be transferred to the liquid from each impeller. What should be the diameter of the dispersing turbine? At what speed can the assembly be driven if the specific gassed power input is to be limited to 0.6 kW/m^3 (3 hp per 1000 gal)? See Example 11-1 for physical properties.
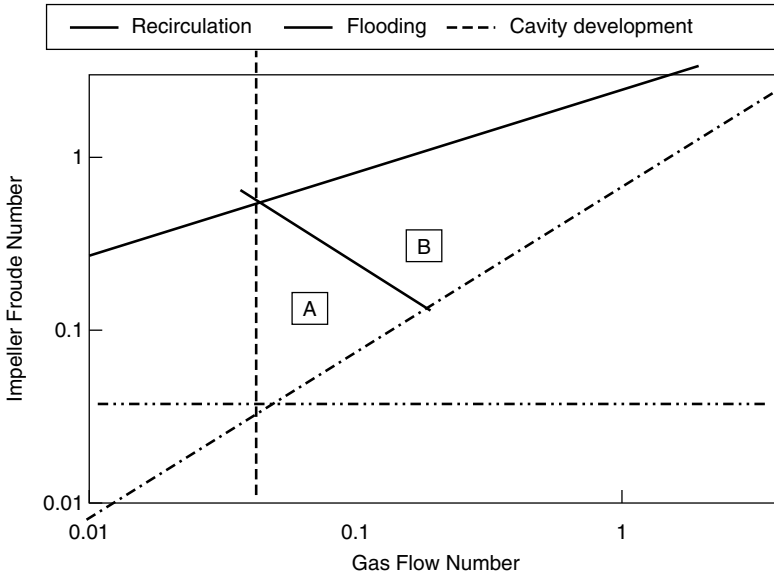
Figure 11-14   Flow map for triple Rushton turbines (T/D = 2.5). Regimes as for Figure 11-8, except that in region A there are large cavities on the lowest impeller only; in region B large cavities are present on all three impellers.

See Table 11-6 for the calculations. The relevant equations, which are solved using TK Solver or a similar program, are

$$P_U = Po \cdot N^3 D^5 \rho_L \qquad P_G = RPD \cdot P_U$$

11-4.3   Agitated Vessels, Boiling, Nongassed

Early studies (Breber, 1986; Smith and Verbeek, 1988; Smith and Smit, 1988) demonstrated the general similarities between the ventilated cavities formed during the dispersion of gases with agitators and those developed in unsparged boiling systems. However, there are major differences in performance between boiling and gas–liquid systems. During boiling, the RPD is essentially independent of the boil-up rate (Smith and Katsanevakis, 1993). Figure 11-15 illustrates results obtained with a 0.18 m diameter Rushton turbine. It is clear that neither the total boil-up rate nor changes in the flow field when vapor from the immersion heaters is directed into or away from the impeller have any effect on the relationship between impeller speed and the RPD. This implies that vapor does not load the impeller in the same manner as does noncondensable gas, and that generation in the low-pressure regions behind the impeller blades is limited.

In boiling systems the processes of the initiation and further development or collapse of vapor cavities are crucial. Conditions in the vapor cavities behind the

Table 11-6

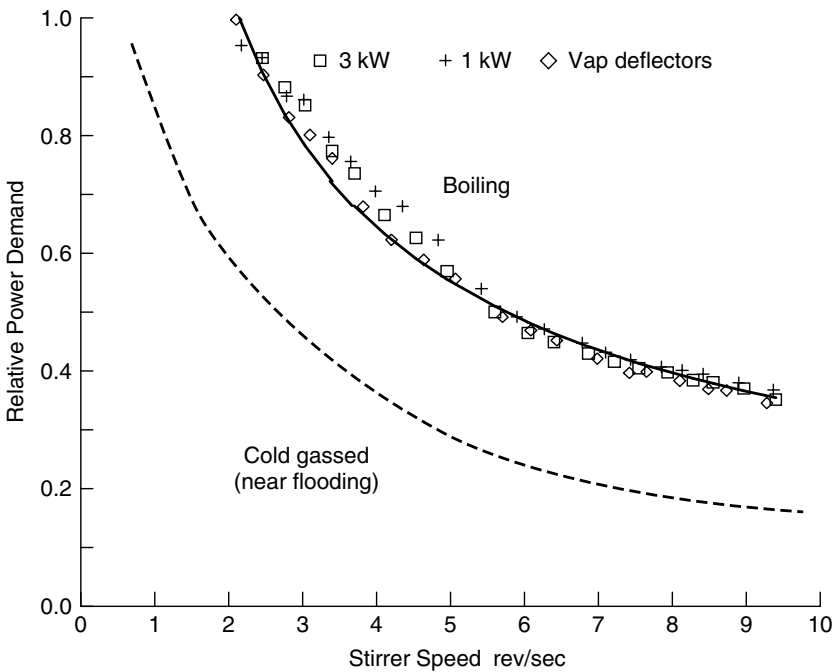| Name	SI Value	SI Unit	U.S. Engg. Value	U.S. Engg. Unit
V	20	m^3	5 280	gal
T	2.34	m	7.66	ft
H	4.67	m	15.33	ft
D_1	0.934	m	3.06	ft
D_2	0.712	m	2.34	ft
N	2.11	s^{-1} or rps	127	rpm
Po_1	1		1	
Po_2	5		5	
Pu_1	6 670	W	8.94	hp
Pu_2	8 570	W	11.5	hp
RPD_1	0.9		0.9	
RPD_2	0.7		0.7	
Pg_1	6 000	W	8.05	hp
Pg_2	6 000	W	8.05	hp
P_{tot}	12 000	W	16.1	hp
Specific power	0.6	W/kg	3.05	hp/gal

Figure 11-15   Power demand of a 0.18 m Rushton turbine with different boil-up rates and vapor flow arrangements. (From Smith and Katsanevakis, 1993.)

impeller blades can be represented by the ratio between the nominal stagnation pressure on the front of the impeller blade, near the tip, $\frac{1}{2}\rho v_t^2$, and the difference between the pressure within the cavity and that at the free liquid surface. At a submergence S, measured to the midplane of the impeller, the latter pressure difference is approximately that due to the nominal hydrostatic head (ρgS), so that we can define an *agitation cavitation number*, C_{Ag}, now sometimes referred to as the *Smith number* (Sm):

$$Sm = C_{Ag} = \frac{2gS}{v_t^2} = \frac{2}{\pi^2}\left(\frac{S}{D}\right)\frac{1}{Fr} \tag{11-11}$$

This is similar to a traditional cavitation number except that the pressure within the vapor cavity is strongly affected by both local fluid mechanics and thermal factors. It was shown by Smith and Katsanevakis (1993) that the RPD in a boiling agitated system can be described adequately by relationships of the form

$$RPD = \frac{P_B}{P_U} = A\left(\frac{2Sg}{v_t^2}\right)^B = AC_{Ag}^B = A \cdot Sm^B \tag{11-12}$$

The constant A, which is often about unity, depends on the impeller type. (see Table 11-7). Impellers with a high gas-handling capacity, such as hollow-blade disk designs, have the highest values. As will also be seen in Table 11-7, the exponent B varies considerably with impeller type but is about 0.4 for Rushton and pitched blade turbines. Figure 11-16 reproduces some results for a six-blade Rushton turbine working at various submergences and boil-up rates. In this case the constant A in eq. (11-12) is 0.74.

A critical $(C_{Ag})_{crit}$ (or Sm_{crit}) can be defined as that value above which the power draw is essentially the same as when this impeller, is ungassed. For a Rushton impeller, this value is about 2.1 and values for other impellers are given

Table 11-7 Impeller Constants for Unsparged Boiling

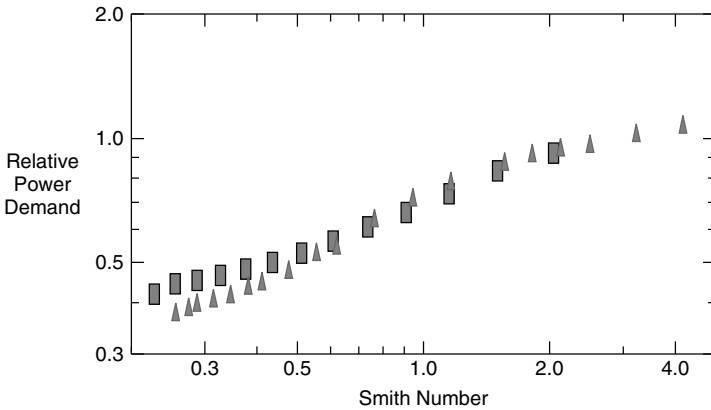| Impeller	Constant A	Exponent B	Critical C_{Ag}
Rushton turbine	0.69	0.4	2.15
PBT_D (down-pumping)	0.74	0.4	2.10
PBT_U (up-pumping)	0.90	0.4	1.30
Chemineer CD-6	1.17	0.2	0.46
Chemineer BT-6	1.16	0.1	0.23
Chemineer Maxflow$_D$	1.03	0.4	0.93
Chemineer Maxflow$_U$	1.61	0.4	0.30
Lightnin A315$_D$	1.16	0.4	0.69
Lightnin A340$_D$	1.07	0.4	0.84
Lightnin A340$_U$	1.12	0.2	0.57

Figure 11-16 Boiling power demand, Rushton turbine. (From Gao et al., 2001a.)

in Table 11-7. Using this critical value, we can write

$$RPD = \left[\frac{C_{Ag}}{(C_{Ag})_{crit}} \right]^B = \left(\frac{Sm}{Sm_{crit}} \right)^B \tag{11-13}$$

The values do not appear to be very sensitive either to D/T or to absolute scale.

Figures 11-17 and 11-18 show data from Smith et al. (2001a) relating to various hollow-blade and hydrofoil impellers from which the values in Table 11-7 have been derived. Modern hydrofoil impellers, which are designed to have good gas-handling characteristics, almost maintain their cold ungassed power levels when up-pumping. In this respect they behave almost as if cavitation does not occur. This will be a very desirable feature of these impellers when used in evaporative crystallizers. Later work (Smith and Tarry, 1994) confirmed that the
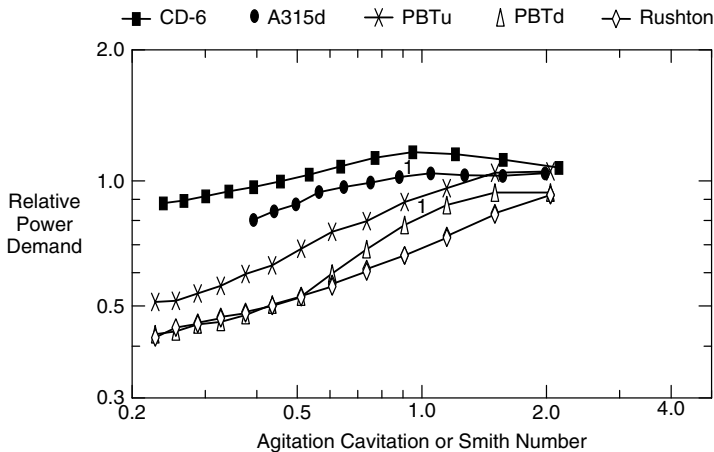

Figure 11-17 Boiling RPD for common impellers. (From Gao et al., 2001a.)
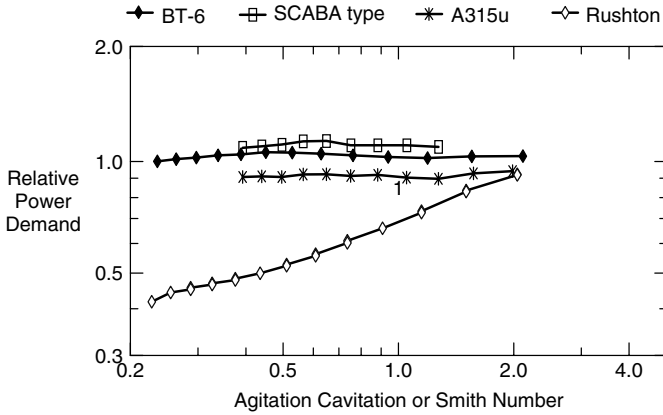
Figure 11-18   Boiling RPD for modern gas-dispersing impellers. (From Gao et al., 2001.)

identical relationship is valid with boiling solutions in which the elevation of boiling point would have the same effect as that of significant increases in impeller submergence. It is also unlikely that liquid viscosity will have a significant influence as long as the Reynolds number is high. These two facts encourage the conclusion that the results will be valid for all low viscosity liquids.

The locus of the limiting power appropriate to flooding an 0.18 m diameter Rushton impeller at a submergence of 0.3 m is also shown in Figure 11-15. The much higher relative power demand of an impeller in rapidly boiling liquid compared with that in the near-flooded, cold-sparged condition at the same shaft speed (i.e., of Fr or Sm) is evident. These boiling cavitation and (cold) gas flooding lines represent limits between which a sparged boiling reactor might be expected to operate.

Example 11-3: Impeller Power in a Boiling Crystallizer.   An upward-pumping pitched blade impeller of 0.6 m in diameter is to be specified for a boiling crystallizer in which it is submerged by 0.7 m. If the critical Smith number for this impeller is 1.3 with RPD obeying a $Sm^{0.4}$ law, and the RPD is not to be lower than 60% of the ungassed value, what is the maximum speed at which the impeller should be driven?

See Table 11-8 for the calculations. The relevant equations, which are solved using TK Solver or a similar program, are

$$Fl_G = \frac{Q_G}{ND^3} \qquad Fr = \frac{N^2D}{g} \qquad P_U = Po \cdot N^3 D^5 \rho_L$$

$$P_G = RPD \cdot P_U \qquad Sm = \frac{2gS}{v_t^2} = \frac{2}{\pi^2}\left(\frac{S}{D}\right)\frac{1}{Fr} \qquad v_t = \pi ND$$

$$RPD = \left(\frac{Sm}{Sm_{crit}}\right)^B \qquad \text{where } B = 0.4$$

Table 11-8

Name	SI Value	SI Unit	U.S. Engg. Value	U.S. Engg. Unit
RPD	0.6		0.6	
Sm	0.36		0.36	
Sm_{crit}	1.3		1.3	
S	0.7	m	2.30	ft
g	9.81	m/s^2	32.2	ft/sec^2
v_t	6.15	m/s	20	ft/sec
D	0.6	m	1.97	ft
N	3.26	s^{-1} or rps	196	rpm

11-4.4 Agitated Vessels, Hot Gassed Systems

Unsparged boiling and cold sparging generate two quite different sets of conditions with large differences between the physical properties of the liquid and gas phases. The cavitation line for Figure 11-15 is based on liquid at its boiling-point generating vapor, while the flooding correlation refers to cold systems with little further vaporization. It has been shown that at a given speed [i.e., a fixed Froude or agitation cavitation (Smith) number] most impellers draw more power in a boiling system than in cold, preflooding, gassed conditions. The interactions of gas rate and impeller operation need to be understood so that the transitional hot sparged gas case can be quantified for industrially important conditions.

When an inert gas is passed through a boiling liquid, there is a change in the thermodynamic equilibrium. Since the bubbles consist of a mixture of vapor and inert gas, the partial vapor pressure of the condensable components is less than the total pressure at which the liquid was previously boiling. The liquid is therefore superheated relative to the mixed gas phase and there will be an immediate increase in the evaporation rate so that latent heat can remove the excess energy. The liquid temperature will fall until the energy supply and removal rates are in balance. A steady equilibrium temperature will be established when there are constant net heat input and gas throughput rates.

Saturation is rapid. Figure 11-19 shows the results of a simplified calculation suggesting that bubbles leaving a sparger are brought to within 90% of saturation in about 500 ms (Gao et al., 2001). This suggests that calculations based on complete saturation are accurate enough for most design purposes. The evaporation of the liquid into the bubbles removes heat from the system. Saturated bubbles will contain vapor to a partial pressure that will correspond to the temperature of the liquid and is less than the total pressure of the system. It follows that even when there is a heat source, no continuously sparged liquid can be at its true boiling point.

The equilibrium temperature is sensitive to the sparged gas and heat supply rates but is independent of the impeller speed, a result confirmed by experiment (Figure 11-20). This simplifies the analysis since a constant vapor pressure can
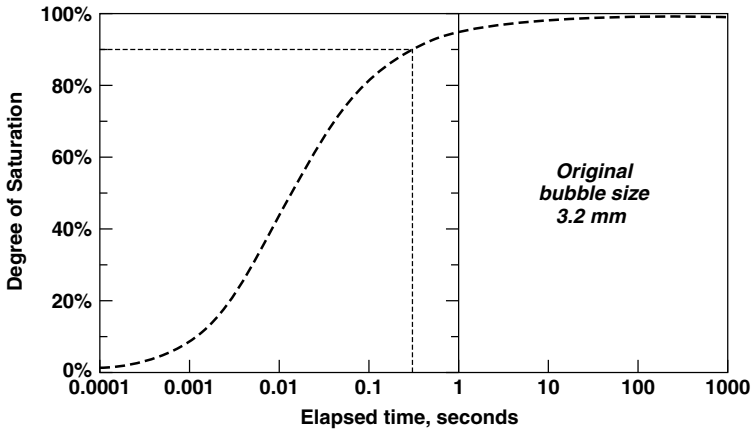
Figure 11-19   Saturation of an air bubble introduced into boiling water.
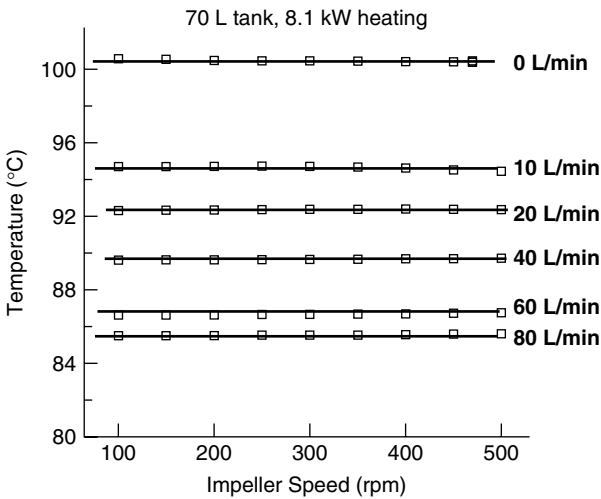
Figure 11-20   Temperature of heated sparged water showing the independence of impeller speed.

be assumed for a given gas rate, and this allows reasonable estimates to be made of the combined gas and vapor flow loading the impeller.

When an existing boiling reactor is sparged, the sparged gas rate can be corrected using the vapor pressure of the liquid at the temperature measured. Assuming that the partial pressure of the vapor p_v is then known, the total volumetric rate, Q_{GV}, is given by

$$\frac{Q_{GV}}{Q_G} = \frac{p_0}{p_0 - p_v} \tag{11-14}$$

When the liquid vapor pressure is known in terms of the usual relationship, $p_v = Ae^{b/\theta}$, the correction can be expressed as

$$\frac{Q_{GV}}{Q_G} = \frac{1}{1 - e^{b(1/\theta_1 - 1/\theta_0)}} \tag{11-15}$$

where θ_0 is the boiling point at the ambient pressure p_0 and θ_1 is the temperature measured during sparged operation. This relationship will always be true even if there has not been sufficient time for the equilibrium conditions consistent with the heat balance to be established.

Some RPD results from experiments in a dish-bottomed vessel of 0.44 m diameter with three 1.2 kW heaters and a 0.18 m Rushton turbine are shown in Figure 11-21 using the log(RPD) versus log(Sm) format (after Smith and Milling-ton, 1996). Most of the values fall between the pool boiling cavitation and gas flooding lines, with higher gas supply rates corresponding to lower values of the RPD. As can be seen from the figure, within the accuracy of the measurements the relative power demand of a sparged "boiling" system is independent of the impeller speed until the impeller speed becomes low enough for the data points to concatenate onto the cold flooding line. Many other experiments have confirmed this behavior.

11-4.5 Prediction of Power by CFD

If the methods referred to earlier are used with care, CFD can predict the power number of an impeller in a single-phase system to within 20%. A well-chosen grid with local refinement around the impeller and at least 200 000 cells is required. The only successful method seems to be to integrate the torque on the impeller. Summation of energy dissipation, ε, over the vessel does not give the
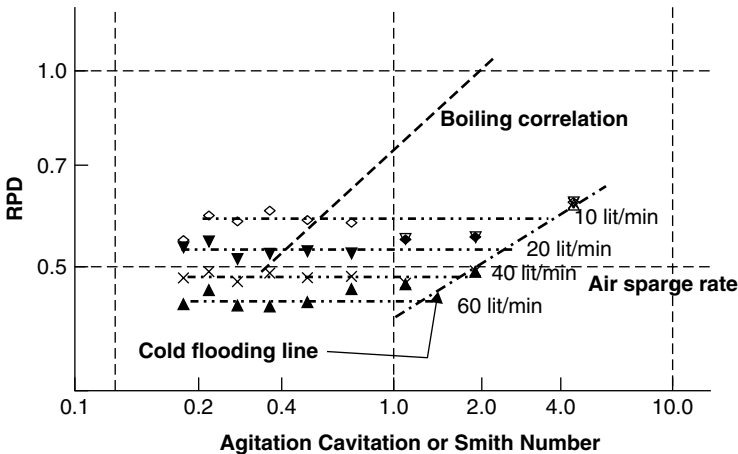

Figure 11-21 Relative power demand in aerated hot 70 L reactor.

correct answer, probably because of the shortcomings of the turbulence models; this is illustrated by the underprediction of ε in the discharge region of disk turbine impellers (Montante et al., 2001). CFD methods have not yet been developed to the point that they will predict the correct effect of gassing on power demand.

11-5   GAS HOLD-UP OR RETAINED GAS FRACTION

11-5.1   In-line Mixers

As remarked earlier, because in-line static mixers are plug flow devices, the gas fraction is comparatively easy to determine from the ratio of mean gas flow rate to total flow rate, with adjustment for bubble "slip" if the flow orientation is non-horizontal. Often, vertical downflow is preferred, since the gas–buoyancy leads to the bubble velocity being less than the liquid velocity, so the gas fraction (and hence the gas–liquid interface area) is greater than for other configurations. While there is much literature on bubble slip velocities, the predictions are said to be unreliable (Zuber and Findlay, 1965) and it is usually preferred to use empirical correlations of the gas fraction based on measurements [such as those in Middleton (1978)], although so far these all seem to be for air–water systems with negligible depletion of bubble size, so may need adjustment for other systems.

When gases are dispersed in liquids of high vapor pressure, there are significant effects due to vaporization or condensation of the liquid. For example, if the pressure surrounding an air bubble in water at around 97°C, which has a vapor pressure of about 0.9 bar, is reduced from 1.2 bar to 1 bar, the volume of the bubbles will increase threefold, not by the 20% or so that would be the case at room temperature (see Figure 11-23). This effect will be particularly important in changing the phase ratio of a two-phase flow through a static mixers operating with a large overall pressure drop.

11-5.2   (Cold) Agitated Vessels, Nonboiling

Gas fraction in agitated vessel is difficult to predict a priori, but in the homogeneous regime, scale-up can be made reasonably accurately using empirical correlations. These are best expressed in the form

$$\phi = \alpha' \left(\frac{P}{\rho V} \right)^{\beta'} (v_s)^{\gamma'} \tag{11-16}$$

where the constants α', β', and γ' are independent of scale. Although such equations are unsatisfactory in principle both because the $P/\rho V$ and v_s terms are often mutually dependent and because of the need for α' to have noninteger dimensions in order to provide dimensional consistency, they have been more

successful than alternative formulations. The implication is the rather counter-intuitive result that the impeller design or configuration is only of secondary importance, provided that the energy is transferred to the liquid.

The value of α' depends on the physical properties of the liquid, in a way that is in general difficult to predict (hence the recommendation to obtain at least one measurement at semitech or pilot scale during process development, and use the correlation for scale-up only). The published data are for aqueous systems, in which the addition of any solute that exhibits surface activity (this includes electrolytes and alcohols as well as surfactants) has a large impact on the gas fraction; for example, a system in which water gives, say, $\phi = 0.1$ and d = 4 mm may give $\phi = 0.25$ and d = 0.5 mm with a solution of a simple electrolyte (above a plateau concentration). The considerable literature on this effect currently aligns observations with a reduction of bubble coalescence caused by the solute via gradients of surface tension repressing drainage of the liquid film between approaching bubbles. Such effects could also occur with small concentrations of water in organic liquids or with small particles caught at the interface. For engineering purposes, the situation has been simplified to cover (for the homogeneous regime) two "extreme" classes of liquid system—coalescing and noncoalescing systems—with separate correlations for gas fraction and mass transfer; but there is no guarantee that all industrial systems fit between these classes.

Values of β' and γ' vary in the literature between 0.2 and 0.7, but generally, $\beta' = 0.48$ and $\gamma' = 0.4$ are quite reliable (Smith et al., 1977). More recent work (Gao et al., 2001) has led to the equation (expressed in W, m, s units)

$$\phi = 0.9 \left(\frac{P}{\rho V} \right)^{0.20} (v_s)^{0.55} \qquad (11\text{-}17)$$

for hold-up in vessels with multi-impeller agitators dispersing air in water at ambient temperature. It would be better to have separate correlations for each flow regime; for example, as the Reynolds number is decreased into the transitional region, β' tends to fall and γ' to rise (Cooke et al., 1988). The same trends occur in β' and γ' as gas superficial velocity v_s rises into the heterogeneous regime; eventually (above $v_s = 0.08$ m s^{-1} and $P/\rho V = 1$ W/kg), the total gas fraction actually decreases slightly with increased $P/\rho V$, and the fraction of small bubbles remains constant, with the large bubble fraction increasing as v_s is increased (Gezork et al., 2000). The latter work was carried out with one liquid system (air–polypropylene glycol solution) which gives very high gas fractions (up to 0.55), and no general correlations for this regime are yet available. The presence of large bubbles implies that it may not be an optimal regime for mass transfer.

These equations are for operation at ambient temperature. In the fully turbulent regime there is a dependence of void fraction on temperature which is discussed below. This gives $\phi \propto \mu^{0.55}$. Measurements of the void fraction distribution in gas-sparged vessels clearly show a region of high gas fraction in the violently

agitated regions near the impeller plane. There may also be gas accumulation in the liquid downflow centrally above a radial pumping impeller and near the walls below the impeller plane.

11-5.3   Agitated Vessels, Boiling (Nongassed)

Bubbles can survive in a hot liquid only if the temperature is high enough that the vapor pressure of the liquid matches the local pressure. This implies that vapor generation in a well-mixed liquid is limited to boiling near the free surface, possibly in low-pressure regions behind impeller blades and in any superheated liquid that may be near heat sources. In the case of boiling water at 1 bar, a superheat of 1 K will sustain a bubble at a depth of about 35 cm, so this is the maximum depth that bubbles can exist in a tank in which the temperature is as uniform as that. Visual observation in pilot scale rigs confirms that vapor generation is limited to the topmost few centimeters of the vessel, and the vertical distribution shown in Figure 11-22 is typical.

The situation is rather different at 10 bar. Because of the steeply rising vapor pressure, a water temperature of 1 K superheat will support bubbles to a depth of about 7.5 m. Since large vessels, with their greater likelihood of temperature inhomogeneity, frequently operate at high pressure, the void distribution in them can be expected to be distributed much more uniformly and to approach those more typical of gassed systems.
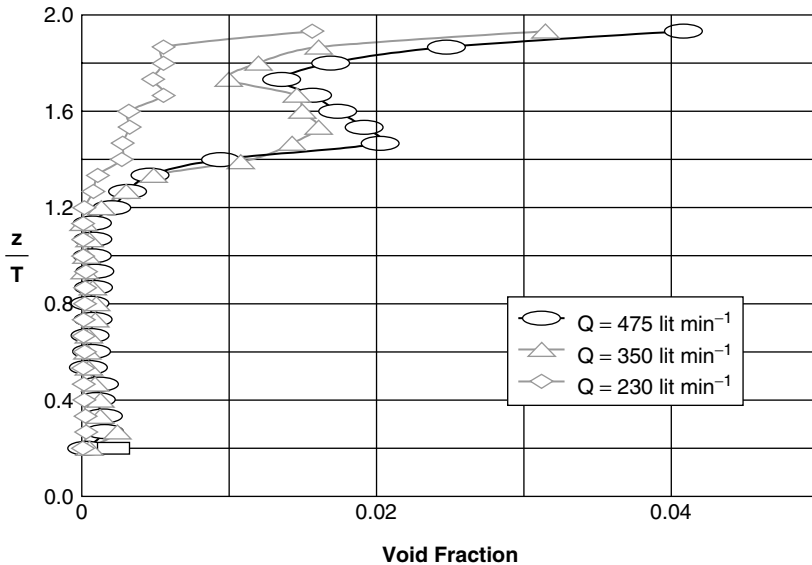

Figure 11-22   Vertical void fraction distributions at three boil-off rates in a boiling reactor with twin radial pumping 18 cm CD6 impellers at 240 rpm.

11-5.4 Hold-up in Hot Sparged Reactors

When gas is sparged into a hot liquid, there is an immediate change in the thermodynamic status as the liquid vaporizes into the bubbles. As noted above, this process continues until the latent heat required removes all that is available. In continuous operation the liquid will settle at a temperature below its nominal boiling at a value determined by the rate of supply of sparge gas and heat. Any sparged or evolved gas will produce this effect. The vapor dilutes the sparged gas, so reduces the driving force for mass transfer.

Although the effects of pressure are less spectacular than in purely boiling conditions, they cannot be neglected. Figure 11-23 illustrates the difference when a small air bubble is released into open tanks of hot and cold water at a depth of 2 m: at ambient temperature the bubble expands by about 20%, whereas at 97°C the expansion is 300%. The effect will be less marked at high pressure, and again, the closer the liquid is to its boiling point at the operating pressure, the greater the effect, so that void distributions in purely boiling liquids at high pressure can be expected to be closer to those in sparged systems. Sparged hold-up measured in hot systems differs markedly from that at room temperature. Experimental measurements suggest that in an air–water system around 80°C, void fractions are at least 30% lower than at room temperature.

Overall void fraction measurements (made by a radar probe detecting the surface level averaged over several seconds) are shown in Figure 11-24. Similar data confirm the lower gas holdup in heated systems. In this figure the sharp fall-away in void fraction at low shaft power (i.e., at low speeds) seen at room temperature is visually correlated with the loss of radial pumping action by the asymmetric BT-6 impeller.

Extensive work with configurations involving up-pumping hydrofoils, which have become a generally favored arrangement for large gas–liquid reactors, has led to a correlation for overall gas retention that is a function of the absolute temperature. Specifically, in an air–water system with multiple impellers, the
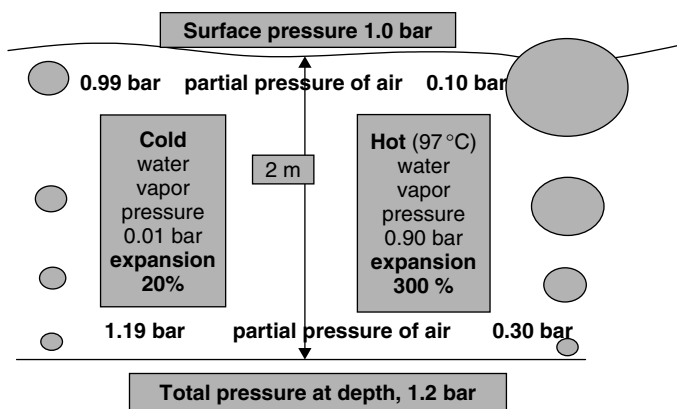
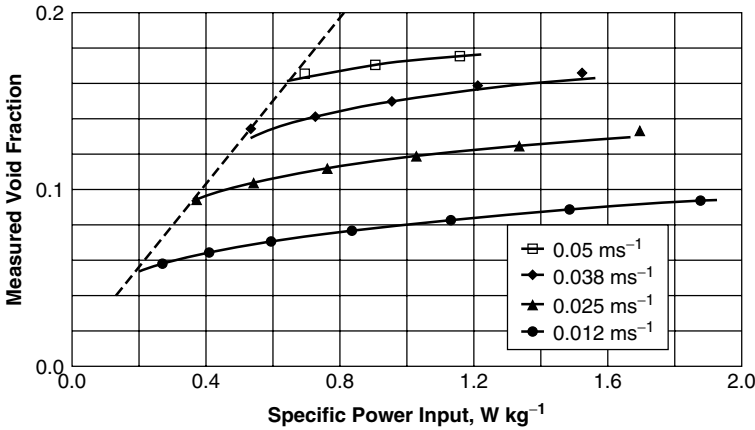**Figure 11-23** Expansion of air bubbles rising in cold and hot water.

Figure 11-24 Overall void fractions with a multiple impeller agitator CD6 + 2MFU.

average void fraction

$$\phi = 70 \times 10^6 \left(\frac{P}{\rho V}\right)^{0.20} (v_s)^{0.55} \theta^{-3.2}$$

where $P/\rho V$ is the specific power input (W/kg), v_s the superficial gas velocity (m/s), and θ the absolute temperature (K). This equation is consistent with that by Gao et al. (2001) given above for ambient holdup data.[2] In a vessel with a single impeller agitator, the void fraction will be lower, about 65% of this predicted value. Since vapor pressure and liquid-phase viscosity have similar dependence on temperature, there is not enough evidence to decide which is controlling, but broadly similar behavior can be expected whatever the composition of the liquid phase.

Example 11-4: Void Fraction in a Gas–Liquid Reactor. A void fraction of 7% is measured in an aerated reactor containing water at 20°C. What will be the void fraction if the reactor is operated at the same specific power input and superficial gas velocity (after allowing for the contribution of water vapor) at 90°C?

SOLUTION: Void fraction varies with absolute temperature, $\theta^{-3.2}$. For this example

$$7 \left(\frac{363.2 \text{ K}}{293.2 \text{ K}}\right)^{-3.2} = 3.5\%$$

The mean residence time of gas passing through a reactor at 20°C (when the partial pressure of water is negligible) is 1 min [i.e., the sparge rate is 1 vvm (1 volume of gas per volume of liquid per minute)], at which flow rate the void

---

[2] This conclusion has not been confirmed in a system of very high purity (Shaper et al., 2002).

fraction is 7%. What will be the mean residence time if the temperature is raised to 90°C (when the partial pressure of water is 0.9 bar)?

The oxygen content will be reduced from 21% to 2.1% and the residence time reduced from 1 min to 31 s. Mass transfer might be expected to be about 20 times as difficult except that diffusion coefficients will be increased (by about $\theta^{3/2}$, i.e., $\approx 40\%$) at the higher temperature.

11-5.4.1 Void Fraction Profiles with Multiple-Impeller Agitators.

Figure 11-25 shows data obtained with two 18 cm radial flow CD6 impellers in tank of T = 44 cm, H = 2T. The highest void fraction occurs just above the level of the uppermost impeller, with a peak value in cold operation that is about 40% higher than that just above the lower impeller. In hot operation (generating about 250 L/min of steam into about 130 L/min of sparged air), although the void profile has an overall shape which is generally similar to that at room temperature, the gas fraction is clearly considerably less at all levels. In hot conditions the void fraction near the upper impeller is nearly twice that at the lower impeller. When the liquid is boiling, with a vapor generation rate giving a similar off-gas volume, the voids are limited to the top few centimeters of the reactor since efficient liquid mixing eliminates significant superheat.

Figure 11-26 shows comparable data when the agitator is a combination of a radial impeller with two up-pumping wide blade hydrofoils. This provides a rather different picture from that with twin radial impellers. The highest void fraction again develops just above the plane of the uppermost impeller, whatever the operating temperature. The maximum void fraction is spectacular, approaching 50% at room temperature. Again, hot sparged conditions generate similar void fraction profiles, but over the entire reactor height the gas fraction is lower than at room temperature. The contribution of the middle impeller to gas retention
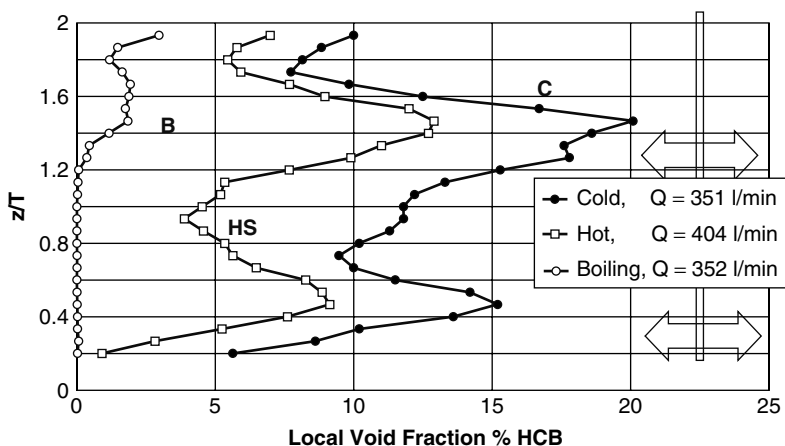

Figure 11-25 Void profiles in cold and hot sparged and boiling conditions with twin CD6 impellers. (Data from Smith et al., 2001a.)
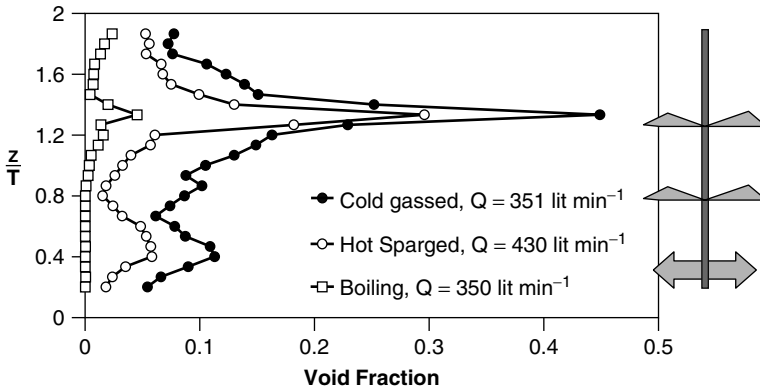
Figure 11-26 Void distribution with a multiple-impeller agitator (CD6 with two MaxfloW up-pumping hydrofoils). Note the high local void fraction just above the upper impeller.

is slight, but the effect on liquid circulation almost certainly remains important. Truly boiling conditions again have very low void fractions throughout the tank, with some evidence of vapor bubbles being released from the topmost impeller.

The very strong liquid circulation induced by the hydrofoils forces gas through the bottom (radial) impeller to the extent that the discharge from the impeller has a strong upward component. The conditions differ from the usual buoyancy-induced flooding in that the dispersing action of the impeller appears not to be badly affected. This combination with up-pumping hydrofoils is currently popular as a means of ensuring good top-to-bottom mixing in tall reactors. Again the large peak in void fraction is seen just above the level of the uppermost impeller. The profiles depend on temperature, with significantly less gas retained in a hot system and very few vapor bubbles being found below the liquid surface in boiling conditions.

11-6   GAS–LIQUID MASS TRANSFER

This section is concerned mainly with predicting or scaling-up the mass transfer rate between gas and liquid, in which the controlling factor is film diffusion on the liquid side of the interface, as described by the mass transfer coefficient, k_L. Ideally, perhaps, this should be done from a basis of predicting local bubble sizes and gas fractions, using perhaps CFD, but this is not established within the realms of process engineering. The traditional method is (as for gas fraction) to use empirical correlations for the mass transfer factor $k_L a$, and to use this in mass balance equations:

$$\text{overall transfer rate} = k_L a.V.(C^* - C_L)_{mean} \tag{11-18}$$

This has the advantage of not requiring knowledge of bubble sizes, but also has some inherent disadvantages which are set out later in this section. Evidently, it will also be necessary to use an appropriate value of the mean for $(C^* - C_L)$, which, as discussed in Section 11-3, will in general be between those for the ideal backmixed and plug flow cases. It should be noted that this is important also for the extraction of $k_L a$ values from laboratory concentration measurements and may not have been observed correctly in the derivation of some older correlations.

11-6.1 Agitated Vessels

The homogeneous region correlations for $k_L a$ (again like those for gas fraction) for the turbulent regime are best expressed in the form

$$k_L a = \alpha'' \left(\frac{P}{\rho V} \right)^{\beta''} (v_s)^{\gamma''} \tag{11-19}$$

where P includes shaft power and gas buoyancy power $[QHg\,(\rho_L - \rho_G)]$ but not gas kinetic energy (Middleton et al., 1994). Typical values for the air–water system at 20°C are $\alpha'' = 1.2$, $\beta'' = 0.7$, and $\gamma'' = 0.6$, with P in watts, V in m^3, v_s in m/s, $k_L a$ in s^{-1}, and α'' dimensioned appropriately (Middleton, 1997). However, it has been found (e.g., by Smith et al., 1977) that whereas the indices β'' and γ'' do not change with liquid type, impeller type, or scale, α'' is a strong function of liquid type and properties, the noncoalescing value being about twice that for coalescing systems. Thus such correlations can be used for scale-up purposes but not for general prediction. However, two concerns remain: one is the need for fractionally dimensioned constants, and the other is that [as shown in Smith et al. (1977)] the correlations are actually composed of smaller, very nonlinear curves, so should not be extrapolated outside their v_s range (in this case, 0.004 to 0.02 m/s). It should also be noted (also for gas fraction), especially for disk turbines, that $P/\rho V$ is itself a function of v_s, so the variables in the correlation are not independent. This may explain why the indices β'' and γ'' vary between workers and data sets even when the $k_L a$ values may be similar. It is therefore recommended to use only those correlations that cover the relevant ranges of $P/\rho V$ and v_s, and not to extrapolate.

For extension into transitional Reynolds numbers (range 100 to 10^6), Cooke et al. (1988) obtained

$$k_L a \propto \left(\frac{P}{\rho V} \right)^{0.5} (v_s)^{0.3} \mu_{app}^{-1} \tag{11-20}$$

to ±30% for aqueous suspensions of fibers and several combinations of impellers at scales of 20 to 60 L, with H = T, and with a different value of the constant, with H = 3T. The P term in these correlations includes the contribution of gas buoyancy $[Q_G Hg(\rho_L - \rho_G)]$.

Although it is commonly assumed that when agitation conditions are sufficiently intense for effective gas–liquid dispersion, the liquid mixedness will be

good. It is worth checking this, particularly for large vessels [noting that, on scaling up at constant $P/\rho V$ in the turbulent regime, N will decrease in proportion to $(\text{scale})^{-2/3}$ and mixing time with $1/N$]. If it turns out that mixing time is longer than mass transfer time (90% mass transfer time $= 2.3/k_L a$), preferably the liquid mixing should be improved; otherwise, a more complex design calculation with interlinked zones of different driving force (and even perhaps local values for $k_L a$) will be necessary.

Example 11-5: Impeller Size and Speed for Mass Transfer. Assume that 0.2 mol/s of gas A is to be absorbed into a coalescing type of aqueous solution of B in a baffled vessel of 2 m³ liquid capacity with a DIN torispherical base. What is the required design if 99% of gas A is to be absorbed and reacted?

The temperature θ is 300 K; the pressure at the sparger is 1.5 bar abs., and the inlet concentration of A in gas, y_{A0}, is 0.1 mol/mol. Henry's constant He $= 10^{-8}$ mol fr./Pa; molar volume of liquid $M_V = 50\,000$ g-mol/m³.

SOLUTION: Calculate the gas flow rate from the mass balance and absorption efficiency, η:

$$N_0 y_{A0}\eta = k_L a V(\Delta C)_{\text{mean}} = J$$

where N_0 is the inlet molar flow rate of gas and y_{A0} is the concentration of A at the inlet.

$$N_0 = \frac{J}{y_{A0}\eta} = \frac{0.2 \text{ mol/s}}{0.1 \times 0.99} = 2.0 \text{ mol/s}$$

$$P_0 Q_0 = N_0 R\theta \qquad \text{ideal gas law applied at the inlet}$$

$$Q_0 = \frac{N_0 R\theta}{P_0} = \frac{2.0 \text{ mol/s} \times 8.314 \text{ m}^3 \cdot \text{Pa/mol} \cdot \text{K} \times 300 \text{ K}}{152\,000 \text{ Pa}} = 0.0332 \text{ m}^3/\text{s}$$

Calculate the vessel dimensions for a DIN torispherical base, specifying that $H = T$:

$$H = T = \left(\frac{V}{0.7320}\right)^{1/3} = \left(\frac{2}{0.7320}\right)^{1/3} = 1.40 \text{ m}$$

Calculate the gas superficial velocity at the inlet:

$$v_{s0} = \frac{4Q_{G0}}{\pi T^2} = \frac{4 \times 0.033 \text{ m}^3/\text{s}}{\pi \times (1.40 \text{ m})^2} = 0.022 \text{ m/s}$$

Calculate the pressure at the surface. This is given approximately by

$$P_1 = P_0 - \rho g H = 152\,000 \text{ Pa} - 1000 \text{ kg/m}^3 \times 9.81 \text{ m/s}^2$$
$$\times 1.40 \text{ m} = 138\,000 \text{ Pa}$$

The partial pressure of the reactant at the base is given by

$$p_{A0} = y_{A0}P_0 = 0.1 \times 152\,000 = 15\,200 \text{ Pa}$$

The partial pressure of the reactant at the surface is given by:

$$p_{A1} = y_{A1}P_1 = 0.001 \times 138\,000 \text{ Pa} = 138 \text{ Pa}$$

The saturation concentrations of the reactant at the base and the surface are given by

$$x_{A0}^* = \text{He} \cdot p_{A0} = 1 \times 10^{-8} \times 15\,200 = 1.52 \times 10^{-4} \text{ mol A/mol liquid}$$
$$x_{A1}^* = \text{He} \cdot p_{A1} = 1 \times 10^{-8} \times 132 = 1.32 \times 10^{-6} \text{ mol A/mol liquid}$$

Calculate the mean concentration driving force. Assume that the reaction is rapid such that the concentration of A in the bulk liquid phase is approximately zero. Assume also that the gas recirculation ratio α is low, approaching plug flow.

$$(\Delta C)'_{mean} = \frac{\Delta C_0 - \Delta C_1}{\ln(\Delta C_0/\Delta C_1)} = \frac{(1.52 \times 10^{-4} - 0) - (1.38 \times 10^{-6} - 0)}{\ln[(1.52 \times 10^{-4} - 0)/(1.38 \times 10^{-6} - 0)]}$$
$$= 3.20 \times 10^{-5} \text{ mol A/mol liquid}$$

Converting units yields

$$(\Delta C)_{mean} = (\Delta C)'_{mean} \times M_V = 3.20 \times 10^{-5} \times 50\,000 = 1.60 \text{ mol/m}^3$$

Calculate the mass transfer coefficient required:

$$k_L a V(\Delta C)_{mean} = J$$
$$k_L a = \frac{J}{V(\Delta C)_{mean}} = \frac{0.2 \text{ mol/s}}{2 \text{ m}^3 \times 1.60 \text{ mol/m}^3} = 0.063 \text{ s}^{-1}$$

To calculate the shaft power required; the correlation chosen for $k_L a$ is

$$k_L a = 1.2 \left(\frac{P}{\rho V}\right)^{0.7} (v_s)^{0.6}$$

(Note that preferably the constant in the $k_L a$ correlation is confirmed from the results of semitech scale tests.) Therefore;

$$\frac{P}{\rho V} = \left[\frac{k_L a}{1.2(v_s)^{0.6}}\right]^{1/0.7} = 0.39 \text{ W/kg}$$

The shaft power required will therefore be

$$P = 780 \text{ W}$$

$$P = \text{Po} \cdot \text{RPD} \cdot \rho N^3 D^5$$

Specify a BT-6 impeller with a ring sparger (Po $= 2$), with D $= 0.4$, T $= 0.56$ m. Assume that RPD is approximately 0.9 (this will be checked later). The required impeller speed is therefore

$$N = 2.0 \text{ s}^{-1}$$

Calculate the Reynolds number:

$$\text{Re} = \frac{\rho N D^2}{\mu} = \frac{1000 \times 2.0 \times 0.56^2}{10^{-3}} = 6.3 \times 10^5$$

confirming that the impeller flow is turbulent. Confirm the value of RPD:

$$\text{gas flow number Fl}_G = \frac{Q_G}{ND^3} = \frac{0.0332}{2.0 \times 0.56^3} = 0.094$$

Hence RPD $= 0.9$ is correct (see Table 11-4).

Confirm the estimated gas recirculation ratio α: If the impeller had been a Rushton disk turbine, the correlation of Section 11-6.1 would have applied, giving a value of 0.14 for α, confirming the approximation to plug flow of the gas assumed above. No correlation is available for the BT6 impeller, but the flow pattern is similar.

11-6.2   In-line Mixers

With static mixers in the turbulent regime, scale-up can be made using a correlation of almost the same form as that for vessels:

$$k_L a = \alpha''' \left(\frac{P}{\rho V} \right)^{\beta'''} (v_s)^{\gamma'''} \tag{11-21}$$

and $\beta''' = 0.42$ and $\gamma''' = 0.42$ have been found to fit data for coalescing and non-coalescing liquids for several mixer types and scales [in agreement with Holmes and Chen (1981)]. For air–water systems at 20°C, a value for α''' of 0.38 is obtained (with P in watts, V in m^3, $k_L a$ in s^{-1}): however, α''' seems to vary slightly with liquid and mixer type and possibly scale, so fitting it from small scale tests (during process development) with the actual process fluids is advised. Note that $k_L a$ values are very high and that except for the fastest reactions, it can usually be assumed that equilibrium is achieved with a few elements.

## 11-6.3   Gas–Liquid Mass Transfer with Reaction[3]

When the reaction rate is comparable to that of the mass transfer through the diffusion film, interactions must be taken into account. The interactions can be delineated as five regimes, as shown in Figure 11-27. These are identified by the

REGIME	CONDITIONS	IMPORTANT VARIABLES	CONCENTRATION PROFILES
I *Kinetic control* Slow reaction	$\sqrt{\dfrac{t_D}{t_R}} < 0.02$	Rate α ϵ_L α k_{nm} α $(C_{AL}^*)^n$ α $(C_{BL})^m$ Independent of a (if a adequate) Independent of k_L	LIQUID, FILM, BULK, GAS; C_{AL}^*, C_{BL}, C_{AL}
II *Diffusion control* Moderately fast reaction in bulk of liquid $C_{AL} \approx 0$	$0.02 < \sqrt{\dfrac{t_D}{t_R}} < 2$ Design so that $\dfrac{\epsilon_L}{a} > 100 \dfrac{D_{AL}}{k_L}$	Rate α a α k_L α C_{AL}^* Independent of k_{nm} Independent of ϵ_L (if ϵ_L adequate)	C_{AL}^*, C_{BL}, C_{AL}
III *Fast reaction* Reaction in film $C_{AL} \approx 0$ (pseudo first order in A′)	$2 < \sqrt{\dfrac{t_D}{t_R}} < \dfrac{C_{BL}}{qC_{AL}^*}$ $C_{BL} \gg C_{AL}^*$	Rate α a α $\sqrt{k_{nm}}$ α $(C_{AL}^*)^{(n+1)/2}$ Independent of k_L Independent of ϵ_L	C_{BL}, C_{AL}^*, C_{AL}
IV *Very fast reaction* General case of III	$2 < \sqrt{\dfrac{t_D}{t_R}}$ $C_{BL} \sim C_{AL}^*$	Rate α a depends on k_L, k_{nm}, C_{AL}^*, C_{BL} Independent of ϵ_L	C_{AL}^*, C_{BL}, C_{AL}
V *Instantaneous reaction* Reaction 'at interface'. Controlled by transfer of B to interface from bulk. $J \alpha k_L a$	$\sqrt{\dfrac{t_D}{t_R}} \gg \dfrac{C_{BL}}{qC_{AL}^*}$	Rate α a α k_L Independent of C_{AL}^* Independent of k_{nm} Independent of ϵ_L	C_{BL}, C_{AL}^*, C_{AL}

Figure 11-27   Regimes of gas–liquid mass transfer with reaction. (From Middleton, 1997; reproduced by permission of Butterworth-Heinemann.)

[3] This material is taken from Middleton (1997) by permission of Butterworth-Heinemann.

value of the *Hatta number*, Ha, which is defined as the square root of the ratio of the diffusion time, t_D, to the reaction time, t_R. For a reaction of the type

$$nA + mB \rightarrow products$$
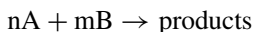
these are defined as follows:

$$t_D = \frac{D_{AB}}{k_L^2} \tag{11-22}$$

$$t_R = \frac{n+1}{2k_{mn}C_{LA}^{n-1}C_{LB}^m} \tag{11-23}$$

For regimes III and IV the reaction effectively enhances the mass transfer rate, and an "enhanced" effective value of k_L is often used, defined as k_L^*:

$$k_L^* = \left[\frac{2D_{AB}k_{nm}(C_{LA}^* - C_{LA})^{n-1}C_{LB}^m}{n+1} \right]^{0.5} \tag{11-24}$$

Note that this is now a function of the reaction rate, not the hydrodynamics. If heat of reaction is significant, this expression must be modified to allow for the effects of local temperature on gas solubility and reaction rate (Mann and Moyes, 1977).

The regime dictates the choice of reactor. From Figure 11-27, the following choice of equipment for each regime can be inferred:

- *Regime I:* reaction in bulk, modest $k_L a$: bubble column
- *Regimes II, IV, and V:* high a and $k_L a$: stirred vessel
- *Regime III:* all reaction in film, high a: thin-film reactor (packed column or spinning disk)

It should also be noted that as the reaction rate increases, it becomes more likely that the gas-side resistance will become important, so this should be checked if the gas phase is multicomponent.

11-7   BUBBLE SIZE

The apparent success of $P/\rho V$ as a correlating parameter for ϕ and $k_L a$ in the turbulent regime implies that it is strongly linked to bubble size as well as to liquid circulation. Indeed, $P/\rho V$ can be equated to the vessel-average value of ε, the turbulent energy dissipation rate at the smallest scales of turbulence, if it is assumed (classically) that all the power eventually dissipates at these scales. Several workers have postulated that bubble breakup occurs (finally) by impact of turbulent eddies at this smallest (Kolmogorov) scale, presumably via pressure fluctuations distorting the bubble sufficiently to disrupt it. Hinze (1979)

balanced this external force with the restoring surface tension to obtain a critical Weber number ($We = \tau d/\sigma$) above which breakup will occur, with for turbulent breakup, $\tau = 2\rho(\varepsilon d)^{2/3}$; thus, d is the maximum bubble size to survive. There are, however, some conceptual problems with applying this. First, breakup occurs only in the regions of highest stress (in the impeller vortices of an agitated vessel or the wall shear layers in static mixers), and the ratio of maximum to mean ε (i.e., $P/\rho V$) differs between impeller types, but the same correlations for $k_L a$ apply to different impeller types. Second, the Kolmogorov scale of turbulence in the discharge of typical impellers ($\varepsilon \approx 10$ W/kg) is $(\nu^3/\varepsilon)^{1/4} \approx 0.02$ mm, which is considerably smaller than the final bubble size, so a mechanism whereby sufficiently large bubble distortions are produced by this mechanism, and for sufficiently long time scales for breakup to occur, is difficult to imagine. Breakup has been observed to occur only in the blade and blade vortex region, and several possible mechanisms have been postulated [see, e.g., Kumar et al. (1991) for liquid droplets] involving bubble (or drop) stretching by shear and elongational flows. Rationalization of the correlations cited above with these observations is still awaited. The bimodal bubble size distributions found in the heterogeneous regime also await fundamental explanation.

11-8   CONSEQUENCES OF SCALE-UP

It is evident that having made a choice of scale-up relationship, other factors will be affected in different ways; there is often no way to scale up all the significant factors together, so priorities have to be chosen. An example of this is given in Middleton (1997), to which reference should be made for full details. A summary is given here.

In the example a gas–liquid reaction with particulate solids (e.g., a catalyst) operating in regime II in a stirred reactor with a Rushton turbine is to be scaled up. The primary process requirement is for the same degree of reaction conversion at each scale, which means the same number of moles of gas transferred per mole of liquid fed:

$$\frac{k_L aV(C_A^* - C_A)}{C_{LBfeed}Q_L} = \text{constant} \tag{11-25}$$

Assume for simplicity that $C_A = 0$ (a good approximation for regime II) and that the degree of gas backmixing is the same at all scales (this should be checked at the end of the calculation and reiterations performed if necessary). Given a constant feed concentration at all scales,

$$k_L aVC_L \propto Q_L \tag{11-26}$$

Sometimes it is necessary for the outlet gas concentration to be constant (e.g., with hazardous gases); then from the mass balance this becomes

$$k_L aV \propto Q_G \tag{11-27}$$

Substituting a suitable correlation for $k_L a$, for example

$$k_L a \propto \left(\frac{P}{V}\right)^{0.7} (v_S)^{0.6} \tag{11-28}$$

and a curve fit for the gassed power curve, such as

$$P = N^{3.3} D^{6.3} Q_G^{-0.4} \qquad \text{(not necessarily reliable!)} \tag{11-29}$$

an expression such as

$$N^{3.4} T^{6.0} \propto Q_L \tag{11-30}$$

results.

Another constraint will then fix the design. In this example maintaining $N > N_{JS}$ for the suspension of the catalyst particles is important, so $NT^{0.76} =$ constant could be added (although not strictly applicable to gassed systems), giving

$$Q_G \propto Q_L \propto T^{3.4} \tag{11-31}$$

This scale-up method has the effects, on increasing the scale, of:

- Increasing v_S, so foaming and entrainment become more likely
- Decreasing P/V
- Decreasing the heat transfer flux per unit throughput
- Nearer approach to poor gas dispersion
- Longer liquid mixing time

NOMENCLATURE

a	gas–liquid interfacial area per unit volume of liquid (m^2/m^3)
c	constant in eq. (11-1)
C	off-bottom clearance of impeller (m)
C_L	saturation concentration of solute gas in bulk liquid (mol/m^3)
C^*	concentration of solute gas in liquid at interface (mol/m^3)
C_{ag}	agitation cavitation number, eq. (11-11)
d	surface mean bubble size (m)
D	impeller diameter (m)
D_{AB}	molecular diffusivity of A in B (m^2/s)
Fl_G	gas flow number, Q_G/ND^3 (–)
Fr	Froude number, $N^2 D/g$ (–)
H	liquid height (m)
J	gas flux (mol/s)
k_L	mass transfer coefficient (m^2/s)
N	impeller speed (rps)
N_{js}	just suspended speed for solids suspension (rps)
P	power draw (W)
P_G	gassed power draw (W)

P_U ungassed power draw (W)
Po   power number $(-)$
q   mass transfer enhancement coefficient due to reaction $(-)$
Q_L liquid volumetric flowrate (m^3/s)
Q_G mean gas volumetric flowrate (m^3/s)
RPD   relative power demand, P_G/P_U $(-)$
S   submergence of the impeller below the liquid surface (m)
S_m Smith number $2gS/v_t^2$
t_D diffusion time (s)
t_M mixing time (s)
t_R reaction time (s)
T   vessel diameter (m)
U   superficial velocity (m/s)
v_s gas superficial velocity (m/s)
v_t impeller tip speed (m/s)
V   volume of liquid (m^3)
W   blade width (m)
We   Weber number $\tau d/\sigma$ $(-)$

Greek Symbols

α gas recirculation ratio $(-)$
ε turbulent energy dissipation rate (m^2/s^3)
ε_L liquid hold-up $(-)$
ϕ gas volume fraction
μ viscosity (kg/ms)
μ_{APP} apparent viscosity (kg/ms)
ν kinematic viscosity (m^2/s)
θ absolute temperature (K)
ρ density (kg/m^3)
σ surface tension (N/m)
τ local shear stress (N/m^2)

REFERENCES

Bin, A. K., and J. M. Smith (1982). Mass transfer in a plunging jet absorber, *Chem. Eng. Commun.*, **15**, 367–383.

Breber, G. (1986). The decrease in power number of impellers due to cavitation phenomena, *Paper 77c*. AIChE Meeting, Miami Beach, FL.

Bruijn, W., K. van't Riet, and J. M. Smith (1974). Power consumption with aerated Rushton turbines, *Trans. Inst. Chem. Eng.*, **52**, 88–104.

Bujalski, W., A. W. Nienow, S. Chatwin, and M. Cooke (1987). The effect of scale on power number for Rushton disc turbines, *Chem. Eng. Sci.*, **42**, 317–326.

Chapman, C. M., A. W. Nienow, J. C. Middleton, and M. Cooke (1983). Particle–gas–liquid mixing in stirred vessels, *Chem. Eng. Res. Des. (Trans. Inst. Chem. Eng. A)*, **61**, 71–82, 167–182.

Cooke, M., J. C. Middleton, and J. R. Bush (1988). Mixing and mass transfer in filamentous fermentations, *Paper B1*, *Proc. 2nd International Conference on Bioreactors*, pp. 37–64.

Deckwer, W.-D. (1992). *Bubble Column Reactors*, Wiley, Chichester, West Sussex, England.

Gao, Z., J. M. Smith, D. Zhao, and H. Müller-Steinhagen (2000). Void fraction and mixing in sparged and boiling reactors, *Proc. 10th European Mixing Conference*, Delft, The Netherlands, Elsevier, Amsterdam, pp. 213–220.

Gao, Z., J. M. Smith, and H. Müller-Steinhagen (2001). The effect of temperature on the void fraction in gas–liquid reactors, *Proc. 5th Symposium on Gas–Liquid–Solid Systems*, Melbourne, Australia.

Gezork, K. M., W. Bujalski, M. Cooke, and A. W. Nienow (2000). The transition from homogeneous to heterogeneous flow in a gassed stirred vessel, *Chem. Eng. Res. Des. (Trans. Inst. Chem. Eng. A)*, **78A**, 363–370.

Gezork, K. M., W. Bujalski, M. Cooke, and A. W. Nienow (2001). Mass transfer and hold-up characteristics in a gassed, stirred vessel at intensified operating conditions, *Proc. ISMIP4*, Toulouse, France [submitted to *Chem. Eng. Res. Des. (Trans. Inst. Chem. Eng. A)*].

Hari-Prajitno, H., V. I. Mishra, K. Takemaka, W. Bujalski, A. W. Nienow, and J. McKemmie (1998). Gas–liquid mixing studies with multiple up and down pumping hydrofoil impellers: power characteristics and mixing times, *Can. J. Chem. Eng.*, **76**, 1056–1068.

Hinze, J. O. (1979). *Turbulence*, McGraw-Hill, New York.

Holmes, T. L., and T. L. Chen (1981). Gas–liquid contacting with horizontal static mixing systems, presented at the AIChE Annual Meeting, New Orleans, LA.

Kumar, S., R. Kumar, and K. S. Gandhi (1991). Alternative mechanisms of drop breakage in stirred vessels, *Chem. Eng. Sci.*, **46**, 2483–2489.

Lockhart, R. W., and R. C. Martinelli (1944). Proposed correlation of data for isothermal two phase, two component flow in pipes, *Chem. Eng. Prog.*, **45**, 39–48.

Mann, R., and M. Moyes (1977). Exothermic gas absorption with chemical reaction, *AIChE J.*, **23**, 17–23.

Metzner, A. B., and R. E. Otto (1957). Agitation of non-Newtonian fluids, *AIChE J.*, **3**, 3–10.

Michel, B. J., and S. A. Miller (1962). Power requirements of gas–liquid agitated systems, *AIChE J.*, **8**, 264–266.

Middleton, J. C. (1978). Motionless mixers as gas–liquid contacting devices, *Paper 74e*, presented at the AIChE Annual Meeting, Miami Beach, FL.

Middleton, J. C. (1997). Gas–liquid dispersion and mixing, in *Mixing in the Process Industries*, N. Harnby, A. W. Nienow, and M. F. Edwards, eds., Butterworth—Heinemann, Oxford.

Middleton, J. C., M. Cooke, and L. Litherland (1994). The role of kinetic energy in gas–liquid dispersion, *Proc. 8th European Mixing Conference*, *Inst. Chem. Eng. Symp. Ser.*, **136**, 595–602.

Montante, G., K. C. Lee, A. Brucato, and M. Yianneskis (2001). Numerical simulations of the dependency of flow pattern on impeller clearance in stirred vessels, *Chem. Eng. Sci.*, **56**, 3751–3770.

Nagel, O., H. Kuerten, and B. Hegner (1973). The interfacial area in gas–liquid contact apparatus, *Chem. Ing. Tech.*, **45**, 913–920.

Nienow, A. W., D. J. Wisdom, and J. C. Middleton (1977). The effect of scale and geometry on flooding, recirculation and power in gassed stirred vessels, *Proc. 2nd European Mixing Conference*, Cambridge, pp. 17–34.

Nienow, A. W., M. Konno, and W. Bujalski (1986). Studies on three phase mixing: a review and recent results, *Chem. Eng. Res. Des. (Trans. Inst. Chem. Eng. A)*, **64**, 35–42.

Schaper, R., A. B. de Haan, and J. M. Smith (2002). Temperature effects on the hold-up in agitated vessels, *Chem. Eng. Res. Des. (Trans. Inst. Chem. Eng. A*, **80**, 887–892.

Skelland, A. H. P. (1967). *Non-Newtonian Flow and Heat Transfer*, Wiley, New York.

Smith, J. M., and A. Katsanevakis (1993). Impeller power demand in mechanically agitated boiling systems, *Chem. Eng. Res. Des. (Trans. Inst. Chem. Eng. A)*, **71A**, 145–152, 466.

Smith, J. M., and C. A. Millington (1996). Boil-off and power demand in gas–liquid reactors, *Chem. Eng. Res. Des. (Trans. Inst. Chem. Eng. A)*, **74A**, 424–430.

Smith, J. M., and L. Smit (1988). Impeller hydrodynamics in boiling reactors, *Proc. 6th European Conference on Mixing*, Pavia, ltaly, pp. 297–304.

Smith, J. M., and K. Tarry (1994). Impeller power demand in boiling solutions, *Chem. Eng. Res. Des. (Trans. Inst. Chem. Eng. A)*, **72A**, 739–740.

Smith, J. M., and D. G. F. Verbeek (1988). Impeller cavity development in nearly boiling liquids, *Trans. Inst. Chem. Eng.*, **66**, 39–46.

Smith, J. M., K. van't Riet, and J. C. Middleton (1977). Scale up of agitated gas–liquid reactors for mass transfer, *Proc. 2nd European Conference on Mixing*, pp. F4-51 to F4-66.

Smith, J. M., M. M. C. G. Warmoeskerken, and E. Zeef (1987). Flow conditions in vessels dispersing gases in liquids with multiple impellers, in *Biotechnology Processes*, C. S. Ho and J. Y. Oldshue, eds., AIChE, New York, pp. 107–115.

Smith, J. M., Z. Gao, and J. C. Middleton (2001a). The unsparged power demand of modern gas dispersing impellers in boiling liquids, *Chem. Eng. J.*, **84**, 15–22.

Smith, J. M., Z. Gao, and H. Müller-Steinhagen (2001b). Void fraction distributions in sparged and boiling reactors with modern impeller configurations, *Chem. Eng. Process.*, **40**, 489–497.

Van de Sande, E., and J. M. Smith (1973). Surface entertainment of air by high velocity water jets, *Chem. Eng. Sci.*, **28**, 1161–1168.

Van de Sande, E., and J. M. Smith (1974). Mass transfer with plunging water jets, in *Multi-phase Flow Systems, Inst. Chem. Eng. Symp. Ser.*, **38**(J3), 1–11.

Van't Riet, K. (1976). Turbine agitator hydrodynamics and dispersion performance, Ph.D. dissertation, University of Delft, The Netherlands.

Warmoeskerken, M. M. C. G., and J. M. Smith (1982). Description of the power curves of turbine stirred gas dispersions, *Proc. 4th European Conference on Mixing*, Noordwijkerhout, The Netherlands, pp. 237–246.

Warmoeskerken, M. M. C. G., and J. M. Smith (1986). Flow regime maps for Rushton turbines, *Paper W-624*, presented at the 3rd World Congress of Chemical Engineering, Tokyo.

Warmoeskerken, M. M. C. G., and J. M. Smith (1989). Hollow blade turbine impellers for gas dispersion and mass transfer, *Chem. Eng. Res. Des. (Trans. Inst. Chem. Eng. A)*, **67A**, 193–198.

Warmoeskerken, M. M. C. G., J. Speur, and J. M. Smith (1984). Gas–liquid dispersion with pitched blade turbines, *Chem. Eng. Commun.*, **25**, 11–29.

Zhao, D., Z. Gao, H. Müller-Steinhagen, and J. M. Smith (2001). Liquid-phase mixing times in sparged and boiling agitated reactors with high gas loading, *Ind. Eng. Chem. Res.*, **40**, 1482–1497.

Zlokarnik, M. (1979). Sorption characteristics of slot injectors and their dependency on the coalescence behaviour of the system, *Chem. Eng. Sci.*, **34**, 1265–1271.

Zuber, N., and J. A. Findlay (1965). Average volumetric concentration in two-phase flow systems, *J. Heat Transfer ASME*, **87C**, 453–468.

Immiscible Liquid–Liquid Systems

DOUGLAS E. LENG

Leng Associates

RICHARD V. CALABRESE

University of Maryland

12-1 INTRODUCTION

12-1.1 Definition of Liquid–Liquid Systems

In this chapter we describe the use of agitated vessels and other equipment to create immiscible liquid–liquid dispersions. The primary purpose is to help the reader become acquainted with the physical and interfacial phenomena involved with coalescence and dispersion, and how to use these phenomena in practice. The goal is to predict mean drop size and drop size distribution for a given design, set of properties, and operating conditions. The subject matter is complex, often failing to predict accurate information. Unforeseen impurities, interfacial "scum," phase inversions, and poorly defined objectives complicate reliable predictions for the practitioner.

The term *immiscible liquid–liquid system* refers to two or more mutually insoluble liquids present as separate phases. These phases are referred to as the *dispersed* or *drop phase* and the *continuous* or *matrix phase* and are given subscripts of d and c, respectively. The dispersed phase is usually smaller in volume than the continuous phase, but under certain highly formulated conditions, it can represent up to 99% of the total volume of the system. Immiscible liquid–liquid systems can also contain additional liquid, solid, or gas phases.

Agitation plays a controlling role in the liquid–liquid systems considered herein. It controls the breakup of drops, referred to as *dispersion*; the combining of drops, known as *coalescence*; and the suspension of drops within the

system. The magnitude and direction of convective flows produced by an agitator affect distribution and uniformity throughout the vessel as well as the kinetics of dispersion. Agitation intensity is also important. Intense turbulence found near the impeller leads to drop dispersion, not coalescence. Lower turbulence or laminar/transitional conditions found elsewhere in the vessel promote coalescence by enabling drops to remain in contact long enough for them to coalesce. Laminar shear also leads to drop dispersion. If a drop is stretched beyond the point of critical elongation, it breaks. If not, it returns to its prestressed state as it enters a more quiescent region.

12-1.2   Practical Relevance

12-1.2.1   Industrial Applications.   Immiscible liquid–liquid systems are found extensively throughout the chemical, petroleum, and pharmaceutical industries. The rate of chemical reactions is often mass transfer controlled and affected by interfacial area. Examples include nitration, sulfonation, alkylation, hydrogenation, and halogenation. For example, the nitration of aromatic compounds involves use of a continuous phase of concentrated mixed acids ($HNO_3 + H_2SO_4$) and a dispersed organic phase to be nitrated. Dispersion, coalescence, and suspension are all involved, along with heat and mass transfer. The nitronium ion from the continuous phase is transported to the drop surface, where reaction occurs. Water, a by-product of the reaction, transfers to the continuous phase. Nitration reactions are exothermic, and reaction rates and temperatures are controlled by interfacial area, created by agitation. Failure to suspend drops adequately can lead to catastrophic results, as described in Section 12-9.

The petroleum industry depends on efficient coalescence processing to remove aqueous brine drops in crude refinery feed streams to prevent severe corrosion of processing equipment. Control of mean drop size and drop size distribution (DSD) is vital to emulsification and suspension polymerization applications. Extraction processes depend on repeated drop coalescence and dispersion to accomplish the required mass transfer.

Coalescence, dispersion, and suspension phenomena are complex and scale dependent. Nevertheless, some industrial processes can be simplified, as suggested in Table 12-3, if they are either noncoalescing or slowly coalescing. This simplifies design and scale-up. Coalescence can usually be neglected, for practical purposes, in applications where the volume fraction of dispersed phase, $\phi \leq 0.1$. This is particularly true if surfactants and/or interfacial contaminants are present.

12-1.2.2   Design Scope. Stirred vessels, rotor–stator mixers, static mixers, decanters, settlers, centrifuges, homogenizers, extraction columns, and electrostatic coalescers are examples of industrial process equipment used to contact liquid–liquid systems. Although this chapter emphasizes stirred vessels, the fundamentals of phase behavior are applicable to a broad range of other equipment types. Immiscible liquid–liquid systems are processed in batch, continuous, and semicontinuous modes.

In the case of stirred vessels, the resulting mean drop size and drop size distribution depend on the selection, placement, and operational speed of the agitator. Excessive speed leads to hard-to-separate emulsions. Inadequate speed can cause phase separation. Coalescence and dispersion are both fluid motion-dependent rate processes. Drop sizes depend on flow, shear, turbulence, and dispersion time as well as on physical and interfacial system properties.

12-1.3 Fundamentals

An agitated liquid–liquid process involves many simultaneous, interdependent phenomena, such as dispersion, coalescence, suspension, heat and mass transfer, and chemical reaction. Previously described nitration requires control of the interfacial area rather than specific drop size, but some processes require precise control of drop size. For example, equipment for suspension polymerization processes must be capable of producing uniform beads of specified size range as well as providing for heat transfer and drop suspension.

Flow patterns and turbulence in stirred vessels are complex phenomena that can often be better appreciated using modern tools such as laser Doppler velocimetry (LDV), particle image velocimetry (PIV), and computational fluid dynamics (CFD). All show turbulence consisting of high-energy eddies near the impeller, and lower-energy eddies located farther away. Turbulence intensities near the impeller can be ≈40 times greater than the mean for the entire vessel. Turbulence intensities are very low in regions close to the wall and at the top and bottom of the vessel. Flow patterns are sensitive to impeller geometry, the number of impellers, and their position in the vessel. The reader is referred to Chapters 2 and 6 for more detail. Since drop size depends on flow-dependent dispersion and coalescence phenomena, it can be concluded that certain regions of the vessel are dominated by dispersion while others are dominated by coalescence. When a drop is contained within a larger eddy, it rotates within that eddy and does not break up. However, if it encounters an eddy of its size or smaller, it can be deformed and dispersed. When drops suspended in gentle flows collide, they often remain in contact long enough to coalesce.

12-1.3.1 Breakup, Coalescence, and Phase Inversion. Drop deformation is caused by mechanical forces induced by the surrounding fluid and is resisted by surface and internal viscous forces. Drop breakage occurs when fluid forces exceed the combined resistance force. Figure 12-1 shows different types of drop deformation due to different disruptive forces. Impact drop collisions (walls, impeller blades, and baffles) lead to lenticular deformation, uniform shear leads to cigar-shaped deformation, and turbulent conditions lead to bulgy deformation. It is common practice to refer to all fluid dynamical forces that cause drop deformation as *shear forces* regardless of the controlling mechanisms. These include shear and extension in laminar flow, and pressure fluctuations in turbulent flow.

An elongated drop does not necessarily break. In simple shear flows, differences in surface drag establish an internal rotation or circulation within the drop that helps stabilize it. This circulation does not develop for the case of bulgy deformation.
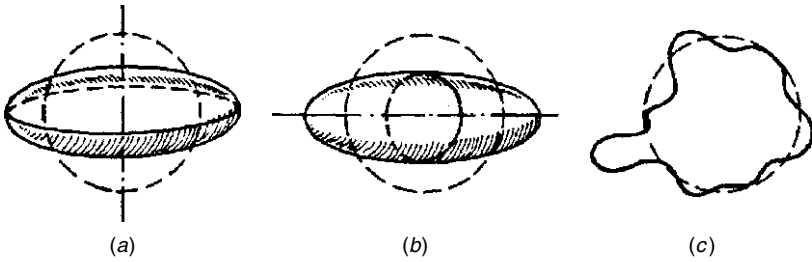
Figure 12-1   Basic types of globule deformation: (*a*) lenticular; (*b*) cigar-shaped; (*c*) bulgy. (Reproduced from Hinze, 1955.)

Surface forces due to interfacial tension attempt to minimize surface area by forcing the elongated drop to return to its original spherical shape. Breakage does not occur unless a critical deformation is reached during stretching. The drop either breaks or reverts to a condition of lower deformation as it passes to a region of lower shear rate. Dispersion also occurs by collisions with solid surfaces such as impeller blades, baffles, and vessel walls. Impeller selection and tank geometry are important in preventing this undesirable, uncontrolled form of dispersion. Fluid shear forces are mostly responsible for drop dispersion in stirred tanks, but impingement can be important in static mixers and rotor-stator machines. This topic is discussed in Section 12-2.

Coalescence is the combining of two or more drops, or a drop with a coalesced layer. The two-step process involves collision followed by film drainage. The drainage step depends on the magnitude and duration of the force acting on the drop(s), to squeeze out the separating film to a critical thickness, believed to be in the range ≈ 50 Å. In the case of a drop coalescing to a settled layer, the force is gravitational. The rate of film thinning also depends on the interfacial tension and the viscosity of the phases. Collision frequency depends on both agitation rate and the volume fraction of the dispersed phase. Not all collisions result in coalescence. If the contact is of short duration, critical thickness is not reached during contact, and the drops separate. The coalescence rate is the product of the collision rate and the coalescence efficiency. The mobility of the liquid–liquid interface also affects the film drainage rate. Clean, mobile interfaces promote efficient film drainage and lead to higher coalescence probability. As drops collide, a flattened disk forms at the leading drop surfaces. The diameter of this disk is important. If the system has a low interfacial tension, a large disk forms and more continuous phase fluid is trapped. This increases the task of drainage and reduces coalescence probability. A viscous continuous phase lowers drainage rates and therefore coalescence probabilities. Coalescence probabilities have been correlated in terms of the ratio of the contact time to drainage time. Section 12-3 deals with this subject quantitatively.

Phase inversion is the transitioning of water dispersed in oil (w/o) to oil dispersed in water (o/w), or vice versa. It can occur in more concentrated systems as a result of changes in stabilization, physical properties, or phase proportions.

For example, if chemical changes result in one phase becoming more viscous, that phase will tend to become the continuous phase. If this phase was originally the continuous phase, no inversion occurs, but if it was the dispersed phase, inversion is likely to occur. This phenomenon is discussed in Section 12-5.

The initial dispersion of two settled layers can create either (o/w) or (w/o) systems, often both temporarily. This is shown in Figure 12-34. However, the continued addition of one phase normally makes that phase the continuous phase. Surface-active materials also influence which phase ultimately becomes the dispersed phase.

12-1.3.2 Terms Used to Represent Mean Drop Size and Drop Size Distribution.

The following expressions describe the common drop size notation used in this chapter. The volume fraction of dispersed phase is ϕ, the total interfacial area per unit volume of mixed phases is a_v, and d_{max} is the maximum drop size. The Sauter mean diameter, d_{32}, is defined by

$$d_{32} = \frac{\sum_{i=1}^{i=m} n_i d_i^3}{\sum_{i=1}^{i=m} n_i d_i^2} \tag{12-1}$$

where m is the number of size classes describing the DSD, n_i the number of drops, and d_i the nominal diameter of drops in size class i. The subscripts indicate that d_{32} is formed from the ratio of the third to second moments of the DSD.

The mean diameter of choice is often d_{32}, since it is directly related to ϕ and a_v by

$$d_{32} = \frac{6\phi}{a_v} \tag{12-2}$$

Another commonly used mean drop diameter is the mass mean diameter where d_{43} is the ratio of the fourth to third moments of the DSD. Since drop mass is proportional to the cube of diameter, eq. (12-3) represents a mass-weighted average.

$$d_{43} = \frac{\sum_{i=1}^{i=m} n_i d_i^4}{\sum_{i=1}^{i=m} n_i d_i^3} \tag{12-3}$$

The number mean diameter is given by

$$d_n = \frac{\sum_{i=1}^{i=m} n_i d_i}{\sum_{i=1}^{i=m} n_i} \tag{12-4}$$

For consistency, the number mean diameter should be referred to as d_{10}, since it represents the ratio of the first to zero moments of the DSD. Although eq. (12-4) is the most common statistical definition of the mean, it is seldom used in the analysis of liquid–liquid dispersions since it provides little useful practical information.

We define d_{10} as 10% by volume of all drops smaller than d_{10}, d_{50} is defined as 50% by volume of all drops smaller than d_{50}, and d_{90} as 90% by volume of all drops smaller than d_{90}. These drop diameters are determined from plots of size

distribution data in terms of the cumulative volume frequency, defined below. In practice, d_{50} and d_{32} are close in value and are often used interchangeably. Overall mass transfer coefficients are commonly reported as $k_m a_v$ where k_m is the mass transfer coefficient and a_v is the interfacial area per unit volume, defined by eq. (12-2).

Drop sizes depend on many factors that are discussed throughout this chapter. For any given system, drop sizes are never uniform; rather, they exist in a continuous size spectrum. The large end of the drop size spectrum is controlled by agitation intensity, and the small end by the physics of drop breakage events. The DSD is sometimes bimodal or trimodal. Multimodal distributions are usually a result of multiple breakage mechanisms and unusual breakage patterns, such as those that result when viscous and/or viscoelastic drops are dispersed. Certain coalescence events can also lead to bimodal drop size distributions.

The DSD is usually represented in a discrete or histogram form in terms of number frequency, $f_n(d_i)$, or volume frequency, $f_v(d_i)$, given by

$$f_n(d_i) = \frac{n_i}{\sum_{j=1}^{m} n_j} \quad \text{and} \quad f_v(d_i) = \frac{n_i d_i^3}{\sum_{j=1}^{m} n_j d_j^3} \tag{12-5}$$

The DSD can also be described in a continuous or cumulative form (e.g., fraction up to size d). The cumulative number frequency $F_n(d_k)$, is defined by

$$F_n(d_k) = \frac{\sum_{i=1}^{k} n_i d_i}{\sum_{j=1}^{m} n_j d_j} = \int_0^{d_k} P_n(d') \, d \, d' \tag{12-6}$$

where d_k is the size of drops in the kth size class, d' is a dummy variable of integration, and $P_n(d)$, a continuous function, is the number probability density for drops of diameter d. The discrete and continuous distribution functions are related by $f_n(d_i) = P_n(d_i)\Delta d_i$, where d_i is the nominal diameter and Δd_i is the bin width for size class i.

An industrially important quantity is the cumulative volume frequency $F_v(d_k)$. For example, it relates to the yield of suspension polymerization products as defined by product specifications. It is defined by

$$F_v(d_k) = \frac{\sum_{i=1}^{k} n_i d_i^3}{\sum_{j=1}^{m} n_j d_j^3} = \int_0^{d_k} P_v(d') \, d \, d' \tag{12-7}$$

where $P_v(d)$ is the volume probability density function and $f_v(d_i) = P_v(d_i)\Delta d_i$.

Cumulative drop size distributions can be plotted conveniently on linear or log probability paper. A straight line on linear or normal probability paper means that the drop sizes follow a *normal* or *Gaussian distribution*. If data form a straight line on log probability paper, the distribution is referred to as *lognormal*.

The probability density functions for the normal and lognormal distributions are given in eqs. (12-8) and (12-9), respectively:

$$P_x(d) = \frac{1}{(2\pi)^{1/2}\sigma_{SD}} \exp\left[-\frac{1}{2}\left(\frac{d-\overline{d}}{\sigma_{SD}}\right)^2\right] \tag{12-8}$$

$$P_x(d) = \frac{1}{(2\pi)^{1/2}\sigma_{SD}}\frac{1}{d} \exp\left\{-\frac{1}{2}\left[\frac{\ln(d/\overline{d})}{\sigma_{SD}}\right]^2\right\} \tag{12-9}$$

For the number distribution, the dummy subscript x equals n, and the mean, $\overline{d}$, and standard deviation, σ_{SD}, are number-averaged quantities. For the volume distribution, x equals v, so $\overline{d}$ and σ_{SD} are volume-averaged quantities.

Figures 12-10 and 12-12 are examples of cumulative frequency plots for distributions that are normally distributed in volume. Values of d_{10}, d_{50}, and d_{90} (defined above) are readily determined for $100F_v$ equal to 10, 50, and 90, respectively. The slopes of the curves are a measure of the breadth of the distribution. A steeper slope means a narrower size distribution.

A commonly used measure of the breadth of a size distribution is the coefficient of variation, CoV. This can be determined easily from normal or lognormal plots of cumulative frequency data. The smaller the value of the CoV, the narrower the drop size distribution:

$$CoV = \frac{d_{16} - d_{84}}{2\,d_{50}} \tag{12-10}$$

where d_{16} is the drop diameter in the spectrum where 16% of drops are smaller than d_{16}. Similarly, d_{84} is the size where 84% are smaller, and d_{50} is the midpoint.

Empirical relations such as the Schwarz–Bezemer equation, given by eq. (12-11), are used to relate the Sauter mean diameter, d_{32}, to the maximum drop size, d_{max}. a^* is an empirical constant.

$$d_{32} = \frac{a^*}{1 + a^*/d_{max}} \tag{12-11}$$

All batch agitation-formed dispersions show transient behavior. Initially, the distribution is broad, due to incomplete dispersion. With continued agitation the distribution becomes narrower as large drops continue to disperse. This is described in more detail in Section 12-2.

In chemical processing, typical dispersion drop sizes range from 1000 μm $\geq$ $d_{32} \geq$ 50 μm. Certain products, such as paint, personal care, and pharmaceutical products, require submicron sizes for reasons of shelf-life stability. Microdispersions are liquid–liquid systems where d_{32} lies between 0.5 and 50 μm.

Table 12-1   Drop Size Classification of Immiscible Liquid–Liquid Systems

Drop Size	Comments	Equipment/Agents
<0.5 μm	Stabilized by Brownian motion; nonsettling	Emulsifiers, ultrasonic devices, rotor–stator mixers, high-pressure homogenizers; surface agents usually required
0.5–3.0 μm	Marginally stable; can cream and separate	Rotor–stator and impingement mixers, static mixers
>3.0 μm	Usually unstable; coalescence and phase separation common when agitation ceases	Static mixers, in-line mixers, and stirred vessels

Emulsions are liquid–liquid systems where d_{32} is less than 0.5 μm. Table 12-1 gives characteristics of liquid–liquid systems based on drop size.

12-1.4   Process Complexities in Scale-up

Successful scale-up means that larger scale operations are fully anticipated and understood. Usually, the performance will be poorer than witnessed on a smaller scale. Scale-up must address several interdependent, flow-sensitive physical processes occurring simultaneously. These are dispersion, dispersion kinetics, coalescence, and drop suspension, as mentioned previously.

Scale-up is system dependent. For example, the scale-up of a dilute, neutral-density, noncoalescing system is a matter of balancing shear with dispersion time. However, the scale-up of a concentrated coalescing liquid–liquid system is much more complex. For this case, scale differences in fluid flow in the vessels result in different proportions of the vessel causing coalescence and dispersion. The small vessel tends to be dominated by dispersion, and the large one, by coalescence. This is due to coalescence being promoted by gentle shear leading to soft, long-duration collisions, while dispersion requires unsteady intense shear. In turbulent flow, rates of drop deformation, collision, and film drainage are governed by the small scale turbulence structure, which is somewhat insensitive to tank size. However, the amount of time that drops spend in the high-shear and quiescent regions depends on mean circulation time, governed by impeller pumping rate and macroscale turbulence phenomena. These are strongly influenced by tank size, so the balance of these rates is not readily scaled. These widely different conditions exist in all stirred vessels. In light of these complexities, scaling up liquid–liquid systems using "rules" such as constant tip speed or power per volume can lead to failures. Scale-up practices are discussed in Section 12-8.

12-1.4.1 Drop Suspension.   A completely suspended condition is necessary to control and ensure a steady and predictable DSD. Segregation and layering in all cases lead to inferior results. The ease with which a suspension forms depends on phase density differences, agitation rate, impeller type/size, and its

location within the vessel. The formation of a suspension starting from separated, settled phases is determined by empirical equations such as those developed by Pavlushenko and Yanishevskii (1958), Nagata (1975), and Skelland and Seksaria (1978). These are discussed in Section 12-6.

12-1.4.2 Role of Surfactants, Solid Particles, and Other Materials. Surfactants, dispersants, surface-active colloids, and very fine solids are all used to control drop size by stabilizing the system against coalescence. They are present at low concentrations, usually less than 1% based on the continuous phase. Composition and functionality are varied. Surfactants and suspending agents reduce the interfacial tension and drop size, and stop or reduce coalescence by affecting interfacial mobility. Fine solids act as structures preventing drop surfaces from touching. A commercialized process, known as limited coalescence, using solid suspending agents, is described in Section 12-9. Polymeric compounds that accumulate at drop surfaces are also used as suspending agents. When adsorbed, they can totally prevent coalescence.

12-1.5 Classification by Flow Regime and Liquid Concentration

12-1.5.1 Flow Regimes: Laminar, Transition, and Turbulent. Flow regimes are separated by the value of the Reynolds number, Re, the ratio of inertial to viscous forces. The impeller Reynolds number is

$$Re = \frac{D^2 N \overline{\rho}}{\overline{\mu}} \tag{12-12}$$

where $\overline{\rho}$ and $\overline{\mu}$ are the bulk density and viscosity of the mixed phases, respectively. For dilute dispersions (defined below) they are equal to those for the continuous phase. Laminar conditions exist when $0 \leq Re \leq 10$, transition flow occurs when $10 \leq Re \leq 10^4$, and fully turbulent flow occurs when $Re > 10^4$. Despite this generalization, it is common to find turbulent conditions near the impeller and transitional or laminar conditions elsewhere in the stirred vessel. This is particularly true for non-Newtonian fluids.

12-1.5.2 Dispersed Phase Concentration. The dispersed phase concentration is usually expressed as a volume fraction, ϕ. Coalescence, dispersion, and settling are all affected by dispersed phase concentration. For example, coalescence rates increase with increasing ϕ. This is due to both an increase in collision frequency and to rheological changes that enable longer contact intervals to be obtained. A high dispersed phase concentration also affects small scale turbulent eddies, reducing their intensity and making them less able to disperse drops. Therefore, the amount of information available and the means by which we approach the design process depend significantly on drop phase concentration. It is useful to categorize liquid–liquid systems with respect to their dispersed phase concentration as defined below.

Dilute Systems: $\phi < 0.01$. Ideally, a dilute system is one in which dispersion is affected only by hydrodynamics, and each drop is a single entity experiencing continuous phase fluid forces. Coalescence is neglected because few collisions occur. These simplifications enable a fairly fundamental treatment of dispersion to be made. Coalescence can become significant for clean systems at $\phi \geq 0.05$.

Moderately Concentrated Systems: $\phi < 0.2$. The behavior and technical treatment of systems in this concentration range depend on coalescence behavior. Ideal dilute dispersion theories may still apply, particularly if the system is noncoalescing. A simple test to detect coalescence is to agitate or shake a sample for 5 min and then watch it settle and coalesce. If only a trace of coalesced layer appears on the surface after 5 min, the system can be considered to be stable. The system is considered to be strongly coalescing if complete separation occurs in less than 30 s. Obviously, many results fall between these limits. More details coalescence tests are given in Section 12-3.1.5.

Even in the presence of coalescence, it is possible to predict the DSD for moderately concentrated systems. For $\phi < 0.2$, the drop phase does not appreciably affect the structure of the continuous phase flow field above the scale of the drop size. This allows single-phase flow concepts that describe the mechanical forces causing drop deformation, collisions, and film drainage to be used.

More Concentrated Systems: $\phi > 0.2$. This range is common in industry. Fast coalescence is probable for clean systems. Sprow (1967b) found that with coalescing systems, drop sizes were position dependent within the vessel. This behavior is very complex and extremely difficult to scale-up, since coalescence and dispersion dominate in different regions of the vessel, as described earlier. A special case is suspension polymerization. It is typically a concentrated system where $\phi \approx 0.5$ and coalescence is prevented by the use of polymeric suspending agents. This enables theories based on dilute systems to be used. This is described fully in Section 12-8. Overall, it is more difficult to predict mean drop size and DSD in systems of high dispersed phase concentration.

Other Considerations. The presence of a third phase can affect liquid–liquid dispersion and coalescence. Fine solids have little effect on drop dispersion but often affect coalescence. Gas bubbles affect dispersion by reducing the effective continuous phase viscosity and lead to a loss in momentum transport, hence dispersion capability. Tiny gas bubbles reduce probability of coalescence by interfering with film drainage rates between colliding drops. This subject is complex and is best studied experimentally at different scales.

Mass transfer to and from drops affects coalescence. Mass transfer creates concentration gradients in the region of the thinning film. Depending on the interfacial tension–concentration characteristics of the system, this can lead to Marangoni effects, causing surface flows and internal circulation within the drops. Such movement accelerates film drainage and increases the probability of coalescence.

12-1.6   Scope and Approach

Liquid–liquid dispersion is among the most complex of all mixing operations. It is virtually impossible to make dispersions of uniform drop size, because of the wide range of properties and flow conditions. Our chapter provides a fundamental framework for analysis and understanding of dispersion and coalescence, based often on idealized experiments and theories. This framework can be applied to more complicated processes, including scale-up. Throughout the chapter, references are made to state-of-the-art information, often not yet proven in practice. The chapter concludes with commercialization advice and recommendations.

Section 12-2 deals with liquid–liquid dispersion, while in Section 12-3 we discuss coalescence. Section 12-4 gives an introduction to the methods used for population balance models, along with references for further reading. In Section 12-5 we describe more concentrated dispersed phase systems, including phase inversion. Section 12-6 deals with other considerations, such as suspension, mass transfer, and other complexities, Section 12-7 with equipment used in liquid–liquid operations, Section 12-8 with scale-up, and Section 12-9 provides industrial examples. Nomenclature and references then follow. Although every attempt has been made to make this a stand-alone chapter, space limitations occasionally make it necessary to refer to other chapters in the book.

12-2   LIQUID–LIQUID DISPERSION

12-2.1   Introduction

12-2.1.1   *Breakup of Single Drops in Laminar and Turbulent Flow*.   The breakup of a single drop in laminar and turbulent flow fields forms the starting point for this section. Although not industrially relevant, it shows in the simplest possible form what occurs when fluid forces act on a drop, and thus provides important insight. The progeny of a single breakage event may be few and orderly or may be many drops of broad size distribution.

Simple laminar shear or extension flow produces orderly dispersion since the flow field surrounding the drop is constant and continuous. In contrast, simple turbulent flows produce more random breakup events, due to the time-dependent nature of fluid–drop interactions. The effect of breakage mechanism on the resulting DSD is sometimes counterintuitive.

Simple theories are described in which breakup results when disruptive forces in the surrounding fluid exceed cohesive forces, due to interfacial tension and drop viscosity. The results for a single drop are then extended to dilute dispersions in order to predict and correlate data for the DSD. The methodology is extended to more concentrated noncoalescing systems of wider practical importance as well as other dispersion devices. The scope includes a broad range of factors. Although most of the section is devoted to the development of the equilibrium mean drop size and DSD, dispersion kinetics and the time evolution of the DSD are included.

12-2.1.2   Description of Forces Causing Breakup. The forces acting to deform a drop in simple laminar flow can be characterized by the shear or extension rate (velocity gradient) in the surrounding fluid. In turbulent flows, these forces are best characterized in terms of the energy dissipation rate, since it is not practical to resolve the instantaneous velocity gradients. The two approaches are consistent, since in general, the energy dissipation rate is the product of the stress and velocity gradient tensors.

In stirred vessels, the forces causing drop dispersion are extremely nonuniform. Velocity gradients or deformation rates are highest near the impeller and diminish rapidly with distance from the impeller. Turbulent energy dissipation rates per volume of fluid in the impeller region are often ≈40 times greater than the average or power draw per unit volume for the tank. Some regions are apt to be turbulent, while others can be laminar. From the point of view of the drop, it seems obvious that it matters little how the force or disruptive energy is produced. This allows for a more general application of the dispersion process.

In laminar flow, the spatially dependent flow field is time periodic to the stationary observer but steady in time with respect to the rotating stirrer blades. However, the flow field as seen by a drop as it moves through regions of varying shear appears time dependent. This transient nature of the deformation process is important. Once deformed, a drop passing to a less intense region tends to return to a spherical shape. However, if it has already reached a critical state of deformation, it will become unstable and break up. In some instances, a deformed drop will remain stable in a steady force field and will not break until the force is relaxed. This is because internal circulation stabilizes it. For a drop exceeding the critical deformation, if internal circulation stops before the drop begins to return to its spherical state, it is likely to disperse. Newton's law of viscosity, or an appropriate non-Newtonian constitutive equation, can be used to describe the forces acting on the drop in laminar flow.

Turbulent flows contain a spectrum of eddies of different size, intensity, and lifetime. However, each eddy has an element of simple shear or extension, and creates forces that lead to drop deformation. The drop sees a time-dependent deformation field even if the Reynolds-averaged velocity field does not vary in space. This is illustrated in Figure 12-2 and is explained more fully in Chapter 2. In reality, forces in turbulent stirred vessels arise from both spatial and temporal velocity fluctuations. These arise from mean velocity gradients, interacting turbulent eddies and impingement of jetlike flows on walls, baffles, and impeller blades.

Figure 12-3 contrasts the time-averaged and instantaneous velocity fields acquired in a turbulent stirred tank. The probability of drop dispersion in such a transient flow field depends on two time scales. One characterizes the turbulent stretching force and the other the restorative surface force. It should be noted that drop viscosity opposes both deformation and relaxation. Observe the nature of flow in the data shown in Figure 12-3. The top view shows the time-averaged velocity field acquired by both LDV (laser Doppler velocimetry) and PIV (particle image velocimetry). These data show regions of high and low liquid velocity and
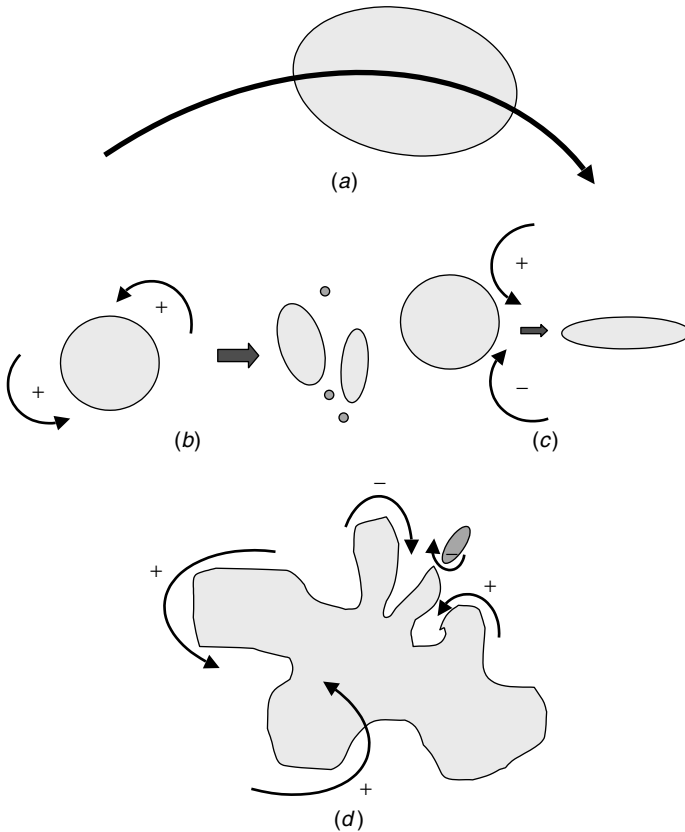
Figure 12-2 Scalar deformation in a turbulent field: (*a*) convection by large eddies; (*b*) erosion by co-rotating eddies; (*c*) elongation by counterrotating eddies; (*d*) multiple scales of turbulent deformation. (From Kresta and Brodkey, Chapter 2, this volume.)

are useful to predict overall convective or bulk mixing. The lower two pictures, acquired by PIV, show instantaneous transient velocity fields. These transient fields create forces leading to drop breakage. However, even if a large quantity of these data were available, a detailed analysis of drop dynamics is not currently possible. Therefore, it is more practical to employ mechanistic theories that relate drop deformation to local energy dissipation rates.

12-2.2 Breakup Mechanism and Daughter Drop Production in Laminar Flow

To the authors' knowledge, there are practically no data or fundamental analysis for drop dispersion in stirred tanks under laminar flow conditions. There are several reasons for this somewhat surprising occurrence. Viscous formulations are often produced in highly specialized equipment and exhibit complex and varied
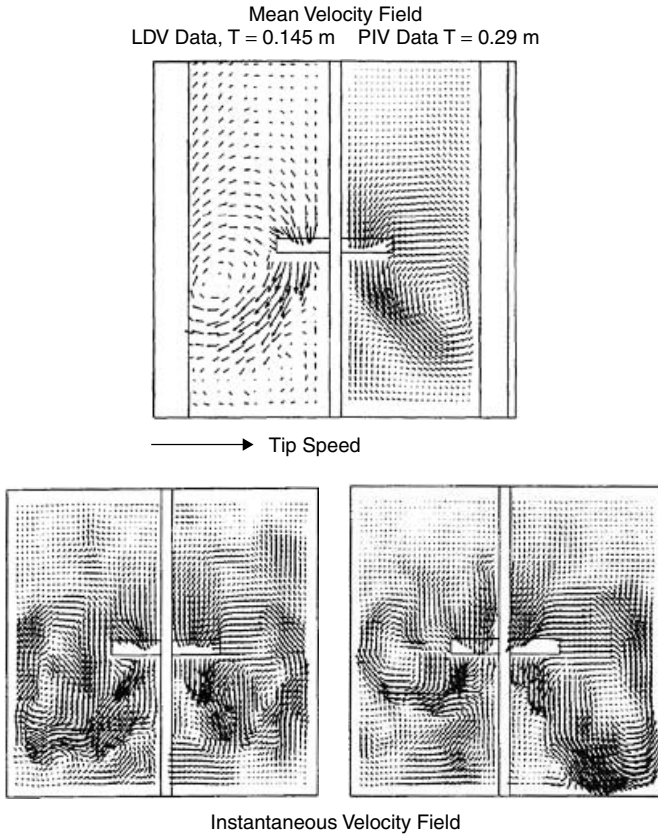
Mean Velocity Field
LDV Data, T = 0.145 m   PIV Data T = 0.29 m

⟶ Tip Speed

Instantaneous Velocity Field

Figure 12-3   Comparison of time-averaged and instantaneous velocity fields in a turbine stirred vessel. (Reproduced from Bakker et al., 1996.)

rheological behavior, so that results are not readily generalized. Drop size data are difficult to acquire, due to limited measurement techniques and numerous handling and disposal issues. Despite this, dispersion does certainly take place under laminar conditions, and it is important. For example, the continuous addition of low viscosity monomer to a stirred mass polymerization system results in monomer dispersion in a viscous matrix phase. Drops are formed long before they dissolve. Product quality often depends on how rapidly the monomer can be made available to growing polymer chains. Another example is given in Section 12-5 where Figure 12-24 shows a steady rotational shear flow and the initial creation of a water-in-oil dispersion prior to phase inversion.

From an analytical viewpoint, the flow fields in laminar devices are highly dependent on geometry, and individual drops experience varied deformation paths of long time scale that are difficult to analyze. Even if Lagrangian tracking of deformation and breakup history of many drops were possible, it would be difficult to apply this information to real-life systems. Therefore, most studies

have focused on single drops in highly idealized flow fields such as simple shear and/or extension. These studies have led to a better understanding of drop dispersion and form a basis for process design and scale-up by judicious application of this fundamental information.

It is not our purpose to provide a complete discussion of drop deformation and breakup in idealized laminar flow fields. There have been numerous studies that have been reviewed by Rallison (1984), Stone (1994), and others. Only the most practically relevant studies are discussed below. Of central importance is to predict and/or correlate the size above which a parent drop of known physical properties (that is subjected to an imposed deformation) will become unstable and break up into smaller drops. This size is referred to as the *critical* or *maximum stable drop size*, d_{max}.

If the breakup of a single drop in an idealized laminar flow is confined to low Reynolds number (creeping flow), inertial forces can be neglected. Nondimensionalization of the resulting Stokes equations reveals that drop size data can be correlated in terms of a capillary number, $Ca = \mu_c G a / \sigma$, and a viscosity ratio, μ_d / μ_c. G is the deformation rate (shear or extension rate). The capillary number is the ratio of the viscous force acting to deform the drop to the surface force opposing deformation. This is illustrated in Figure 12-4, which shows the critical stability curve for Newtonian fluids in simple shear flow (SSF) and simple extensional flow (SEF). A drop at conditions above the curve is unstable and will break. The drop is stable at conditions below the curve. Consider a drop of known physical properties at the critical capillary number. Then *a* is the radius of the largest drop that exists for a deformation rate G; or G is the smallest deformation rate required to break a drop of radius *a*. Note that the shape of the curves for shear and extensional flows are quite different.
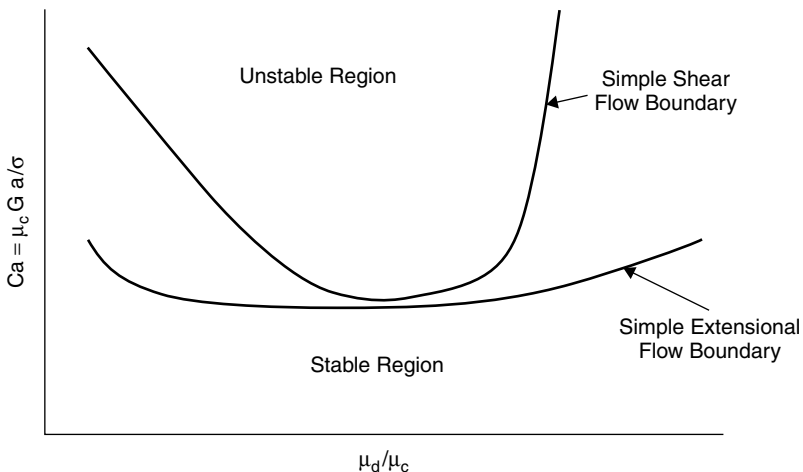

Figure 12-4 Critical stability curves for simple shear (SSF) and simple extensional (SEF) flow.

In SSF or Couette flow, it is not possible to break a drop if the viscosity ratio is greater than about 3. The deformed drop shape is stabilized by internal circulation. It has been concluded that extension is more effective than shear at breaking drops. With respect to practical flows, it is important not to interpret this statement too literally since in practical applications, a single steady shear gradient rarely exists. Bear in mind that the physical definitions of shear and extension depend on the environment seen by the drop along its trajectory, while the mathematical definitions are related to the choice of coordinate system.

Taylor (1934) was first to establish an analytical relationship between the degree of deformation of a drop and the deformation rate. For SSF this is given by

$$D_{crit} = \frac{L_d - B_d}{L_d + B_d} = \frac{G a \mu_c}{\sigma} \frac{1.19 (\mu_d/\mu_c) + 1}{(\mu_d/\mu_c) + 1} = Ca \cdot f(\mu_d/\mu_c) \qquad (12.13)$$

where L_d and B_d are the length and breath of the deformed drop and D_{crit} is the critical deformation for breakage. Since then there has been considerable effort, both analytically and computationally, to determine the critical or maximum stable drop size in a variety of idealized laminar flow situations. The reader is again referred to the reviews referenced above.

Karam and Bellinger (1968) and Grace (1982) studied drop deformation and breakup in simple shear flow. The conditions for breakage were observed within a glass-walled Couette apparatus consisting of independently controlled, counterrotating concentric glass cylinders. When the rotational speeds were about equal, the centroid of a drop would remain stationary, enabling deformation and breakage information to be observed and recorded. Drop data from two breakage
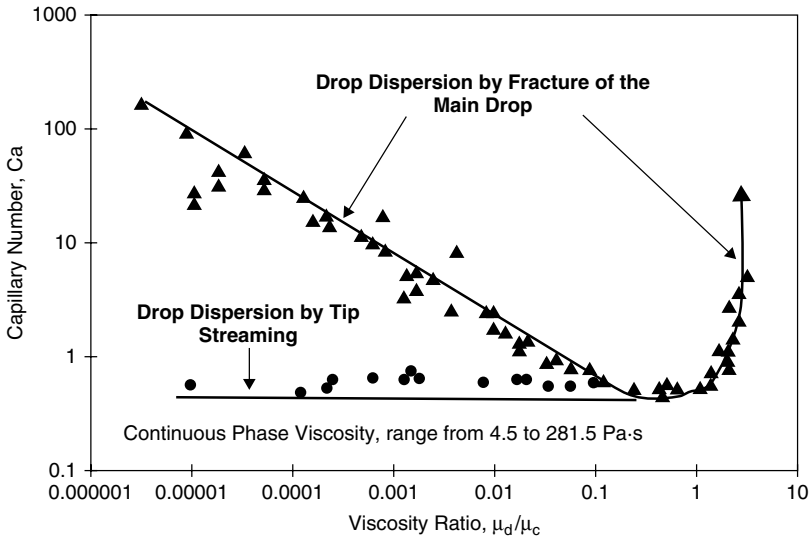

Figure 12-5 Drop stability data for simple shear flow. (Data of Grace, 1982.)
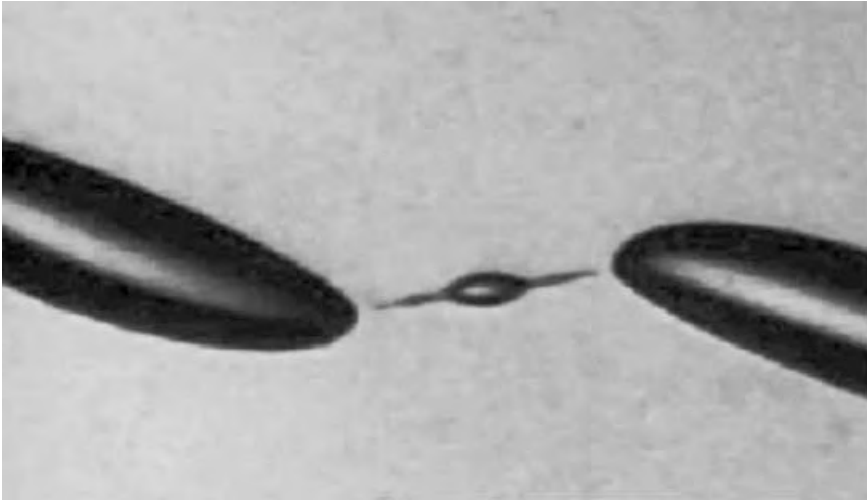
Figure 12-6 Breakup of a drop in simple shear flow. (Photo from Grace's archives; courtesy of E.I. DuPont de Nemours & Co.)

modes are shown in Figure 12-5. Typical breakage patterns showing the breakage of the main drop into orderly size daughter drops and the shedding of smaller drops from the tip ends of the main drop are given in Figure 12-6.

Bentley and Leal (1986) and Stone et al. (1986) studied deformation and breakup of a drop in a four-roll mill that allowed specification of idealized flows with various degrees of shear and extension. In addition to determining the critical deformation rate under steady conditions, the following experiments were performed. Drops were deformed to a steady nonspherical shape. After stopping the flow motion, the stability of the drop was monitored as it relaxed to a sphere. This enabled the conditions leading to breakup to be determined. Tjahjadi and Ottino (1991) studied the breakup of drops subjected to both stretching and folding.

There have been fewer studies to observe drop breakup and the resulting daughter drop size distribution. Figure 12-6 shows a typical breakage pattern for fracture of the main drop in SEF. Observe there are three distinct drop diameters that form upon breakup of the parent drop. As the imposed deformation rate exceeds the critical value required to just break the drop, a larger number of daughter drops are formed. Figure 12-7 correlates daughter drop production with the ratio of imposed to critical shear rate (G/G_{crit}). It shows that tens to thousands of daughters can result. Tjahjadi et al. (1992) measured relaxation of a stretched drop in SSF. They included details of satellite drop production as the drop broke up while trying to regain its initial spherical shape.

In a more recent study, Marks (1998) observed the deformation and breakup of a drop in SSF that was exposed to a steady shear rate greater than G_{max}. His results show that the breakage mechanism and breadth of the daughter DSD
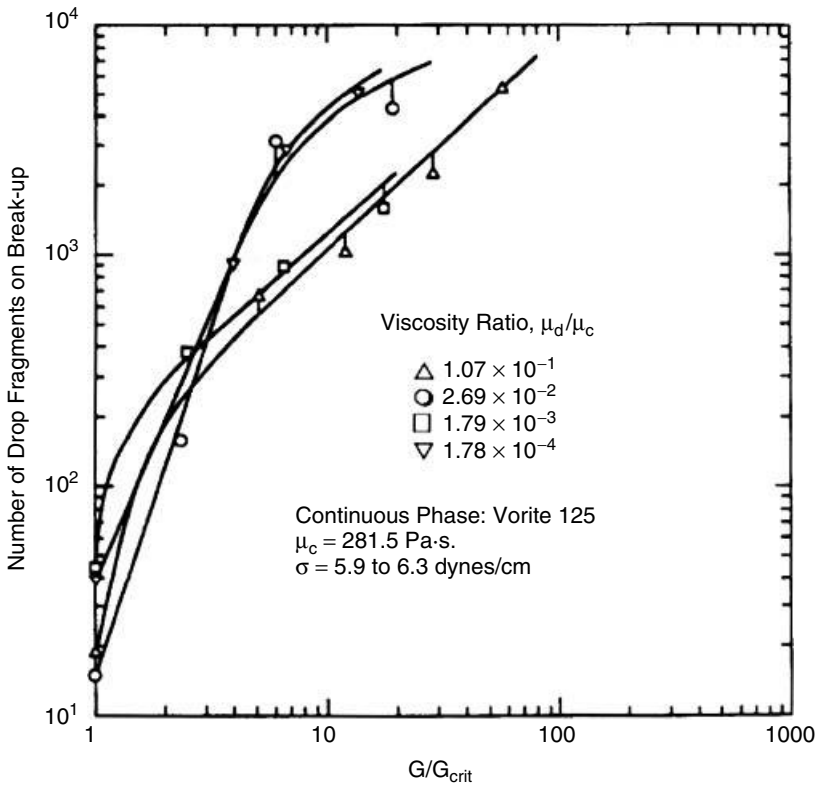
Figure 12-7 Number of drop fragments from breakup of a single drop in SSF as a function of the ratio of imposed to critical shear rate, G/G_{crit}. (Data of Grace, 1982.)

depend uniquely on G/G_{crit}. Furthermore, there was no further breakage of the largest fragments formed. If an application requires a narrow size distribution, it is important to operate as close to the critical shear rate as possible and to provide for a uniform deformation field. Alternatively, one can ramp up the deformation rate temporally or spatially to continue the break up the largest existing fragments.

In the absence of data for practical flows, the engineer must make use of the insights gained from these idealized studies. The literature for blending of immiscible polymers in extruders may also provide useful insights.

12-2.3 Drop Dispersion in Turbulent Flow

In contrast to laminar flow, there are numerous studies of drop dispersion in practical turbulent flows, particularly for dilute systems, when coalescence can be neglected. Data are relatively easy to acquire, since water and other nontoxic Newtonian fluids serve as the continuous phase and waste disposal issues are

minimized in dilute systems. With respect to mixing flows, most of the studies have been conducted on a bench scale in fully baffled batch stirred vessels equipped with a single Rushton (RDT) impeller. Fortunately, the small scale turbulence structure that determines ultimate drop size is independent of geometry, and turbulent time scales are such that statistically repeatable results can be obtained. This allows the development of mechanistic analysis coupled with similarity arguments to develop correlations for mean drop size and DSD that when applied carefully, perform adequately under extrapolation to larger scale. On the other hand, there are few observations of the breakup of single drops in practical turbulent flows, since these experiments are quite difficult to perform.

We begin by considering mechanistic theories that allow correlation of equilibrium mean drop size in dilute systems. An example of their application is given. Drop size distributions are then discussed. The predictive approach is extended to other contacting devices and to moderately concentrated noncoalescing systems. Some additional factors are considered, followed by a discussion of transient effects and time to achieve equilibrium.

12-2.3.1 Mechanistic Models and Correlation of Mean Drop Size.

Mechanistic models for maximum stable drop size in turbulent flow are based on arguments put forth by Kolmogoroff (1949) and Hinze (1955). The stress acting to deform a drop of size d is given by

$$\tau_c = \rho_c \overline{v'(d)^2} = \rho_c \int_{1/d}^{\infty} E(k)\, dk \qquad (12\text{-}14)$$

where $\overline{v'(d)^2}$ is the mean-square velocity difference across the surface of the drop of diameter d, E(k) the energy spectral density function, and k the wavenumber or inverse eddy length. Only energy contained in eddies of scale smaller than $k = 1/d$ is considered, since larger eddies carry rather than deform the drop.

For energy dissipation rates that commonly occur in stirred vessels, final drop sizes are small compared to the turbulence macroscale but large compared to the Kolmogoroff microscale, defined by

$$\eta = \left(\frac{\nu_c}{\varepsilon} \right)^{1/4} \qquad (12\text{-}15)$$

Therefore, eddies that interact with the drops to determine the ultimate DSD fall within the inertial subrange of turbulence. These eddies are locally isotropic and E(k) can be described by Kolmogoroff's (1941a,b) theory of local isotropy:

$$E(k) = \beta_K \, \varepsilon^{2/3} \, k^{-5/3} \qquad (L_T \gg d \gg \eta) \qquad (12\text{-}16)$$

$\beta_K \sim 3/2$ is the Kolmogoroff constant. When eq. (12-16) is used in (12-14), the result is

$$\tau_c \approx \rho_c \, \varepsilon^{2/3} \, d^{2/3} \qquad (L_T \gg d \gg \eta) \qquad (12\text{-}17)$$

It should be noted that ε is the local energy dissipation rate, which varies widely throughout stirred tanks and other contacting devices.

Cohesive forces due to interfacial tension and drop viscosity oppose drop deformation. The surface force per unit area is given by

$$\tau_s \approx \frac{\sigma}{d} \tag{12-18}$$

According to Hinze (1955), the viscous stress within the drop is

$$\tau_d \approx \mu_d \frac{(\tau_c/\rho_d)^{1/2}}{d} \tag{12-19}$$

This is Newton's law of viscosity, with the characteristic velocity within the drop, $(\tau_c/\rho_d)^{1/2}$, related to the turbulent stress on the surface.

An examination of eqs. (12-17) to (12-19) reveals that there exists a maximum stable drop size, d_{max}, above which the disruptive forces are sufficient to break the drop, and below which the drop is stabilized by surface and internal viscous forces. For $d = d_{max}$, the disruptive force exactly balances the cohesive forces, so that

$$\tau_c = \tau_s + \tau_d \tag{12-20}$$

Low Viscosity Dispersed Phase. If the drop is inviscid, τ_d is negligible, and only the surface force contributes to drop stability. According to eq. (12.20), we can then equate (12-17) and (12-18) and rearrange to obtain

$$d_{max} = C_1 \left(\frac{\sigma}{\rho_c}\right)^{3/5} \varepsilon_{max}^{-2/5} \tag{12-21}$$

where the constant C_1 must be determined empirically. Given the broad spatial distribution in energy dissipation rate in a stirred vessel, the maximum stable drop size will not be achieved until all dispersed phase globules experience the highest energy region of the flow. Therefore, d_{max} is determined by the maximum energy dissipation rate. Hence ε is replaced by ε_{max} in eq. (12-21). Furthermore, it will take a large number of impeller passes before equilibrium is achieved. Time to complete dispersion is discussed later in this section.

For geometrically similar turbulent systems, $\varepsilon_{max} \propto \varepsilon_{avg}$, where ε_{avg} is the power draw per unit mass ($P/\rho_c V$) of fluid. For constant power number this gives $\varepsilon_{max} \sim N^3 D^2$. For a dilute system, the equilibrium DSD will consist of drops of size d_{max} and smaller. There is considerable experimental evidence that d_{max} is proportional to d_{32}. This relationship has also been argued mechanistically. Therefore, for geometrically similar systems, eq. (12-21) is equivalent to

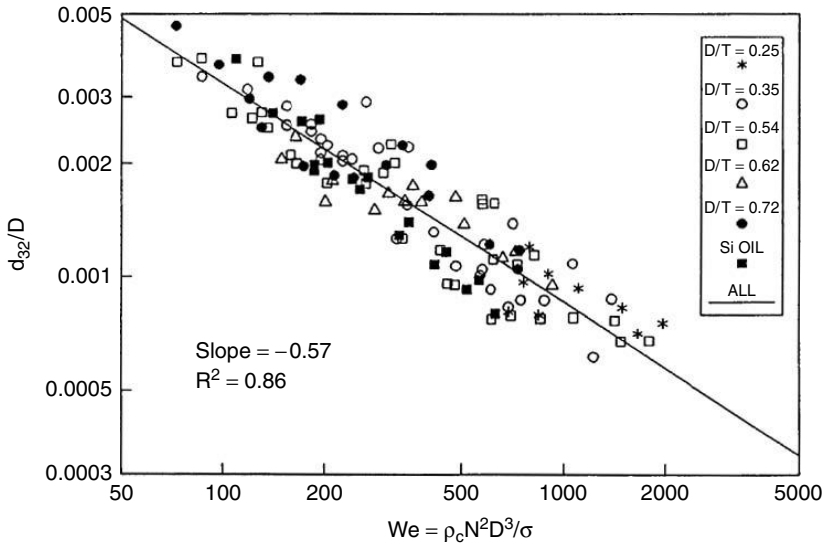$$\frac{d_{32}}{D} = C_2 \cdot We^{-3/5} \tag{12-22}$$

Figure 12-8 Experimental data for 14 different liquid–liquid pairs. (Data of Chen and Middleman, 1967 for a RDT.)

where $We = \rho_c N^2 D^3 / \sigma$ is the ratio of inertial (disruptive) to surface (cohesive) forces. This expression is the well-known Weber number theory, which has been derived and validated by Chen and Middleman (1967), among others. Their substantial data set for a Rushton turbine covered a broad range of physical properties and tank size and is shown in Figure 12-8. The data are best fit by eq. (12-22) with $C_2 = 0.053$.

Equations (12-21) and (12-22) show that dispersed phase systems created by turbulent flow scale-up by maintaining constant ε_{max}; or for practical industrial purposes, by constant P/V. Large Weber numbers result in small drops, and vice versa. These expressions are valid for dilute, noncoalescing systems of low μ_d. It turns out that many stabilized or noncoalescing industrial systems with $\phi > 0.05$ can also be scaled by the constant P/V criterion.

Example 12-1. It is proposed to recover a fermentation product by solvent extraction. The broth has a viscosity of $\mu_c = 0.3$ Pa · s (300 cP). While the broth is viscous, the drop phase is not. The bulk or mixture viscosity is $\overline{\mu} = 0.0386$ Pa · s (38.6 cP). The interfacial tension is $\sigma = 0.003$ N/m (3.0 dyn/cm). The broth has density $\rho_c = 1000$ kg/m³ (1.0 g/cm³), but the bulk or mixture density is 1100 kg/m³ (1.1 g/cm³). The vessel volume is 3.54 m³ (750 gal). The vessel has a diameter T = 1.524 m (5.0 ft) and is equipped with an RDT with D/T = 0.4. Laboratory studies have shown that acceptable extraction results are obtained if the mean drop size is $d_{32} = 50$ μm. Determine the required impeller speed and power draw.

SOLUTION: The solvent will disperse in the broth and the system will be slow to coalesce because of the high broth viscosity. As a result, eq. (12-22) will be used with $C_2 = 0.053$, even though it is not a dilute system. Substituting $d_{32} = 0.005$ cm, D = 61 cm, $\sigma = 3.0$ dyn/cm, $\rho_C = 1.0$ g/cm^3 into eq (12-22) and solving for N yields: N = 48 rpm (0.8 s^{-1}).

The Reynolds number, Re = $D^2 N \overline{\rho}/\overline{\mu}$, is 7700. Flow is nearly fully turbulent, so the use of eq. (12-22) is acceptable. For an RDT, an average power number is $N_p = P/\overline{\rho} N^3 D^5 = 5.0$. Using the bulk density, the power required is P = $N_p \overline{\rho} N^3 D^5 = 0.3$ hp.

Equations (12-21) and (12-22) are independent of the device used. However, C_1, C_2, and $\varepsilon_{max}/\varepsilon_{avg}$ do depend on impeller type and tank geometry. In principle, one can apply data for an RDT to other geometries from knowledge of their respective values of ε_{max}. These can be estimated from LDV measurements (see Chapter 3), as demonstrated by Zhou and Kresta (1998a), who successfully correlated drop size data for several impeller geometries with ε_{max}. Accurate DSD data are even more difficult to acquire than accurate LDV data. This makes measurements of ε_{max} an efficient means to convert literature data for RDTs to other geometries.

A simple concept is to use the impeller swept volume as the dissipation volume to correlate data for different geometries in the absence of data for ε_{max}. The idea is to assume that all power is dissipated uniformly in the volume swept out by the impeller rather than throughout the tank volume. Then, according to eq. (12-21), drop size for different geometry should scale approximately with $N_p^{-2/5}$. McManamey (1979) correlated many systems with other types of impellers using

$$\frac{d_{32}}{D} = C_3 N_p^{-2/5} We^{-3/5} \tag{12-23}$$

In other words, if a turbine other than the RDT is used for dispersion (say turbine X), first calculate d_{32} from eq. (12-22) for the RDT and then correct it by multiplying it with a *factor* represented by the ratios of the power numbers to the $\frac{2}{5}$ power. For example,

$$factor = \left(\frac{N_{p\,Rushton}}{N_{p\,Impeller\,X}}\right)^{2/5}$$

It cannot be overstated that the basis of the mechanistic theory and scale-up criteria discussed here assumes that there is no coalescence and that the drops are large compared to the Kolmogoroff microscale but small compared to the macroscale ($L_T \gg d \gg \eta$). Otherwise, eq. (12-17), and hence (12-21) and (12-22), are not valid. Correlations and scale-up for other criteria are discussed later in this section.

Viscous Dispersed Phases. If the drop is viscous, the internal viscous resistance to deformation cannot be ignored. Both interfacial tension and viscosity contribute

to drop stability and the development of the preceding section can be extended in a straightforward manner. When all of eqs. (12-17) to (12-19) are substituted into (12-20), the result is

$$\frac{\rho_c \varepsilon_{max}^{2/3} d_{max}^{5/3}}{\sigma} = C_4 \left[1 + C_5 \left(\frac{\rho_c}{\rho_d} \right)^{1/2} \frac{\mu_d \varepsilon_{max}^{1/3} d_{max}^{1/3}}{\sigma} \right] \qquad (12\text{-}24)$$

In the limit as μ_d vanishes and/or σ becomes large, the right-hand term in brackets becomes small with respect to unity, and eq. (12-24) reduces to (12-21). In the limit of large μ_d and/or small σ, internal viscous forces predominate over surface forces. The right-hand term in brackets becomes large with respect to unity, and eq. (12-24) reduces to

$$d_{max} = C_6 (\rho_c \rho_d)^{-3/8} \mu_d^{3/4} \varepsilon_{max}^{-1/4} \qquad (12\text{-}25)$$

For the case of geometrically similar systems with constant power number, eq. (12-24) yields

$$\frac{d_{32}}{D} = C_7 \cdot We^{-3/5} \left[1 + C_8 \cdot Vi \left(\frac{d_{32}}{D} \right)^{1/3} \right]^{3/5} \qquad (12\text{-}26)$$

The viscosity group, $Vi = (\rho_c/\rho_d)^{1/2} \mu_d N D/\sigma$ represents the ratio of viscous to surface forces stabilizing the drop. In the limit as $Vi \to 0$, eq. (12-26) yields (12-22). In the limit as $Vi \to \infty$, eq. (12-26) yields the counterpart to eq. (12-25):

$$\frac{d_{32}}{D} = C_9 \left(\frac{\rho_c}{\rho_d} \right)^{3/8} \left(\frac{\mu_d}{\mu_c} \right)^{3/4} Re^{-3/4} \qquad (12\text{-}27)$$

Equation (12-27) can be misleading. Since $Re = \rho_c N D^2/\mu_c$, there is actually no dependence on μ_c. Calabrese et al. (1986a,b) and Wang and Calabrese (1986) extended the work of Chen and Middleman (1967) to dilute dispersions of viscous drops in turbulent stirred vessels equipped with Rushton turbines. They found that the mechanistic correlations were valid for $\mu_d \leq 500$ cP. Figure 12-9 is taken from their substantial data set and verifies that $d_{32} \sim \mu_d^{3/4}$ for large μ_d. Based on their results and several other data sources (ca. 350 data sets), they found that $C_7 = 0.054$ and $C_8 = 4.42$. They also found that the following empirical equation was equally accurate for the RDT:

$$\frac{d_{32}}{D} = 0.053 \ We^{-3/5} (1 + 0.92 Vi^{0.84})^{3/5} \qquad (12\text{-}28)$$

Both correlations collapse to the Chen and Middleman result in the inviscid limit.

According to eqs. (12-21), (12-24), and (12-25), the dependency of drop size on ε_{max} or P/V varies from the $-\frac{2}{5}$ to the $-\frac{1}{4}$ power as μ_d or Vi increases. The ideas discussed earlier about scale-up and application to other impeller types still
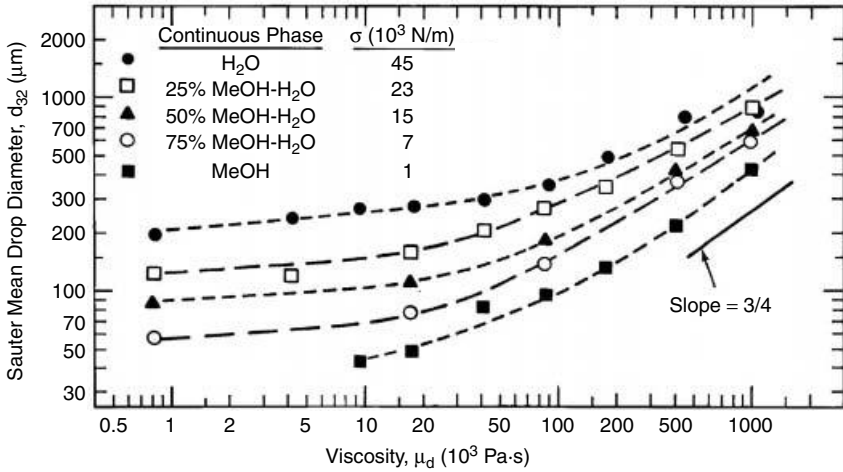
Figure 12-9 Relative influence of μ_d and σ on d_{32} for constant conditions of agitation. Silicone oils dispersed in aqueous methanol solutions. RDT with N = 3.0 rps, D/T = 0.5, T = 0.2 m. (Reproduced from Wang and Calabrese, 1986.)

apply here, except that one additional complexity arises. The power to which you scale ε_{max} or the N_p ratio now varies, depending on the value of viscosity group. Vi is also scale dependent, so an approximate power dependency must be assumed.

For $\mu_d > 500$ cP, dispersion behavior and the dependency of d_{32} on system variables is quite complex. The reader is referred to the original work of Calabrese et al. (1986a).

12-2.3.2 *Equilibrium Drop Size Distribution*. Chen and Middleman (1967) found that for turbulent Rushton turbine stirred vessels, the equilibrium DSD for dilute inviscid dispersions was normally distributed in volume and therefore described by eq. (12-8). Wang and Calabrese (1986) found a similar result for low- to moderate-viscosity dispersed phases ($\mu_d \leq 500$ cP). Figure 12-10 shows that the cumulative volume frequency exhibits straight-line behavior on normal probability coordinates that is indicative of a Gaussian DSD. The distribution broadens with increasing drop viscosity, increasing interfacial tension, and decreasing impeller speed.

Both authors argued that for dynamically similar breakage mechanisms, the equilibrium DSD should only depend on the ratio of disruptive (τ_c) to cohesive (τ_s and/or τ_d) forces acting on the drops. Thus, the individual DSDs could be collapsed to a single correlation by normalization with d_{32}. Defining $X = d/d_{32}$, the volume probability density function becomes

$$P_V(X) = \frac{1}{\sqrt{2\pi}\,\sigma_V} \exp\left(-\frac{X - \overline{X}}{\sqrt{2}\,\sigma_V}\right)^2 \qquad (12\text{-}29)$$
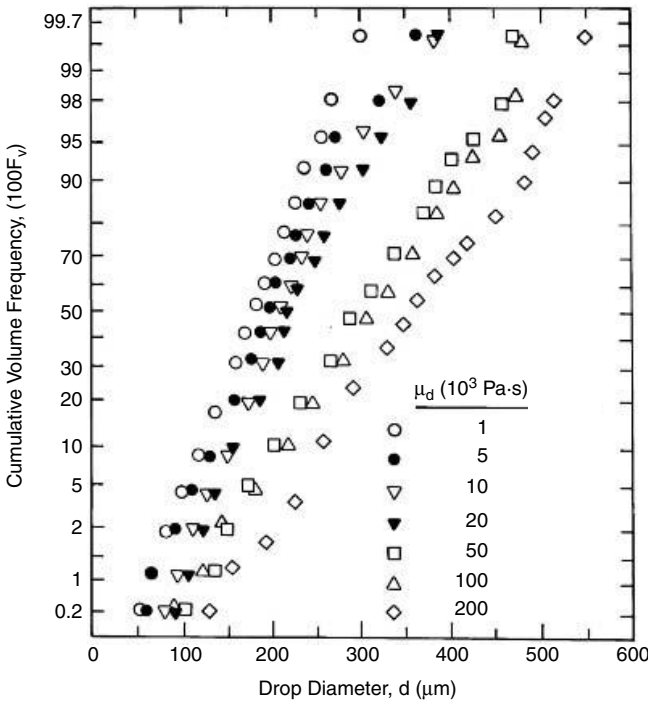
Figure 12-10 Effect of μ_d on DSD. Silicone oils dispersed in water, $\sigma = 0.045$ N/m. RTD with N $= 4.67$ rps, D/T $= 0.5$, T $= 0.15$ m. (Reproduced from Wang and Calabrese, 1986.)

where $\overline{X}$ is the mean of d/d_{32} and σ_v is the volume standard deviation. Chen and Middleman found that their inviscid dispersed phase data were well correlated by $\overline{X} = 1.07$ and $\sigma_V = 0.24$. Wang and Calabrese found essentially the same result ($\overline{X} = 1.07$ and $\sigma_V = 0.23$) for viscous drops with $\mu_d \leq 500$ cP. Therefore, a single correlation can be used to include a broad range of physical properties.

In the absence of direct information, it is reasonable to assume that the functional form of the DSD, and its mean and standard deviation, are not a strong function of scale or geometry. Then, once d_{32} has been estimated, the DSD is known. The solid line of Figure 12-13 (discussed later) is just eq. (12-29) in its cumulative form, with $\overline{X} = 1.07$ and $\sigma_V = 0.24$.

Dispersion behavior becomes more complex for $\mu_d > 500$ cP. The DSD broadens considerably and transitions to a lognormal distribution in volume, due to a shift in the breakage mechanism, resulting in the production of numerous small satellite drops. The reader is referred to the original work of Calabrese et al. (1986a).

12-2.3.3 *Extension to Finite* ϕ. The equations given in Sections 12-2.3.1 and 12-2.3.2 hold strictly only for dilute systems. By *dilute* it is meant that

neighboring drops do not alter the turbulence structure or interfere with the drop breakage forces themselves. Furthermore, coalescence is neglected even for coalescing systems, since collision rates are low. Dilute dispersion studies are typically made at dispersed phase volume fractions of $\phi < 0.01$. In more concentrated systems, say for $0.01 \leq \phi \leq 0.3$, that can be described as noncoalescing, many of the relationships given above can still be used if modified appropriately to account for the effect of phase fraction on turbulence forces. For this to be valid, the dispersion must be well stabilized against coalescence and the high phase fraction cannot alter the rheological behavior of the system. Under these conditions, the presence of droplets tends to suppress small scale turbulent fluctuations and thereby reduce the stress acting to break the drops.

For inviscid drops, eq. (12-22) has been modified both mechanistically and empirically to yield

$$\frac{d_{32}}{D} = C_{10}(1 + b\,\phi)We^{-3/5} \tag{12-30}$$

Doulah (1975) argued mechanistically that if the only effect of the presence of drops was to alter the local energy dissipation rate, $C_{10} = C_2$ and $b = 3$. Brown and Pitt (1970) measured drop size at the tip of an RDT. Their data for $\phi < 0.3$ were well correlated by the Chen and Middleman (1967) correlation with the Doulah correction [eq. (12-30) with $C_{10} = 0.053$ and $b = 3.0$]. Furthermore, the normalized DSD was also well correlated by the Chen and Middleman correlation [eq. (12-29), with $\overline{X} = 1.07$ and $\sigma_V = 0.23$]. Calderbank (1958) and Mlynek and Resnick (1972) found similar correlations for d_{32}. Calabrese et al. (1986b) used the Doulah approach to correct eq. (12-26) and their correlation for viscous drops. In addition to the $(1 + 3\phi)$ term in front of We, they included a $(1 - 2.5\phi)$ term in front of Vi. They suggested that their modified correlation for d_{32} and their original correlation for DSD applied to RDTs for $\mu_d \leq 500$ cP and $\phi < 0.3$. However, they offered no experimental validation. In the absence of additional information, these extensions allow application of the correlations and scale-up procedures discussed above for RDTs and other impellers to noncoalescing systems of higher phase fraction.

It should be noted that numerous researchers have used eq. (12-30) to correlate drop size data for coalescing systems. Both C_{10} and b varied widely and were greater than the values reported above. Except in special circumstances, the use of such correlations is not recommended, since they do not mechanistically account for coalescence, making their performance under extrapolation questionable. This is discussed further in Section 12-3.

12-2.3.4 Extension to Other Devices. Equations (12-17) to (12-27) and (12-30) were the result of mechanistic arguments that were independent of device geometry. They are based on the argument that the equilibrium DSD is such that $L_T \gg d \gg \eta$, so that the turbulent stress is derived from eddies in the inertial subrange of turbulence. The structure (isotropic) and energy content of these eddies do not depend on the large scale motion or how the power is introduced. Therefore, these equations apply to a variety of contactors, provided

that $L_T \gg d \gg \eta$. Scale-up and extension of device specific correlations to other geometries requires knowledge of the $\varepsilon_{max}/\varepsilon_{avg}$ ratio or the power number, or the friction factor in the case of continuous flow devices.

Static Mixers. Middleman (1974) studied the dispersion of dilute inviscid dispersed phases in turbulent flow in a Kenics static mixer. He found that equilibrium was achieved after 10 mixer elements. To ensure equilibrium, Berkman and Calabrese (1988) performed a similar study for viscous dispersed phases in a 24-element static mixer. For a Kenics mixer,

$$\varepsilon_{avg} = V'_s \frac{\Delta P}{\rho_c L_p} = \frac{2V'^3_s f}{D_p} \qquad (12\text{-}31)$$

where V'_s is the superficial velocity, ΔP the pressure drop, L_p the mixer length, f the constant friction factor, and D_p the pipe diameter. The latter authors found that both data sets were well correlated by eq. (12-26) with $C_7 = 0.49$ and $C_8 = 1.38$, with the impeller diameter replaced by the pipe diameter and the Weber number and viscosity groups now defined as $We = \rho_c V^2_s D_p/\sigma$ and $Vi = (\rho_c/\rho_d)^{1/2}\mu_d V'_s/\sigma$. When compared on an equal power per unit mass basis, the RDT produces smaller drops than the static mixer. This is because the RDT focuses energy in the trailing vortices behind the impeller blades, while the static mixer dissipates energy more uniformly. That is, the ratio $\varepsilon_{max}/\varepsilon_{avg}$ is very different in the two devices. It is tempting to conclude that the RDT is more efficient than the static mixer, but this is not the case. The energy in a stirred tank is intensely focused, but the time to reach equilibrium is relatively long. Many drop paths do not pass through the high dispersion zone. This is not the case in a static mixer. All drops are exposed to fairly uniform shear as they pass through the mixer. Berkman and Calabrese (1988) also found that the DSD is well correlated by eq. (12-29), with $\overline{X} = 1.12$ and $\sigma_V = 0.31$. While the mean is almost the same as for the RDT, the distribution is broader. It is not clear if this is real or if improvements in photographic measurement techniques allowed for better capture of the smaller drops.

Rotor–Stator Mixers. Calabrese et al. (2000) studied dilute dispersions of inviscid drops in turbulent flow in Ross ME100LC and Silverson L4R batch rotor-stator mixers. These devices are discussed in Chapter 8. These machines have four blade rotors, are geometrically similar, and discharge the flow radially outward from the mixing head. Although the Power numbers are similar, in magnitude to those for stirred tank turbines, these devices operate at higher speed and energy input, producing smaller drops that are close in size to the Kolmorgoff microscale. Nevertheless, the data for a slotted stator head were well correlated using eq. (12-22) with $C_2 = 0.038$, making the correlation similar to that for an RDT. The authors also found that many smaller drops were produced, resulting in the volume probability density function being a lognormal rather than a Gaussian distribution function [see eq. (12-9)]. A reasonably good correlation for DSD

could still be obtained by normalization with d_{32}. The lognormal distribution had log mean $\overline{X} = 1.01$ and volume log standard deviation $= 0.31$.

Phongikaroon (2001) extended the study of Calabrese et al. (2000) to include viscous dispersed phases produced in the Silverson mixer, with both slotted and disintegrating (round hole) stator heads. Since he studied a broader range of physical properties and rotor speeds, he was able to produce drops at low μ_d and σ and at high N that were smaller than the Kolmorgoff scale. As a result, only the larger values of d_{32} in his data set could be correlated using eq. (12-26). Correlations that result when the restriction $L_T \gg d \gg \eta$ is not valid are discussed below. Phongikaroon (2001) also found that the normalized probability density function was lognormally distributed in volume.

Local Power Per Mass Approach. Davies (1987) showed that values of d_{max} for a wide variety of dispersion devices could be correlated with local power per mass if a rough estimate of $\varepsilon_{max}/\varepsilon_{avg}$ could be obtained. By extending the ideas of McManamey (1979), he argued that this could be accomplished by assuming that all the power is dissipated in a localized, device-specific volume. The results of his analysis of literature data for dilute inviscid dispersed phases, corrected for interfacial tension, are shown in Figure 12-11. The slope of the line bounding the data is $-\frac{2}{5}$, as predicted by eq. (12-21). The rotor–stator data discussed above would lie between the data for agitated vessels and liquid whistles.

Experimental evidence shows that the scale-up procedures discussed above can be applied to a broad range of dispersion geometries, provided that the criterion $L_T \gg d \gg \eta$ is met. Furthermore, a few comprehensive data sets can be used to design a variety of dilute dispersion processes when applied with good judgment
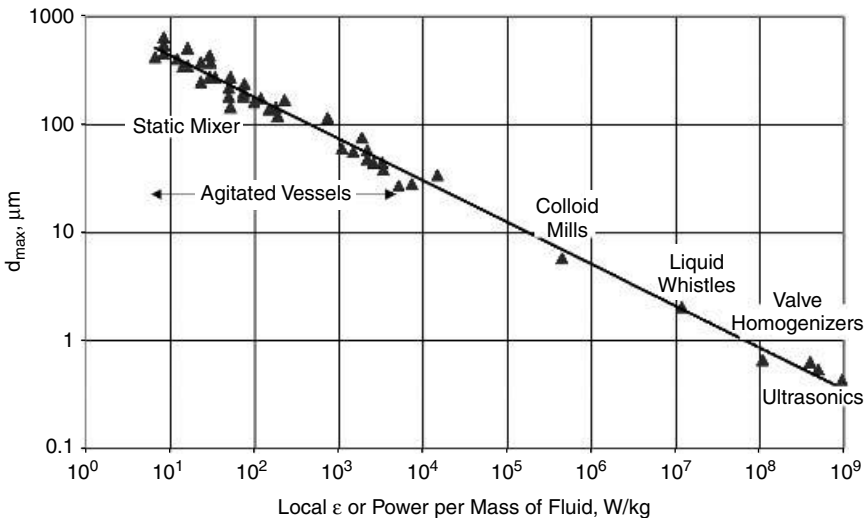

Figure 12-11   Dependence of drop size on local power draw for various dispersion devices. (After Davies, 1987.)

by a skilled practitioner. Scale-up recommendations and examples are given in Section 12-8.

12-2.3.5 Additional Factors for Dilute Turbulent Dispersions

Fine Scale Intermittency. Baldyga and Bourne (1992) argued that the equilibrium drop size was ultimately determined by violent but relatively rare bursts of turbulent energy. Therefore, on long time scales the ultimate value of ε_{max} in eq. (12-21), (12-24), and (12-25) is determined by the intermittent nature of the fine scale turbulence. They redeveloped the mechanistic theory of Section 12-2.3.1 to show that different dependencies on system parameters would result. For instance, for inviscid dispersed phases, the dependency of d_{32}/D on Weber number, would be to a power less than the value $-\frac{3}{5}$ given by eq. (12-22) and could be as low as -0.93. Although the theory is well grounded, it is difficult to implement from a practical viewpoint. It is not clear how much time is needed to experience the ultimate turbulent burst or how system dependencies would vary at very long times. Other factors that complicate the interpretation are discussed below.

More Sophisticated Models. More sophisticated models have been developed to predict equilibrium mean drop size. For instance, Arai et al. (1977), Lagisetty et al. (1986), and Clark (1988) have used a Voigt (spring and dashpot) model to account for the interaction between interfacial and dispersed phase viscous forces rather than assume that they were additive, as in eq. (12-20). Although this approach is more realistic, it has not resulted in more reliable data correlation. Models have been developed for non-Newtonian drops (Lagisetty et al., 1986; Koshy et al., 1988b) and for drop breakup in the presence of drag reducing agents (Koshy et al., 1989). Unfortunately, they have only been weakly validated by data.

Other Breakage Regimes. The models and correlations discussed above are based on the Kolmogoroff (1949) theory for the inertial subrange of turbulence. That is, the stress acting to deform the drop is given by eq. (12-17), so the models apply only for $L_T \gg d \gg \eta$. Correlations can be developed for other breakup regimes by replacing eq. (12-17) with an appropriate model for τ_c. For instance, Chen and Middleman (1967) developed a model for inviscid drops that applies when $d \ll \eta$. Shinnar (1961) and Baldyga and Bourne (1993) proposed expressions for τ_c that apply to both viscous and inertial disruptive forces when $d < \eta$. These models were not validated, since stirred vessels are usually not operated at a sufficiently high power draw to produce such small drops. Recently, Calabrese et al. (2000) have developed models for inviscid drops based on the Shinnar arguments to correlate data for d_{32} of order η, produced in high-shear mixers. Phongikaroon (2001) extended these to viscous drops.

Turbulence in laboratory scale vessels may be entirely nonisotropic. That is, the drop size may be of the same order as the turbulent macroscale ($d \sim L_T$) and an equilibrium turbulence subrange may not exist. Konno et al. (1983), Pacek

et al. (1999), and others have shown that in this limit, $d_{32}/D = C_{11} \cdot We^{-1}$ for inviscid drops. Therefore, the exponent on the Weber number varies from $-\frac{3}{5}$ to -1 as the impeller size and speed decrease. Using small tanks, Blount (1995) and others have shown this to be the case. Unfortunately, the fine scale intermittency argument above leads to a similar shift in the We exponent. These considerations illustrate how difficult it is to develop correlations for extrapolation, even for dilute dispersions.

Effect of Surfactants. For dilute dispersions, the presence of surfactants influences drop size only by reducing interfacial tension. To a first approximation, the drop size may be estimated within the framework developed above using the static interfacial tension in the presence of surfactant. However, drop stretching and breakup occur rapidly. As new interface is created, the rate at which surfactant diffuses to the surface may not be sufficient to maintain a constant interfacial tension. The dynamic σ will vary from the static value in the presence of a surfactant to the value for a clean interface. Phongikaroon (2001) found that for this reason, drop sizes produced in a rotor–stator mixer with a surfactant-laden system of known static σ were larger than those produced for a clean system of the same σ.

At high surfactant concentration, the resistance to deformation may be due solely to drop viscosity, and/or the ultimate size may be dictated by thermodynamic considerations. Koshy et al. (1988a) developed a model for drop breakup in the presence of surfactants. Unfortunately, there are few experimental data to support its implementation.

Correlations for Sauter Mean Diameter. Table 12-2 summarizes a large number of correlations for d_{32} in stirred vessels reported before 1990. The table contains many of the studies discussed above. It also contains many studies that are largely empirical. Many apply to low viscosity drops and are based on eq. (12-30). As noted previously, this equation applies only to dispersion-dominated systems stabilized against coalescence. Yet many of the table entries are for coalescing systems at high dispersed phase fraction. As stated previously, the reader should exercise caution in extrapolating such correlations. Coalescence is discussed in Section 12-3. Most of the studies are for RDTs, demonstrating the lack of data for other impellers. Several measurement techniques, including light transmission, in situ photography, and sample withdrawal, are represented. Since these correlations were acquired for a broad spectrum of processing conditions, it is not surprising that the results are varied. Recently, Zhou and Kresta (1998a, b) and Pacek et al. (1999) have acquired data for several other impeller geometries.

12-2.4   Time to Equilibrium and Transient Drop Size in Turbulent Flow

Several investigators, including Chen and Middleman (1967), Arai et al. (1977), and Wang and Calabrese (1986), have reported that after introduction into the tank, several hours are required for a dilute dispersion to reach the equilibrium

Table 12-2 Review of Correlations for Mean Drop Diameter in Liquid–Liquid Stirred Vessels[a]

Authors	Correlation[a]	Physical Properties			Operating Conditions/ Geometric Parameters				Impeller/Measurement Techniques and Comments
		$\dfrac{\rho_d}{\rho_c}$ (g/cm³)	$\dfrac{\mu_d}{\mu_c}$ (cP)	σ (dyn/cm)	D (cm)	T (cm)	ϕ	N (rps)	
Vermeulen et al. (1955)[b]	$\dfrac{d_{32}}{D} = Bf_\phi We^{-0.6}$	$\dfrac{0.693-1.595}{0.693-1.595}$	$\dfrac{0.378-184}{1.81-65.4}$	3.1–55.1	—	25.4, 50.8	0.1–0.4	1.80–6.67	4-blade paddles/in situ (light transmittance)
Rodger et al. (1956)	$\dfrac{d_{32}}{D} = B(D/T)^{-b} We^{-0.36}$	$\dfrac{0.761-1.101}{1.0}$	$\dfrac{0.578-3.91}{1.0}$	2.1–49	5.1–30.0	15.5, 45.7	0.5	1–20	6-blade RT/in situ (photography, light transmittance)
Calderbank (1958)	$\dfrac{d_{32}}{D} = 0.06(1 + 3.75\phi)We^{-0.6}$ $\dfrac{d_{32}}{D} = 0.06(1 + 9\phi)We^{-0.6}$	—	—	35–40	5.8–25.4	17.8, 38.1	0–0.2	—	4-blade paddles/in situ (light transmittance); 6-blade RT/in situ (light transmittance)
Shinnar (1961)	$\dfrac{d_{32}}{D} = BWe^{-0.6}$ (breakage control) $\dfrac{d_{32}}{D} = B(\sigma D)^{-3/8}We^{-3/8}$ (coalescence control)	—	$\dfrac{22.5}{0.4}$	—	12.7	29.0	0.05	2.6–10.5	No experiments; paddle turbine/sample withdrawal

Table 12-2 (*continued*)

Authors	Correlation[a]	Physical Properties			Operating Conditions/ Geometric Parameters				Impeller/Measurement Techniques and Comments
		$\dfrac{\rho_d}{\rho_c}$ (g/cm³)	$\dfrac{\mu_d}{\mu_c}$ (cP)	σ (dyn/cm)	D (cm)	T (cm)	ϕ	N (rps)	
Chen and Middleman (1967)	$\dfrac{d_{32}}{D} = 0.053 We^{-0.6}$	$\dfrac{0.703-1.101}{0.997-1.001}$	$\dfrac{0.52-25.8}{0.890-1.270}$	4.75–48.3	5.1–15.2	10.0–45.7	0.001–0.005	1.33–16.7	6-blade RT/in situ (photograph)
Sprow (1967a)	$\dfrac{d_{32}}{D} = 0.0524 We^{-0.6}$	$\dfrac{0.692}{1.005}$	$\dfrac{0.51}{0.99}$	41.8	3.2–10.0	22.2, 30.5	0–0.015	4.2–33.4	6-blade RT, modified turbine/sample withdrawal (Coulter counter)
Brown and Pitt (1970)	$\dfrac{d_{32}}{D} = 0.051(1 + 3.14\phi)We^{-0.6}$	$\dfrac{0.783-0.838}{0.972-0.998}$	$\dfrac{0.59-3.30}{1.0-1.28}$	1.9–50.0	10	30	0.05–0.3	4.2–7.5	6-blade RT/in situ (photograph)
Van Heuven and Beek (1971)	$\dfrac{d_{32}}{D} = 0.047(1 + 2.5\phi)We^{-0.6}$	$\dfrac{-}{0.998}$	—	8.5–49.5	3.75–40.0	12.5–120	0.04–0.35	—	6-blade RT/ encapsulation, sample withdrawal
Mlynek and Resnick (1972)	$\dfrac{d_{32}}{D} = 0.058(1 + 5.4\phi)We^{-0.6}$	$\dfrac{1.055}{1.0}$	$\dfrac{-}{1.0}$	41	10	29	0.025–0.34	2.3–8.3	6-blade RT/in situ (photograph) sample withdrawal (drop withdrawal) encapsulation)

Reference	Correlation								Apparatus
Weinstein and Treybal (1973)[c]	$d_{32} = 10^{(-2.316+0.672\phi)}\overline{\nu_c}^{0.0722}$ $\times\,\varepsilon^{-0.194}(\sigma g_c/\rho_c)^{0.196}$ (batch process) $d_{32} = 10^{(-2.066+0.732\phi)}\overline{\nu_c}^{0.047}$ $\times\,\varepsilon^{-0.204}(\sigma g_c/\rho_c)^{0.274}$ (continuous process)	$\dfrac{0.831-0.997}{0.831-0.997}$	$\dfrac{0.722-7.43}{0.722-7.43}$	3.76–36.0	7.62–12.7	24.5, 37.2	0.079–0.593	2.5–10.33	6-blade RT, unbaffled tank/in situ (light transmittance)
Brown and Pitt (1974)[d]	$d_{32} = B(\sigma/\rho_c\varepsilon_{avg}t_{circ})^{0.6}$	$\dfrac{0.783-0.838}{0.972-0.998}$	$\dfrac{0.59-3.30}{1.0-1.28}$	1.9–50.0	10, 15	30	0.05	2.1–7.5	6-blade RT/in situ (light transmittance)
Coulaloglou and Tavlarides (1976)	$\dfrac{d_{32}}{D} = 0.081(1+4.47\phi)We^{-0.6}$ (continuous process)	$\dfrac{0.972}{1.0}$	$\dfrac{1.3}{1.0}$	43	10.0	24.5	0.025–0.15	3.2–5.2	6-blade RT/in situ (photomicrography)
Godfrey and Grilc (1977)	$\dfrac{d_{32}}{D} = 0.058(1+3.6\phi)We^{-0.6}$ $d_{32} = 10^{(-3.18+0.74\phi)}$ $\times\,\varepsilon_{avg}^{-0.2755}(\sigma/\rho_c)^{0.1787}$	$\dfrac{0.783-0.829}{0.986-0.997}$	$\dfrac{2.05-8.6}{0.89-1.19}$	1.9–34.5	5.1	15.2	0.05–0.5	8.33–15.0	6-blade RT, unbaffled square tank/sample withdrawal
Arai et al. (1977)[e]	$\dfrac{d_{max}}{d_{max,0}} = (1+9Vi')^{3/5}$	$\dfrac{0.879-0.922}{1.00}$	$\dfrac{0.78-1500}{0.97}$	22	Incorrect value of (D/10) is given in the paper	12.7	<0.003	2.5–13.7	6-blade RT/In situ (photograph)

Table 12-2 (*continued*)

Authors	Correlation[a]	Physical Properties			Operating Conditions/ Geometric Parameters				Impeller/Measurement Techniques and Comments
		$\dfrac{\rho_d}{\rho_c}$ (g/cm^3)	$\dfrac{\mu_d}{\mu_c}$ (cP)	σ (dyn/cm)	D (cm)	T (cm)	ϕ	N (rps)	
Lagisetty et al. (1986)	$\dfrac{d_{max}}{D} =$ $0.125(1+4.0\phi)^{1.2}We^{-0.6}$	$\dfrac{0.88\text{--}1.47}{0.78,\,1.0}$	Non-Newtonian $\dfrac{}{1.0,\,2.1}$	20, 45.2, 50	7.25	14.5	0.02	3.33–10	6-blade RT/sample withdrawal; correlation is based on Voigt model; limited experiments used for verification of the model
Calabrese et al. (1986a)[f]	$\dfrac{d_{32}}{d_0} = (1+11.5Vi'')^{5/3}$, $Vi'' < 1$ (moderate viscosity, μ_d)	$\dfrac{0.960,\,0.970}{0.997}$	$\dfrac{96.0,\,486}{0.893}$	37.8	7.1–19.6	14.2–39.1	<0.0015	0.93–5.95	6-blade RT/In situ (photograph)
	$\dfrac{d_{32}}{D} = 2.1(\mu_d/\mu_c)^{3/8}Re^{-3/4}$ (high viscosity, μ_d)	$\dfrac{0.971\text{--}0.975}{0.997}$	$\dfrac{971\text{--}10\ 510}{0.893}$	37.8	7.1–19.6	14.2–39.1	<0.0015	0.93–5.95	—
Wang and Calabrese (1986)[g]	$\dfrac{d_{32}}{D} = 0.053We^{-0.6}$ $\times (1 + 0.97Vi^{0.79})^{3/5}$	$\dfrac{0.834\text{--}0.986}{0.792\text{--}0.997}$	$\dfrac{0.81\text{--}459}{0.52\text{--}0.89}$	0.21–47	7.1–15.6	14.2–31.2	<0.002	1.4–4.7	6-blade RT/In situ (photograph)

Calabrese et al. (1986b)[g]	$\dfrac{d_{32}}{D} = 0.053 We^{-0.6}$ $\times (1+0.91 Vi^{0.84})^{3/5}$	$\dfrac{0.692-1.101}{0.792-1.005}$	$\dfrac{0.51-520}{0.52-1.27}$	0.21–48.3	7.1–19.6	14.2–39.1	<0.005	0.93–33.4	Mainly 6-blade RT/Correlate Sprow (1967b), Arai et al. (1977), Calabrese et al. (1986a), and Wang and Calabrese (1986)
Berkman and Calabrese (1988)[h]	$\dfrac{d_{32}}{D} = 0.49 We'^{-0.6}$ $\times [1+1.38 Vi''' (d_{32}/D_p)^{1/3}]^{3/5}$	$\dfrac{0.852-0.967}{\sim 1}$	$\dfrac{0.63-204}{-}$	31.8–41.6	—	1.91	0.00057–0.001	—	Kenics static mixer/In situ (photograph)
Nishikawa et al. (1987a)	$\dfrac{d_{32}}{D} = 0.095 N_p^{-2/5} We^{-0.6}$ $\times (1+2.5\phi^{2/3})(\mu_d/\mu_c)_d^{1/5}$ $\times (\mu_d/\mu_c)_c^{1/8}$ (breakup region) $\dfrac{d_{32}}{D} = 0.035 N_p^{-1/4} We^{-3/8} D^{-3/8}$ $\times (1+3.5\phi^{3/4})(\mu_d/\mu_c)_d^{1/5}$ $\times (\mu_d/\mu_c)_c^{1/8}$ (coalescence region)	$\dfrac{0.81}{0.972}$	$\dfrac{17.0}{0.356}$	17.9	12.5	25.0	0.0045–0.36	1.3–5.0	6-blade RT/sample withdrawal; the suffix d or c outside the bracket (μ_d/μ_c) means to keep the viscosity of dispersed phase or the viscosity of continuous phase constant

(continued overleaf)

Table 12-2 (*continued*)

Authors	Correlation[a]	Physical Properties			Operating Conditions/ Geometric Parameters				Impeller/Measurement Techniques and Comments
		$\dfrac{\rho_d}{\rho_c}$ (g/cm³)	$\dfrac{\mu_d}{\mu_c}$ (cP)	σ (dyn/cm)	D (cm)	T (cm)	ϕ	N (rps)	
Nishikawa et al. (1987b)[i]	$\dfrac{d_{32}}{D} =$ $0.095 N_p^{-2/5} We^{-0.6} (T/T_0)^{-2/5}$ $\times (1 + 2.5(T/T_0)^{1/2}\phi^{2/3})$ $\times (\mu_d/\mu_c)_d^{1/5} (\mu_d/\mu_c)_c^{1/8}$ (breakup region) $\dfrac{d_{32}}{D} = 0.035 N_p^{-1/4} We^{-3/8}$ $\times (T/T_0)^{-1/4}$ $\times (1 + 3.5(T/T_0)^{1/2}\phi^{3/4})$ $\times (\mu_d/\mu_c)_d^{1/5}$ $\times (\mu_d/\mu_c)_c^{1/8} D^{-3/8}$ (coalescence region)	$\dfrac{0.81}{0.972}$	$\dfrac{17.0}{0.356}$	17.9	T/2	12–50	0.005–0.36	1.0–10.0	6-blade RT/sample withdrawal; the suffix d or c outside the bracket (μ_d/μ_c) means to keep the viscosity of dispersed phase or the viscosity of continuous phase constant

| Chatzi et al. (1989) | $\dfrac{d_{32}}{D} = 0.056(1 + 10.97\phi)We^{-0.6}$ | $\dfrac{0.8792, 0.9014}{0.9881, 0.9971}$ $\dfrac{0.4591, 0.7303}{0.5502, 0.9147}$ | 7.4, 11.5 | 7.5 | 15 | 0.01–0.03 | 2.50–5.00 | 4-blade turbine/sample withdrawal; suspending agent (polyvinyl alcohol added in the tank) |

Reproduced from Zhou and Kresta (1998a).

[a] B and b are constants.

[b] f_ϕ is the ratio of the actual mean diameter to that at $\phi = 0.1$.

[c] $\nu_c = \mu_c/\rho_c =$ continuous-phase kinematic viscosity. For batch process; $\varepsilon = [Pg_c/V(1 - \overline{\phi})\rho_c]$ (V is the volume of the fluids). For continuous process: $\varepsilon = [(P - 6Q_d\sigma/\overline{d_{32}})g_c]/V(1 - \overline{\phi})\rho_c$ (Q_d is the flow rate of dispersed phase; g_c is the gravitational constant).

[d] t_{circ} is the circulation time.

[e] Based on a Voigt model; $d_{max,0}$ is the value of d_{max} when $Vi' \rightarrow 0$; $Vi' = \mu_d\varepsilon_{avg}^{1/3}d_{max}^{1/3}/\sigma$.

[f] d_0 is the d_{32} for an inviscid dispersed phase ($Vi'' \rightarrow 0$); $Vi'' = (\rho_c/\rho_d)^{1/2}(\mu_d\varepsilon_{avg}^{1/3}d_{32}^{1/3}/\sigma)$.

[g] $Vi = (\mu_dND/\sigma)(\rho_c/\rho_d)^{1/2}$.

[h] $We' = \rho_cV_s^2D_p/\sigma$ and $Vi''' = (\rho_c/\rho_d)^{1/2}(\mu_dV_s/\sigma)$. D_p is the pipe diameter, and V_s is the superficial velocity.

[i] T_0 is a reference tank diameter.

DSD. This implies that breakage rate slows considerably as d approaches d_{max}. The long time behavior of d_{32} is uncertain. As drop sizes decrease with time, the energy required for them to disperse further increases continually. This amounts to shrinking the effective dispersion volume. Since all dispersing drops must pass through this shrinking volume, it explains the long times required to reach an equilibrium state. Lam et al. (1996) argued that their data supported the idea that turbulent intermittency caused d_{32} to decrease without limit. Blount (1995) and others have found that d_{32} actually increased at very long times. This could be due to very slow coalescence rates becoming important as breakage ceases; or possibly to Ostwald ripening or to redispersion of dispersed phase liquid collected on impeller, tank, and baffle surfaces. These considerations could have limited practical consequence, since the time to reach equilibrium decreases drastically for coalescing systems as the dispersed phase volume fraction increases. Hong and Lee (1985) measured times to equilibrium of less than 10 min for $0.05 < \phi < 0.2$. The time to achieve a dynamic equilibrium between breakage and coalescence appears to be much shorter than that to achieve inconsequential breakage in the absence of coalescence. In large scale vessels the time to reach equilibrium is longer than on the bench scale.

Using an intuitive approach, several researchers have proposed that the time for d_{32} to reach equilibrium could be described by analogy to reaction kinetics:

$$\frac{d\Omega}{d\theta} = -\alpha_1 \Omega^{\alpha_2} \quad \text{where} \quad \Omega = \frac{d_{32}(t) - d_{32}^{\infty}}{d_{32}^{\infty}} \quad \text{and} \quad \theta = N\,t \qquad (12\text{-}32)$$

where N is the impeller speed, $d_{32}(t)$ the Sauter mean diameter at time t, and d_{32}^{∞} its value at equilibrium. The terms α_1 and α_2 are analogous to the reaction rate constant and reaction order, respectively. An implicit assumption is that the entire DSD evolves similarly. For $\alpha_2 = 1$, $d_{32}(t)$ decays exponentially. Hong and Lee (1985) found this to be the case for stirred tank systems undergoing simultaneous breakage and coalescence ($0.05 < \phi < 0.2$). Al Taweel and Walker (1997) argued that data for a dilute dispersion in a Lightnin static mixer were well correlated by $\alpha_2 = 2$, where t was the transit time through the mixer.

12-2.4.1   Prediction of Transient Drop Size Distribution.   The initial stage of forming a dilute dispersion shows a broad size distribution. This is illustrated in Figure 12-12. Narsimhan et al. (1980) and Sathyagal et al. (1996) have acquired similar data. As stirring continues, drops of all size continue to break to form smaller droplets. Both impeller speed and physical properties affect the dispersion time and breadth of the DSD. Faster speeds tend to hasten dispersion and give a narrower DSD. Increases in interfacial tension and drop viscosity result in longer dispersion time and broader distributions.

The aforementioned investigators found that after a relatively short time, the DSD became normally distributed in volume, like the equilibrium DSD discussed in Section 12-2.3.2. Both Narsimhan et al. (1980) and Chang (1990) found that the data from many experiments could be collapsed to a single curve
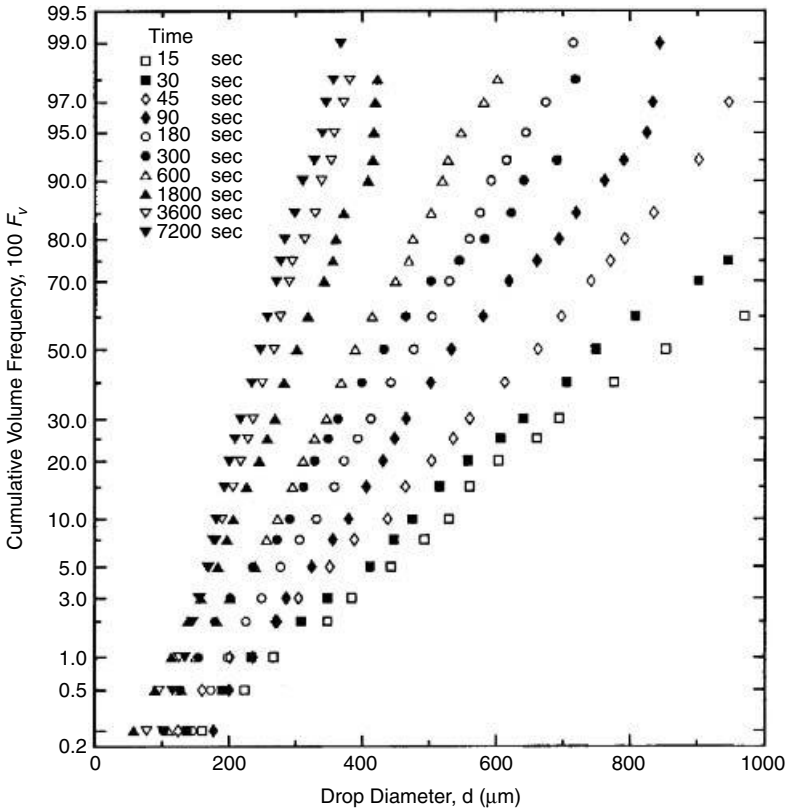
Figure 12-12 Effect of stirring time on DSD for a paraffin oil dispersed in water, $\sigma = 0.048$ N/m, $\mu_d = 0.040$ Pa $\cdot$ s. For RDT with N = 4.67 rps, D/T = 0.5, T = 0.21 m. (Data of Chang, 1990.)

by normalization with the instantaneous $d_{32}(t)$. This is shown in Figure 12-13. Therefore, the instantaneous DSD can be described by eq. (12-29), where $X(t) = d/d_{32}(t)$ and the mean and the volume standard deviation are defined similarly. Chang found that his data for a RDT were well correlated by $\overline{X} = 1.07$ and $\sigma_V = 0.27$ for both inviscid and viscous drops with $\mu_d \leq 0.140$ Pa $\cdot$ s. This is essentially the same result as for the equilibrium DSD of Section 12-2.3.2, as should be expected. Therefore, for dilute systems, a single correlation describes the time evolution of the DSD provided that $d_{32}(t)$ is known. The correlation also fits the data of Narsimhan et al. for a flat-blade turbine.

Chang (1990) used a population balance framework (discussed in Section 12-4) to develop correlations for $d_{32}(t)$. For nonviscous oils dispersed in water, he obtained

$$\frac{d_{32}(t)}{d_{32}^{\infty}} = \left(\frac{3.8 \times 10^3}{Nt}\right)^{1/6} \qquad \text{for } 100 < Nt < 3800 \qquad (12\text{-}33)$$
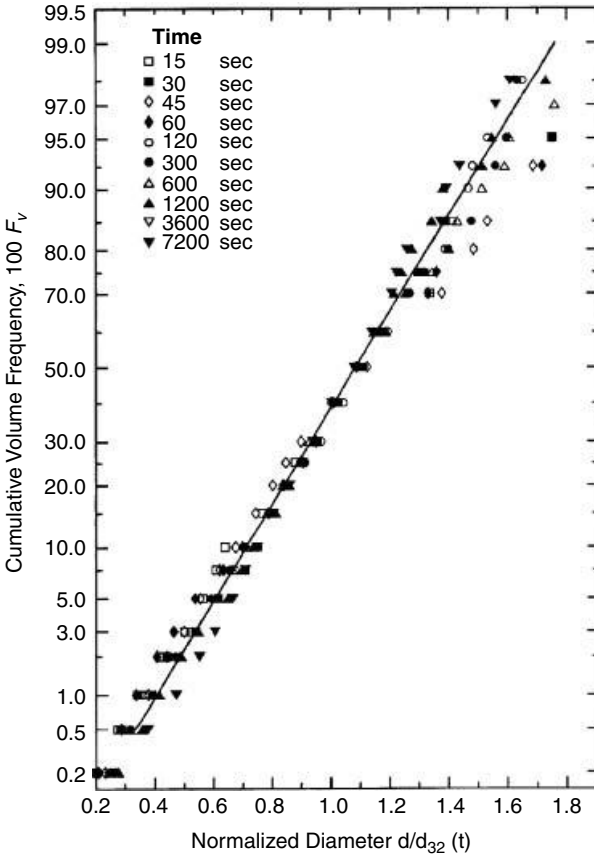
Figure 12-13   Normalized transient DSD for a paraffin oil dispersed in water, $\sigma = 0.048$ N/m, $\mu_d = 0.140$ Pa · s. For RDT with $N = 3.0$ rps, $D/T = 0.5$, $T = 0.21$ m. (Data of Chang, 1990.)

For viscous oils ($0.040 < \mu_d \leq 0.140$ Pa · s) dispersed in water, he obtained

$$\frac{d_{32}(t)}{d_{32}^{\infty}} = \left(\frac{2.1 \times 10^4}{Nt}\right)^{1/6} \qquad \text{for } 100 < Nt < 21\ 000 \qquad (12\text{-}34)$$

In his experiments with a single RDT, the tank mean circulation time was given by $N\,\bar{t}_{circ} = 3.8$. The inviscid drops reached equilibrium after about 1000 impeller passes. The viscous drops approached equilibrium more slowly, requiring about 5500 impeller passes.

Chang's results can be used to estimate the time evolution of the DSD as follows. The equilibrium Sauter mean diameter, now called d_{32}^{∞}, can be estimated using the correlations developed in Section 12-2.3.1. The value of $d_{32}(t)$ can then be obtained from the more appropriate of eq. (12-33) and (12-34). The

DSD follows from eq. (12-29) with $\overline{X} = 1.07$ and $\sigma_v = 0.27$. Chang (1990) and Calabrese et al. (1992) have summarized the method.

For impellers other than the RDT, the estimation of d_{32}^{∞} was discussed above. The dimensionless DSD for the radial impeller studied by Narsimhan et al. (1980) is also fit by $\overline{X} = 1.07$ and $\sigma_v = 0.27$, so it is reasonable to apply these values to approximate the DSD for other impellers. The weak link is prediction of $d_{32}(t)$, since it is directly dependent on circulation time. If the circulation time is known relative to the RDT work of Chang (1990), it may be possible to guess the decay rate by reference to eq. (12-32) and (12-33), since it is the number of impeller passes that determine the time to achieve equilibrium. The reader is reminded that these methods apply only to dilute dispersions and will significantly overestimate the dispersion time in the presence of coalescence.

12-2.5 Summary

Estimations of mean drop size and drop size distribution is complex, even for non-coalescing systems. They depend on the completeness of the dispersion process, local turbulent intensities (which in turn depend on impeller selection), vessel and impeller design, and operating conditions. They also depend on physical and interfacial properties which are often affected by the presence of surfactants, suspending agents, and impurities. Furthermore, concentration of the dispersed phase plays an important role. Drop size distributions are also affected by the violence of drop breakage. When barely enough energy is available to cause breakage, the result is for relatively few daughter drops to form. If the breakage event is caused by excessive energy, often orders-of-magnitude more daughter drops form. We have tried to summarize the state of knowledge for dilute systems and how this information can be applied to more concentrated dispersions. Reliable data are available for relatively few process geometries, so engineering judgment is required to apply these data to other configurations. It is difficult to predict the time to achieve a steady DSD, since this depends on drop concentration and circulation/residence time. Even in the absence of detailed information, it is important to make a rough estimate of the dispersion time relative to the process time.

Most of the studies discussed above were carried out at a bench scale. If scale-up is involved, further complications can arise. These are discussed in Section 12-8.

12-3 DROP COALESCENCE

12-3.1 Introduction

12-3.1.1 Basic Principles. Coalescence is the process of combining two or more drops to form one or more larger drops. It occurs when drops, suspended in a moving fluid, collide with one another as shown in Figure 12-14. Coalescence also occurs when drops rise or settle due to gravity to a condensed layer, as in a
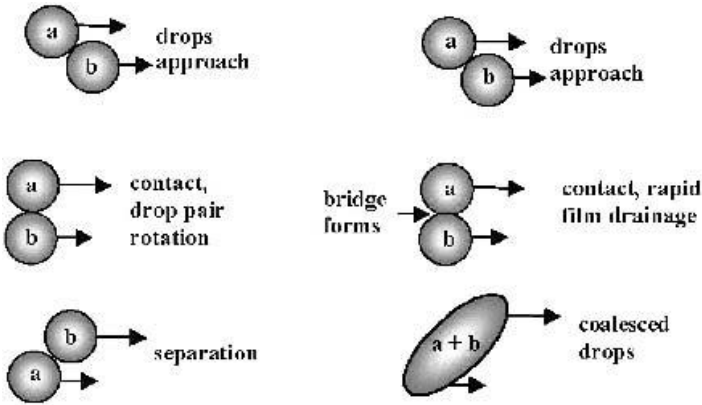
Figure 12-14 Rebounding and coalescence of two drops in shear flow.

decanter. It is also caused by impacts, such as when drops collide with impeller blades, baffles, vessel walls, static mixer elements, or fibers in coalescers. *Coalescence efficiency*, defined as the probability of coalescence per collision, depends on the collision force, the cleanliness of the interface, and the time of contact.

From an industrial viewpoint, coalescence is undesirable for some processes and desirable for others. For example, coalescence during suspension polymerization is undesirable and leads to reactor setup, or buildup of polymer on vessel walls and agitation equipment. On the other hand, mass transfer processes, such as extraction, centrifugation, and decantation, depend on coalescence to achieve desirable rates of operation. Coalescence between drops leads to intimate mixing in the newly formed larger drop.

Coalescence depends on the collision rate, which increases with dispersed phase concentration. To quantify this process, it is convenient to define a collision frequency $\xi(d, d')$, between drops of diameter d and d', which is independent of concentration. The collision frequency depends on agitation rate and drop size. As shown in Figures 12-14 and 12-17, the collision of two drops does not ensure coalescence. As the drops approach each other, a film of continuous phase fluid keeps them apart. Coalescence depends on the rupture of this film. It must drain to a critical thickness before coalescence can occur. The critical drainage time is the time it takes for the film to thin sufficiently that rupture occurs; or in other words, coalescence occurs only if the collision interval, referred to as the *contact time*, exceeds the critical film drainage time. The probability that this will occur is called the *coalescence efficiency*, $\lambda(d,d')$. It depends on a different set of hydrodynamic factors as well as drop size and physicochemical variables. Because collision frequency and coalescence efficiency depend on different factors, their contributions to coalescence are treated separately. As a result, the coalescence frequency $\Gamma(d, d')$ between two drops of diameter d and d' is defined as

$$\Gamma(d, d') = \xi(d, d')\lambda(d, d') \qquad (12\text{-}35)$$

For fine aerosol particles, $\lambda \to 1.0$ and the agglomeration rate is the collision rate. However, for liquid–liquid systems, the coalescence efficiency is often small and rate limiting. Therefore, classical agglomeration theory (e.g., Smoluchowski equation) cannot be directly applied to liquid–liquid dispersions. Coalescence is known as a second-order process ($\sim n^2$) since the coalescence rate is proportional to $\Gamma(d, d')n(d)n(d')$, where $n(d)$ and $n(d')$ represent an appropriate measure of the number of drops of size d and d', respectively.

12-3.1.2 *Empirical Approach for Turbulent Stirred Vessels*.

In turbulent stirred vessels with small but finite ϕ, drop size often varies linearly with dispersed phase concentration. For low viscosity drops, Figure 12-15 shows a linear relationship up to $\phi = 10\%$, between ϕ and drop size, expressed as $d_{32}(\phi)/d_{32}(0)$, presumably at the same agitation rate. $d_{32}(\phi)$ is the equilibrium Sauter mean diameter at dispersed phase fraction ϕ, while $d_{32}(0)$ is its counterpart for a dilute dispersion ($\phi \to 0$). This ratio also shows dependence on impeller type and D/T. Larger D/T impellers (e.g., Intermigs in Figure 12-15), promote gentler agitation throughout the vessel, enhancing coalescence. In the earlier work of Vermeulen et al. (1955), the degree of coalescence was less than for the Todtenhaupt et al. (1991) data of Figure 12-15. This could be due to different physical properties and impurities. As discussed below, coalescence rates depend on many factors and are operation dependent. However, the Vermeulen et al. data did show that the dependence of d_{32} on ϕ was nonlinear at high ϕ.

For inviscid dispersed phases, $d_{32}(0)$ is given by eq. (12-22). Since the curves of Figure 12-15 are fit by an empirical equation of the form $d_{32}(\phi)/d_{32}(0) =$
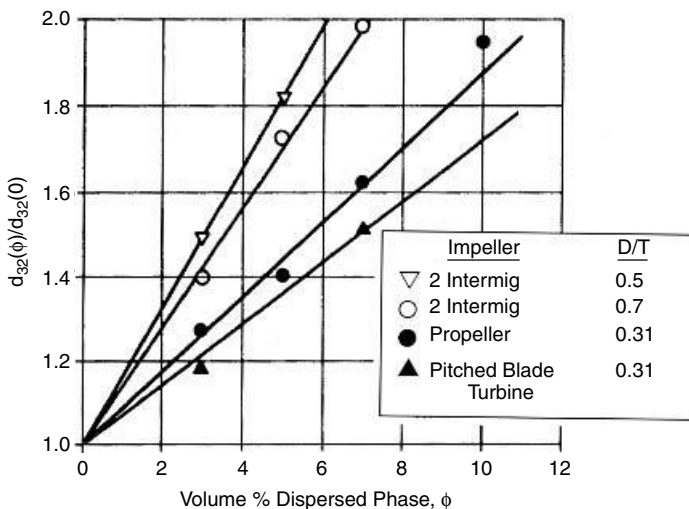

Figure 12-15 Typical dependence of drop size on dispersed phase concentration for a coalescing system. $d_{32}(\phi)/d_{32}(0)$ increases with ϕ due to coalescence. (Reproduced from Todtenhaupt et al., 1991.)

$1 + b\phi$, the data should be correlated by an equation of the form of eq. (12-30). Early investigators treated coalescence as an addendum to dispersion theory, where b ranged from 3 to 9, depending on the system and the investigator. As discussed previously, Table 12-2 summarizes much of the work done using this approach.

The use of eq. (12-30), a breakage equation, to correlate data for coalescing systems can be further rationalized by reference to eq. (12-35). Since the $b\phi$ term represents the coalescence frequency, the use of eq. (12-30) suggests that there is a constant coalescence efficiency represented by b and a constant collision rate that is proportional to ϕ. Presently, there is no systematic way to relate b to the many factors governing coalescence, and there is no way to extend the approach to viscous drops. This empirical approach, although simple to use, lacks technical interpretation and is therefore risky to apply for scale-up work.

12-3.1.3 Factors Influencing Coalescence. Drop coalescence is not as well understood as drop breakage, since the relevant physical mechanisms are more complex and data acquisition (sampling and analysis) becomes more difficult with increasing dispersed phase concentration. The collision frequency is determined largely by the dynamics of the continuous phase flow field, which determines the trajectories of the colliding drops. Calculations that account for the effect of drop deformation and other drop-surrounding fluid interactions on collision rate are difficult, and it is often assumed that the drops are rigid and behave as inertialess fluid points. For laminar flow, these calculations depend strongly on geometry and are tedious for realistic processing equipment.

For turbulent flows, the collision rate depends on the frequency at which eddies bring drops into contact. Since the drops are usually small compared to the macroscale ($L_T \gg d \gg \eta$, as in Section 12-2.3.1), isotropic turbulence theory can be used to model the collision frequency, the force with which two drops collide, and the time that they remain in contact before subsequent eddies carry them apart. These factors depend on the drop size and the magnitude of the energy dissipation rate, which depends on the impeller speed and diameter. For instance, Coulaloglou and Tavlarides (1977) show that for equal drop size and $L_T \gg d \gg \eta$, the collision frequency, $\xi(d, d)$, is given by

$$\xi(d, d) = C_{12}d^{7/3}\varepsilon^{1/3} = C_{13}d^{7/3}N D^{2/3} \qquad (12\text{-}36)$$

They show further that the approach force is given by $F \sim (d^8\varepsilon^2)^{1/3}$ and the contact time is given by $t_c \sim (d^2/\varepsilon)^{1/3}$. These quantities, derived from turbulence theory, are required inputs to models for the drainage rate of the laminar film and the coalescence efficiency, as described below.

The collision frequency and approach force increase with drop size and agitation rate. For monodisperse drops, the collision rate is of order $n^2(d)\xi(d, d)$. Contact times increase with drop size and decrease with agitation rate. Coulaloglou and Tavlarides (1977) have also modified these results to apply to unequal-sized drops.
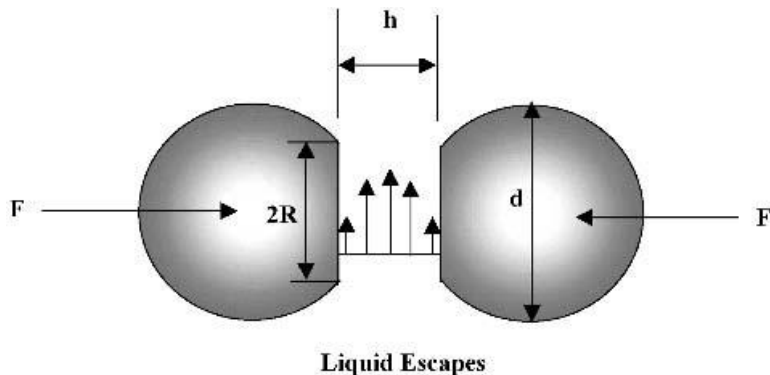
Figure 12-16   Film drainage and thinning for deformable equal-sized colliding drops.

The collision efficiency is much more difficult to quantify. Consider the collision of two equal-sized drops as illustrated by Figure 12-16. The drops approach each other with a transient force F. This force squeezes out the film of continuous phase fluid, of thickness h, trapped between the drops. The contact time should be sufficiently long so that a critical thickness is achieved, whereupon film rupture and coalescence will take place. During the impact or contact period, the drops deform and flatten, thereby increasing the surface area of contact. The degree of flattening, characterized by disk radius R in Figure 12-16, affects the film drainage time since the amount of entrapped film and the resistance to drainage both increase with increasing contact area. The film-thinning rate also depends on the mobility of the interface between the drops and the draining film. If the interface is rigid, the drop fluid remains stationary and is not dragged in the direction of the draining film. A rigid interface offers the maximum resistance to film drainage due to a no-slip condition at the film–drop interface. A mobile interface is one in which the drop phase fluid is dragged in the direction of film drainage, so that the velocity is equal on both sides of the interface. A mobile interface offers the minimum resistance to film drainage, due to a "complete slip" condition at the film–drop interface. It was shown by Murdoch and Leng (1971) that when interfaces are immobile, the drainage flow develops a parabolic velocity profile instead of the plug flow profile that exists for mobile surfaces. Most interfaces are partially mobile, falling somewhere between the two limits. The film drainage time increases as the interface becomes less mobile.

Physicochemical factors affecting coalescence efficiency are complex and often difficult to quantify. A high drop viscosity promotes coalescence by increasing resistance to leading surface deformation during impact, but it inhibits coalescence by making film drainage more difficult. The latter factor is usually dominant. Suspension polymerizations go through a sticky stage. This is caused by the collision of partially polymerized drops having sticky surfaces.

Interfacial tension is an important physicochemical factor. Decreasing the interfacial tension inhibits coalescence since it leads to greater flattening for a

given impact force. Surfactants, suspending agents, and certain impurities reduce coalescence by immobilizing drop-film interfaces and increasing disk size, due to lower interfacial tension. Small quantities of surface-active impurities can significantly reduce coalescence rates. Suspending agents and surfactants are designed to act in the same way. Suspending agents are adsorbed more slowly at the interface than surfactants, due to their higher molecular weights and thus slower diffusion rates. Typical molecular weights for surfactants ≈ 300 and for suspending agents $\approx 30\,000$. However, once polymeric suspending agents are adsorbed at the drop interface, they can form physically coherent "skins," which are a solid polymer network and prevent coalescence for days, even at stagnant conditions.

The film drainage time is also affected by the magnitude and duration of collision forces, which depend not only on external hydrodynamic conditions but also on the electrochemical state of the interface. It would appear at first glance that higher approach forces would lead to faster film drainage. But this is not necessarily the case, since increasing this force promotes more flattening, and excessive pressure buildup, resulting in rebounding of drop pairs. This is another reason why coalescence is promoted by "gentle collisions."

In certain cases when drops approach one another, repulsive forces begin to act. For instance, increasing the pH inhibits coalescence in water–organic systems due to increased surface adsorption of OH^-, causing stronger repulsive forces. Tobin and Ramkrishna (1992) found that absorption of CO_2 from the headspace in a stirred tank decreased the pH and caused an increased coalescence rate of organic drops in water. Ionic surfactants inhibit coalescence by increasing electrostatic repulsive forces. For such systems, increasing the ionic strength by the addition of electrolytes promotes coalescence by decreasing the effect of double-layer protection. In summary, electrical charges can create either a force of attraction or a force repulsion between drops. Coalescers employed by the petroleum industry use charged plates to promote coalescence of saltwater drops in crude petroleum fractions.

It is difficult to develop a single model for coalescence efficiency because of the numerous factors influencing the film drainage rate and therefore the coalescence frequency. Even if all impurities could be eliminated, it would still be difficult to interpret the most systematic experiments in surfactant-free and charge-neutral systems. For instance, in a turbulent stirred tank, increasing the agitation rate (N or ε) at constant ϕ increases the collision rate by increasing the collision frequency directly and by increasing the number of drops, due to increased dispersion. However, increased agitation decreases the coalescence efficiency by increasing the approach force and by decreasing the contact time. The decrease in drop size inhibits coalescence due to decreased collision frequency but will promote coalescence by reducing drop flattening. Uncontrolled impurities, unqualified electrical forces, and other interfacial phenomena will further complicate interpretation. As a result, considerable judgment must be exercised when scaling-up from lab scale studies or in using empirical correlations. Mechanistic models are discussed below.

Fundamental studies have focused on the more complex film drainage step, by precisely monitoring the coalescence of a single drop at a plane interface or the interaction between two colliding drops under precisely controlled conditions. These studies elucidate the complexities of the coalescence process.

12-3.1.4 *Coalescence Mechanisms in Mixing Flows*. As explained previously, coalescence between colliding drops occurs when the film of continuous phase fluid separating them thins to a critical thickness during contact. Once the critical thickness is reached, a hole opens up which enlarges rapidly, resulting in coalescence and internal drop mixing. Sometimes the combination is so rapid that internal pressures cause satellite drops to be ejected from opposite ends of the newly formed oscillating drop. If the force holding drops in contact is brief and insufficient drainage occurs, coalesce will not take place.

The approach forces needed to bring about film drainage can be hydrodynamic, hydrostatic, or physicochemical. As discussed above, hydrodynamic forces are bought about by shear (laminar or turbulent) and are of finite duration. Such forces can be intense but are definitely not constant during drop contact. Forces can also be due to gravity acting on density differences between the drops and the continuous phase. Gravitational forces are constant and are of long duration. They control coalescence times for drops approaching settled layers. The film thinning mechanism still applies even though there is no critical time beyond which departure occurs. The time for an emulsion or suspension to settle completely can be quite long, particularly if the phases have similar densities or if interfaces contain surfactants, repulsive charges, or impurities.

Solid surfaces, particularly those easily wetted by the dispersed phase, can be major collectors of drops. In the case of a rotating impeller, drops collect and coalesce on blade surfaces to form a condensed film. As this film grows in thickness, it flows under centrifugal forces to the impeller tips and disperses into tiny drops. This process is similar to the breakup of a cylindrical liquid jet. A film of dispersed phase can also collect on free surfaces, baffles, tank walls, and the impeller shaft, where the surface vortex meets the shaft. In the case of emulsion and suspension polymerization, coalescence also leads to fouling of heat transfer surfaces.

Electrostatic forces are used in electrostatic precipitators to coalesce aqueous brine from crude oil. Fibrous beds are used to coalesce flowing drop suspensions where fibers are chosen that will be wetted by the dispersed phase. As the drop suspension is forced through the bed, drops coalesce and build up a wet layer on the fibers. This layer continues to thicken until drag forces caused by the flow result in break-off. The departing drops, however, are much larger than the incoming drops, so the device achieves its desired function. Centrifuges amplify gravitational forces. The cream separator is a good example.

12-3.1.5 *Practical Classification of Coalescing Systems*. While it has been stated repeatedly that coalescence is highly complex and that scale-up is difficult, not all liquid–liquid systems are complex. A simple way to characterize

systems is to measure the time for a dispersion to separate. The tested system is thoroughly agitated to form either a water-in-oil (w/o) or oil-in-water (o/w) dispersion, depending on the system under investigation. Following 3 to 5 min of vigorous agitation or shaking, the system is allowed to settle and the time to form two distinct layers is noted. Complete separation may not occur, but two distinct layers ought to be visible. Guidelines for scale-up, based on separation time, are given in Table 12-3. When applying this method, be aware that density differences affect both settling time and the forces acting on the drops that cause film drainage. If coalescence appears to be severe and undesirable, reverse the phases if possible and repeat the test. Finally, compare the times for coalescence to see which phase should be dispersed.

A more quantitative method is to use a baffled stirred vessel containing a light transition probe similar to the one described by Rodger et al. (1956). Record the probe output at moderately high levels of agitation. After a constant baseline is established, reduce the agitation to just maintain full suspension and observe changes in the recorded output. The probe can be calibrated to read interfacial area. The slope at the time just after speed transition is proportional to the rate of coalescence under dynamic as opposed to static conditions. This method is insensitive to effects of density difference and is described by Howarth (1967).

If the interfacial area appears to remain constant after decreasing the agitation, the system can be considered to be noncoalescing. If not, the steepness of the

Table 12-3   Characterization of the Coalescibility of Immiscible Liquid–Liquid Systems

Time to Separate	Characterization	Process Implication
<10 s	Very fast coalescence	Expect severe scale-up problems for agitated vessels, provide more dispersion opportunities. For example, use multiple impellers, provide for strong flow at the top and bottom of the vessel. Consider use of long static mixers.
<1 min	Fast coalescence	Scale-up problems can be managed by careful selection of mixing equipment. Use multiple impellers, eliminate unnecessary internals, and provide for complete circulation.
2–3 min	Moderate coalescence	Problems are less severe, design for coalescence. Use large impellers for dispersion and flow. Maintain ample flow at the top/bottom surfaces. Often can treat this case as noncoalescing.
>5 min	Slow coalescence	Application can be treated as dispersion only.

slope is a measure of the severity of coalescence. Care must be taken when choosing the slow speed to ensure that settling does not occur.

12-3.2   Detailed Studies for Single or Colliding Drops

12-3.2.1   *Coalescence of a Single Drop with a Plane Interface*. Numerous studies have dealt with the coalescence of a single drop at a plane interface created by a settled, coalesced layer. These studies involve measurement of the elapsed time from drop arrival at the interface to coalescence. Many factors influence the rest or film drainage time, including the age of the interface. Times are correlated using film drainage theory. The approach force acting on the drop is constant and caused by gravity (density difference). Although drop rest time studies are relatively simple compared to dynamic measurements, they yield useful information concerning film drainage rates and the critical film thickness necessary for coalescence to occur. The nearly static system permits in situ transient film thickness measurements to be made (e.g., by interferometry) during the thinning process. The earliest studies were reported by Gillespie and Rideal (1956), followed by Charles and Mason (1960), Allan and Mason (1962), MacKay and Mason (1963), Jeffreys and Hawksley (1965), Lang and Wilke (1971a, b), Hartland and Jeelani (1987), Hartland (1990), and others.

The simplest model for film drainage assumes that the conditions affecting the drainage rate are time invariant. By analogy to squeezing flow between parallel disks (lubrication approximation), the rate at which the film thins is given by

$$\frac{dh}{dt} = -\alpha_3 h^3 \tag{12-37}$$

The interface is assumed to be mobile but motionless. The initial separation distance is h_0, and h is the separation distance after time t. The constant α_3 accounts for all the factors that determine the drainage time. Integration of eq. (12-37), with initial condition $h = h_0$ at $t = 0$, leads to

$$\frac{1}{h^2} - \frac{1}{h_0^2} = \alpha_4 t \tag{12-38}$$

Estimation of the initial film thickness h_0 is not critical, since initial thinning is fast. After a short time, $h^{-2} \gg h_0^{-2}$, allowing evaluation of the drainage rate constant α_4, from precise measurements of film thickness versus time. Estimates for the film thickness at rupture from 25 to 500 Å have been reported. Studies involving mass transfer from drops show that in the presence of mass transfer, coalescence times are much shorter.

12-3.2.2   *Coalescence of Two Colliding Drops*. Refer again to Figure 12-16, which is a schematic diagram showing the collision between two drops of equal diameter d. The leading edges of both deformable drops become flattened on collision. This deformation creates a parallel disklike geometry.

Therefore, the dynamics of film drainage can be represented as a squeezing flow between two disks of radius R, separated by distance h, that approach each other due to force F. The relationship governing this process is given by eq. (12-39), which applies only to an immobile interface:

$$\frac{dh}{dt} = -\frac{2F}{3\,\pi\,\mu_c R^4}h^3 \tag{12-39}$$

The reasoning is similar to that for drops resting at a flat liquid–liquid interface. Equation (12-37) is the same as eq. (12-39) with $\alpha_3 = 2F/3\pi\mu_c R^4$ equal to a constant. The rate of film thinning (dh/dt) depends, among other things, on the approach force F and the radius R of the disks. The approach force and disk radius are not independent, since $F \sim \pi R^{2\cdot}(4\sigma/d)$. That is, the excess pressure in the film must be on the order of the Young–Laplace pressure. Using this result to substitute for R leads to

$$\frac{dh}{dt} = -\frac{32\,\pi\,\sigma^2}{3\,\mu_c d^2\,F}h^3 \tag{12-40}$$

Equation (12-40) shows that the film drainage rate is inversely proportional to the approach force, again demonstrating that coalescence is promoted by gentle collisions. Integration of eq. (12-40) with initial condition $h = h_0$ at $t = 0$ and final condition $h = h_c$ at $t = \tau$ leads to

$$\tau = \frac{3\mu_c d^2 F}{64\pi\sigma^2}\left(\frac{1}{h_c^2} - \frac{1}{h_0^2}\right) \tag{12-41}$$

where h_c is the critical thickness required for film rupture. The initial distance h_0 is usually much greater than h_c, so that $h_c^{-2} - h_0^{-2} \approx h_c^{-2}$. The time required for film rupture is τ. Coalescence occurs only if the contact time t_c is greater than τ. There are several versions of this equation that reflect variable approach force, circulation in the drop, and the mobility of the drop interface. Further details can be found in Murdoch and Leng (1971), Scheele and Leng (1971), and Chesters (1991). Further discussion is given in Section 12-3.3.

Scheele and Leng (1971) and Murdoch and Leng (1971) investigated the coalescence behavior of colliding drop pairs. Anisole drops ($\Delta\rho = 0$, d = 3 mm) suspended in water were fired at one another from nozzles and their movement filmed at 1000 fps. Figures 12-17 and 12-18 show the interaction patterns for drop pairs that rebound (bouncing) and coalesce, respectively. As drops left the nozzle, an oscillation was established that affected the curvature of the leading edge at impact. Drops having more pointed leading edges at impact coalesced, as seen in Figure 12-18. Drops striking with a blunt leading edge usually bounced apart, as seen in Figure 12-17. As they traveled toward each other, the leading-edge shape oscillated between pointed and blunt. Therefore, changing the nozzle spacing changed the shape of the leading surface at impact. The measured coalescence efficiencies varied with separation distance from 25 to 100%, as determined
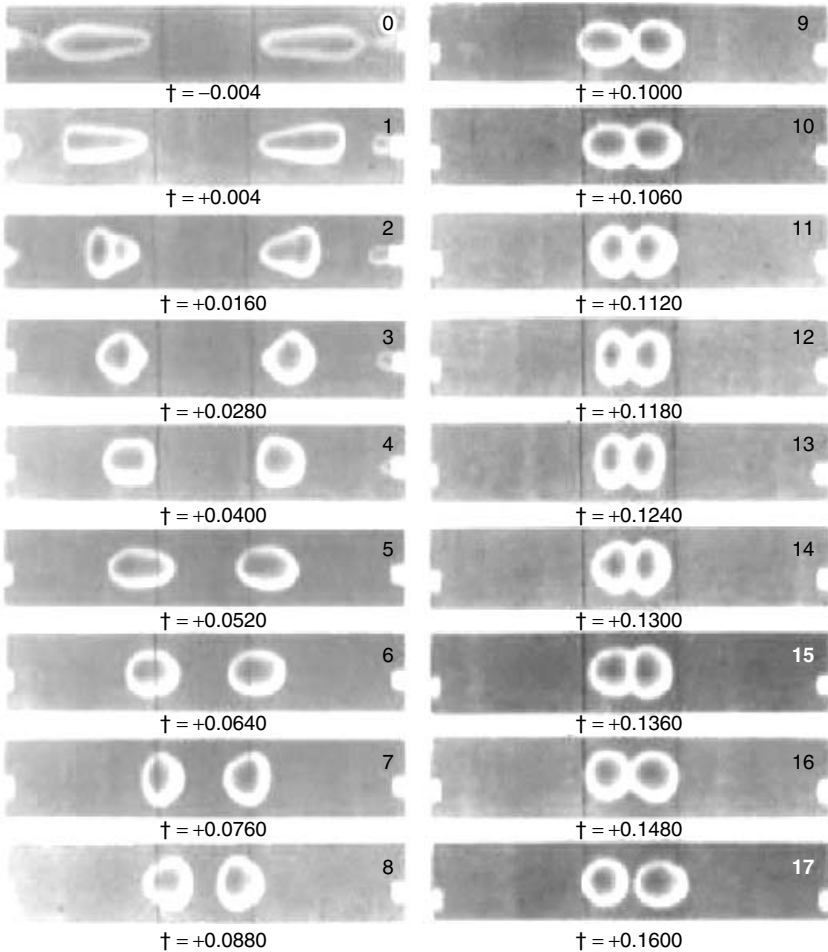
Figure 12-17 Rebounding (bouncing) of colliding anisole drop pairs in water. Times are in seconds before (−) or after (+) drops become independent of the nozzle. (Reproduced from Scheele and Leng, 1971.)

by witnessing 100 events per distance setting. Figure 12-19 shows that coalescing pairs (upper half) had smaller disk radii during contact than bouncing pairs (lower half). The run numbers refer to a specific filmed experiment of single drop pair collisions.

    There are many theories of how actual rupture occurs and at what thickness it happens. For example, a hypothesis by Vrij (1966) suggests that as hydrodynamic thinning proceeds, a point is reached where van der Waals attractive forces dominate over surface (interfacial tension) forces. Therefore, surface waves develop and become unstable, creating a hole where the film is thinnest. Film thickness at rupture was estimated to be in excess of 100 Å.
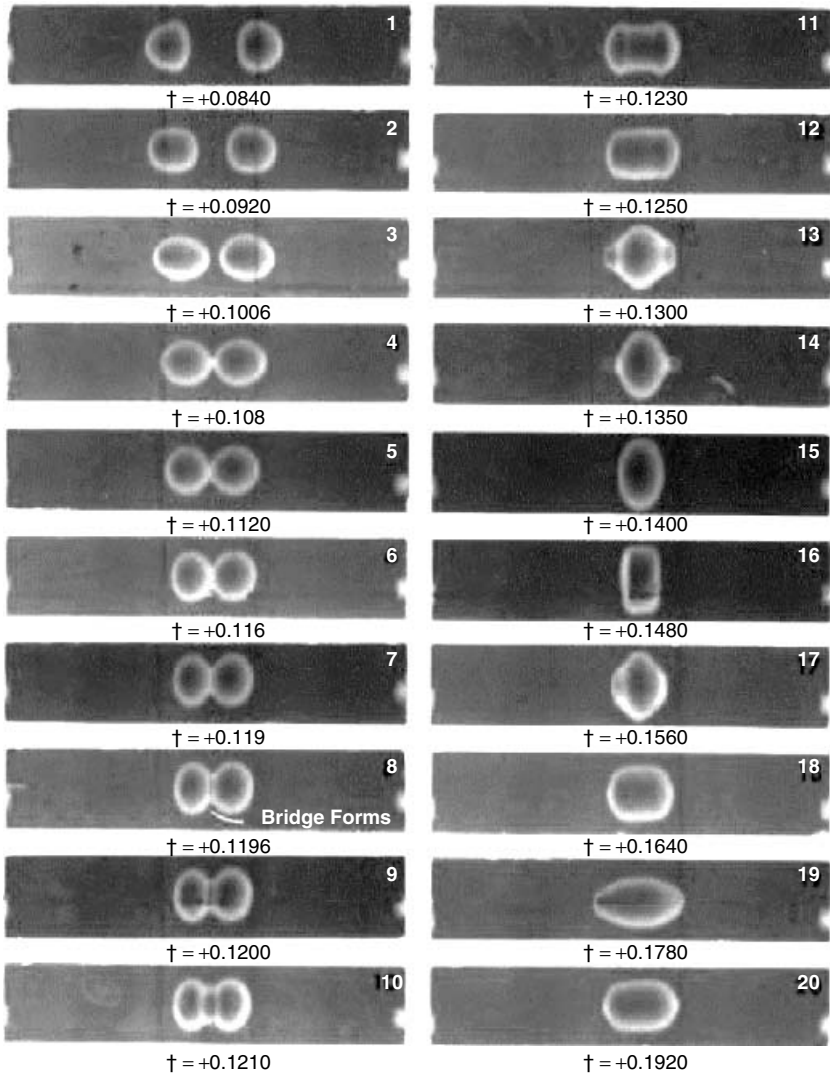
Figure 12-18   Coalescence of colliding anisole drop pairs in water. Times are in seconds after (+) drops become independent of the nozzle. (Reproduced from Scheele and Leng, 1971.)

12-3.2.3 Practical Implications of Single Drop and Drop Pair Studies. The observations made from detailed single drop and drop pair studies have several practical implications, which complement the discussion of Section 12-3.1:

- If sufficient drainage occurs during the contact interval, a critical thickness is reached and the drops will coalesce. This requires that τ in eq. (12-41) be
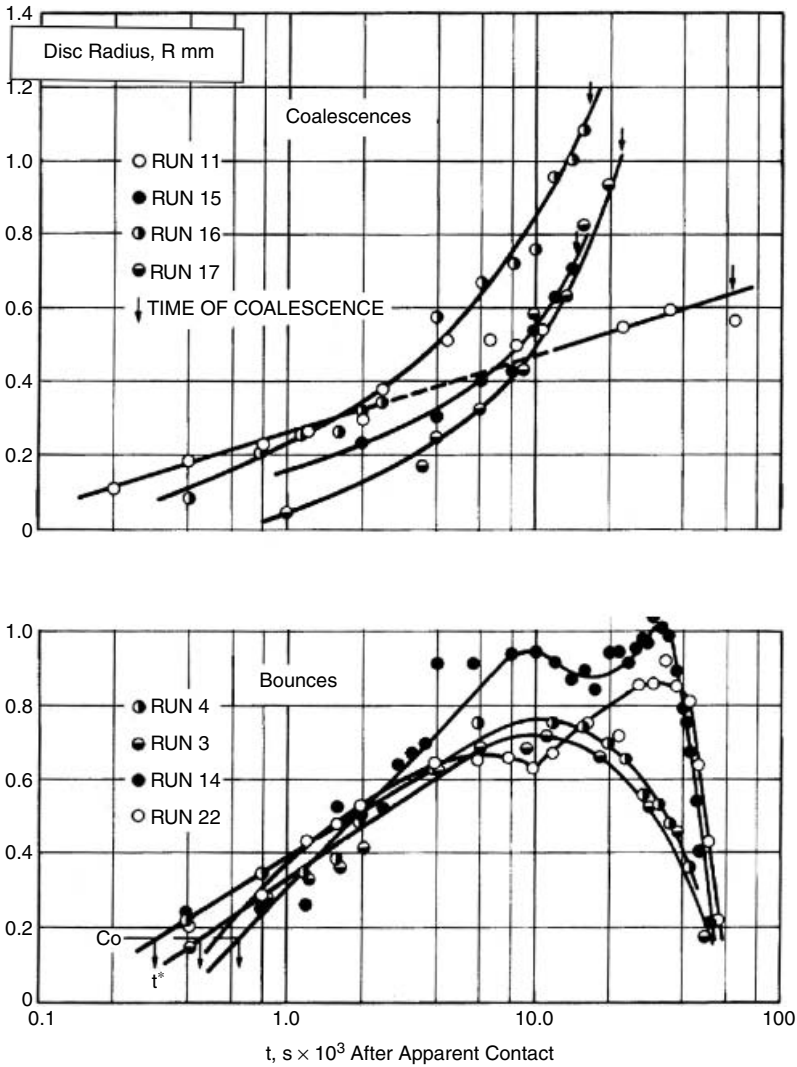
Figure 12-19 Expansion/contraction of apparent contact radius with time for coalescing and bouncing drops. (Reproduced from Scheele and Leng, 1971.)

equal to or less than the contact time. If insufficient drainage occurs during the contact interval, the drops depart one another. A higher contact force, F, decreases drainage rates by creating larger disk radii, thereby increasing the time required for coalescence.

- Low interfacial tension leads to greater flattening upon contact, thereby trapping more continuous phase fluid. This increases the drainage time and decreases the likelihood of coalescence. Surfactants normally lower

the interfacial tension, σ, and therefore reduce coalescence probability. Adsorbed surfactants also immobilize the drop–film interface. This also affects the slip velocity of the draining film, further reducing coalescence probability.

- A higher continuous phase viscosity increases the resistance to film drainage by partially immobilizing the drop–fluid interface. This reduces coalescence probability. If two similar volumes of immiscible liquids are dispersed, the fluid having the higher viscosity will normally become the continuous phase. The first attempts to produce suspension polymers used sugar to thicken the suspending phase and to retard coalescence.

- Solids trapped in the thinning film prevent critical thicknesses from being reached, and therefore reduce coalescence probability. Solid particles have been used as suspending agents in suspension polymerization processes.

- The argument put forth in Section 12-2, that P/V be maintained constant for scale-up in order to maintain equal drop size under turbulent conditions, does not hold true for scaling-up of coalescing systems.

12-3.3   Coalescence Frequency in Turbulent Flow

One of the earliest attempts to quantify coalescence frequencies was the work of Howarth (1967). A procedure was used that is similar to the one described in Section 12-3.1.5. A steady dispersion was established at a high agitation rate. The stirrer speed was then lowered so that only coalescence occurred, at least initially. Howarth defined a global or macroscopic coalescence frequency as the initial slope of a plot of interfacial area (related to d_{32}) versus time and demonstrated that systematic experiments could be conducted to determine the effect of various system variables on coalescence rate. Since the coalescence frequency depends strongly on drop diameter, most models are based on the approach discussed below.

The coalescence frequency, $\Gamma(d, d')$, is the product of the collision frequency, $\xi(d, d')$, and coalescence probability, $\lambda(d, d')$, as shown by eq. (12-35). A schematic diagram illustrating how models for $\Gamma(d, d')$ are developed for flow-driven collisions is given in Figure 12-20. The diagram follows the overview given by Chesters (1991). From a hydrodynamic viewpoint, two separate models are developed. The model for the external flow surrounding the drops produces the collision frequency, $\xi(d, d')$, approach force, F, and contact time, t_c. This model can be for laminar or turbulent flow, depending on the contacting equipment and process variables. The model for the internal flow yields the film drainage time. This model is that for a squeezing flow, driven by F and constrained by t_c of the external model. Given the dimensions of the draining film, this is a viscous model, usually assumed to be a lubrication flow.

The coalescence efficiency is determined by comparing the time to reach critical thickness with the available contact time determined by the external flow model. The approach of Figure 12-20 allows development of a variety of models. Whereas the form of $\xi(d, d')$ depends on the process flow field, that for $\lambda(d, d')$
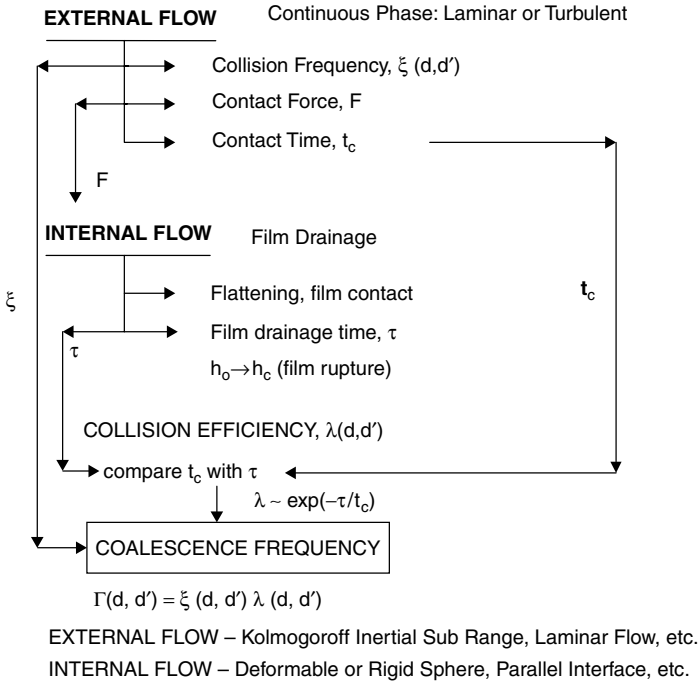
Figure 12-20 Model for coalescence frequency.

depends on interface mobility and the physicochemical and electrostatic state of the interface. Chesters (1991) demonstrates how laminar and turbulent models for $\xi(d, d')$ are developed, as well as how models for $\lambda(d, d')$ that apply to rigid spheres and mobile, partially mobile, and immobile interfaces are developed. His review is excellent and does not need repeating here. Chesters gives an example by application of the method to simple shear flow. Here we provide one of the earliest examples of the approach in the form of the model developed by Coulaloglou and Tavlarides (1977) for turbulent stirred tank systems.

The model developed by Coulaloglou and Tavlarides (1977) for turbulent stirred tanks applies to drops whose collision rates are determined by interaction with eddies that fall within the inertial subrange of isotropic turbulence ($L_T \gg d \gg \eta$). For equal-sized drops, assuming uniform energy distribution throughout the vessel, the collision frequency is given by eq. (12-36). For unequal-size drops, these authors obtained

$$\xi(d, d') = C_{14}(d^2 + d'^2) \cdot (d^{2/3} + d'^{2/3})^{1/2} \, \varepsilon^{1/3} \tag{12-42}$$

where ε is the energy dissipation rate typical of the quiescent regions of the tank; $\varepsilon/\varepsilon_{avg} \leq 0.1$. Equation (12-42) was derived by assuming that the collision mechanism was similar to that for molecules in the kinetic theory of gases. As shown in Figure 12-20, the coalescence efficiency, $\lambda(d, d')$, is described in terms

of the time, τ, required for sufficient film drainage to take place compared to the time that drops remain in contact with one another, t_c. If $t_c > \tau$, coalescence occurs, and if $t_c < \tau$, drops fail to coalesce. This is a simple concept, having a somewhat unrealistic yes or no criterion. Accordingly, coalescence efficiency for drop diameters d and d' is expressed as

$$\lambda(d, d') = C_{15}\, e^{-\tau/t_c} \tag{12-43}$$

For drops having immobile interfaces, Coulaloglou and Tavlarides (1977) show the drainage time for unequal size drops to be

$$\tau = \frac{3}{16}\frac{\mu_c F}{\pi\sigma^2}\left(\frac{1}{h_c^2} - \frac{1}{h_o^2}\right)\left(\frac{d\,d'}{d + d'}\right)^2 \tag{12-44}$$

Equation (12-44) reduces to (12-41) for $d = d'$. The drops are brought into contact by eddies whose size is of order $d + d'$. Consistent with eq. (12-14), $\overline{v'(d + d')^2}$ is the mean-square turbulent velocity difference across these eddies and is given by

$$\overline{v'(d + d')^2} \approx \varepsilon^{2/3}(d + d')^{2/3} \tag{12-45}$$

This is consistent with eq. (12-17). The authors argue that the average contact force, F, is given by

$$F \approx \rho_c \overline{v'(d + d')^2}\left(\frac{d\,d'}{d + d'}\right)^2 \tag{12-46}$$

Combining eq. (12-45) and (12-46) and substituting into eq. (12-44) yields

$$\tau = \frac{\mu_c\rho_c\varepsilon^{2/3}(d + d')}{\sigma^2}\left(\frac{1}{h_c^2} - \frac{1}{h_o^2}\right)\left(\frac{d\,d'}{d + d'}\right)^2 \tag{12-47}$$

The contact time, t_c, is proportional to the eddy arrival time for eddies of size $d + d'$:

$$t_c \approx \frac{(d + d')^{2/3}}{\varepsilon^{1/3}} \tag{12-48}$$

Since drop volumes are additive upon coalescence, it is convenient to write quantities in terms of drop volume, v, rather than diameter. Inserting eqs.(12-47) and (12-48), into (12-43) with $d \sim v^{1/3}$ gives the following result for coalescence efficiency when the interface is immobile:

$$\lambda(v, v') = C_{15}\exp\left[-\frac{C_{16}\rho_c\mu_c\varepsilon}{\sigma^2}\left(\frac{v^{1/3}\,v'^{1.3}}{v^{1/3} + v'^{1/3}}\right)^4\right] \tag{12-49}$$

Equation (12-49) expresses the coalescence efficiency in terms of drop volumes (v, v'), physical properties (μ_c, ρ_c, σ), and the energy dissipation rate, ε, for quiescent regions of the vessel. It should be noted that for fully mobile and rigid

interfaces, the drop viscosity does not play a role. For a partially mobile interface, the drop viscosity contributes to interface immobility.

It is thus possible to combine eqs. (12-42) and (12-49) using (12-35) to give the coalescence frequency under agitated conditions:

$$\Gamma(v, v') = C_{17}(v^{2/3} + v'^{2/3}) \cdot (v^{2/9} + v'^{2/9})^{1/2} \, \varepsilon^{1/3}$$

$$\times \exp\left[-\frac{C_{16}\rho_c\mu_c\varepsilon}{\sigma^2} \left(\frac{v^{1/3}v'^{1/3}}{v^{1/3} + v'^{1/3}} \right)^4 \right] \qquad (12\text{-}50)$$

For equal-sized drops, eq. (12-50) is reduced to

$$\Gamma(v, v') = C_{19}v^{7/9}\varepsilon^{1/3} \exp\left[-\frac{C_{18}\mu_c\rho_c\varepsilon v^{4/3}}{\sigma^2} \right] \qquad (12\text{-}51)$$

As noted earlier, ε is the local energy dissipation rate, so eq. (12-50 and 51) can be used for spatially dependent calculations. For constant power number and relatively uniform energy dissipation in the circulation region of the tank, $\varepsilon \sim N^3D^2$ and the dependency on impeller speed and diameter can be established. The terms in eq. (12-50) are consistent with practice and our discussion in Section 12-3.1.3. The coalescence frequency $\Gamma(v, v')$ is independent of the volume fraction of dispersed phase. The coalescence rate can be obtained from the coalescence frequency by accounting for the number of drops of size v and v'. This is best demonstrated by reference to the population balance equations discussed in Section 12-4.

Although difficult to apply in practice, models for coalescence rate provide an appreciation for the physical phenomena that govern coalescence. They also provide an appreciation for why it is difficult to interpret stirred tank data or even to define the appropriate experiment. For instance, it can be clearly seen from eq. (12-49) to (12-51) that the collision frequency increases with ε, whereas the coalescence efficiency decreases with ε. For constant phase fraction, the number of drops also increases with ε. The models for coalescence of equal-sized drops are quite useful to guide the interpretation of data that elucidate the time evolution of both mean diameter and drop size distribution during coalescence. To this end, Calabrese et al. (1993) extended the work of Coulaloglou and Tavlarides (1977) to include turbulent stirred tank models for rigid spheres and deformable drops with immobile and partially mobile interfaces. The later model accounts for the role of drop viscosity. In practice, models for unequal-sized drops are even more difficult to apply, but they do suggest that rates are size dependent. They are useful in the application of the population balance models discussed in Section 12-4.

Numerous authors have developed models for coalescence frequency. These include the models of Muralidhar and Ramkrishna (1986), Das et al. (1987), Muralidhar et al. (1988), Tsouris and Tavlarides (1994), and Wright and Ramkrishna (1994), for turbulent stirred tanks, as well as those of Davis et al. (1989),

Vinckier et al. (1998), and Lyu et al. (2002) for laminar flows and extruder applications. The models differ in how they describe the film drainage and/or drop collision process. Although the effect of surface charge and absorbed surfactant at the interface can be addressed in principle, these are rarely considered, due to their complexity. Although some models have been validated in a global sense, there has been little quantitative validation of dependencies on system variables.

12-3.4 Conclusions, Summary, and State of Knowledge

It is obvious that coalescence is a complex phenomenon. Here we have focused on creating an overall understanding rather than presenting an exhaustive literature review. We apologize for the omission of important studies not reported. We conclude this section by reiterating some important points and by providing additional practical observations.

- One must consider whether coalescence is desirable or undesirable for the application.
- Although it is difficult to apply the fundamental equations of this section, it is useful to use them to determine the effects that variables have on coalescence rates.
- There are regions close to the impeller where dispersion predominates. For scale-up under geometrically similar conditions, the effective dispersion volume shrinks with increasing vessel size.
- There are large regions in a vessel where coalescence can occur. Gentle agitation promotes coalescence because it provides for longer contact times enabling more film drainage to take place.
- Bench scale processes may occur at steady-state conditions, while larger scale industrial processes may not.
- Coalescence rates depend on both dispersed phase concentration and physicochemical factors. Except for strongly coalescing systems, coalescence effects are minimal at concentrations less than 5%.
- In practice, it is helpful to characterize coalescence rates by the simple methods presented in Section 12-3.1.5.
- Models for coalescence frequency show the importance of agitation rate, physicochemical phenomena, and interfacial properties on coalescence. This information is broadly useful for explaining the behavior of stirred vessels, decanters, extractors, and centrifuges, as well as how to prevent coalescence. It is also useful in the determination of which phase will tend to dominate as the continuous phase and in the interpretation of phase inversion phenomena.
- Scale-up is discussed in Section 12-8. Since different scale vessels have different proportions of drop time spent in coalescence and dispersion zones, it is a major challenge to design for duplicate results. One promising approach is to use CFD to create circulation time and energy dissipation rate profiles

at the various scales under consideration. Assuming that coalescence dominates in regions where $\varepsilon_{local}/\varepsilon_{avg} < 0.1$ and that dispersion dominates in regions where $\varepsilon_{local}/\varepsilon_{avg} \geq 10$. CFD enables one to see what effects design variables have on the size of and residence time in these regions. For example, using more or larger impellers in the larger vessel can be a way to increase the dispersion region and decrease the circulation time. CFD can guide the selection process.

- Surfactants, suspending agents, and other stabilizers can make a system totally noncoalescing. For such systems, scale-up becomes a dispersion and kinetics problem.

12-4 POPULATION BALANCES

12-4.1 Introduction

Population balances are a set of mathematical tools that enable one either to predict the time evolution of the DSD or to determine specific information, such as breakage frequency and daughter size distribution, or collision frequency and coalescence efficiency, from an analysis of time-variant drop size data. They were first developed by Valentas et al. (1966) and Valentas and Amundson (1966), as applied to liquid–liquid dispersions. These techniques have been used for both batch and continuous systems and for steady state as well as unsteady conditions.

Population balances are analogous to material balances, but instead of applying them to each chemical species, they are applied to each drop size class comprising the entire DSD. Therefore, accumulation and depletion terms are referred to as *birth* and *death rates* for a drop of specific diameter or volume. Figure 12-21 shows a general scheme for the events taking place. Within the enclosure, or control volume, are drops of volume v. The population of these drops is determined as follows. Drops of volume v enter by convection and because they are formed by the coalescence of smaller drops and the breakage of larger drops. Drops of volume v leave by convection and because they are depleted as they themselves break and/or coalesce. It is important to note that both breakup and coalescence produce a gain and a loss to the control volume or size class, as indicated by the arrows.

As discussed above, population balance models account for the influent and effluent of drops into the control volume. The control volume can be the entire tank or a particular region of the tank. The resulting equations are referred to as *integro-differential equations*. Analytical solutions of these equations exist only for unreasonably simplistic assumptions. Usually, the equations are solved by numerical methods, either by direct numerical integration or by a statistical simulation such as a Monte Carlo technique. Several authors opt for simplifying assumptions, such as imparting similarity conditions on one or more variables. One similarity argument can be illustrated by reference to Figure 12-13, which shows that the shape of the DSD is time independent. The solution methods are beyond the scope of this chapter.
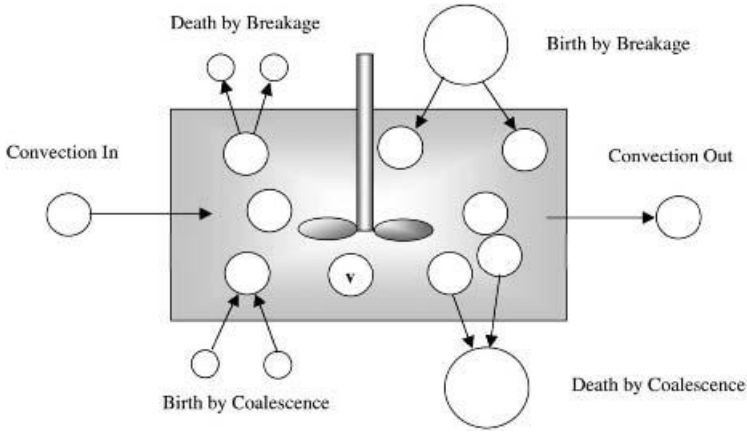
Figure 12-21   Population balance events for drops of volume v.

In addition to liquid–liquid systems, the population balance equation (PBE) has been applied to crystallization, grinding, interphase heat and mass transfer, multiphase reactions, and floatation.

12-4.2   History and Literature

There are two principal ways in which population balances have been used in liquid–liquid systems. These involve using experimentally or phenomenologically derived models for the breakage frequency and resulting daughter size distribution (known as the breakage kernel), along with similarly derived models for collision frequency and coalescence efficiency, to compute the evolution of the drop size distribution. The other procedure, referred to as the *inverse problem*, is to use transient drop size distribution data to compute or infer the breakage frequency and kernel, or the collision frequency and coalescence efficiency. From a computational point of view, the latter is more complex. Tavlarides and Stamatoudis (1981) give an excellent review of population balance models for stirred vessels. These authors address reaction and mass transfer as well as coalescence and dispersion. The theory, solution, and general application of population balance equations are well described in a book by Ramkrishna (2001). Table 12-4 lists some of the important contributions to the literature. The table includes methods used, results, and some conclusions. It is meant to be representative rather than comprehensive.

12-4.3   Population Balance Equations

The most general form of the population balance equation, applicable for a flow system, can be written

$$\frac{\partial n_d}{\partial t} + \nabla \cdot (\overline{U}\, n_d) - \dot{B}_d + \dot{D}_d = 0 \tag{12-52}$$

For a given drop size, n_d is the number of drops, $\dot{B}_d$ the birth rate, $\dot{D}_d$ the death rate, and $\overline{U}$ the velocity vector.

The complete population balance equation given by Coulaloglou and Tavlarides (1977) in the form of number density over drop volume for a CSTR is given by:

$$\frac{\partial}{\partial t}[N_T(t)A(v, t)] = \int_v^{v_{max}} \beta(v', v)\upsilon(v')g'(v')N_T(t)A(v', t)\, dv'$$

$$- g'(v)N_T(t)A(v, t) + \int_0^{v/2} \xi(v - v', v')\lambda(v - v', v')$$

$$\times N_T(t)A(v - v', t)N_T(t)A(v')\, dv' - N_T(t)A(v, t)$$

$$\times \int_0^{v_{max}-v} \xi(v, v')\lambda(v, v')N_T(t)A(v', t)\, dv'$$

$$+ N_{T0}(t)A_0(v, t) - N_T(t)A(v, t)f_e(v) \qquad (12\text{-}53)$$

where $N_T(t)$ is the total number of drops in the vessel at time t; $A(v, t)$ the number probability density for drops of volume v at time t; $\beta(v', v)$ the breakage kernel or the number probability density of daughter drops of volume v formed by the breakup of a parent drop of volume v'; $\upsilon(v')$ the mean number of daughter drops resulting from breakage of a parent drop of volume v'; $g'(v')$ the breakage frequency of drops of volume v'; $\xi(v, v')$ the collision frequency of drops of volume v with drops of volume v'; $\lambda(v, v')$ the coalescence efficiency between drops of volume v and drops of volume v'; $N_{T0}(t)$ the number feed rate of drops at time t; $A_o(v,t)$ the number probability density of drops of volume v at time t in the feed; and $f_e(v)$ the escape frequency of drops of volume v in the product stream.

The first two terms on the right represent the addition (birth) and loss (death) of drops of volume v due to breakage. The next two terms deal with formation and loss due to coalescence, and the last two terms represent droplet flow into and out of the vessel. The last two terms are eliminated for batch operation. If the system is noncoalescing, the middle two terms are eliminated. If the system is purely coalescing (no breakage), the first two terms are eliminated. Purely coalescing systems exist, at least initially, when the impeller speed is decreased. At steady state, eq. (12-53) can be written as

$$N_{TS}A(v)[g'(v) + \gamma(v) + f_e(v)]$$

$$= N_0A_o(v) + \int_v^{v_{max}} \beta(v', v)\upsilon(v')g'(v')N_{TS}A(v')\, dv'$$

$$+ \int_0^{v/2} \xi(v - v', v')\lambda(v - v', v')N_{TS}A(v - v', v')N_{TS}A(v')\, dv' \quad (12\text{-}54)$$

where

$$\gamma(v) = \int_0^{v_{max}-v} \xi(v, v')\lambda(v, v')N_{TS}A(v')\, dv'$$

Here $N_T(t) = N_{TS}$ and $N_{T0}(t) = N_0$, since the number of drops in the vessel and in the feed remain constant. Furthermore, $A(v,t) = A(v)$ and $A_0(v,t) = A_0(v)$. Many variations of eq. (12-53) and (12-54) exist, and the nature of the problem dictates the selection of terms to be used. As stated previously, these equations are in the form of number density over drop volume. That is, number probability density functions are applied to a drop of specified volume. It is often more convenient to use volume probability density functions for a drop of specified diameter. This form, given for a batch, noncoalescing system in eq. (12-55) represents volume density over drop volume. It was applied successfully by Konno et al. (1983):

$$\frac{\partial P_v(d, t)}{\partial t} = \int_d^{d_{max}} P_v(d', t)g'(d')\beta'(d', d)\, dd' - P_v(d, t)g'(d) \qquad (12\text{-}55)$$

where $P_v(d, t)$ is the volume probability density for drops of size d at time t; $g'(d)$ the breakage frequency of a drop of size d; and $\beta'(d, d')$ the breakage kernel or the number of daughter drops of size d formed by the breakup of a parent drop of size d′. Note that β' as defined in eq. (12-55) is equivalent to the product of υ and β in eq. (12-53).

12-4.4   Application of PBEs to Liquid–Liquid Systems

To apply practically the equations given in Section 12-4.3, it is important to have experimental data. As mentioned earlier, there are two approaches shown in Table 12-4. The direct approach is to use phenomenological models for the breakage and coalescence terms in the appropriate PBE to solve for the DSD. Favorable comparison of experimental and computed DSDs leads to the confirmation of phenomenological expressions. An excellent review of models for the breakage terms, including direct comparison to breakage rate data, is given by Lasheras et al. (2002). The other approach, referred to as the *inverse method*, uses transient drop size distribution data as input, and the solution of the PBE yields quantitative breakage and coalescence information, such as $\xi(v, v')$, $\lambda(v, v')$, $\beta(v, v')$, and $g'(v)$. The experimental and numerical procedures used to determine these quantities are discussed by Ramkrishna (2001) and others listed in Table 12-4. They will not be repeated here.

   The numerical solution of the PBE often leads to errors. Some of these include discretization errors, truncation errors, round-off errors, and propagated errors. Inverse problems are particularly stiff. Experimental errors include determining when steady state has been reached, noise in the tails of the DSD, sampling and analysis errors, and uncertainties that arise when in situ measurements cannot be made.

12-4.5   Prospects and Limitations

Despite the fact that PBE technology has been around since the 1960s, little practical industrial use has been made of it. Part of this is due to the formidable task of solving these equations, and part is due to the difficulty in obtaining quality

Table 12-4 Population Balance Studies in Stirred Vessels

Reference	Year	Methods	Problem Type	Conclusions
Bajpai et al. (1976)	1976	—	Direct	Coalescence followed by immediate redispersion into drops of specified distribution. Numerical results are compared with data from the literature.
Coulaloglou and Tavlarides (1977)	1977	Iterative technique backward marching from largest size increment	Direct	Used phenomenological models to develop breakage and coalescence rate and distribution functions. Used these to predict the DSD, which compared favorably with CSTR data.
Narsimhan et al. (1980)	1980	Similarity hypothesis	Inverse problem	Experimental DSD data for dilute system used to extract breakage frequency; led to validation of similarity hypothesis.
Tavlarides and Stamatoudis (1981)	1981	—	—	A major review of population balance work, including mass transfer and chemical reactions.
Tavlarides (1981)	1981	Monte Carlo methods	Direct	Used phenomenological models describing coalescence and dispersion to predict DSD, with results compared with experiments. A review.
Rod and Misek (1982)	1982	Monte Carlo methods	Inverse problem	Compared Monte Carlo simulation with exact solution of PBEs. Concluded MC methods are adequate and efficient for calculating rate parameters in response to DSD data.
Bapat et al. (1983)	1983	Interval of quiescence Monte Carlo method	Direct	Used breakage and coalescence functions to predict spatially varying drop size distribution and mass transfer rates.

(continued overleaf)

701

Table 12-4 (*continued*)

Reference	Year	Methods	Problem Type	Conclusions
Tavlarides and Bapat (1983)	1983	—	—	General review, including PBE modeling.
Narsimhan et al. (1984)	1984	Discretized drop volume intervals	Direct	Dilute dispersion data; observed similarity behavior for DSD. Compared DSD predicted by PBE with measurements; good agreement.
Rajamani et al. (1986)	1986	Monte Carlo methods	—	Compared time-driven with event-driven methods, applied to batch liquid–liquid dispersion.
Jeon and Lee (1986)	1986	—	Various	Showed applicability of PBEs to solving mass transfer problems. Using various assumptions, it was shown that all were in close agreement with experimental DSD and mass transfer data.
Laso et al. (1987a, b)	1986	Discrete model; size classes defined by geometric series	Direct	Developed a computationally efficient discrete model for breakage and coalescence; breakage and coalescence rates determined by optimizing the fit of experimental DSD data.
Muralidar and Ramkrishna (1988)	1988	Similarity hypothesis for PBE	Inverse problem; applicable if DSDs are self-preserving	1. Transient DSD data for purely coalescing systems used to determine coalescence efficiencies. 2. Mechanistic models developed for coalescence efficiency that include physical and turbulence information regarding drop motion, rest time, etc.

Reference	Year	Approach	Problem type	Description
Chang et al. (1991)	1991	Discrete size classes	Direct	Calculated DSD for different breakage frequencies. Size classes defined.
Calabrese et al. (1993)	1993	Discrete size classes	Both direct and inverse problem	Calculated DSD from described breakage model, and breakage frequencies from DSD data.
Alvarez et al. (1994)	1994	Quasi-steady state assumed for population dynamics	Direct	Applied PBE to suspension polymerization using breakage-coalescence parameters from the literature. Predicted DSD in agreement with published data.
Wright and Ramkrishna (1994)	1994	Similarity hypothesis	Inverse problem	Experimental data for purely coalescing system used with PBE to extract and develop correlation for coalescence frequency.
Chatzi and Kiparissides (1994)	1994	Numerical solutions	Direct	Steady-state distributions were calculated and found to be in generally good agreement with experimental data. Used to help determine effectiveness of polymeric suspending agent, and its performance vs. composition.
Sathyagal et al. (1995)	1995	Similarity transformation used	Inverse problem	Transient dilute dispersion DSD data used to extract breakage frequencies and kernels.
Ramkrishna (2001)	2001	—	—	Book covering all aspects, including theory and solution, of population balance equations.

data required for analysis. This is particularly true for coalescence phenomena, as discussed in Section 12-3. Recall that the number of drops, the collision rate, and the coalescence efficiency depend in a complicated and often competing way on agitation rate, drop diameter, and physicochemical variables, making validation of phenomenological models difficult.

Another limitation is that the breakage and coalescence kernels and frequency information tend to be specific to the equipment used to acquire the data. It is highly scale dependent; all quantities are flow dependent. Once information is obtained using PBEs, it cannot be used, with confidence, for scale-up work. At a specific scale, however, system information can prove useful. For example, the effect of surfactant concentration, stirring rate, impeller design, phase composition, and so on, could all be interpreted in terms of $\xi(v, v')$, $\lambda(v, v')$, $\beta(v, v')$, and $g'(v)$. This information could be used to improve and control product quality.

Vastly improved and faster computers can overcome the previously expensive task of solving the equations. In the past, simplifying assumptions have been used to shorten computation time. Today, and in the future, the most rigorous numerical techniques should be employed to eliminate the compromises of the past.

We expect that in the near future, CFD technology that has proven valuable in characterizing differences in flow behavior due to scale can be coupled with PBEs to give reasonably accurate drop size information, including scale effects, for estimating interfacial area and drop size uniformity.

12-5   MORE CONCENTRATED SYSTEMS

12-5.1   Introduction

Most industrial liquid–liquid applications fall into the category of being more concentrated systems. We identify more concentrated systems as $\phi > 0.20$ by volume fraction of dispersed phase. Industrial examples include suspension and emulsion polymerization, extraction, and separations, including decantation, centrifugation, and electrostatic precipitation. Because practice is as much an art as a science, much of the industrial experience on concentrated systems is proprietary and not published, contrasting the vast amount of academic work published for dilute and "clean" systems.

Concentrated liquid–liquid systems often involve dispersion and coalescence as well as rheological complexities. Data conflicts are common, often arising from the presence of impurities, sometimes unknown to investigators. There is also the challenge of obtaining representative samples and analyzing them. Describing the microscale interactions between the drops and the surrounding fluid, necessary for theoretical interpretation, is seldom a goal. That is, for concentrated systems, the small scale structure of the continuous phase turbulence is unknown and the drop–eddy interactions are undetermined. Salts, surface-active materials, and other impurities lead to system-specific behavior, complicating the development of industrial technology. As a result, many of the points discussed in this section are tied to specific process examples.

Dispersion, coalescence, and suspension phenomena are all important in concentrated liquid–liquid dispersions. Convective mixing patterns are also affected by the changes in rheology brought about by high dispersed phase concentrations. Heat transfer becomes more critical because of high concentrations of reactive materials often in the dispersed phase. For example, heat is managed in emulsion polymerization by controlling the addition rate of monomer fed to the reactor. Certain smaller scale processes can maintain temperature control through jacket cooling. For highly exothermic reactions, reflux condensers are used. If the end product is not shear sensitive, cooling by recirculation through an external heat exchanger is often used.

As discussed in previous sections, turbulent eddies are affected by high dispersed phase concentrations. Elasticlike behavior of deformable drops "cushion" eddies, reducing momentum transport. This means drop dispersion is limited to a smaller region closer to the impeller than for dilute systems.

Coalescence is also different in concentrated systems. Drop coalescence in dilute and moderate concentration systems was shown to originate from drop–drop collisions, contact with surfaces, or settling to a nondispersed, settled layer. Turbulence-induced collisions lead to brief contact intervals during which the separating film thins due to shear forces acting on the drop pairs. The total extent of thinning during contact determines coalescence probability, as shown in Section 12-3. Drops are closer together in concentrated systems (sometimes touching), and relative drop movement due to eddy fluctuations is less. This leads to longer contact intervals and a higher coalescence probability. In the case of highly concentrated systems, drops move relative to one another due to the local velocity gradient. Collisions, as we have described previously, are not likely to occur.

Gravitational effects are also different for concentrated systems. Quiescent settling of dilute dispersions leads to a gradient in both drop size and phase fraction. For $\rho_d < \rho_c$, the largest drops concentrate near the liquid surface and the smallest drops are closest to the lower cleared layer. Coalescence rates for unprotected drops are also accelerated due to the greater hydrostatic force on the settled drops, promoting faster film drainage. Dense drop populations lead to slower, hindered drop settling.

Surface-active materials are used to stabilize dispersions in industrial applications when coalescence must be prevented, as for suspension and emulsion polymerization processes. Concentrated dispersions are more likely to undergo phase inversion. This complex coalescence-dominated phenomenon is discussed later in this section.

12-5.2   Differences from Low Concentration Systems

Differences and similarities are illustrated by example. Suspension and emulsion polymerizations are examples of industrial processes having high drop concentrations, where coalescence is prevented by the use of suspending agents/emulsifiers. Polyvinyl alcohol (PVA) is typical of the aqueous suspending agents used. Concentrates of $\approx 2\%$ of partially hydrolyzed PVA are diluted to ≈ 0.05 to 0.2%

for use in polymerization reactions. This concentration is usually sufficient to prevent coalescence once drop interfaces become sufficiently covered. The stabilizing efficiency depends on its chemical composition (degree of hydrolysis for PVA) and its molecular weight. The typical phase ratios are close to $1:1$ or $\phi \sim 0.5$. Monomer containing an initiator is dispersed into water containing the suspending agent. Agitation continues at ambient temperatures to establish desired drop size and consistency. The temperature is then increased to the point where free radicals are formed form the initiator and polymerization begins. Each drop formed by agitation becomes a polymer particle of similar, but slightly smaller, size compared to the liquid drop. Heat transfer is seldom a problem, since drops have a large surface/volume ratio, and water, the suspending medium, provides good conduction and convection for heat transfer to the jacketed vessel walls. Suspension polymerization reactions are typically low viscosity operations. Vivaldo-Lima et al. (1997) have given an excellent review of suspension polymerization.

Leng and Quarderer (1982) show that for certain applications, dilute dispersion theories can be applied successfully to concentrated noncoalescing systems. It was shown that boundary layer shear on impeller surfaces controlled drop dispersion for drops in the size range 300 to 1000 μm and turbulence-controlled dispersion for smaller drops. The expressions given by eqs. (12-73) and (12-74) were supported by data from bench to production scale experiments. These results give encouragement that some industrially complex noncoalescing systems behave similarly to dilute systems. The result is not surprising since flow patterns were simple and independent of scale, rheology was close to Newtonian, and shear brought about drop dispersion. Additional details are given in Section 12-8.3.

12-5.3   Viscous Emulsions

12-5.3.1   Emulsion Viscosity and Stability. Drop sizes for emulsions are less than 0.1 μm, as distinguished from dispersions, which contain larger drops. Emulsions typically contain high concentrations of emulsifiers, and the dispersed phase volume fraction can be as high as 99%. Such high internal phase compositions often have unusually high viscosity and display complex rheological behavior. The apparent emulsion viscosity is much higher than single-component viscosities, and this is due both to large quantities of adsorbed surface-active materials and to large interfacial areas, causing internal flow resistance. In certain industrial applications, the viscosity of such systems has been found to be several hundred poise. Latex paints and similar products are strongly formulated to provide optimum film uniformity, durability, and adhesion. Balances of short-range forces stabilize these emulsions. These are electrostatic and steric repulsion forces and London–van der Waals attraction forces. The addition of an electrolyte reduces the repulsion forces and causes the emulsion to coalesce.

Emulsion polymerization involves simultaneous nucleation and growth phenomena. Monomer is first dispersed into drops enabling the aqueous phase to become saturated. Monomer moves by a convection–diffusion mechanism to growing micelles or suspended particles. Although nucleation and growth occur simultaneously, growth continues after nucleation stops. The growth phase stops when the monomer supply or free-radical generation is exhausted. Emulsion polymerization reactions are nearly always exothermic. Heat transfer is managed by a combination of controlled monomer feeding and the use of external heat transfer surfaces, such as reflux condensers or heat exchangers arranged in a circulation loop. Pumped circulation can be used only when dealing with shear stable products. The role of agitation is to disperse monomer into drops and to provide adequate movement for suspension and heat transfer. Despite the presence of stabilizers, many latex products are shear sensitive and prone to coagulation. Coagulum is undesirable and costly to remove. Agitation equipment should be chosen to minimize coagulum formation. A common design consists of a baffled jacketed glass-lined steel vessel equipped with a three-blade retreat curve impeller, shown in Figure 12-28. Use of glass-lined equipment helps prevent fouling and leads to higher product quality.

12-5.3.2 Drop Dispersion. Both turbulence and shear can break up drops in concentrated systems, but due to the dampening of eddies, it is likely that mean shear plays an important role in drop dispersion. This effect has been quantified by Coulaloglou and Tavlarides (1977) and shown by

$$N^*_{eff} = \frac{N^*}{1 + \phi} \tag{12-56}$$

where N^*_{eff} is the rotational speed necessary for equivalent dispersion for a volume fraction ϕ, equivalent to that for a dilute system operating at a speed N^*. Drop dispersion occurs only near the impeller, and coalescence occurs throughout the rest of the vessel, similar to dilute dispersion. The high dispersed phase fraction leads to a higher collision rate.

12-5.4 Phase Inversion

12-5.4.1 General Description. Phase inversion is a commonly observed and practiced phenomenon in which the continuous phase becomes the dispersed phase, and vice versa. Coalescence is the fundamental phenomenon involved with phase inversion. Figure 12-22 shows schematically the steps occurring during phase inversion. The left column shows the preinverted condition. The middle column shows bridging and coalesce taking place, and the right column shows the inverted condition. The bottom row shows how irregular bridging (center) leads to drops in drops (right column), as rapid coalescence traps some of the
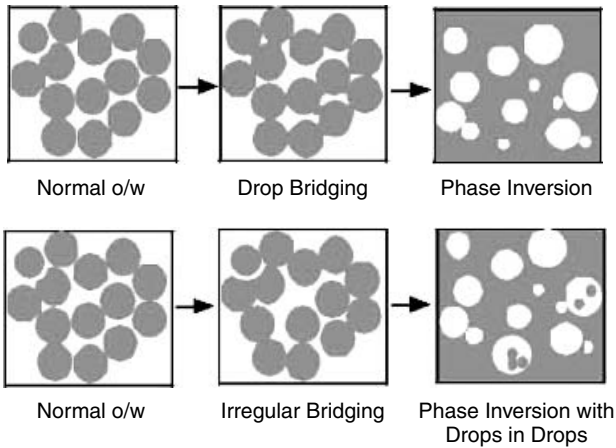
Figure 12-22   Sequences in phase inversion.

continuous phase. The condition shown in the bottom right view is metastable, usually existing only temporarily, but not always.

Although conflicting information exists on the subject of phase inversion, the following conclusions can be made:

- Coalescence, not dispersion, dominates as the controlling mechanism in phase inversion. Factors discussed in Section 12-3 affecting film drainage rates, such as agitation rate, interfacial tension, interface mobility, μ_c, and contact time, all apply.
- Inversion behavior is system specific.
- Surface-active agents play an important role, affecting film drainage rates.
- Every system has an operating region in which the oil phase is continuous, a region in which the aqueous phase is continuous and an ambivalent region where either phase can be continuous.
- The probability for phase inversion increases as drops get closer together. For uniform drops, the distance between drops is $s_d/d = (c_p/\phi)^{1/3} - 1$, where s_d is the separation distance between drops, d the drop diameter, ϕ the volume fraction dispersed phase, and c_p a packing parameter (0.7404 for face-centered cubic or hexagonal packing).
- The phase boundaries, or volume fractions at which phase inversion occurs, depend to some extent on initial conditions, path and agitation intensity, resulting in an *ambivalent region*. Beyond a certain point, phase inversion becomes independent of operating conditions.
- Several studies show metastable conditions of drops in drops, or water in oil in water.

12-5.4.2   Physical Description. Phase inversion is the transformation from o/w to w/o or from w/o to o/w. Sometimes phase inversion is initiated as a

result of physical property changes brought about by chemical reaction. Both o/w and w/o phases usually coexist temporarily during the inversion process. For example, if the dispersed aqueous phase becomes viscous (as a result of polymerization) and coalescence occurs, it becomes the continuous phase as a result of inversion. However, if the continuous oil phase were to thicken, it would remain the continuous phase and no inversion would take place.

12-5.4.3 *Phase Inversion Boundaries/Regime Map and Ambivalent Region*.
Figure 12-23 is an example of a regime map. The region above the curves is where oil is always the continuous phase. Water is the continuous phase in the region below the curves. Between the two sets of lines is the ambivalent region, where either o/w or w/o systems can exist. The top arrow shows o/w going to w/o as more oil is added to the system. The bottom arrow shows the inversion of a w/o to an o/w system as water is added. Both the upper and lower boundary lines show a weak dependence on agitation rate, becoming even less dependent at higher levels of agitation.

Pacek et al. (1994a) have developed an effective video technique for concentrated liquid–liquid systems enabling phase inversion to be recorded in situ. Pacek et al. (1993, 1994b) found that when water was dispersed in oil at $\phi > 0.25$, water drops appeared in oil (drops in drops), but drops in drops did not appear when oil was dispersed in water.

Surfactant concentration can also be used to drive phase inversion. At high surfactant concentration, agitation and the method of addition may play a less
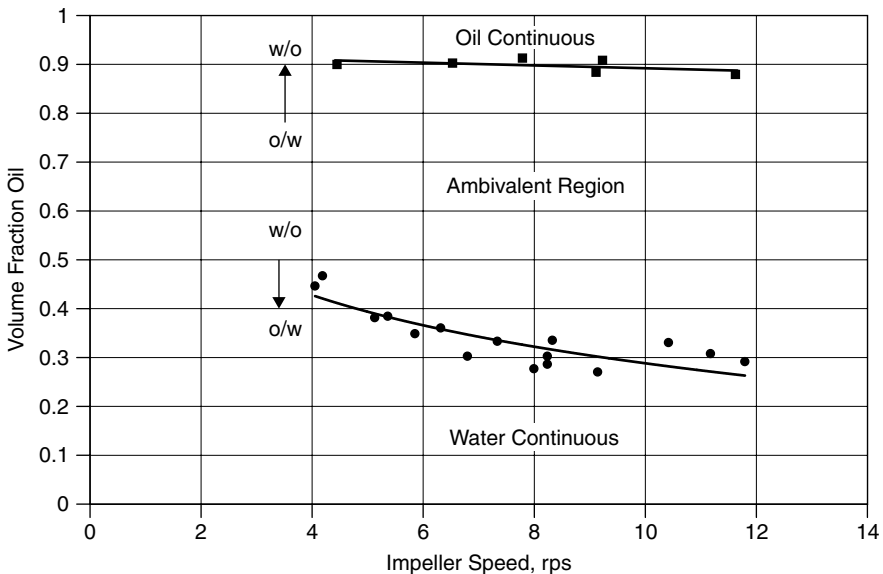

Figure 12-23 Phase inversion boundaries for the kerosene–water system showing oil and water continuous regions and an ambivalent region. (Data of Kinugasa et al., 1997.)
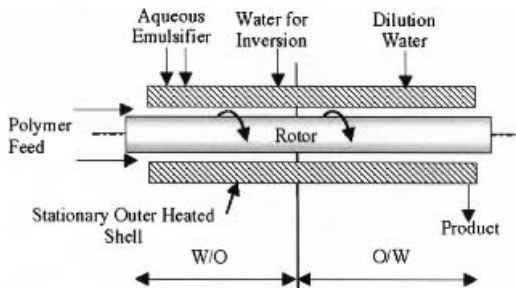
Figure 12-24   Continuous Couette-type phase inversion emulsifier.

important role. Systematic studies on the effect of surfactant concentration and mixing on phase inversion and emulsion drop size have been carried out by Brooks and Richmond (1991, 1994a–c).

12-5.4.4   *Other Types of Phase Inversion*. Synthetic emulsions were prepared by phase inversion at The Dow Chemical Company. A long Couette-like concentric cylinder apparatus was developed and is shown in Figure 12-24. All feed streams were precisely metered and controlled. Polymer in the form of either a melt or solution is fed in as shown on the left. Two aqueous streams are added to permit the gradual buildup of a w/o (polymer) phase. These aqueous streams contain significant quantities of surfactant. The third addition of water forces phase inversion, similar to that shown in Figure 12-23. A final water addition is for dilution to obtain the desired solids concentration. Typically, the final product contained 40 to 60% solids consisting of 0.1 to 1.0 μm particles in water. A wide variety of both heat- and solvent-plasticized feeds were demonstrated. The variables maintained constant for successful scale-up were shear rate and dispersion time. The process is more fully described in patents issued to Warner and Leng (1978) and Leng et al. (1985). The process was commercialized.

   High capillary numbers were obtained as a result of high-shear rate (typically, 200 s^{-1}), high continuous phase viscosity, and low interfacial tension. Once steady-state conditions are established, cooling to the outer cylinder is applied to compensate for heat generation caused by viscous energy dissipation. Overheating leads to lower viscosity and in a reduction of shear stress required for dispersion. Different feed streams were used, requiring different feed preparation. Some polymers required use of solvents to adjust viscosity, whereas for others, simple heating was sufficient to pump in the feed. When solvents were used, they were removed by continuous stripping.

12-6   OTHER CONSIDERATIONS

12-6.1   Introduction

Section 12-6 provides a discussion of drop suspension, dispersion formation, and the interrelationships between dispersion, coalescence, and suspension. Additional

topics include the role of surfactants and suspending agents, Oswald ripening, mass and heat transfer, and the effect of the presence of solids and gas bubbles on dispersion and coalescence.

12-6.2 Suspension of Drops

Settling and coalescence are common when the dispersed and continuous phases are of different density and when agitation provides only minimal circulation throughout the vessel. It is therefore important to determine the minimum speed for drop suspension. Most reported work is semiempirical and follows the approach of Zwietering (1958) for the just suspended state of solids in liquids.

There are analogies between the minimum impeller speed N_{js} for solids suspension and N_{min} for drop suspension. Both depend on density difference, continuous phase viscosity, and impeller diameter. However, N_{js} depends directly on particle size, while N_{min} depends instead on interfacial tension and the other physical properties that determine drop size. Skelland and Seksaria (1978) determined the minimum speed to form a liquid–liquid dispersion from two settled (separated) phases of different density and included the sensitivity to impeller location. The vessels used were fully baffled. They determined N_{min} for systems of equal volumes of light and heavy phase. Studies included use of single impellers placed midway in the dense phase (C = H/4), at the o/w interface (C = H/2) and midway in the lighter phase (C = 3H/4). They also examined the use of dual impellers located midway in both phases. Several impeller types were tested, including a propeller (Prop), a 45° pitched blade turbine (PBT), a flat-blade turbine (FBT), and a curved-blade turbine (CBT). Their results are correlated by the following equation, which is dimensionless:

$$\frac{N_{min}D^{0.5}}{g^{0.5}} = C_{20}\left(\frac{T}{D}\right)^{\alpha_5}\left(\frac{\mu_c}{\mu_d}\right)^{1/9}\left(\frac{\Delta\rho}{\rho_c}\right)^{0.25}\left(\frac{\sigma}{D^2\rho_c g}\right)^{0.3} \tag{12-57}$$

$\Delta\rho = |\rho_d - \rho_c|$. The magnitude of the constants C_{20} and α_5, given in the Table 12-5, are a measure of the ease of suspension formation. Low C_{20} values indicate that dispersions are formed at low speeds. Large C_{20} values (single impellers) suggest that higher speeds are required for minimum suspension. Turbines at the o/w interface require lower speed than in other locations. Radial flat-blade turbines placed in the light phase appear to be inefficient.

In an earlier study, Nagata (1975) determined minimum agitation conditions for forming a dispersion using a baffled cylindrical vessel and four-blade turbine impellers of $D/T = \frac{1}{3}$, placed at C = T/2. The following equation shows his dimensional correlation:

$$N_{min} = C_{21}T^{-2/3}\left(\frac{\mu_c}{\rho_c}\right)^{1/9}\left(\frac{\rho_c - \rho_d}{\rho_c}\right)^{0.26} \tag{12-58}$$

The value of C_{21} is 750 for normal centered agitation and 610 for off-center agitation with eccentricity D/4. Units are ρ_c (kg/m³), ρ_d (kg/m³), μ_c (kg/m · s),

Table 12-5   Constants for Use in Eq. (12-57)

Type	Clearance	C_{20}	α_5
Prop.	H/4	15.3	0.28
Prop.	3H/4	9.9	0.55
Prop.	H/2	15.3	0.39
Prop.	H/4 + 3H/4	5.2	0.92
PBT	H/4	6.8	1.05
PBT	3H/4	6.2	0.82
PBT	H/2	3.0	1.59
PBT	H/4 + 3H/4	3.4	0.87
FBT	H/4	3.2	1.62
FBT	3H/4	[a]	[a]
FBT	H/2	4.0	0.88
FBT	H/4 + 3H/4	[a]	[a]
CBT	H/4	3.6	1.46
CBT	3H/4	[a]	[a]
CBT	H/2	4.7	0.80
CBT	H/4 + 3H/4	4.3	0.54

[a] Insufficient data for correlation purposes.

T (m), and N_{min} (rpm). Off-center locations are seldom used, but the vortex due to eccentricity creates an efficient means to help form dispersions. The lack of dependency on μ_d indicates that only low viscosity dispersed phases were considered.

Pavlushenko and Yanishevskii (1958) determined the minimum speed for suspension in experiments that he conducted in a 0.3 m baffled vessel. The following equation gives his dimensional result, where SI units are used and N has units of rps.

$$N_{min} = \frac{5.67 \Delta\rho^{0.08} \mu_c^{0.06} \mu_d^{0.04} \sigma^{0.15} T^{0.92}}{\rho_c^{0.33} D^{1.87}}$$

(12-59)

Armenante and Tsai (1988) studied the effects of many variables on N_{min}. Their results for inviscid dispersed phases are given by

$$N_{min} = C_{22}(g\,\Delta\rho)^{5/12}\sigma^{1/12}\rho_c^{-0.5}D^{-2/3}\left(\frac{T}{D}\right)^{0.67}\left(\frac{H}{D}\right)^{0.33}N_P^{-1/3}$$

(12-60)

The results in terms of minimum Reynolds number are given by

$$Re_{min} = C_{23} \cdot Su^{1/12}Ar^{5/12}\left(\frac{T}{D}\right)^{0.67}\left(\frac{H}{D}\right)^{0.33}N_P^{-1/3}$$

(12-61)

where $Su = \rho_c \sigma D/\mu_c^2$ is the Suratman number, $Ar = g\rho_c \Delta\rho D^3/\mu_c^2$ is the Archimedes number, and Np is the power number. The equation was found to be in good agreement with other work.

Armenante and Huang (1992) and Armenante et al. (1992) found practically no advantage in using multiple impellers for determining N_{min}. This is similar to the result for solid–liquid suspension. However, multiple impellers were useful in improving dispersed phase uniformity. Results agreed with the work of Skelland and Seksaria (1978).

We recommend use of eq. (12-57) in the absence of direct experimental data. It describes more specific impeller arrangements than the other work reported and is confirmed by the more recent work of Armenante and co-workers. These bench scale minimum-speed equations have not been validated by scale-up experiments, so caution is advised. For important applications, we recommend that scale-up experiments be conducted on a minimum of a fourfold volume scale using eq. (12-57) to guide in the variable selection and correlation.

12-6.3   Interrelationship between Suspension, Dispersion, and Coalescence

Church and Shinnar (1961) described the interrelationship between suspension, dispersion, and coalescence. Figure 12-25 shows drop size as a function of agitator speed in a turbulent process vessel. A stable region exists in the center area bounded by three lines representing dispersion, coalescence, and suspension phenomena. Consider constant impeller speed. If a large drop exists above the upper dispersion line, it will continue to break up until the dispersion line is reached. Breakage can result in some drops whose size lies below the lower coalescence line. These drops will continue to coalesce until the coalescence line is reached. Inside the bounded region, equilibrium is established between dispersion and coalescence.

A drop existing to the left of the suspension line will only be suspended when the speed is increased to the intersection of that drop size with the suspension line. If agitation speeds are to the right of the suspension line, the drops are always suspended. In the figure, the equations for the three lines apply to
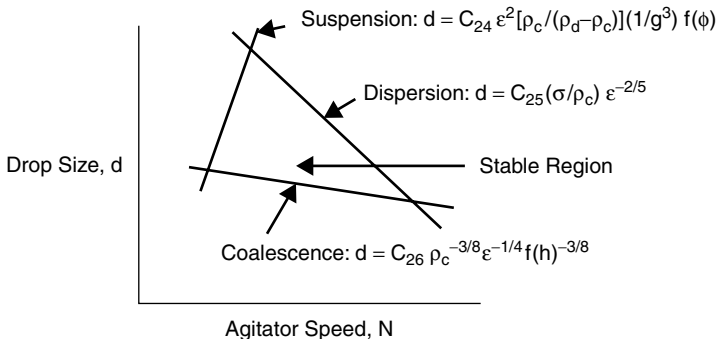

Suspension: $d = C_{24}\, \varepsilon^2 [\rho_c/(\rho_d - \rho_c)](1/g^3)\, f(\phi)$

Dispersion: $d = C_{25}(\sigma/\rho_c)\, \varepsilon^{-2/5}$

Drop Size, d

Stable Region

Coalescence: $d = C_{26}\, \rho_c^{-3/8} \varepsilon^{-1/4} f(h)^{-3/8}$

Agitator Speed, N

Figure 12-25 Stable region concept for liquid–liquid processing in a stirred vessel. (After Church and Shinnar, 1961.)

inviscid dispersed phases. Symbols are defined in the "Nomenclature" section. The dispersion equation is analogous to eq. (12-21). Church and Shinnar (1961) derived the suspension and coalescence equations. Although somewhat simplistic compared to later work, they well illustrate the concept.

An extension of the Church and Shinnar concepts as they apply to suspension polymerization is as follows. In suspension polymerization, a conflict exists between suspension and dispersion since large uniform drops must be formed. Suspension of these large drops is often a problem, due to the phase density difference. The speed necessary for the prevention of "layering out" can produce smaller than desired beads. Figure 12-26 depicts the interaction between suspension and dispersion in the process vessel. For given properties and equipment, drop size decreases with increasing impeller speed, but the size of drops that can be suspended increases with speed. For a given system and reactor design, the largest practical drop size lies at the intersection of the two lines. Different agitation designs and suspending agents can shift the position of these lines, as suggested by the lighter lines on the figure, to meet bead size requirements.

12-6.4   Practical Aspects of Dispersion Formation

Placing a turbine (RDT) in the aqueous or lower phase, close to the interface, can make o/w dispersions. A central interfacial vortex forms with the commencement of impeller motion. This directs a stream of the lighter oil phase to the impeller, where it disperses. The volume of oil layer decreases with continued dispersion until it is exhausted. Placing the turbine in the oil, or upper phase, close to the interface can make w/o dispersions. A water-containing vortex forms, allowing water to be dispersed into the lighter oil phase.

Dispersions may also be formed by the continuous addition of one phase into another under agitation conditions. This method offers a safe procedure for handling exothermic reactions such as nitration and emulsion polymerization. The amount of phase addition will determine if phase inversion occurs as discussed in Section 12-5.4.
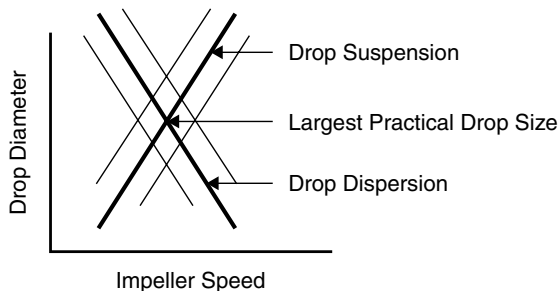

Figure 12-26   Relationship between drop suspension and dispersion.

Listed below are some general recommendations for o/w and w/o systems:

- Use multiple turbines if the system is rapidly coalescing to provide additional dispersion capability. Axial flow turbines can also be used to achieve better uniformity in circulation.

- Avoid excessive dispersion in noncoalescing systems. Creation of tiny hard to coalesce drops can become a real problem if phase separation is required later. Test the system using bench scale equipment to see if and at what speed undesirably small drops form.

- Use at least one axial flow hydrofoil-type impeller of high D/T (i.e., $0.4 \leq$ D/T ≤ 0.6) in addition to the RDT for systems having large phase density differences.

- Interfacial tension controls the ease of drop breakage. Systems of low inter-facial tension ($\sigma \leq 10$ dyn/cm or 0.01 N/m) require much lower power for dispersion than do those of high interfacial tension ($\sigma \geq 30$ dyn/cm or 0.03 N/m). We described this in more detail in Section 12-2.

- Baffling is always required for liquid–liquid dispersion, with the exception of suspension polymerization and certain highly shear-sensitive emulsion polymerizations.

12-6.5 Surfactants and Suspending Agents

Surfactants are organic compounds, often liquids, that have a hydrophobic and a hydrophilic portion of the molecule. Typical molecular weights range from 100 to 400. Suspending agents are usually polymeric in nature. They also have a hydrophobic portion, often the polymer backbone, and a hydrophilic group added to the backbone. Typical molecular weights range from 10 000 to 40 000. They are often only sparingly soluble in water. In practice, surfactant and/or sus-pending agents inhibit coalescence. This means that drop sizes are controlled by dispersion rather than by equilibrium between dispersion and coalescence, thus simplifying scale-up. The problem becomes one of dispersion kinetics and sus-pension. Suspending agent/surfactant concentrations are application dependent. However, typical concentrations are about 0.2 wt % for suspending agents and about 1 wt % for surfactants based on water content.

Surfactant/suspending agent molecules adsorb at liquid–liquid interfaces until equilibrium is reached between the adsorbed layer and the bulk fluid. The interfa-cial tension decreases with increasing bulk concentration until the critical micelle concentration (CMC) is reached. The interfacial tension remains constant beyond the CMC. Figure 12-27 shows a typical dependence of interfacial tension on surfactant concentration. Surface viscosity behavior is different. The viscosity remains practically constant up to the CMC and increases beyond it. The CMC is an equilibrium phenomenon. As surface area is created by agitation, surfac-tant molecules leave the CMC cluster, transfer to the aqueous phase, and then transfer to the liquid–liquid interface. Adsorption and protective action are not
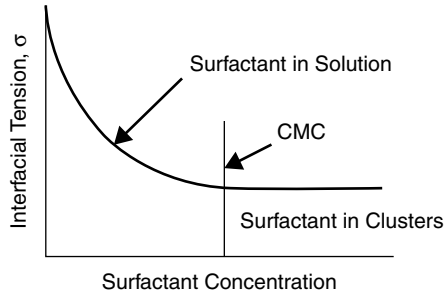
Figure 12-27   Interfacial tension dependence on surfactant concentration.

instantaneous. The diffusion-dependent adsorption rate is faster for lower molecular weight materials. To illustrate this point, an attempt to produce uniform drops using a static mixer failed because newly made drops collided with one another and coalesced faster than they could be protected. The age of all drops produced in a static mixer is the same, whereas in a stirred tank, a large age distribution exists. If a protected drop collides with an unprotected drop, the pair does not coalesce; but the collision of two unprotected drops can result in coalescence.

Unlike surfactants, suspending agents usually create a viscous or semisolid skin over the surface of the drops. This makes coalescence impossible. Furthermore, dispersion is governed by viscous rather than interfacial resistance. Suspending agents used in suspension polymerization include materials such as polyvinyl alcohol and derivatized methylcellulose. In industry, the composition of effective suspending agents is closely guarded technology.

Approximations can be made to estimate how much surfactant is needed to maintain a desired dispersion. This is illustrated by example.

Example 12.2. Suppose that a dispersion is to be 50% oil dispersed in water and consist of 50 μm drops. The surfactant molecular weight is 350. Assume that the molecular dimensions of the surfactant are 4 Å × 7 Å and that drop stability is obtained when surfaces are 50% covered. Estimate the surfactant requirement.

SOLUTION: Let c_s be the surfactant concentration in g/L. The molar concentration is then $(c_s/350)$ g-mol/L. The number of surfactant molecules in solution can be obtained using Avogadro's number and is $(c_s/350)$ (6.023×10^{23}) molecules/L. The interfacial surface area is $(c_s/350)$ (6.023×10^{23}) (4×7) Å^2/L. A 50% ($\phi = 0.5$) o/w dispersion having $d_{32} = 50$ μm has a specific surface area of $a_v = 6 \times 0.5/50 \times 10^4$ cm^2/cm^3 [refer to eq. (12-2)]. This converts to 6×10^5 cm^2/L or 6×10^{21}Å^2/L. Since stability is reached with only 50% coverage, the surfactant needs to cover only 3×10^{21}Å^2/L. Equating molecular area to drop surface area gives $c_s = 0.062$ g/L. Since the surfactant is supplied to the water phase (50% of total volume), the aqueous phase needs to contain 0.124 g/L or 0.0124 wt % surfactant.

12-6.6 Oswald Ripening

Ostwald ripening is a phenomenon resulting from slight differences in solubility due to differences in drop or crystal size. Small drops are slightly more soluble in the surrounding phase than large ones. This causes small drops, over time, to decrease in size and larger ones to get larger. The driving force for this phenomenon comes from consideration of the minimum surface free energy and is best explained in fundamental texts on phase equilibria.

Nyvlt et al. (1985) showed that for the case of a pure crystal of species A, the relationship between the bulk solubility of A in solution $c_{A\infty}$ and the solubility of a small particle of radius $\bar{r}$ in the same solution $c_{A\bar{r}}$ is given by

$$\bar{r} = \frac{\beta_S \hat{V}_A \hat{E}_S c_{A\infty}}{(c_{A\bar{r}} - c_{A\infty})(kT)_b} \tag{12-62}$$

where β_S is a shape factor for the crystal, $\hat{V}_A$ the molecular volume of A, $\hat{E}_S$ the specific surface energy of the particle, and $(kT)_b$ the product of the Boltzmann constant and absolute temperature. As $\bar{r} \to \infty$, $c_{A\bar{r}} \to c_{A\infty}$. An alternative interpretation of eq. (12-62) is that for a solution at concentration $c_{A\bar{r}}$, $\bar{r}$ is a critical particle radius. Smaller particles will disappear due to their higher solubility, and larger particles will grow due to their lesser solubility. Ostwald ripening is diffusion controlled and is often important for long-term storage of emulsified or formulated products. A model for Ostwald ripening in emulsions has been developed by Yarranton and Masliyah (1997).

12-6.7 Heat and Mass Transfer

Many industrially important chemical reactions occur in liquid−liquid systems since heat and mass transfer can be very efficient in agitated heterogeneous stirred reactors. The reaction usually takes place in the dispersed phase. Transport rates depend on the slip velocity between the phases as shown in eqs. (12-63) and (12-64). They are applicable only to single drops that are larger than the turbulent macroscale and are presented for illustrative purposes only. A tank-specific correlation is given later. The heat transfer coefficient, h_T, for a single sphere is given by

$$\frac{h_T d}{k_{cf}} = 2.0 + 0.6(Re_\infty)^{1/2}(Pr_f)^{1/3} \tag{12-63}$$

The mass transfer coefficient, k_m, is given by

$$\frac{k_m d}{D_{AB}} = 2.0 + 0.6(Re_\infty)^{1/2}(Sc_f)^{1/3} \tag{12-64}$$

The Reynolds number $Re_\infty = dv_\infty \rho_f/\mu_f$, the Prandtl number $Pr_f = C_{pf}\mu_f/k_{cf}$, and the Schmidt number $Sc_f = \mu_f/\rho_f D_{AB}$ are based on the physical properties

(density ρ_f, viscosity μ_f, heat capacity C_{pf}, thermal conductivity k_{cf}, and mass diffusivity D_{AB}) of the surrounding fluid.

The Reynolds number includes v_∞, the drop velocity relative to its surroundings or slip velocity. If drops move with the surrounding fluid, v_∞ is negligible, and heat and mass transfer rates depend solely on conduction and diffusion, respectively. If drops are suspended as in fluidization, heat and mass transfer coefficients will increase due to increased slip velocity.

The mass transfer rate, $\dot{m}_A$, of species A into or out of a drop depends on the interfacial area, πd^2, the concentration driving force, ΔC_A, and the mass transfer coefficient, k_m, as shown by

$$\dot{m}_A = k_m \pi d^2 \Delta C_A \tag{12-65}$$

where ΔC_A is the difference in concentration of species A inside and outside the drop. The actual driving force for interphase mass transfer is the difference in chemical potential. Therefore, one of these concentrations must be adjusted using a partition coefficient, or equivalent, so that ΔC_A is defined relative to either the drop or continuous phase. Increasing agitation intensity increases mass transfer in two ways. Since drop size decreases, interfacial area is increased. Eddy motion increases, causing an increase in slip velocity.

Mass transfer can affect the rate of film thinning between drops and hence coalescence rate. When mass transfer is not uniform, surface concentration and interfacial tension gradients are established. This leads to a phenomenon known as the *Marangoni effect*. Differences in concentration result in differences in interfacial tension and surface pressure that cause surface flows that facilitate film drainage and coalescence. Coalescence affects mass transfer since the coalescing drops can have different composition.

Skelland and Moeti (1990) and Skelland and Xien (1990) measured mass transfer rates using an electrical conductivity probe for drops suspended in an agitated vessel. Results of 180 different systems were correlated by

$$\frac{k_m d}{D_m} = 1.237 \times 10^{-5} (Sc_c)^{1/3} Re^{2/3} Fr^{5/12} \left(\frac{D}{d}\right)^2 \left(\frac{d}{T}\right)^{1/2} \left(\frac{\rho_d d^2 g}{\sigma}\right)^{5/4} \phi^{-1/2}$$

$$\tag{12-66}$$

where D_m is the mass diffusivity of the solute in the continuous phase, $Fr = N^2 D/g$ is the impeller Froude number, Re the impeller Reynolds number, and $Sc_c = \mu_c/\rho_c D_m$ is the Schmidt number.

12-6.8   Presence of a Solid Phase

Solids affect coalescence in some instances by slowing the rate of film drainage. They can also have the opposite effect of helping to bridge the film, thereby increasing the probability of coalescence. Dispersion is less sensitive to the presence of solids. At low solids concentration there is little effect. At continuous phase concentrations above 10 vol %, a higher average viscosity tends to

reduce coalescence and create higher shear stresses. Therefore, drop sizes become smaller with increasing solids content. "Limited Coalescence" is a patented, high concentration dispersed phase process that utilizes solids to stabilize against coalescence. It is described fully in Section 12-9.2.3.

12-6.9 Effect of a Gas Phase

Gas bubbles play a complicating role in both dispersion and coalescence. The effects of gas bubbles are size dependent. Large bubbles (larger than drops) interfere with momentum transfer. This results in a loss of shear stress and the ability to transport momentum necessary for drop dispersion. Large bubbles often collect drops in their wake or in the trapped liquid between them. When bubbles are trapped in the liquid film, buoyancy forces create a squeezing flow that enhances drop coalescence. On the other hand, microbubbles, located in the film drainage region between drops, interfere with film drainage and thus reduce coalescence rates.

12-7 EQUIPMENT SELECTION FOR LIQUID–LIQUID OPERATIONS

12-7.1 Introduction

Any impeller in a vessel capable of pumping fluid and providing shear can produce liquid–liquid dispersions. The impellers commonly used for immiscible liquid–liquid systems include disk turbines, pitched blade turbines, propellers, hydrofoils, paddles, retreat curve impellers, and other proprietary designs. We showed in Section 12-2 that drop size depends on maximum energy dissipation rate. More specifically, eq. (12-23) shows that the power number of an impeller affects drop size. In this section we deal with equipment used for two common industrial applications: creating the maximum interfacial area and creating uniformly sized drops.

Most drop dispersion results from shear forces created by a rotating impeller. To a lesser extent, drop dispersion occurs by drops impinging on baffles and vessel walls, and by streaming from dispersed phase liquid collected on impeller blades and other surfaces. Dispersion in a static mixer involves both shear forces and drop impingement on the leading edges of mixer elements. Although the major emphasis of this section is on stirred vessels, other contacting equipment is also considered.

12-7.2 Impeller Selection and Vessel Design

12-7.2.1 Impeller Selection. Design for liquid–liquid contactors includes impeller geometry, number of impellers required, D/T ratio, and location in the vessel. Commonly used impellers are classified as producing shear or flow. If the application requires high interfacial area (small drop diameters), a high-shear impeller, such as the Rushton turbine shown on the left in Figure 12-28, is a

good choice. These turbines are also known as radial disk turbines (RDT) and by other vendor designations, such as the Lightnin R100 or Chemineer D6. If moderate, yet gentle shear is required, such as for emulsion polymerization, the retreat curve impeller, shown in the center of Figure 12-28, is commonly chosen. When larger drops of a narrow size distribution are required, the loop impeller, shown in the right view of Figure 12-28, is a reasonable choice. Broad blade paddles are also used. Acceptable substitutes for the RDT include the Scaba and Chemineer's BT6 and CD6 impellers, commonly used for gas–liquid mixing.

RDTs produce strong radial flows and intense turbulence. When the impeller flow meets the vessel wall, it divides, forming two distinct circulation zones, as shown in Figure 12-29. Baffles increase dispersing power by increasing power draw and eliminating vortexing.
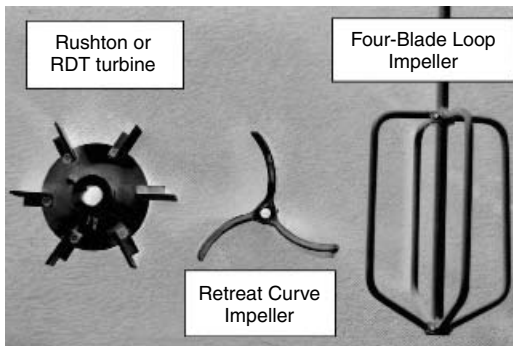

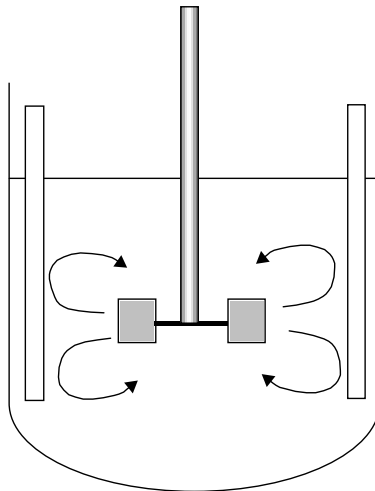**Figure 12-28**   Some impellers used for liquid–liquid dispersion.

Figure 12-29   Overall flow pattern for a radial disk turbine in a baffled vessel.

Other high-shear impellers include the tapered blade ChemShear impeller and dispersing disks such as the Cowles impeller. These provide excellent shear, but far less flow than the RDT. They are used primarily in small scale batch applications where dispersion time is not critical. Pitched blade turbines (PBT) are used when large density differences could lead to a suspension problem. They require higher speed to create the same drop size as the RDT, since they have a lower power number. The flow discharge angle for PBTs varies with Reynolds number and blade angle.

Impeller size is conveniently specified in terms of the D/T ratio. This helps conceptualization and scale-up. This ratio varies from 0.25 to 0.40 for RDTs and from 0.4 to 0.6 for flow-type hydrofoils and propellers. D/T ratios for retreat curve, glassed steel impellers are larger, usually ranging from 0.5 to 0.8. Vertical placement of the impeller depends on vessel shape and application. For example, for dispersion by continuous addition of a dense phase fluid into a less dense fluid, the impeller should be placed fairly low in the vessel at a clearance $C \approx H/4$ to H/5, where H is the liquid height. For dispersion of light liquids, it is good practice to place a single impeller between $0.2 \leq C/H \leq 0.5$. The subject of impeller type and location with respect to drop suspension was covered in Section 12-6.

The production of pharmaceuticals and specialty chemicals frequently requires the same vessel and agitation equipment be used for each processing step. Therefore, a gas–liquid dispersion step might require special impellers for that operation. If a liquid–liquid processing step is also required, the equipment chosen for the gas–liquid step will usually be well suited for liquid–liquid dispersion. For such multiuse applications, it is essential to use a variable speed drive. It is common to have to deal with slurries. Care must be taken to ensure adequate mixing during off-loading, so impellers are often located close to the bottom for such applications.

Multiple impellers are recommended if $H/T \gg 1.2$ or if $\Delta\rho > 150$ kg/m^3. Assuming a less dense dispersed phase, the second or top impeller often is a hydrofoil placed midway between the RDT and the surface of the liquid. This impeller produces high flow at low power, provides excellent circulation, and complements the flow pattern produced by the RDT. The diameter of the second impeller is usually greater than the RDT, typically $D/T \geq 0.45$. A good practice is to distribute the total power to $\approx$20% for the hydrofoil and $\approx$80% for the RDT. Since the power number, N_p, is known for each turbine, setting the power distribution enables the diameter of the hydrofoil to be determined. The vertical position of the upper turbine must ensure that fluid reaches the lower impeller, but must avoid gas entrainment that could occur if placement is too close to the liquid surface. Flow from a PBT does not complement that from a RDT and is therefore not recommended. Power requirements are discussed in Section 12-7.3. Table 12-6 lists equipment options for different drop sizing objectives (desired result). If d_{32} must be less than 30 μm, the use of a stirred tank is not recommended, so other devices are also included in the table.

Mass transfer among drops is enhanced by repeated coalescence and redispersion. This is very important in liquid–liquid extraction. Disk turbines used in

Table 12-6   Common Types of Equipment Used for Liquid–Liquid Dispersion

Description	Impeller Types	Batch or Continuous	Desired Result	Comments
Stirred tanks; baffles	Flat, pitch, and disk type	Either	$30 \leq d_{32} \leq 300 \ \mu m$	General; mass transfer operations
Stirred tanks; baffles	Retreat curve	Either	$30 \leq d_{32} \leq 300 \ \mu m$	General; emulsion polymerization[a]
Stirred tanks; no baffles	Paddle, loop, special types	Batch	$100 \leq d_{32} \leq 1000 \ \mu m$	Suspension polymerization; suspending agent required
Static/in-line mixers	None	Continuous	$10 \leq d_{32} \leq 200 \ \mu m$	Dispersant or protective colloid needed
Rotor–stator mixers	Slotted ring or impeller, along with slotted stator	Either, often continuous	$1 \leq d_3 \leq 50 \ \mu m$	Sparse data for scale-up; need extensive testing
Impingement mixers	None	Continuous	$1 \leq d_{32} \leq 50 \ \mu m$	Sparse data; work with vendors
Valve homogenizers; ultrasonic mixers	None	Usually continuous	$0.1 \leq d_{32} \leq 10 \ \mu m$	Sparse data; work with vendors; feed is predispersed

[a] Drop size refers to monomer drops. Latex products are much smaller particles, in the range 0.1 to 0.5 μm.

extraction are operated at moderately low speed to avoid over dispersing, thus forming hard to coalesce drops. Suspension polymerization applications require production of nearly monodispersed drops, since these become the final product. Figure 12-30 shows a loop impeller that creates low, uniform shear for suspension polymerization. It was described by Leng and Quarderer (1982) and is discussed in Section 12-8. Four long vertical arms produce regions of relatively uniform shear and provide wall movement for heat transfer. This design is not easily adaptable to systems of large phase density difference, due to weak axial flow. D/T ratios are between 0.6 and 0.8. Two- and four-blade backswept square paddles can also used. Baffling is kept to a minimum to minimize shear.

12-7.2.2 Tank Geometry. It is essential to avoid stagnant regions in liquid–liquid operations, regardless of the process. This means that use of flat- and cone-bottomed tanks and tall slender vessels should be avoided if possible. Placing baffles away from the wall, to permit flow between the wall and the baffle, prevents dispersed phase buildup on surfaces. Internal heating coils and ladders should also be avoided if possible. Optimum flow patterns normally
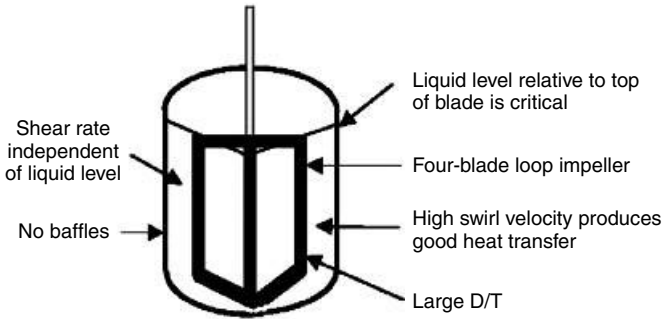
Figure 12-30   Low-shear agitation for suspension polymerization.

develop when the overall vessel shape is $1 < H/T < 1.2$. It is certainly possible to operate successfully well beyond this range, as shown later in this section, but the design must provide for excellent flow throughout the vessel.

For mass transfer dependent reactions, agitation must promote dispersion, discourage coalescence, and prevent settling. Usually, a single impeller can accomplish these tasks for vessels of $H/T \leq 1.2$ and for $0.9 < \rho_d/\rho_c < 1.1$. However, additional impellers are used when $H/T \geq 1.2$ or when ρ_d/ρ_c is outside the limits cited above. The selection of a second impeller was discussed in Section 12-7.2.1. Dispersions of 1 mm drops are easily suspended in square vessels ($H = T$) and normally do not require use of a second impeller.

High-pressure autoclaves are sometimes designed as tall, slender vessels to minimize construction cost due to wall thickness. Figure 12-31 shows such an
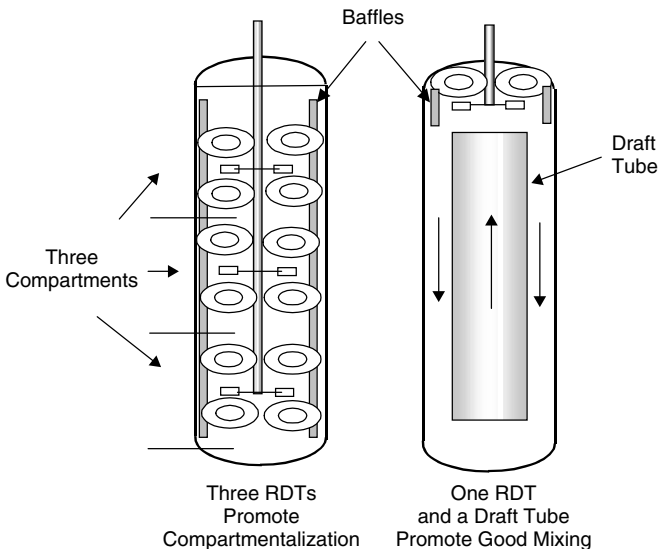

Figure 12-31   Internal arrangements for tall vessels.

application. The slender shape complicates efficient top-to-bottom mixing. A solution is to use a draft tube, with a tube/tank diameter ratio of ~0.7, and a top entering Rushton turbine. This is shown in the right-hand view. This design avoids compartmentalization problems leading to poor circulation, shown by the design on the left. Multiple RDTs set up circulation cells around each impeller. Reaction modeling shows results for this design to be consistent with those for a multistage CSTR. The preferred design of Figure 12-31 was commercialized and operated for over 20 years, for a high-pressure reaction requiring both high shear and circulation. Its features are discussed further in Section 12-8.

12-7.2.3   *Forming Dispersions*. The initial condition is important in forming dispersions, as illustrated in Figures 12-32 and 12-33. In these examples, oil is the lighter or upper phase. If the lower phase is to be dispersed in the upper phase, the RDT is placed in the upper phase and an up-pumping axial flow turbine is placed in the lower phase. Figure 12-32 shows the suggested arrangement. When the upper oil layer is to be dispersed in the lower water layer, the arrangement shown in Figure 12-33 is recommended. Here the axial flow turbine pumps downward. Both figures show the use of a RDT for dispersion and a propeller to improve circulation. Single impellers can also be used. Often, both o/w and w/o regions initially coexist. The amount of each phase, and the relative rates of coalescence (o/w versus w/o) during transient conditions, determines whether the final system is o/w or w/o. Figure 12-34 shows the ideal location for a single turbine.

12-7.2.4   *Baffles and Baffle Placement*. Baffles increase the axial velocity component that promotes circulation and reduce the tangential or swirl velocity. This lower tangential velocity leads to a higher relative velocity and shear rate near the impeller. Higher rates of shear and circulation result in faster overall dispersion. Good surface movement helps prevent settled layers from forming. Poor surface movement can lead to surface coalescence and the formation of a condensed layer. Baffles help prevent this. However, suspension polymerization reactors use little or no baffles to help reduce shear and therefore produce larger drops.

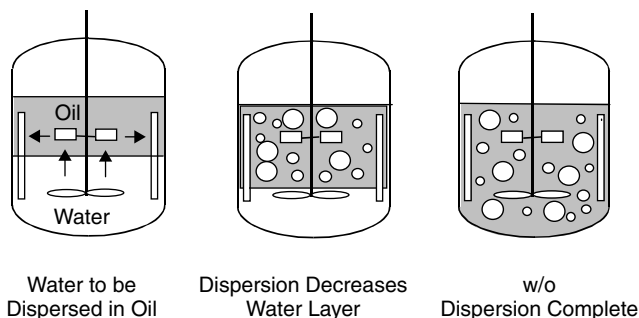

Water to be   Dispersion Decreases   w/o
Dispersed in Oil   Water Layer   Dispersion Complete

Figure 12-32   Dual impeller arrangement for water-in-oil dispersion. Propeller is upward pumping.

Oil to be Dispersed in Water

Dispersion Decreases Oil Layer

Nearly Complete Dispersion of Oil in Water

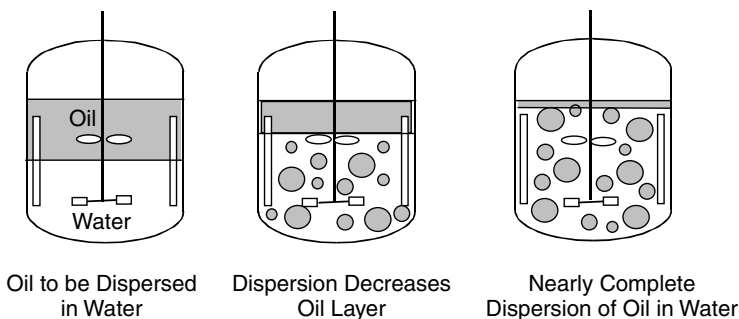**Figure 12-33** Dual impeller arrangement for oil-in-water dispersion. Propeller is downward pumping.

Single Impeller at o/w Interface
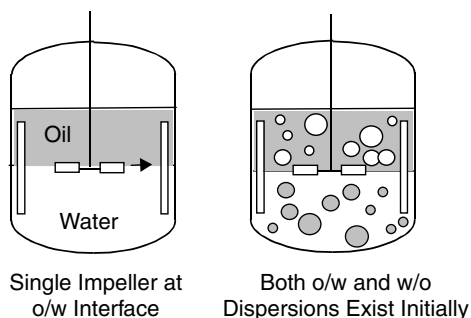
Both o/w and w/o Dispersions Exist Initially

Figure 12-34 Single RDT placed at oil–water interface.

Short baffles, H/3 in length and T/12 in width, located just below the liquid surface, can be used to promote improved axial flow while producing only a slight increase in effective shear rate. They are positioned well above the plane of the impeller and are able to convert tangential into axial momentum without significantly increasing shear rates. If phase density differences are great enough to require better overall circulation, narrow width baffle designs (<T/12) should be considered. Baffles used in glass-lined equipment (beavertail or "D" or finger designs) have proven beneficial, since the degree of baffling can be adjusted by changing the baffle angle relative to the flow. However, baffles can cause dispersed phase and polymer buildup, stagnation, and some loss of heat transfer through the wall, due to lower tangential velocities at the wall. A nonfouling design is to provide weak baffling by welding four 90° angle sections to the vessel walls, to create triangular fins. Baffles cause an increase in power supplied to the vessel and therefore reduce drop size.

As a general rule, four equally spaced baffles should be used. The baffle width should be T/10 to T/12 and should be located a minimum distance of T/72 from the wall. This enables liquid to pass between the baffle and the wall. Baffles should extend from just below the surface of the liquid to the lower end of the
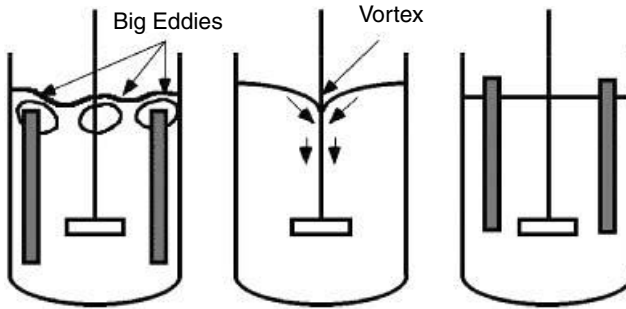
Figure 12-35   Importance of baffling to surface conditions.

straight wall, or in the case of dish-bottomed vessels, the lower tangent line. For good mixing, Nagata (1975) proposed suspending baffles from the top of the vessel a radial distance two-thirds out from the center and to submerge them to a depth of H/3. This arrangement is commonly found in glass-lined vessels, where baffles are suspended from the top head. However, for conventional vessels, top-mounted baffles are seldom used.

As noted above, correct baffle placement can improve surface flow. The location of the top edge of the baffles relative to the liquid surface is important in creating eddies that are helpful in facilitating drop suspension. When baffle tips are just below the surface, unrestricted eddy motion facilitates engulfment of surface materials into the bulk liquid. If baffles extend through the surface, they create local stagnation, causing slow surface engulfment and sometimes pooling. This is shown in Figure 12-35. The left-hand view shows how ideally placed baffles can aid in creating surface motion. The center view shows that a central vortex forms when no baffles are used. Although poor from a mixing point of view, the vortex can assist in the engulfment of feed streams. The right-hand view shows baffles extending through the surface and creating stagnation and poor surface mixing.

12-7.2.5 Location of Feed and Exit Streams. When rapid initial mixing is required, direct feed injection through a dip pipe to the impeller is often used for nonplugging conditions. Other considerations, such as differences in phase densities, need to be considered. Low density liquids are introduced near the bottom and heavy liquids near the top of the vessel. Feed discharge onto the surface is not recommended.

Most batch processes are drained from the bottom of the vessel, but for continuous processes, removal can be from any well-mixed region. It is good practice to keep feed and exit locations as far apart as possible to prevent "short-circuiting."

12-7.3   Power Requirements

The questions to address when estimating power requirements are:

- How much power is needed for the desired result?
- Which impeller(s) size and speed will deliver that power?
- What vessel geometry, shape, and baffling are to be used?

As discussed in Section 12-2, the ultimate drop size is determined by ε_{max}, not ε_{avg}. However, most correlations for drop size use ε_{avg}, since data for ε_{max} are not readily available. Many investigators, starting with Corrsin (1964), determined that $\varepsilon_{max}/\varepsilon_{avg} \simeq 40$. Once T, D/T, and ε_{avg} have been selected, it is a straightforward task to calculate the operating speed, motor power, and torque. The power number, N_p, is needed for the calculation. Power numbers for different impellers are a function of impeller Reynolds number and are found in Chapters 6 and 9. Once N_p is known, the hydraulic power is calculated from

$$P = \frac{N_p \, \overline{\rho} \, D^5 \, N^3}{f_{conv}} \tag{12-67}$$

If the units are P in hp, D in ft, N in rpm, and $\overline{\rho}$ in lb/ft^3, the conversion factor is $f_{conv} = 17{,}710$. If the units are P in kW, D in meters, N in rps, and $\overline{\rho}$ in kg/m^3, then $f_{conv} = 0.001$. The vessel average power per unit mass, $\varepsilon_{avg} = P/V \overline{\rho}$.

12-7.4   Other Considerations

12-7.4.1   Time to Reach Equilibrium.   As discussed previously, studies over the past two decades have shown that large differences in turbulence energy and shear exist in different regions of stirred vessels. Turbulence is highest near the impeller surfaces and lowest near vessel walls and the free surface. As a result, the power input is not evenly dissipated throughout the tank, so that d_{max} is achieved only when the last drop of size $d > d_{max}$ experiences the region of maximum energy dissipation, ε_{max}. For example, in tests witnessed by one of the authors, a 1000 gal suspension polymerizer took over 30 h to reach terminal dispersion conditions. A light transmission probe was used to measure the transient interfacial area. Most industrial processes using noncoalescing liquid–liquid systems operate at transient drop size conditions. Steady-state (equilibrium) conditions are reached more quickly in coalescing systems.

Equation (12-68) shows an empirical relationship developed by Hong and Lee (1983, 1985) for the time to reach equilibrium, t_{eq}. They conducted 181 experiments (representing five different liquid–liquid systems) and two scale sizes. The range of dispersed phase volume fraction was $0.05 < \phi < 0.20$.

$$N\,t_{eq} = 1995.3 \left(\frac{D}{T}\right)^{-2.37} \left(\frac{We}{Re}\right)^{0.97} \frac{\mu_d}{\mu_c} Fr^{-0.66} \tag{12-68}$$

The time for a dilute system to reach equilibrium was discussed in Section 12-2.4.

12-7.4.2 Breakage and Coalescence Regimes.

As stated previously, dispersion depends on maximum local energy, ε_{max}, and coalescence depends on gentle shear. For coalescing systems, drops will coalesce in the more quiescent regions of a stirred vessel and will disperse close to the impeller. This is illustrated by the work of Sprow (1967b), shown in Figure 12-36. Using a small baffled stirred vessel and a coalescing system consisting of methyl isobutyl ketone in water, Sprow found that drop size varied with agitator speed and with location in the vessel. Position C represents a location where dispersion controls. At this location he found that $d_{32} \sim N^{-1.5}$, which is a much stronger speed dependence than the $N^{-1.2}$ prediction of the Weber number theory given by eq. (12-22). Position D is well away from the impeller where gentle flow promotes coalescence. Drops in this region were less sensitive to agitation with $d_{32} \sim N^{-0.75}$. Coalescence dominates at position D but dispersion dominates at C. Since $\varepsilon \sim N^3 D^2$, then $\varepsilon^{-1/4} \sim N^{-0.75}$, and Sprow's data at position D are consistent with those of Church and Shinnar (1961) for the coalescence line in Figure 12-25. Sprow's results imply that coalescence and dispersion rates are as fast or faster than overall mixing and circulation rates. This may be the exception, not the rule.
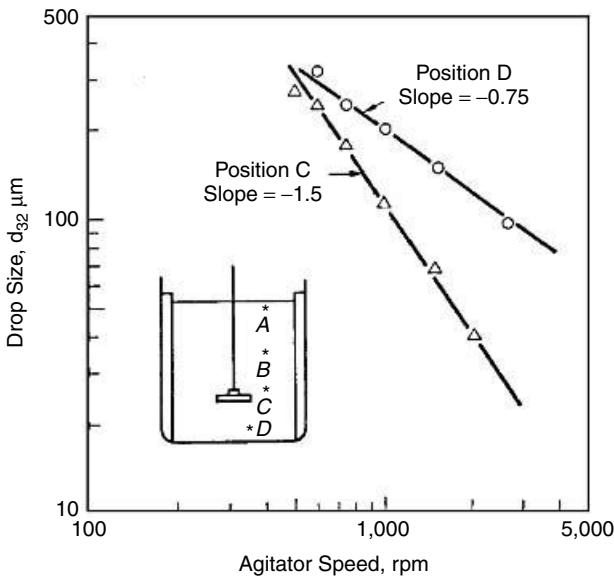

Figure 12-36 Drop size dependence on impeller speed and spatial location for a coalescing system. (From Sprow, 1967b, reproduced with permission of AIChE © 1967.)

For example, Hong and Lee (1983, 1985) argued that Sprow's results were exaggerated. Using light transmission probes to measure interfacial area, they found only a small spatial variation in drop size. We can only conclude that spatial dependence can occur and is system dependent. It is less apt to be a problem, even for coalescing systems, if the vessel has short circulation times.

12-7.4.3 *Circulation Time*.

As stated previously, both time to equilibrium and the competition between coalescence and dispersion depend on circulation time. Holmes et al. (1964) performed bench scale experiments in a baffled flat-bottomed vessel with $H = T$ and $C/T = \frac{1}{2}$. For turbulent flow their data were well correlated by

$$N \bar{t}_{circ} = C_{27} \left(\frac{T}{D} \right)^2 \tag{12-69}$$

where $\bar{t}_{circ}$ is the mean circulation time and $C_{27} = 1.0$ for their RTD and vessel geometry. Middleton (1979) considered the effect of scale and performed experiments in three vessels of similar geometry, ranging from $0.61\ m < T < 1.8\ m$. However, in his work $C/T = \frac{1}{3}$. His data were well correlated by

$$N \bar{t}_{circ} = 0.5 V^{0.3} \left(\frac{T}{D} \right)^3 \tag{12-70}$$

There appears to be mechanistic arguments as well as further experimental evidence to support both correlations. It is apparent that other variables, such as C/T, H/T, bottom geometry, and so on, will significantly influence circulation time.

An intuitive approach is to assume that V/Q_V gives the mean circulation time, where Q_V is the volume flow from the impeller. The latter quantity is usually correlated in terms of flow number, $N_q = Q_V/ND^3$. Then

$$N \bar{t}_{circ} = \frac{V}{N_q \cdot D^3} \tag{12-71}$$

Equations (12-69) and (12-70) both indicate that the intuitive approach of eq. (12-71) is too optimistic. However, it has been applied successfully in limited cases.

12-7.5 Recommendations

- Select RDTs for demanding applications. As discussed in Section 12-2, this is presently the only well-studied geometry.
- Use dished/elliptical-bottomed vessels of overall proportions of $H/T = 1$ to 1.2. These give better circulation and minimize creation of dead zones.
- Use multiple dispersing impellers, full baffles (either conventional or those proposed by Nagata), and larger D/T impellers if strongly coalescing systems are involved. Minimize circulation time through the use of

secondary large high-flow impellers. $\bar{t}_{circ}$ is reduced by a factor of 2 if two equal-sized RDTs are used in place of one.

12-8 SCALE-UP OF LIQUID–LIQUID SYSTEMS

12-8.1 Introduction

Scale-up of agitated immiscible liquid–liquid systems can be a challenge that should not be taken lightly. The problems arise from incomplete or inaccurate process information and few quantitative tools to deal with complex technology. In this section we describe some proven practices for scale-up and caution that liquid–liquid dispersion technology is highly system specific.

Most problems are not observed in glass bench scale equipment because unrealistically high rates of circulation mask coalescence and suspension problems. These problems usually surface at the time of scale-up. Throughout this chapter it has been emphasized that production scale vessels are dominated by coalescence, whereas small vessels are dominated by dispersion. As discussed previously, Sprow (1967b) worked with a coalescing system in a small bench scale vessel and found that different regions of the vessel responded differently to agitation. The technology to cope with these complex issues lags other mixing operations, such as blending and solids suspension. Often, all three flow-dependent phenomena—dispersion, coalescence, and drop suspension—must be dealt with simultaneously.

A successful scale-up does not mean that identical results are obtained at two different scales, but rather, that the scale-up results are predictable and acceptable. Problem correction at large scale is costly, time consuming, and sometimes not possible (see Section 12-9.2.2). Scale-up errors can lead to losses in capacity, quality, safety, and profits. For example, an explosion resulted from increasing agitation for an inadequately suspended mixed acid nitration. Faster agitation created a large increase in interfacial area at reaction temperatures and led to an uncontrolled exothermic reaction and property loss.

The scale-up of certain liquid–liquid processes can be straightforward. Dilute dispersions are the easiest processes to scale up. The most difficult ones involve simultaneous coalescence, dispersion, suspension, mass transfer, and chemical reaction. If multiple complex reactions are involved, inadequate mixing often leads to yield losses.

The first step is to understand the goals of the process and to acquire accurate data for all components, including physical, chemical, and interfacial properties as well as reaction kinetics. This also includes the influence of minor impurities. Differences in the quality of raw materials need to be considered.

It is important to undertake bench scale studies that simulate the poorer mixing conditions in the larger vessel. For example, simulate the large scale vessel circulation time. Although dispersion is apt to be unrealistic, coalescence and settling problems can be observed. Examination of the flow patterns in the proposed full scale vessel using CFD can help visualize potential problems related

to design. Once the CFD model has been developed and validated, design and operating parameters can be compared to determine design sensitivities. One observation seems to hold universally—better results are always obtained in small equipment.

Identify applications by types likely to cause problems, and separate these from more trivial applications. For example, mixing is critical in the following applications:

- Chemical reactors/polymerizers in which reaction rates are equal to, or faster than, mixing rates
- Competing chemical reactions when yields depend on good mixing
- Mass transfer dependent reactions involving coalescence and dispersion

Less demanding tasks include:

- Heat transfer
- Reactors involved with slow chemical reactions

12-8.2 Scale-up Rules for Dilute Systems

Many processes have been scaled successfully using ND^X = constant. This simple rule is based on years of industrial experience. To apply it, the tank Reynolds number must be greater than 10^4 and vessels must be geometrically similar. Table 12-7 lists the rule and the application best suited to the rule. Other operations, such as blending and solids suspension, are included to provide the reader

Table 12-7 "Rules" for Scale-up of Geometrically Similar Vessels at Turbulent Conditions, Based on ND^X = Constant

Value of X	Rule	Process Application
1.0	Constant tip speed, constant torque/volume	Same maximum shear; simple blending; shear-controlled drop size.
0.85	Off-bottom solids suspension	Used in Zwietering equation for N_{js}, for easily suspended solids; also applies to drop suspension (see Section 12-6.2).
0.75	Conditions for average suspension	Used for applications of average suspension difficulty.
0.67	Constant P/V	Used for turbulent drop dispersion; fast settling solids; reactions requiring micromixing; gas–liquid applications at constant mass transfer rate.
0.5	Constant Reynolds number	Similar heat transfer from jacket walls; equal viscous/inertial forces.
0.0	Constant speed	Equal mixing time; fast/competing reactions.

with an overview of how the exponent on impeller diameter varies from operation to operation. One can see from the table that different scale-up rules apply for suspension, dispersion, heat transfer, and reaction, making it necessary to focus on the most important or limiting task. As mentioned earlier, the indiscriminate use of rules can lead to problems.

Example 12.3. Consider scale-up of a process for a dilute (noncoalescing) liquid–liquid system. For inviscid drops,

$$d_{max} = C_1 \left(\frac{\sigma}{\rho_C} \right)^{0.6} \varepsilon_{max}^{-2/5} \tag{12-21}$$

SOLUTION: Assume similar geometry, $Re > 10^4$, an equal ratio of $\varepsilon_{max}/\varepsilon_{avg}$ on both scales and identical physical properties. For $N_p = $ constant, $\varepsilon_{avg} \sim N^3 D^2$. Then eq. (12-21) for scale 1 and scale 2, with the condition $d_{max}(1) = d_{max}(2)$, can be written

$$\frac{d_{max}(1)}{d_{max}(2)} = 1 = \left[\frac{\varepsilon_{avg}(2)}{\varepsilon_{avg}(1)} \right]^{2/5} = \left[\frac{P/V(2)}{P/V(1)} \right]^{2/5} = \frac{N(2)^{1.2}D(2)^{0.8}}{N(1)^{1.2}D(1)^{0.8}} \tag{12-72}$$

Since $(ND^{0.67})^{1.2} = N^{1.2}D^{0.8}$, eq. (12-72) is consistent with Table 12-7, row 4.

Equation (12-72) can be used to calculate the speed required for a $T = 3.0$ m vessel with $D/T = \frac{1}{3}$, to achieve the same drop size as a $T = 1.0$ m geometrically similar vessel operating at 200 rpm. Substituting $N(1) = 200$ rpm, $D(1) = 0.33$ m, and $D(2) = 1.0$ m into eq. (12-72) gives $N(2) = 95.5$ rpm.

12-8.3 Scale-up of Concentrated, Noncoalescing Dispersions

Dilute, low viscosity dispersions are nearly always controlled by turbulence. At high dispersed phase concentrations, small scale turbulent eddies are damped out by the drops and bulk viscosity increases. As a result, laminar shear forces can control drop dispersion in concentrated systems. Turbulence theories developed for dilute dispersions can sometimes apply to concentrated, noncoalescing systems. However, in other cases, they may not. This is illustrated, by example, below for the scale-up of a suspension polymerization application, described by Leng and Quarderer (1982).

The system consisted of free radical initiated styrene–divinylbenzene monomers dispersed in water containing 0.2% dissolved polyvinyl alcohol. The dispersed phase was 50 vol %. The process was to be carried out in a vessel containing a loop impeller (see Figure 12-28) operating at low-shear conditions. Bench scale studies showed important variables to be speed, impeller diameter, baffling, selection of the suspending agent, and continuous phase viscosity. Polymerization reactions were completed and bead size distributions were determined by sieve analysis.

Theories based on laminar and turbulent dispersion conditions were developed, and tested by comparing bead size against each specific variable. Results showed that beads of size greater than 300 μm were formed under laminar shear-controlled conditions, and smaller beads were formed under turbulence-controlled conditions.

Leng and Quarderer (1982) reasoned that dispersion occurred in the boundary layer adjacent to the loop impeller surfaces and that the impeller vertical elements could be approximated by cylinders moving through the suspension at the relative impeller tip speed. When laminar shear forces predominated, it was shown that

$$d_{max} = C_{28}\sigma \left(\frac{D_C}{\mu_c \rho_c}\right)^{1/2} \frac{1}{[ND(1-k_v)]^{3/2}} \left(\frac{(\mu_d/\mu_c)+1}{1.19(\mu_d/\mu_c)+1}\right) f(\mu_d/\mu_c) \quad (12\text{-}73)$$

where D_C is the diameter of the cylinder and k_v is the ratio of the tangential velocity at the impeller tip to the tip speed. All other variables follow earlier use.

The equation for turbulent dispersion was based on the classical development of Chen and Middleman (1967) (see Section 12-2), with the energy dissipation term calculated for drag on a cylinder. Two cases were assumed for the dissipation volume in the wake region behind the cylindrical impeller blade. The first was that an eddy length proportional to the cylinder diameter determined the dissipation volume. The second was that this volume was proportional to the velocity of the cylinder (tip speed) and a characteristic eddy decay time. Equation (12-74) results from the second case. It showed reasonable agreement with data taken at higher speeds.

$$d_{max} = C_{29} \left(\frac{\sigma}{\rho_c}\right)^{3/5} \frac{1}{(ND)^{4/5}(1-k_v)^{2/5}} \quad (12\text{-}74)$$

Typical low-speed laboratory results showing the effect of impeller speed and baffling are given in Figure 12-37. Using paddle impellers, Aiba (1958) found that $k_v = 0.6$ for unbaffled and 0.3 for baffled conditions. These values were used to correct for baffling effects. Uncorrected data fell on two parallel lines of the same slope. In Figure 12-37, $d_{max} \sim N^{-1.5}$, confirming the validity of eq. (12-73) based on the bench scale data. Other laboratory scale results are given in the paper.

Scale-up experiments were conducted in four larger scale vessels, ranging in volume from 0.082 to 15.1 m^3. The D/T ratio varied from 0.478 to 0.676. For each vessel, the impeller speed that gave $d_{max} \approx 1000$ μm was determined. Identical physical properties and chemical composition were used at all scales. Then, according to eq. (12-73), for d_{max} to be the same on all scales, the quantity $D_C^{1/2}/(ND)^{3/2}$, based on the measured speed, must be the same on all scales. Table 12-8 shows values of this quantity. The numbers in the second column appear to be scale independent. This supported the hypothesis that dispersions were formed by laminar shear. Equation (12-74) did apply to runs made at higher impeller speeds.
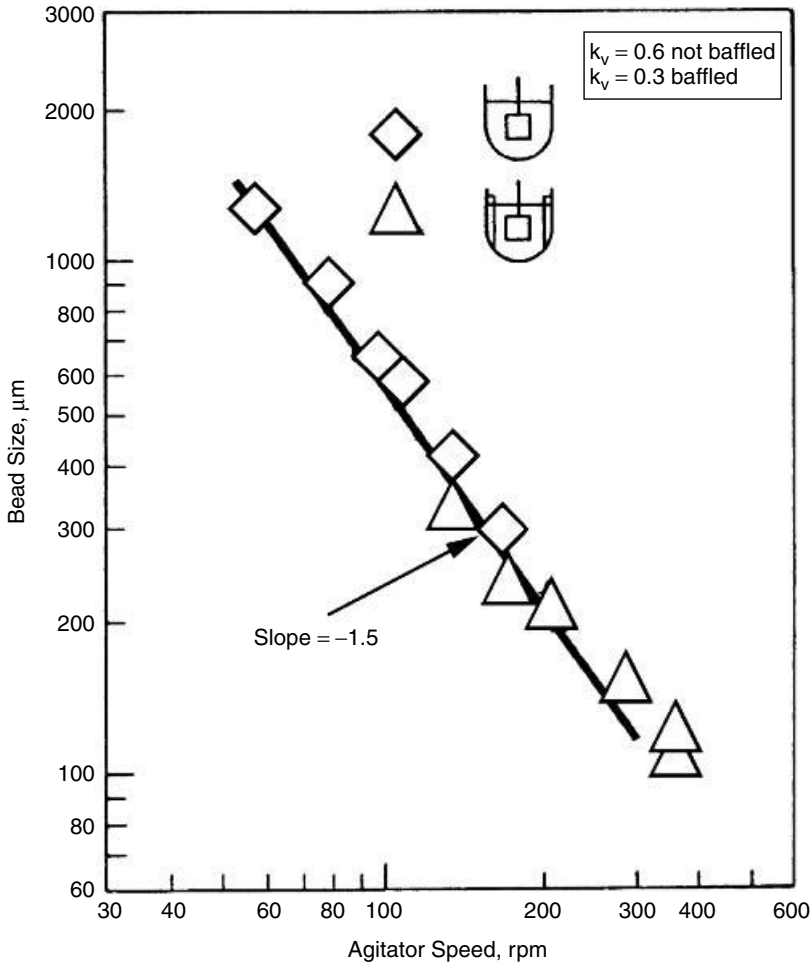
Figure 12-37   Suspension bead size versus agitation rate for styrene/DVB. (Reproduced from Leng and Quarderer, 1982.)

Table 12-8   Validation of Eq. (12-73) for Scale-up

Reactor Volume (m^3)	$Dc^{1/2}/(ND)^{3/2}$
0.082 (laboratory)	7.5×10^{-4}
0.1135	7.5×10^{-4}
0.330	6.0×10^{-4}
2.840	4.8×10^{-4}
15.15 (production)	5.5×10^{-4}

Source: Data of Leng and Quarderer (1982).

12-8.4 Scale-up of Coalescing Systems of All Concentrations

No exact method exists to assure successful scale-up of strongly coalescing systems. The following considerations are offered.

- Does the process require coalescing or noncoalescing conditions? Extractions require coalescence; suspension and emulsion polymerization processes do not.
- Few industrial systems are rapidly coalescing. Impurities, salts, and residues often ensure slow coalescence.
- Coalescence rates can be characterized using either the static or dynamic method described in Section 12-3.1.5 and Table 12-3.
- Make the more viscous phase continuous if coalescence is to be minimized. Consider adding a thickener to the continuous phase.
- Suspending aids, such as polymeric suspending agents, detergents, or fine solids, reduce or stop coalescence.
- A static mixer in a recirculation loop can complement conventional agitation in the vessel.
- The use of multiple and larger diameter impellers can increase the "effective" dispersion zone.
- CFD can be used to examine flow field details for both the small scale and the proposed larger scale vessels, and to map out regions of constant energy dissipation rate. The dispersion volume can be approximated as the region in which $\varepsilon_{local}/\varepsilon_{avg} \geq 3.0$. Similarly, the coalescence region is where $\varepsilon_{local}/\varepsilon_{avg} \leq 0.1$. The probability of success upon scale-up will improve if the volume ratio of the dispersion to coalescence regions is scale independent.

12-8.5 Dispersion Time

Dispersion kinetics is discussed in Section 12-2.4 for dilute systems and in Section 12-7.4.1 for more concentrated systems. As stated previously, dispersion kinetics in turbulent stirred vessels follows a first-order rate process, and rate constants depend on interfacial tension, drop size, and flow conditions (Hong and Lee 1983, 1985). Figure 12-38 shows a typical drop size versus dispersion time relationship for a batch vessel. Upon introduction of the dispersed phase, the drop size falls off rapidly and approaches the ultimate size within a factor of 2 or so, at times that are often short compared to the process time. However, the decay to equilibrium size is quite slow. This is why equilibrium drop size correlations perform adequately despite the fact that the process time is often smaller than the time to equilibrium.

Dispersion time adds a complication to the scale-up of liquid–liquid systems. For a coalescing system, a small vessel reaches d_{32}^{∞} in a shorter time than the larger one. This is illustrated in Figure 12-39. A steady d_{32}^{∞} is reached at time
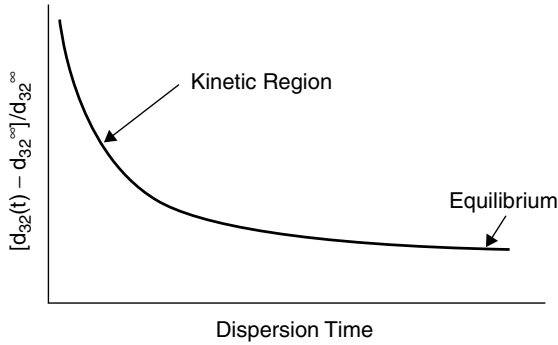
Figure 12-38 Drop size as a function of dispersion time in a batch vessel.
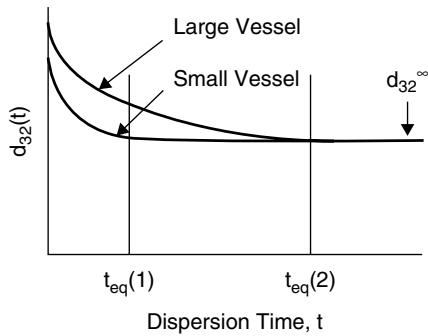
Figure 12-39 Typical dispersion times in vessels of different size.

$t_{eq}(1)$ in the small vessel, but not until time $t_{eq}(2)$ in the large one. If the large vessel is required to have the same dispersion time as the bench scale, the agitation rate must be increased beyond the value for equal drop size. The mean drop size can be smaller and the drop size distribution may be affected.

12-8.6 Design Criteria and Guidelines

Table 12-9 gives a summary of practical guidelines for scale-up of coalescing and noncoalescing systems. Based on the static test for coalescibility, described in Section 12-3.1.5 and Table 12-3, a non/slowly coalescing system has a settling time that is greater than 5 min. A rapidly coalescing system has a settling time of less than 1 min. In Table 12-9, the scale-up limitation refers to the ratio of vessel volumes (large V_L to small V_S) that should not be exceeded. That is, for non/slowly coalescing systems, it is safe to scale-up by a factor of 100 in volume, but for rapidly coalescing systems, scale-up should be limited to a 10 to 20 fold increase in volume.

Table 12-9 Guidelines for Scale-up of General Purpose Liquid–Liquid Stirred Vessels

Feature	Non/Slowly Coalescing System	Rapidly Coalescing System
Scale-up criterion	P/V = constant	Circulation time = constant
Scale-up limitation, V_L/V_S	100 : 1	10 : 1 to 20 : 1
Baffles	Yes but not for suspension polymerization	Yes
Impellers	RDT and optional axial flow/hydrofoil impeller	Multiple RDTs and axial flow/hydrofoil impeller for better circulation
D/T	0.3–0.5	≥0.5
Time to reach terminal drop size	Long times for large vessels	Short times under 30 min for most coalescing systems (all vessel sizes)
Geometric similarity	Maintain close similarity	Use more and larger turbines in larger vessel; do not try to maintain geometric similarity
Speed/drives	Variable or fixed speed	Variable speed capability is essential; consider overdesign to meet unpredicted performance
Risk	Low to moderate risk	High risk

12-9 INDUSTRIAL APPLICATIONS

12-9.1 Introduction

Common problems encountered in the industrial applications of liquid–liquid systems include (1) failure to meet requirements for interfacial area, often due to effects of coalescence, (2) failure to meet requirements for drop size distribution, (3) failure to meet requirements for drop suspension and process heat transfer, and (4) failure to recognize problems caused by interfacial debris and tiny drops.

Every problem is unique. Sometimes, differences in quality of raw materials lead to unexpected by-products that prevent coalescence. When coalescence is required for separation, filters, centrifuges, and fibrous bed coalescers can sometimes alleviate these problems.

12-9.2 Industrial Applications

Several examples of industrial scale-up problems are given below. In some cases the problems were corrected. For others, less than ideal performance had to be accepted.

12-9.2.1   *Inverse Suspension Polymerization*.   *Inverse suspension polymerization* refers to the polymerization of an aqueous monomer dispersion in an organic continuous phase. For this application, the aqueous dispersed phase consisted of initiated monomer dissolved in water, and the continuous phase was xylene containing a dissolved polymeric suspending agent. On the production scale, polymerization was rapid relative to dispersion, and a viscoelastic dispersed phase was initially produced. Viscoelasticity proved to be a problem during the dispersion step. Deformation and drop breakage of the elastic drops was partly due to tip streaming, and that led to considerable quantities of undesirable fines, dusty particles that caused problems for the customer. Laboratory studies failed to reveal the problem, since dispersion was fast and complete prior to polymerization. In the production plant dispersion was incomplete at the time of initiation.

The problem was solved using initially fast agitation to establish the desired particle size, followed by slower agitation just prior to initiation. This way, dispersion was completed before the elasticity developed. Coalescence was not a problem due to the presence of the suspending agent.

12-9.2.2   *Pharmaceutical Process Scale-up*.   The second step in the synthesis of a pharmaceutical intermediate was to reduce an organic reactant, using powdered zinc and concentrated HCl as the reducing agent. This reduction reaction was mass transfer controlled. Studies in a 10 L glass reactor gave acceptable reaction rates that served as a basis for production goals. The large reactor was a typical 3500 gal glass-lined vessel, containing beavertail baffles and a single retreat curve impeller located at the bottom. Production results were unexpectedly poor. Low yields and reaction rates (17 times slower than expected) were observed. Laboratory tests in glass vessels showed that after stopping agitation, complete coalescence took place in seconds. This evidence suggested that coalescence was the cause of the problem. The large reactor was controlled by coalescence, not by dispersion, as was the case in the laboratory vessel. Loss of much needed interfacial area explained the results.

Agitation in the production scale equipment was changed to include dual glass-lined impellers of $D/T = 0.45$, consisting of a lower four-blade FBT and an upper four-blade 45° PBT. This was an attempt to increase the volume of the dispersion region and to improve circulation. The modified system did improve reaction rates, but not to the degree desired.

12-9.2.3   *Limited Coalescence*.   Limited coalescence is a commercialized process (Ballast et al., 1961) that produces uniform polymer particles. The principle involves providing the correct amount of very fine particles to interfere with film drainage, thereby suppressing coalescence. Inorganic materials, such as zinc oxide or silica, and organic materials, such as sulfonated polyvinyl toluene, have been used. A given number of particles support a given surface area. Since agitation creates more surface area by dispersion, fewer particles are available per unit area to protect against coalescence. Drop sizes then grow by coalescence, which then reduces the total interfacial area. Therefore, ultimate drop size is a

result of a dynamic equilibrium process that depends on the number of particles present, not on agitation intensity. The process is fine-tuned by the use of wetting agents that control the position of the particles relative to the o/w interface. Solids partially wet by the oil phase move into the drop and are less able to prevent coalescence. Nonwetted particles are located at the drop surface, where they effectively prevent coalescence. While drop size is controlled by coalescence phenomena, vigorous agitation is required for good mixing and drop–drop interactions.

12-9.2.4 *Agricultural Intermediate*. The first step in producing an agricultural intermediate was to nitrate an aromatic feed. Nitration usually involves a sequence of reactions leading to mono-, di-, and trinitro products. In this case, only the mononitro compound was desired. The nitrating agent consists of an anhydrous mixture of HNO_3 and H_2SO_4. The nitronium ion becomes available to the dispersed organic phase by mass transfer from the continuous phase through the drop surfaces. Laboratory work in a batch CSTR gave favorable results. A continuous fed columnlike apparatus was used for scale-up. The design was a failure because it did not provide adequate suspension and dispersion, and displayed a predominant tailing residence time distribution pattern. Production was slower than expected, and large quantities of multinitrated products resulted from the undesirable residence time distribution.

12-9.2.5 *Largest Surviving Drop Applications*. Under the conditions described below, the maximum mixing intensity can be characterized by measuring the largest surviving drop size using a dilute, noncoalescing test system. The method consists of contacting an aqueous phase, typically containing 0.1 to 0.2 wt % polyvinyl alcohol (PVA) in water, and an oil phase with $\phi = 0.01$ to 0.02. The oil phase can be any nonpolar liquid such as monochlorobenzene, ethylbenzene, toluene, mineral oil, or silicone oils. Samples are withdrawn to allow measurement of drop size. Analysis is usually done photometrically or by using a Coulter counter. The largest drop diameter in the distribution characterizes maximum mixing intensity. In practice, d_{90} is selected rather than d_{max}. It takes a long time to reach equilibrium in large equipment. It is important to dissolve the PVA completely and to disperse for a long enough time to ensure that all drops "see" the region of maximum shear. Three examples using this technique are given below.

Emulsion Polymerization. Emulsion polymerization processes are used to produce synthetic latexes. Changing product requirements dictate producing and testing many new formulations. Agitation disperses drops, provides mixing, and promotes heat and mass transfer. Latexes are usually shear sensitive and agglomerate if exposed to excessive agitation. With each new product there is the question of agitation optimization. Traditionally, optimal conditions were arrived at by trial and error. The surviving drop method was used to calibrate production scale vessels, identify maximum shear rate, and anticipate product quality from studies in smaller 1 to 5 gal scale equipment.

High-Pressure Autoclave. A high-pressure two-phase alkyl phenol reaction was to be scaled up from experimental data collected from sealed rocking bomb bench scale experiments. At any given rocking speed, mixing intensity varies with the amount of liquid in the bomb. For example, a half-full autoclave provides more mixing intensity than a nearly full one. Mixing intensities in the rocking bomb experiments were compared to agitation rates in a stirred autoclave reactor using the surviving drop method. Drop sizes were determined as a function of rocking bomb loading and compared to those versus speed in the stirred autoclave. Figure 12-40 shows the relationship found between the fill level in the bomb and the agitation speed in the stirred autoclave.

The laboratory stirred vessel was actually never used for reaction experiments. It was simply a scaled-down version of the commercial autoclave geometry and operating conditions. Scale-up/scale-down was accomplished using constant P/V and geometric similarity. Reactions in the commercial reactor proved to be identical to results obtained in the rocking bomb autoclave.

High Pressure Reactor Design. Diphenyloxide and orthophenylphenol were produced continuously as co-products in a high-temperature, high-pressure (410°C, 4000 psig) two-phase reactor by reacting sodium hydroxide with monochlorobenzene. Scale-up was a big challenge. Visual appreciation of mixing was impossible, due to reaction conditions. Operations were calculated to be close to supercritical conditions. Minimizing fabrication cost and providing for an 8 min mean residence time led to a design that was 96 in. tall by 18 in. internal diameter. The process demanded intense dispersive mixing, rapid circulation, and a narrow residence time distribution. These were difficult to obtain in the tall cylinder, shown in the right-hand view of Figure 12-31. An experimental $\frac{1}{3}$ scale Lucite vessel containing a top-entering six-blade RDT, a draft tube, and four wall baffles located in the impeller region was constructed. At the bench scale, continuous reactions (with an 8 min residence time) were carried out in a 1.0 L stirred autoclave reactor to determine the critical change over in impeller speed from mass transfer to reaction rate control.
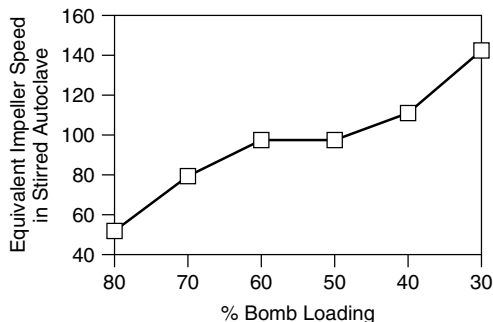

Figure 12-40   Relationship between rocking bomb reactor and lab scale stirred autoclave using the maximum stable drop size as a calibration tool.

The mixing intensity at the critical crossover speed was characterized for the small reactor, employing the maximum stable drop method with mineral oil as the dispersed phase. Similar experiments were run in the $\frac{1}{3}$ scale Lucite prototype vessel. The goal was to find the impeller speed in the $\frac{1}{3}$ scale prototype that gave the same mixing intensity (maximum drop size) as the autoclave operating at the critical change over speed. This information made it possible to establish the speed and power requirements for the production scale vessel. Scale-up was accomplished using equal P/V and circulation time. The commercial scale reactor produced precisely the expected result, and a second identical reactor was installed. This plant operated successfully for over 20 years.

Caution. Example applications using the surviving drop method were for either noncoalescing or slowly coalescing systems. This technique should not be used if the application is a rapidly coalescing system.

12-9.2.6 *Suspension Polymerization: Cross-Linked Polystyrene*. A suspension polymerization process was to be scaled up from a 1000 gal to a 4000 gal vessel. Attempts to do this failed because existing designs produced beads that were too small when suspension needs were met. Correctly sized beads could be made but not adequately suspended. Reactor setups were common. Comparative testing showed that a new impeller design, shown in Figures 12-28 (right view) and 12-30, seemed to meet both needs. It consisted of a four-blade loop-type impeller placed in a nonbaffled vessel. The design provided excellent surface mixing needed for drop suspension, while producing much larger drops of good uniformity. Long vertical arms provided uniform shear as well as good heat transfer to the wall. With reference to Figure 12-26, the new design raised the suspension line, enabling larger drops to be produced.

12-9.2.7 *Suspension Polymerization: Vinyl Polymerization*. A well-established suspension polymerization process was being scaled from existing 3500 gal production reactors to new, more scale-efficient 10 000 gal vessels. The reactor functions consisted of: blending two dense monomers, mixing water with a suspending agent, mixing an initiator with the monomers, dispersing the monomers in the aqueous phase to form an o/w dispersion, and then carrying out the exothermic reaction isothermally. The two reactors (3500 and 10 000 gal) were geometrically similar, and no problems were expected. This was not to be the case. The first three batches in the larger vessel underwent mass polymerization (bulk polymerization), resulting in a difficult to remove mass of polymer. In these reactors, the single retreat curve impeller was located at the bottom of the vessel. Investigative laboratory tests showed that in the 10 000 gal vessel, a dispersion of water (the less dense phase) in the (more dense) mixed initiated monomer phase was formed rather than vice versa. Thus heating resulted in a mass, not a suspension polymerization.

Prior to forming the dispersion, two separated layers existed, with the impeller in the lower monomer phase. A large interfacial vortex formed on starting the

agitator, drawing the upper water layer down, like a tornado, into the impeller, where it was dispersed into the monomer. It is hard to explain why this did not happen in the 3500 gal vessels. Possibly, differences in wall drag had prevented the deep vortex from forming in the older, rough surfaced vessels. Laboratory simulations showed that a second impeller, located in the water phase, would inhibit interfacial vortex formation. This was adapted, and the production plant operated as expected with monomer dispersed in water.

12-9.3   Summary

The applications presented in this section serve to demonstrate that fundamental knowledge must be coupled with practical insight and engineering judgment to solve problems associated with real industrial applications. Apart from certain formulated products, liquid–liquid dispersion is rarely carried out for its own sake. It is usually accompanied by heat/mass transfer and chemical reaction, thereby complicating scale-up.

NOMENCLATURE

a	drop radius (m)
a_v	interfacial area per unit volume (m^{-1})
a^*	constant in eq. (12-11)
$A(v,t)$	number probability density function for drops of volume v at time t
$A_o(v,t)$	value of $A(v,t)$ in vessel feed stream
$A(v)$, $A_o(v)$	steady-state values of $A(v,t)$ and $A_o(v,t)$, respectively
B	baffle width (m)
B_d	breadth of deformed drop (m)
$\dot{B}_d$	birth rate of drops of size d (s^{-1})
$c_{A\bar{r}}$	solubility of a particle of species A of radius $\bar{r}$ in solution (kg-mol/m^3)
$c_{A\infty}$	bulk solubility of species A in solution (kg-mol/m^3)
c_s	surfactant concentration (kg/m^3)
C	clearance from tank bottom (m)
CoV	coefficient of variation
$C_1 \cdots C_{29}$	dimensionless empirical constants
ΔC_A	concentration driving force for mass transfer (kg/m^3)
C_{pf}	heat capacity of fluid (J/kg · K)
d, d'	drop diameter (m)
d_i, d_j, d_k	nominal diameter of drops in size class i, j, and k, respectively (m)
d_{10}, d_{16}, d_{50}, d_{84}, d_{90}	drop diameters defined by cumulative volume frequencies of 0.1, 0.16, 0.5, 0.84, and 0.9, respectively (e.g., 50% of the volume is contained in drops of size d_{50} and smaller) (m)

d_{32}	Sauter mean drop diameter, general use (m)
$d_{32}(t)$	instantaneous Sauter mean diameter (at time t) (m)
d_{32}^{∞}	equilibrium Sauter mean diameter (m)
$d_{32}(0)$	Sauter mean diameter for $\phi \rightarrow 0$ (m)
$d_{32}(\phi)$	Sauter mean diameter for finite ϕ (m)
d_{43}	mass mean drop diameter (m)
d_{max}	maximum stable drop diameter (m)
d_n	number mean drop diameter (m)
$\bar{d}$	average drop diameter in eqs. (12-8) and (12-9) (m)
Δd_i	bin width for size class i in DSD (m)
D	impeller diameter (m)
D_{AB}	mass diffusivity, general use (m^2/s)
D_C	diameter of cylinder (m)
D_{crit}	critical drop deformation
D_m	mass diffusivity in continuous phase (m^2/s)
D_p	diameter of static mixer pipe (m)
$\dot{D}_d$	death rate of drops of size d (s^{-1})
E(k)	energy spectral density function for eddies of wavenumber k
$\hat{E}_S$	specific surface energy of a particle (J/kg-mol)
f	friction factor
f(h)	energy necessary to separate two adhering drops separated by distance h (J)
$f(\phi)$	function of dispersed to continuous phase volume fraction ratio
$f(\mu_d/\mu_c)$	function of dispersed to continuous phase viscosity ratio
$f_e(v)$	escape frequency of drops of volume v from vessel
$f_n(d_i)$	number frequency of drops in size class i
$f_v(d_i)$	volume frequency of drops in size class i
F	approach force acting on drop pairs (N)
$F_n(d_k)$	cumulative number frequency up to drop size d_k
$F_v(d_k)$	cumulative volume frequency up to drop size d_k
g	gravitational acceleration (m/s^2)
g_c	gravitational constant (m/s^2)
g(d), g(v)	breakage frequency of drops of diameter d and volume v, respectively
G	deformation rate (shear or extension) (s^{-1})
G_{crit}	critical deformation rate (shear or extension) (s^{-1})
h	film thickness/separation distance between colliding drops (m)
h_o	initial value of h (m)
h_c	critical film thickness for coalescence to occur (m)
h_T	heat transfer coefficient (W/m$^2 \cdot$ K)
H	height of liquid in vessel (m)
k	wavenumber of eddy (m^{-1})

k_{cf}	thermal conductivity of fluid (W/m · K)
k_m	mass transfer coefficient (m/s)
k_v	ratio of tangential velocity at blade tip to impeller tip speed
$(kT)_b$	product of Boltzmann constant and absolute temperature (N · m)
L_d	length of deformed drop (m)
L_p	length of a static mixer (m)
L_T	turbulent macro length scale (m)
m	number of size classes representing drop size distribution
$\dot{m}_A$	mass transfer rate to/from drop (kg/s)
n(d), n(d′)	number of drops of size d and d′, respectively
n_d	number of drops of size d
n_i, n_j	number of drops in size class i and j, respectively
N	impeller speed (rps)
N_{js}	minimum impeller speed to just suspended solid particles in vessel (rps)
N_{min}	minimum impeller speed to suspend liquid drops in vessel (rps)
$N_T(t)$	total number of drops in vessel at time t
$N_{T0}(t)$	total number of drops in vessel feed stream at time t
N_{TS}, N_0	steady-state values of $N_T(t)$ and $N_{T0}(t)$, respectively
N^*, N^*_{eff}	impeller speeds defined by eq. (12-56); N^* applies to a dilute dispersion and N^*_{eff} to a more concentrated dispersion (rps)
P	power (W)
$P_n(d)$	number probability density function for drop size d
$P_n(d, t)$	number probability density function for drop size d at time t
$P_v(d)$	volume probability density function for drop size d
$P_V(X)$	volume probability density function for dimensionless drop size X
$P_x(d)$	probability density function for drop size d, where x = n or x = v
ΔP	pressure drop in static mixer (Pa)
Q_V	impeller volumetric flow rate (m³/s)
$\bar{r}$	radius of particle undergoing Ostwald ripening (m)
R	radius of disk formed on flattened drop during collision with another drop (m)
t	time (s)
t_c	contact time between two colliding drops (s)
$\bar{t}_{circ}$	mean circulation time in tank (s)
t_{eq}	time to reach equilibrium (s)
T	tank diameter (m)
$\overline{U}$	velocity vector (m/s)

v, v'	volume of drop (m^3)
v$_{max}$	volume of largest drop, (m^3)
v$_\infty$	slip velocity of spherical particle (m/s)
$\overline{v'(d)^2}$	root mean square turbulent velocity difference across drop surface (m/s)
V	volume of tank (m^3)
V$_L$, V$_S$	volume of large (L) and small (S) scale tanks during scale-up (m^3)
$\hat{V}_A$	molar volume of species A (m^3/kg-mol)
V$_s'$	superficial velocity in static mixer (m/s)
W	width of an impeller blade (m)
X = d/d$_{32}$, X(t) = d/d$_{32}$(t)	dimensionless or normalized drop diameter
$\overline{X}$	mean value of X in DSD

Greek Symbols

$\alpha_1 \ldots \alpha_5$	constants
$\beta(v, v')$	frequency of daughter drops of volume v resulting from breakage of a parent drop of volume v'
$\beta'(d, d')$	number of daughter drops of size d resulting from breakage of a parent drop of size d'
β_K	Kolmogoroff constant = 1.5
β_S	crystal shape factor
$\Gamma(d, d')$	coalescence frequency between drops of diameter d and d'
$\Gamma(v, v')$	coalescence frequency between drops of volume v and v'
ε	local energy dissipation rate per mass of fluid (W/kg)
ε_{avg}	average energy dissipation rate per mass of fluid or power draw per mass (W/kg)
ε_{max}	maximum energy dissipation rate per mass of fluid (W/kg)
η	Kolmogoroff microscale of turbulence (m)
$\theta = N t$	dimensionless time in vessel
$\lambda(d, d')$	coalescence efficiency between drops of diameter d and d'
$\lambda(v, v')$	coalescence efficiency between drops of volume v and v'
μ_c	viscosity of continuous phase (Pa · s)
μ_d	viscosity of dispersed phase (Pa · s)
μ_f	viscosity of fluid (Pa · s)
$\overline{\mu}$	bulk viscosity of liquid–liquid mixture (Pa · s)
ν_c	kinematic viscosity of continuous phase, μ_c/ρ_c (m^2/s)
$\xi(d, d')$	collision frequency between drops of diameter d and d'
$\xi(v, v')$	collision frequency between drops of volume v and v'

ρ_c	density of continuous phase (kg/m^3)
ρ_d	density of dispersed phase (kg/m^3)
ρ_f	density of fluid (kg/m^3)
$\overline{\rho}$	bulk density of liquid–liquid mixture (kg/m^3)
$\Delta\rho = |\rho_d - \rho_c|$	density difference between phases (kg/m^3)
σ	interfacial tension (N/m)
σ_{SD}	standard deviation, general (m)
σ_V	volume standard deviation of normalized DSD
τ	time for the film between two coalescing drops to drain to a critical thickness (s)
τ_c	turbulent stress (force per area) acting on surface of drop (N/m^2)
τ_d	internal viscous stress (force per area) resisting drop deformation (N/m^2)
τ_s	stress (force per area) due to interfacial tension resisting drop deformation (N/m^2)
$\upsilon(v), \upsilon(v')$	number of daughter drops formed upon breakage of a parent drop of volume v and v', respectively
ϕ	volume fraction of dispersed phase
$\Omega = \dfrac{d_{32}(t) - d_{32}^{\infty}}{d_{32}^{\infty}}$	dimensionless instantaneous Sauter mean diameter

Dimensionless Groups

Ar	Archimedes number, $g\rho_c\Delta\rho\, D^3/\mu_c^2$
Ca	capillary number, $\mu_c Ga/\sigma$
Fr	Froude number for stirred vessel, $N^2 d/g$
N_p	power number, $P/\rho_c N^3 D^5$
N_q	flow number, Q_V/ND^3
Pr_f	Prandtl number, $C_{pf}\mu_f/k_{cf}$
Re	Reynolds number for stirred vessel (impeller), $\overline{\rho}ND^2/\overline{\mu}$
Re_{∞}	Reynolds number for spherical particle, $\rho_f v_{\infty} d/\mu_f$
Sc_f	Schmidt number, $\mu_f/\rho_f D_{AB}$
Su	Suratman number for stirred vessel, $\rho_c\sigma D/\mu_c^2$
Vi	viscosity group for stirred vessel, $(\rho_c/\rho_d)^{1/2}\mu_d ND/\sigma$; for static mixer, $(\rho_c/\rho_d)^{1/2}\mu_d V_s'/\sigma$
We	Weber number for stirred vessel, $\rho_c N^2 D^3/\sigma$; for static mixer, $\rho_c V_s'^2 D_p/\sigma$

REFERENCES

Aiba, S. (1958). Flow patterns of liquids in agitated vessels, *AIChE J.*, **4**, 485.

Al Taweel, A. M., and L. D Walker (1997). Dynamics of drop breakup in turbulent flow, presented at Mixing XIV, 14th Biennial North American Mixing Conference, Williamsburg, VA, June.

Allan, R. S., and S. G. Mason (1962). Particle motions in sheared suspensions: XIV. Coalescence of liquid drops in electric and shear fields, *J. Colloid Sci.*, **17**, 383–408.

Alvarez, J., J. Alvarez, and M. Hernandez (1994). A population balance approach for the description of particle size distribution in suspension polymerization reactors, *Chem. Eng. Sci.*, **49**, 99–113.

Arai, K., N. Konno, Y. Matunaga, and S. Saito (1977). The effect of dispersed phase viscosity on the maximum stable drop size for breakup in turbulent flow, *J. Chem. Eng. Jpn.*, **10**, 325–330.

Armenante, P. M., and Y.-T. Huang (1992). Experimental determination of the minimum agitation speed for complete liquid–liquid dispersion in mechanically agitated vessels, *Ind. Eng. Chem. Res*., **31**, 1398–1406.

Armenante, P. M., and D. Tsai (1988). Agitation requirements for complete dispersion of emulsions, presented at the AIChE Annual Meeting, Washington, DC, Nov.

Armenante, P. M., Y.-T. Huang, and T. Li (1992). Determination of the minimum agitation speed to attain the just dispersed state in solid–liquid and liquid–liquid reactors provided with multiple impellers, *Chem. Eng. Sci.*, **47**, 2865–2870.

Bajpai, R. K., D. Ramkrishna, and A. Prokop (1976). Coalescence redispersion model for drop-size distributions in an agitated vessel, *Chem. Eng. Sci.*, **31**(10), 913–920.

Bakker, A. J., K. J. Myers, R. W. Ward, and C. K. Lee (1996). The laminar and turbulent flow pattern of a pitched blade turbine, *Trans. Inst. Chem. Eng.*, **74A**, 485–491.

Baldyga, J., and J. R. Bourne (1992). Some consequences for turbulent mixing of fine scale intermittency, *Chem. Eng. Sci.*, **47**, 3943–3958.

Baldyga, J., and J. R. Bourne (1993). Drop breakup in the viscous subrange: a source of possible confusion, *Chem. Eng. Sci.*, **49**, 1077–1078.

Ballast, D. E., S. I. Bates, and R. M. Wiley (1961). Formation of solid beads by congelation of suspended liquid drops, U.S. patent 2,968,066, The Dow Chemical Company.

Bapat, P. M., L. L. Tavlarides, and G. W. Smith (1983). Monte Carlo simulation of mass transfer in liquid–liquid dispersions, *Chem. Eng. Sci.*, **38**(12), 2003–2013.

Bentley, B. J., and L. G. Leal (1986). An experimental investigation of drop deformation and breakup in steady, two-dimensional linear flows, *J. Fluid Mech.*, **167**, 241–283.

Berkman, P. D., and R. V. Calabrese (1988). Dispersion of viscous liquids by turbulent flow in a static mixer, *AIChE J.*, **34**(4), 602–609.

Blount, J. M. (1995). Mechanisms of drop breakage in dilute, agitated liquid–liquid systems, M.S. thesis, University of Maryland, College Park, MD.

Brooks, B. W., and H. N. Richmond (1991). Dynamics of liquid–liquid phase inversion using non-ionic surfactants, *Colloids Surfaces*, **58**, 131–148.

Brooks, B. W., and H. N. Richmond (1994a). Phase inversion in non-ionic surfactant–oil–water systems: I. The effect of transitional inversion on emulsion drop sizes, *Chem. Eng. Sci.*, **49**, 1053–1064.

Brooks, B. W., and H. N. Richmond (1994b). Phase inversion in non-ionic surfactant–oil–water systems: II. Drop size studies in catastrophic inversion with turbulent mixing, *Chem. Eng. Sci.*, **49**, 1065–1075.

Brooks, B. W., and H. N. Richmond (1994c). Phase inversion in non-ionic surfactant–oil–water systems: III. The effect of oil phase viscosity on catastrophic inversion and the relationship between the drop size present before and after catastrophic inversion, *Chem. Eng. Sci.*, **49**, 1843–1853.

Brown, D. E., and K. Pitt (1970). Drop breakup in a stirred liquid–liquid contactor, *Proc. Chemeca '70*, Melbourne and Sydney, Australia.

Brown, D. E., and K. Pitt (1974). Effect of impeller geometry on drop break-up in a stirred liquid contactor, *Chem. Eng. Sci.*, **29**, 345–348.

Calabrese, R. V., T. P. K. Chang, and P. T. Dang (1986a). Drop breakup in turbulent stirred-tank contactors: I. Effect of dispersed phase viscosity, *AIChE J.*, **32**(4), 657–666.

Calabrese, R. V., C. Y. Wang, and N. P. Bryner (1986b). Drop breakup in turbulent stirred-tank contactors: III. Correlations for mean size and drop size distribution, *AIChE J.*, **32**(4), 677–681.

Calabrese, R. V., M. H. Wang, N. Zhang, and J. W. Gentry (1992). Simulation and analysis of particle breakage phenomena, *Trans. Inst. Chem. Eng.*, **70A**, 189–191.

Calabrese, R. V., A. W. Pacek, and A. W. Nienow (1993). Coalescence of viscous drops in a stirred dispersion, *Proc. 1993 Inst. Chem. Eng. Research Event*, January, pp. 651–653.

Calabrese, R. V., M. K. Francis, V. P. Mishra, and S. Phongikaroon (2000). Measurement and analysis of drop size in a batch rotor–stator mixer, *Proc. 10th European Conference on Mixing*, Delft, The Netherlands, Elsevier Science, Amsterdam, pp. 149–156.

Calderbank, P. H. (1958). Physical rate processes in industrial fermentation: I, *Trans. Inst. Chem. Eng.*, **36A**, 443–463.

Chang, K. C. (1990). Analysis of transient drop size distributions in dilute agitated liquid–liquid systems, Ph.D. dissertation, University of Maryland, College Park, MD.

Chang, Y. C., R. V. Calabrese, and J. W. Gentry (1991). An algorithm for determination of size-dependent breakage frequency of droplets, flocs and aggregates, *Part. Part. Syst. Charact.*, **8**, 315–322.

Charles, G. E., and S. G. Mason (1960). The mechanism of partial coalescence of drops at a liquid–liquid interface, *J. Colloid. Sci.*, **15**, 105–122.

Chatzi, E. G., and D. Kiparissides (1994). Drop size distributions in high hold-up fraction dispersed systems: effect of the degree of hydrolysis of PVA stabilizer, *Chem. Eng. Sci.*, **49**(24B), 5039–5052.

Chatzi, E. G., A. D. Gavrielides, and C. Kiparissides (1989). Generalized model for prediction of the steady-state drop size distributions in batch stirred vessels., *Ind. Eng. Chem. Res.*, **28**, 1704–1711.

Chen, H. T., and S. Middleman (1967). Drop size distribution in agitated liquid–liquid systems, *AIChE J.*, **13**(5), 989–995.

Chesters, A. K. (1991). The modelling of coalescence processes in fluid–liquid dispersions, *Trans. Inst. Chem. Eng.*, **69A**, 259–270.

Church, J. M., and R. Shinnar (1961). On the behavior of liquid dispersions in mixing vessels, *Ind. Eng. Chem.*, **53**, 479–484.

Clark, M. M. (1988). Drop breakup in turbulent flow: I. Conceptual and modeling considerations, *Chem. Eng. Sci.*, **43**, 671–679.

Corrsin, S. (1964). The isotropic turbulent mixer: II. Arbitrary Schmidt number, *AIChE J.*, **10**, 870–877.

Coulaloglou, C. A., and L. L. Tavlarides (1976). Drop size distribution and coalescence frequencies of liquid–liquid dispersions in flow vessels, *AIChE J.*, **22**, 289–297.

Coulaloglou, C. A., and L. L. Tavlarides (1977). Description of interaction processes in agitated liquid–liquid dispersions, *Chem. Eng. Sci.*, **32**, 1289–1297.

Das, P. K., R. Kumar, and D. Ramkrishna (1987). Coalescence of drops in stirred dispersion: a white noise model for coalescence, *Chem. Eng. Sci.*, **42**, 213–220.

Davies, J. T. (1987). A physical interpretation of drop sizes in homogenizers and agitated tanks, including the dispersion of viscous oils, *Chem. Eng. Sci.*, **42**, 1671–1676.

Davis, R. H., J. A. Schonberg, and J. M. Rollison (1989). The lubrication force between two viscous drops, *Phys. Fluids A*, **1**, 77–81.

Doulah, M. S. (1975). An effect of hold-up on drop sizes in liquid–liquid dispersion, *Ind. Eng. Chem. Fundam.*, **14**, 137–138.

Gillespie, T., and E. Rideal (1956). The coalescence of drops at an oil–water interface, *Trans. Faraday Soc.*, **52**, 173–183.

Godfrey, J. C., and V. Grilc (1977). Drop size and drop size distribution for liquid–liquid dispersions in agitated tanks of square cross-section, *Proc. 2nd European Conference on Mixing*, Cambridge.

Grace, H. P. (1982). Dispersion phenomena in high viscosity immiscible fluid systems and application of static mixers as dispersion devices in such systems, *Chem. Eng. Commun.*, **14**, 225–277.

Hartland, S. (1990). Coalescence in close packed gas–liquid and liquid–liquid dispersions, *Ber. Bunsenges. Phys. Chem.*, **85**(10), 851–863.

Hartland, S., and S. A. K. Jeelani (1987). Drainage in thin planar non-Newtonian films, *Can. J. Chem. Eng.*, **65**(3), 382–390.

Hinze, J. O. (1955). Fundamentals of the hydrodynamic mechanism of splitting in dispersion processes, *AIChE J.*, **1**, 289–295.

Holmes, D. B., R. M. Voncken, and J. A. Dekker (1964). Fluid flow in turbine stirred, baffled tanks: I. Circulation time, *Chem. Eng. Sci.* **19**, 201–208.

Hong, P. O., and J. M. Lee (1983). Unsteady-state liquid–liquid dispersions in agitated vessels, *Ind. Eng. Chem. Process. Des. Dev.*, **22**, 130–135.

Hong, P. O., and J. M. Lee (1985). Changes of average drop sizes during initial period of liquid–liquid dispersions in agitated vessels, *Ind. Eng. Chem. Process. Des. Dev.*, **24**, 868–872.

Howarth, W. J. (1967). Measurement of coalescence frequency in an agitated tank, *AIChE J.*, **13**, 1007–1013.

Jeffreys, G. V., and J. L. Hawksley (1965). Coalescence of liquid droplets in two-component–two-phase systems: I. Effect of physical properties on the rate of coalescence, *AIChE J.*, **11**, 413–417.

Jeon, Y., and W. K. Lee (1986). Drop population model for mass transfer in liquid–liquid dispersion: I. Simulation and its results, *Ind. Eng. Chem. Fundam.*, **25**(2), 293–300.

Karam, H. J., and J. C. Bellinger (1968). Deformation and breakup for liquid droplets in a simple shear field, *Ind. Eng. Chem. Fundam.*, **1**, 576–581.

Kinugasa, T., K. Watanabe, T. Sonove, and H. Takeuchi (1997). Phase inversion of stirred liquid–liquid dispersions, presented at the International Symposium on Liquid–Liquid Two Phase Flow and Transport Phenomena, Session 13, Antalya, Turkey.

Kolmogoroff, A. N. (1941a). The local structure of turbulence in incompressible viscous fluid for very large Reynolds numbers, *Compt. Rend. Acad. Sci. USSR*, **30**, 301–305.

Kolmogoroff, A. N. (1941b). Dissipation of energy in locally isotropic turbulence, *Compt. Rend. Acad. Sci. USSR*, **32**, 16–18.

Kolmogoroff, A. N. (1949). The breakup of droplets in a turbulent stream, *Dokl. Akad. Nauk.*, **66**, 825–828.

Konno, M., A. Aoki, and S. Saito (1983). Scale effect on breakup process in liquid–liquid agitated tanks, *J. Chem. Eng. Jpn.*, **16**, 312–319.

Konno, M., K. Kosaka, and S. Saito (1993). Correlation of transient drop sizes in breakup process in liquid–liquid agitation, *J. Chem. Eng. Jpn.*, **26**(1), 37–40.

Koshy, A., T. R. Das, and R. Kumar (1988a). Effect of surfactants on drop breakage in turbulent liquid dispersions, *Chem. Eng. Sci.*, **43**, 649–654.

Koshy, A., T. R. Das, R. Kumar, and K. S. Ghandi (1988b). Breakage of viscoelastic drops in turbulent stirred dispersions, *Chem. Eng. Sci.*, **43**, 2625–2631.

Koshy, A., R. Kumar, and K. S. Gandhi (1989). Effect of drag reducing agents on drop breakage in stirred dispersions, *Chem. Eng. Sci.*, **44**, 2113–2120.

Lagisetty, J. S., P. K. Das, R. Kumar, and K. S. Ghandi (1986). Breakage of viscous and non-Newtonian drops in stirred dispersions, *Chem. Eng. Sci.*, **41**, 65–72.

Lam, A., A. N. Sathyagal, S. Kumar, and D. Ramkrishna (1996). Maximum stable drop diameter in stirred dispersions, *AIChE J.*, **42**, 1547–1552.

Lang, S. B., and C. R. Wilke (1971a). A hydrodynamic mechanism for the coalescence of liquid drops: I. Theory of coalescence at a planar interface, *Ind. Eng. Chem. Fundam.*, **10**, 329–340.

Lang, S. B., and C. R. Wilke (1971b). A hydrodynamic mechanism for the coalescence of liquid drops: II. Experimental studies, *Ind. Eng. Chem. Fundam.*, **10**, 341–352.

Lasheras, J. C., C. Eastwood, C. Martinez-Bazan, and J. L. Montanes (2002). A review of statistical models for the break-up of an immiscible fluid immersed into a fully developed turbulent flow, *Int. J. Multiphase Flow*, **28**, 247–278.

Laso, M., L. Steiner, and S. Hartland (1987a). Dynamic simulation of liquid–liquid agitated dispersions: I. Derivation of a simplified model, *Chem. Eng. Sci.*, **42**, 2429–2436.

Laso, M., L. Steiner, and S. Hartland (1987b). Dynamic simulation of liquid–liquid agitated dispersions: II. Experimental determination of the breakage and coalescence rates in a stirred tank, *Chem. Eng. Sci.*, **42**, 2437–2445.

Leng, D. E., and G. J. Quarderer (1982). Drop dispersion in suspension polymerization, *Chem. Eng. Commun.*, **14**, 177–201.

Leng, D. E., W. L. Sigelko, and F. L. Saunders (1985). Aqueous dispersions of plasticized polymer particles, U.S. patent 4,502,888, The Dow Chemical Company.

Lyu, S. P., F. S. Bates, and C. W. Macosko (2002). Modeling of coalescence in polymer blends, *AIChE J.*, **48**(1), 7–14.

MacKay, G. D. M., and S. G. Mason (1963). The gravity approach and coalescence of fluid drops at liquid interfaces, *Can. J. Chem. Eng.*, **41**, 203–212.

Marks, C. R. (1998). Drop breakup and deformation in sudden onset strong flows, Ph.D. dissertation, University of Maryland, College Park, MD.

McManamey, W. J. (1979). Sauter mean and maximum drop diameters of liquid–liquid dispersions in turbulent agitated vessels at low dispersed phase hold-up, *Chem. Eng. Sci.*, **34**, 432–434.

Middleman, S. (1974). Drop size distributions produced by turbulent pipe flow of immiscible fluids through a static mixer, *Ind. Eng. Chem. Process. Des. Dev.*, **13**, 78–83.

Middleton, J. C. (1979). Measurement of circulation within large mixing vessels, *Proc. 3rd European Conference on Mixing*, York, Yorkshire, England, Vol. 1, pp. 15–36.

Mlynek, T., and W. Resnick (1972). Drop size in an agitated liquid–liquid system, *AIChE J.*, **18**, 122–127.

Muralidhar, R., and D. Ramkrishna (1986). Analysis of droplet coalescence in turbulent liquid–liquid dispersions, *Ind. Eng. Chem. Fundam.*, **25**, 554–560.

Muralidhar, R., and D. Ramkrishna (1988). Coalescence phenomena in stirred liquid–liquid dispersions, *Proc. 6th European Conference on Mixing*, Pavia, Italy.

Muralidhar, R., D. Ramkrishna, P. K. Das, and R. Kumar (1988). Coalescence of rigid droplets in a stirred dispersion: II. Band-limited force fluctuations, *Chem. Eng. Sci.*, **43**, 1559–1586.

Murdoch, P. G., and D. E. Leng (1971). The mathematical formulation of hydrodynamic film thinning and its application to colliding drops suspended in a second liquid: II, *Chem. Eng. Sci.*, **26**, 1881–1892.

Nagata, S. (1975). *Mixing Principles and Applications*, Halstead Press, Wiley, New York.

Narsimhan, G., D. Ramkrishna, and J. P. Gupta (1980). Analysis of drop size distributions in lean liquid–liquid dispersions, *AIChE J.*, **26**, 991–1000.

Narsimhan, G., G. Nejfelt, and D. Ramkrishna (1984). Breakage functions of droplets in agitated liquid–liquid dispersions, *AIChE J.*, **30**, 457–467.

Nishikawa, M., F. Mori, and S. Fujieda (1987a). Average drop size in a liquid–liquid phase mixing vessel, *J. Chem. Eng. Jpn.*, **20**, 82–88.

Nishikawa, M., F. Mori, S. Fujieda, and T. Kayama (1987b). Scale-up of liquid–liquid phase mixing vessel, *J. Chem. Eng. Jpn.*, **20**, 454–459.

Nyvlt, J., O. Sohnel, M. Matuchova, and M. Bruol (1985). *The Kinetics of Industrial Crystallization*, Elsevier, Amsterdam.

Pacek, A. W., I. P. T. Moore, R. V. Calabrese, and A. W. Nienow (1993). Evolution of drop size distributions and average drop diameters in liquid–liquid dispersions before and after phase inversion, *Trans. Inst. Chem. Eng.*, **71A**, 340–341.

Pacek, A., I. P. T. Moore, A. W. Nienow and R. V. Calabrese (1994a). A video technique for the measurement of the dynamics of liquid–liquid dispersions during phase inversion, *AIChE J.* **40**, 1940–1949.

Pacek, A. W., A. W. Nienow, and I. P. T. Moore (1994b). On the structure of turbulent liquid–liquid dispersed flows in an agitated vessel, *Chem. Eng. Sci.*, **49**(20), 3485–3498.

Pacek, A. W., S. Chamsart, A. W. Nienow, and A. Baker (1999). The influence of impeller type on mean drop size and drop size distribution in a agitated vessel, *Chem. Eng. Sci.*, **54**, 4211–4222.

Pavlushenko, I. S., and A. V. Yanishevskii (1958). Effective number of revolutions of a stirrer for the dispersion of two mutually immiscible liquids, *Zhur. Priklad. Khim.*, **31**, 1348–1354.

Phongikaroon, S. (2001). Drop size distribution for liquid–liquid dispersions produced by rotor–stator mixers, Ph.D. dissertation, University of Maryland, College Park, MD.

Rajamani, K., W. T. Pate, and D. J. Kinneberg (1986). Time-driven and event-driven Monte Carlo simulations of liquid–liquid dispersions: a comparison, *Ind. Eng. Chem. Fundam.*, **25**(4), 746–752.

Rallison, J. M. (1984). The deformation of small viscous drops and bubbles in shear flows, *Annu. Rev. Fluid Mech.*, **16**, 45–66.

Ramkrishna, D. (2001). *Population Balances*, Wiley, New York.

Rod, V., and T. Misek (1982). Stochastic modeling of dispersion formation in agitated liquid–liquid systems, *Trans. Inst. Chem. Eng.*, **60**(1), 48–53.

Rodger, W. A., V. G. Trice, and J. H. Rushton (1956). Effect of fluid motion on interfacial area of dispersions, *Chem. Eng. Prog.*, **52**, 515–520.

Sathyagal, A. N., D. Ramkrishna, and G. Narsimhan (1995). Solution of inverse problems in population balances: II. Particle break-up, *Comput. Chem. Eng.*, **19**(4), 437–451.

Sathyagal, A. N., D. Ramkrishna, and G. Narsimhan (1996). Droplet breakage in stirred dispersions: breakage functions from experimental drop-size distributions, *Chem. Eng. Sci.*, **51**, 1377–1391.

Scheele, G. F., and D. E. Leng (1971). An experimental study of factors which promote coalescence of two colliding drops suspended in water: I, *Chem. Eng. Sci.*, **26**, 1867–1879.

Shinnar, R. (1961). On the behaviour of liquid dispersions in mixing vessels, *J. Fluid Mech.*, **10**, 259–275.

Skelland, A. H. P., and L. T. Moeti (1990). Mechanisms of continuous-phase mass transfer in agitated liquid–liquid systems, *Ind. Eng. Chem. Res.*, **29**, 2258–2267.

Skelland, A. H. P., and R. Seksaria (1978). Minimum impeller speeds for liquid–liquid dispersion in baffled vessels, *Ind. Eng. Chem. Process. Des. Dev.*, **17**, 56–61.

Skelland, A. H. P., and H. Xien (1990). Dispersed-phase mass transfer in agitated liquid–liquid systems, *Ind. Eng. Chem. Res.*, **29**, 415–420.

Sprow, F. B. (1967a). Distribution of drop sizes produced in turbulent liquid–liquid dispersion, *Chem. Eng. Sci.*, **22**, 435–442.

Sprow, F. B. (1967b). Drop size distributions in strongly coalescing liquid–liquid systems, *AIChE J.*, **13**, 995–998.

Stone, H. A. (1994). Dynamics of drop deformation and breakup in viscous fluids, *Annu. Rev. Fluid Mech.*, **26**, 65–102.

Stone, H. A., B. J. Bentley, and L. G. Leal (1986). An experimental study of transient effects in the breakup of viscous drops, *J. Fluid Mech.*, **173**, 131–158.

Tavlarides, L. L. (1981). Modelling and scale-up of dispersed phase liquid–liquid reactors, *Chem. Eng. Commun.*, **8**, 133–164.

Tavlarides, L. L., and P. M. Bapat (1983). Models for the scale-up of dispersed phase liquid–liquid reactors, *AIChE Symp. Ser.*, **80**, 12–46.

Tavlarides, L. L., and M. Stamatoudis (1981). The analysis of interphase reaction and mass transfer in liquid–liquid dispersions, *Adv. Chem. Eng.*, **11**, 199–273.

Taylor, G. I. (1934). The formation of emulsions in definable fields of flow, *Proc. R. Soc.*, **A146**, 501–523.

Tjahjadi, M., and J. M. Ottino (1991). Stretching and breakup of drops in chaotic flows, *J. Fluid Mech.*, **232**, 191–219.

Tjahjadi, M., H. A. Stone, and J. M. Ottino (1992). Satellite and subsatellite formation in capillary breakup, *J. Fluid Mech.*, **243**, 297–317.

Tobin, T., and D. Ramkrishna (1992). Coalescence of charged droplets in agitated liquid–liquid dispersions, *AIChE J.*, **38**(8), 1199–1205.

Todtenhaupt, P., E. Todtenhaupt, and W. Muller (1991). Handbook of Mixing Technology, Ekato Ruhr und Mischtechnik, Schopfheim, Germany.

Tsouris, C., and L. L. Tavlarides (1994). Breakage and coalescence models for drops in turbulent dispersions, *AIChE J.*, **40**, 395–406.

Valentas, K. J., and N. R. Amundson (1966). Breakage and coalescence in dispersed phase systems, *Ind. Eng. Chem. Fundam.*, **5**, 533–542.

Valentas, K. J., O. Bilous, and N. R. Amundson (1966). Analysis of breakage in dispersed phase systems, *Ind. Eng. Chem. Fundam.*, **5**, 271–279.

Van Heuven, J. W., and W. J. Beek (1971). Power input, drop size and minimum stirrer speed for liquid-liquid dispersions in stirred vessels, *Proc. International Solvent Extraction Conference*, The Hague, The Netherlands, **1**, 70–81.

Vermeulen, T., G. M. Williams, and G. E. Langlois (1955). Interfacial area in liquid–liquid and gas–liquid agitation, *Chem. Eng. Prog.*, **51**, 85F–95F.

Vinckier, I., P. Moldenaers, A. M. Terracciano, and N. Grizzuti (1998). Drop size evolution during coalescence in semi-concentrated model blends, *AIChEJ*, **44**, 951–958.

Vivaldo-Lima, E., P. E. Wood, and A. E. Hamielec (1997). An updated review on suspension polymerization, *Ind. Eng. Chem. Res*, **36**, 939–965.

Vrij, A. (1966). Possible mechanism for the spontaneous rupture of thin free liquid films, *Disc. Faraday Soc.*, **42**, 3505–3516.

Wang, C. Y., and R. V. Calabrese (1986). Drop breakup in turbulent stirred-tank contactors: II. Relative influence of viscosity and interfacial tension, *AIChE J.*, **32**(4), 667–676.

Warner, G. L., and D. E. Leng (1978). Continuous process for preparing aqueous polymer microdispersions. U.S. patent 4,123,403, The Dow Chemical Company.

Weinstein, B., and R. E. Treybal (1973). Liquid–liquid contacting in unbaffled agitated vessels, *AIChE J.*, **19**, 304–312.

Wright, H., and D. Ramkrishna (1994). Factors affecting coalescence of droplets in a stirred liquid–liquid dispersion, *AIChE J.*, **40**(5), 767–776.

Yarranton, H. W., and J. H. Masliyah (1997). Numerical simulation of Ostwald ripening in emulsions, *J. Colloid Interface Sci.*, **196**, 157–169.

Zhou, G., and S. M. Kresta (1998a). Correlation of mean drop size with the turbulence energy dissipation and the flow in an agitated tank, *Chem. Eng. Sci.*, **53**, 2063–2079.

Zhou, G., and S. M. Kresta (1998b). Evolution of drop size distribution in liquid–liquid dispersions for various impellers, *Chem. Eng. Sci.*, **53**, 2099–2113.

Zwietering, T. N. (1958). Suspending of solid particles in liquid by agitators, *Chem. Eng. Sci.*, **8**, 244–253.